

Aus dem Institut für Klinische Biochemie und Pathobiochemie des
Deutschen Diabetes-Zentrums (DDZ)

Leibniz-Zentrum für Diabetes-Forschung an der Heinrich-Heine-
Universität Düsseldorf

(Direktor: Univ.-Prof. Dr. Hadi Al-Hasani)

Analysis of substrate metabolism in peripheral tissues of insulin action

Habilitationsschrift

zur Erlangung der *Venia Legendi* im Fach Pathobiochemie an der
Medizinischen Fakultät der Heinrich-Heine-Universität Düsseldorf

vorgelegt von

Dr. rer. nat. Alexandra Chadt

Düsseldorf 2024

Table of contents

Table of contents	2
Deutsche Zusammenfassung	4
List of original publications underlying this thesis	5
1 Introduction	6
1.1 Insulin resistance and type 2 diabetes (T2D)	6
1.1.1 Etiology of T2D	6
1.1.2 Development of insulin resistance.....	6
1.1.3 Regulation of glucose transporter 4 (GLUT4) translocation in insulin resistance	8
1.1.4 Exercise in the prevention and treatment of insulin resistance and T2D	10
1.2 Rab-GTPase-activating proteins (RabGAPs) as key factors in glycemic control	13
1.2.1 Insulin- and contraction-dependent regulation of RabGAPs	13
1.2.2 RabGAP-mediated control of GLUT4 translocation	16
1.2.3 Naturally occurring RabGAP gene variants.....	18
1.2.4 Investigation of RabGAP function using mouse models	19
1.3 Objectives	22
2 Results	23
2.1 Conventional knockout of <i>Tbc1d1</i> in mice impairs insulin- and AICAR-stimulated glucose uptake in skeletal muscle	23
2.2 Deletion of Both Rab-GTPase-Activating Proteins TBC1D1 and TBC1D4 in Mice Eliminates Insulin- and AICAR-Stimulated Glucose Transport.....	24
2.3 AMPK and TBC1D1 Regulate Muscle Glucose Uptake After - But Not During - Exercise and Contraction	26
2.4 TBC1D4 is Necessary for Enhancing Muscle Insulin Sensitivity in Response to AICAR and Contraction	27
2.5 The RabGAPs TBC1D1 and TBC1D4 Control Uptake of Long-Chain Fatty Acids Into Skeletal Muscle via Fatty Acid Transporter SLC27A4/FATP4	28
2.6 Contraction-Mediated Glucose Transport in Skeletal Muscle Is Regulated by a Framework of AMPK, TBC1D1/4, and Rac1	29

2.7	Depletion of TBC1D4 improves the metabolic exercise response by overcoming genetically induced peripheral insulin resistance.....	31
3	Conclusions	32
3.1	The two RabGAPs TBC1D1 and TBC1D4 represent molecular switches in skeletal muscle substrate utilization.....	32
3.2	TBC1D1 and TBC1D4 regulate both lipid and glucose metabolism in skeletal muscle via a distinct pool of downstream Rab-GTPases.....	34
3.3	Insulin and contraction signaling in skeletal muscle converge at the level of the two RabGAPs TBC1D1 and TBC1D4	38
3.4	Skeletal muscle insulin resistance induced by TBC1D4 depletion can be overcome by moderate exercise endurance training	44
4	References.....	48
5	Abbreviations	55
6	Acknowledgments	57
7	Original publications	58

Deutsche Zusammenfassung

Mutationen der im Skelettmuskel und Fettzellen exprimierten Rab-GTPase-aktivierenden Proteine (RabGAPs) TBC1D1 und TBC1D4 (= AS160) können beim Menschen zur Entstehung schwerer Stoffwechselerkrankungen führen, insbesondere zu extremer Adipositas und Typ-2-Diabetes. Die beiden homologen Proteine TBC1D1 und TBC1D4 stellen direkte Phosphorylierungssubstrate wichtiger Signalkinasen wie der Proteinkinase AKT und der Adenosinmonophosphat-aktivierten Proteinkinase (AMPK) dar und spielen somit eine entscheidende Rolle in der Insulinwirkung in Adipocyten und Muskelzellen.

Durch unsere Forschung haben wir eine nicht redundante Funktion für TBC1D1 und TBC1D4 bei der trainings- und insulinvermittelten Regulierung der Ganzkörperglykämie und des Fettstoffwechsels aufgezeigt. Sie scheinen in der Zelle als molekulare Schalter zu wirken, mit Hilfe derer der Wechsel zwischen verschiedene Energiesubstraten reguliert wird. Aufgrund dieser zentralen Funktion stellen sie vielversprechende Angriffspunkt in der Prävention und Behandlung metabolischer Erkrankungen dar. In einer von uns durchgeführten Studie haben wir aufgezeigt, dass Glukose- und Fettstoffwechsel auf der Ebene der durch RabGAPs aktivierten Rab-GTPasen konvergieren. Des Weiteren konnten wir nachweisen, dass die beiden RabGAPs nicht nur in der Skelettmuskulatur und (im Falle von TBC1D4) im Fettgewebe ihre Funktion ausüben, sondern auch in pankreatischen Betazellen (TBC1D1) und im Herzen (TBC1D4). Des Weiteren konnte eine neue Signalachse im Skelettmuskel identifiziert werden, die aus zwei unabhängigen GTPase-Regulatoren, Rac1 und den beiden RabGAPs TBC1D1/4, besteht. Beide Proteine sind direkte sowie indirekte Ziele der AMPK und vermutlich auch anderer Kinasen. Zudem interagieren sie miteinander, um die vollständige kontraktionsvermittelte Glukoseaufnahme im Skelettmuskel zu erreichen. Schließlich konnten wir zeigen, dass die durch eine Deletion von TBC1D4 verursachte Insulinresistenz durch chronisches Ausdauertraining kompensiert werden kann. Die Untersuchung dieser Regelkreise stellt einen wichtigen Fortschritt im Verständnis der Mechanismen dar, die die Glukosehomöostase regulieren.

Diese kumulative Habilitationsschrift beruht auf 7 begutachteten Originalarbeiten, bestehend aus 2 Erstautorenschaften, 2 Co-Autorenschaften und 3 Letztautorenschaften bzw. korrespondierenden Autorenschaften (Anlagen 1-7).

List of original publications underlying this thesis

1. Dokas J* and **Chadt A***, Nolden T, Himmelbauer H, Zierath JR, Joost HG, Al-Hasani H. (2013) Conventional knockout of *Tbc1d1* in mice impairs insulin- and AICAR-stimulated glucose uptake in skeletal muscle. *Endocrinology* 154(10):3502-14. *Both authors contributed equally. Impact factor 2013: 4.644
1. **Chadt A**, Immisch A, de Wendt C, Springer C, Zhou Z, Stermann T, Holman GD, Loffing-Cueni D, Loffing J, Joost HG, Al-Hasani H. (2015) Deletion of Both Rab-GTPase-Activating Proteins TBC1D1 and TBC1D4 in Mice Eliminates Insulin- and AICAR-Stimulated Glucose Transport. *Diabetes* 64(3):746-59. Impact factor 2015: 8.784
2. Kjøbsted R, Roll JLW, Jørgensen NO, Birk JB, Foretz M, Viollet B, **Chadt A**, Al-Hasani H, Wojtaszewski JFP. (2019): "AMPK and TBC1D1 Regulate Muscle Glucose Uptake After - But Not During - Exercise and Contraction." *Diabetes*. 68(7):1427-1440. Impact factor 2019: 7.720
3. Kjøbsted R, **Chadt A**, Jørgensen NO, Kido K, Larsen JK, de Wendt C, Al-Hasani H, Wojtaszewski JFP. (2019): "TBC1D4 is Necessary for Enhancing Muscle Insulin Sensitivity in Response to AICAR and Contraction." *Diabetes* 68(9):1756-1766. Impact factor 2019: 7.720
4. Benninghoff T, Espelage L, Eickelschulte S, Zeinert I, Sinowenka I, Müller F, Schöndeling C, Batchelor H, Cames S, Zhou Z, Kotzka J, **Chadt A#**, Al-Hasani H. (2020) The RabGAPs TBC1D1 and TBC1D4 Control Uptake of Long-Chain Fatty Acids Into Skeletal Muscle via Fatty Acid Transporter SLC27A4/FATP4. *Diabetes* 69(11):2281-2293. #Corresponding author. Impact factor 2020: 9.461
5. de Wendt C*, Espelage L*, Eickelschulte S, Springer C, Toska L, Scheel A, Bedou AD, Benninghoff T, Cames S, Stermann T, **Chadt A#**, Al-Hasani H. (2021) Contraction-Mediated Glucose Transport in Skeletal Muscle Is Regulated by a Framework of AMPK, TBC1D1/4, and Rac1. *Diabetes* 70(12):2796-2809. *Both authors contributed equally. #Corresponding author. Impact factor 2021: 9.337
6. Springer C, Binsch C, Weide D, Toska L, Cremer AL, Backes H, Scheel AK, Espelage L, Kotzka J, Sill S, Kurowski A, Kim D, Karpinski S, Schnurr TM, Hansen T, Hartwig S, Lehr S, Cames S, Brüning JC, Lienhard M, Herwig R, Börno S, Timmermann B, Al-Hasani H, **Chadt A**. (2024) Depletion of TBC1D4 improves the metabolic exercise response by overcoming genetically induced peripheral insulin resistance. *Diabetes* 12:db230463. Impact factor 2024: Tbd

1 Introduction

1.1 Insulin resistance and type 2 diabetes (T2D)

1.1.1 Etiology of T2D

Type 2 diabetes (T2D) represents the most important metabolic disease in western industrial nations and is mainly caused by disorders of glucose and lipid metabolism. T2D is characterized by chronically elevated blood glucose levels and is associated with an increased risk of developing a large number of secondary complications such as cardiovascular disease (CVD), micro- and macrovascular comorbidities (e. g. diabetic retinopathy) and renal dysfunction [1]. Although the disease was described centuries ago, lifestyle changes, especially since the onset of industrialization, have led to a general decline in physical activity and excessive consumption of high-calorie food. These changes have resulted in a global pandemic of obesity [2]. Recent reports estimate that 537 million adults were living with diabetes in 2021 and project a further increase to 783 million by 2045 [3]. Due to the close relationship between obesity and diabetes, the term "diabesity" was coined already in the 1970s [4] and a causal pathophysiological relationship between the two metabolic disorders is generally accepted. However, while at the population level the link between obesity and its secondary complications is well described, the molecular mechanisms underlying these complications are still poorly understood [5].

1.1.2 Development of insulin resistance

The chronically elevated blood glucose level characteristic of diabetes is the result of an inability of the pancreatic beta cells to produce sufficient amounts of insulin to maintain normoglycemia [6]. The precise control of a complex network of inter-organ communication is necessary to respond adequately to changing external stimuli with adaptations in blood glucose levels [7]. In T2D, a progressive insulin resistance in peripheral tissues is known to precede the onset of diabetes [8]. In particular the skeletal muscle has been shown to be a crucial determinant of glycemic control as it is responsible for over 80% of postprandial glucose clearance from the blood [9]. Similarly, adipose tissue has also been shown to play an important role in regulating insulin sensitivity, not only by importing glucose into cells in response to insulin, but also by controlling the composition of plasma lipids [10]. Insulin resistance is defined as the inability of peripheral organs such as skeletal muscle and adipose tissue to respond to insulin secreted by pancreatic beta cells. Since insulin has a variety of effects on essentially all organs, insulin resistance as a metabolic disease not only

affects glucose metabolism but utilization of energy in general. Whereas in the healthy state, insulin stimulates glucose uptake and glycogen synthesis in the skeletal muscle, glucose transport and lipogenesis in adipose tissue and glycogen synthesis and lipogenesis in the liver, it holds additional inhibitory functions in these tissues. In skeletal muscle, insulin inhibits protein breakdown; in adipocytes, it inhibits lipolysis; and in the liver, glucose production and fatty acid oxidation (FAO) are blocked by high circulating concentrations of insulin [11]. In the state of insulin resistance, all these signaling pathways are counter-regulated, but to a different extent in each person, which makes diagnosis and treatment extremely difficult. While a healthy organism is able to switch between different energy substrates to adapt to changes in metabolic demand, the inability to do so is a hallmark of impaired insulin action and has been described as a state of "metabolic inflexibility" (as opposed to the healthy state of "metabolic flexibility") [12]. Figure 1 provides an overview of the metabolic (in)flexibility of skeletal muscle.

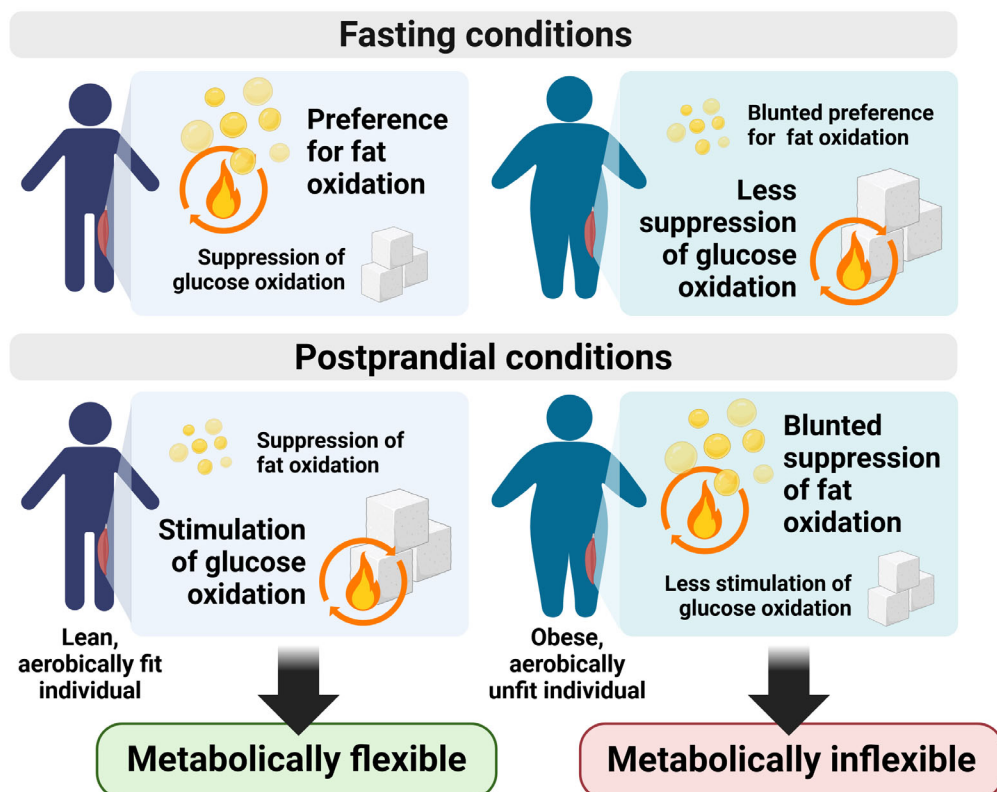


Figure 1: Metabolic (in)flexibility of skeletal muscle. During fasting conditions, lean individuals rely heavily on fat oxidation (A), while obese individuals rely more on glucose oxidation and less on fat (B). When insulin is present (e.g. in the postprandial state), the skeletal muscle of lean individuals suppresses fat oxidation in favor of glucose oxidation (C). Obese individuals exhibit reduced stimulation of glucose oxidation by insulin and blunted suppression of fat oxidation in their skeletal muscles (D). Modified after [13]. (Own illustration, created with Biorender.com)

1.1.3 Regulation of glucose transporter 4 (GLUT4) translocation in insulin resistance

In adipocytes and muscle cells, insulin stimulation (and contraction in skeletal muscle) causes an acute increase in glucose uptake due to an elevated amount of glucose transporter type 4 (GLUT4) on the cell membrane [14]. This process, also known as GLUT4 translocation, represents the fundamental effect of insulin and is still incompletely understood. Containing 12 transmembrane domains, GLUT4 catalyzes the passive transport of glucose across the membrane along a concentration gradient and is exclusively expressed in insulin-sensitive tissues such as adipocytes, the heart and skeletal muscle. In unstimulated cells, the majority of GLUT4 is located in a trans-Golgi-associated membrane compartment (GLUT4-storage vesicles, GSV). Insulin stimulation and, in muscle, contraction, cause fusion of these GLUT4 vesicles with the plasma membrane, consequentially increasing cellular glucose uptake. After termination of the stimulus, the GLUT4 proteins are internalized and sorted back into the intracellular storage compartments [14].

Upon insulin binding to its receptor (IR), the receptor phosphorylates several scaffolding proteins, such as insulin receptor substrate family members (IRS) and Cbl (Casitas B-lineage lymphoma). The tyrosine phosphorylation of IRS proteins creates docking sites for the p85 regulatory subunit of type 1A phosphatidylinositol-3 kinase (PI3K). Phosphatidylinositol 3,4,5-trisphosphate (PIP₃) is generated, which acts as a docking site for pleckstrin homology (PH) domain-containing proteins, such as PDK1 (3-phosphoinositide-dependent protein kinase 1), mTORC2 and AKT. AKT, also known as protein kinase B (PKB), is a serine/threonine kinase that is activated by sequential phosphorylation at Thr308 (by PDK1) and Ser473 (by mTORC2) [15, 16]. There is evidence for an alternative signaling pathway that involves tyrosine phosphorylation of the proto-oncogene Cbl and the Rho-family GTPase TC10, resulting in the translocation of GLUT4 from intracellular vesicles to the plasma membrane. It appears that there is a discrepancy between the reliance of adipocytes and skeletal muscle cells on insulin stimulation. Although the TC10 pathway is regarded as more pertinent in adipocytes, the Rac1 pathway seems to be more relevant in skeletal muscle (Figure 2) [17-19].

To decipher the role of GLUT4 in glucose homeostasis, the *Slc2a4* gene encoding this transporter was disrupted in different mouse tissues by generating knockout mouse models. Surprisingly at that time, ubiquitous knockout of GLUT4 induced cardiac hypertrophy and growth retardation in the animals, but not T2D. In contrast, knockout of the *Slc2a4* gene specifically in adipocytes (aG4KO) or skeletal muscle (mG4KO)

resulted in impaired insulin sensitivity and eventually the development of T2D [20, 21]. Using combined muscle- and adipocyte-specific GLUT4 knockout mice (amG4KO), it was later shown that the specific ablation of the transporter in individual tissues leads to a redistribution of energy substrates, especially lipids, to the liver, and that this fatty liver ultimately causes insulin resistance [22, 23].

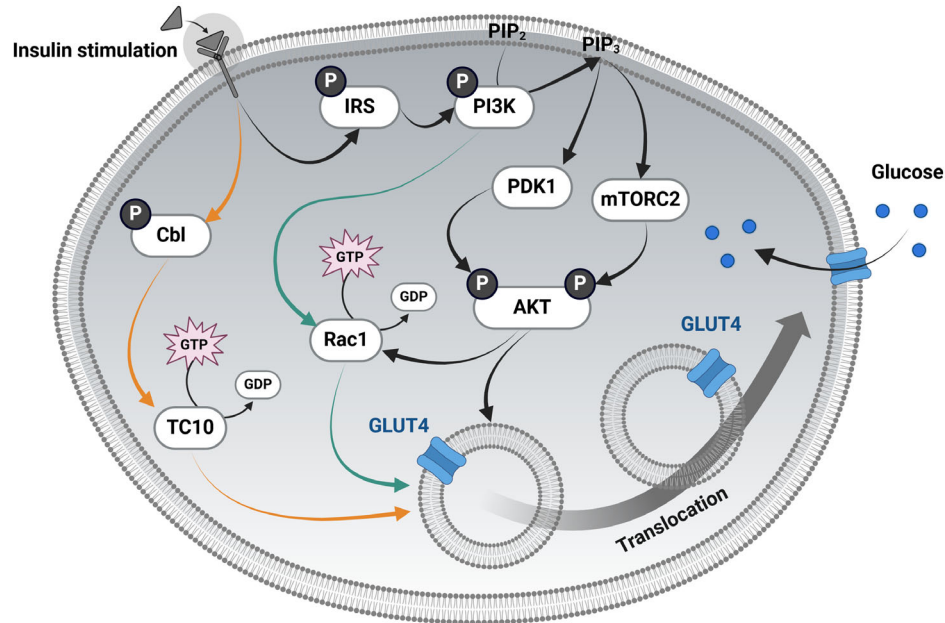


Figure 2: Insulin and contraction signaling in adipocytes and skeletal muscle cells. IRS: Insulin receptor substrate family, Cbl: Casitas B-lineage lymphoma, PI3K: Phosphatidylinositol-3 kinase, PIP₂: Phosphatidylinositol 4,5-bisphosphate, PIP₃: Phosphatidylinositol 3,4,5-trisphosphate, PDK1: 3-phosphoinositide-dependent protein kinase 1, AKT: Protein kinase B (PKB), GLUT4: Glucose transporter 4, mTORC2: mTOR Complex 2. **Orange**: More relevant in adipocytes, **Purple**: More relevant in skeletal muscle. (Own illustration, created with Biorender.com)

In the insulin resistant state, the intracellular signaling mechanisms downstream of the insulin receptor are disturbed, resulting in reduced transport of glucose into the cells and, as a consequence, elevated blood glucose levels. On a genetic level, insulin resistance can be caused by mutations and polymorphisms of the insulin receptor, the IRS proteins, and downstream signaling proteins such as PI3K (Phosphatidylinositol-3 kinase). Extrinsic factors, such as circulating metabolites, inflammatory pathways, and accumulation of toxic lipid species (lipotoxicity), can also negatively affect insulin sensitivity in peripheral tissues [24]. There is strong evidence that diacylglycerols (DAGs) play an important role in the development of skeletal muscle insulin resistance. Studies have shown that elevated DAG levels activate members of the Protein kinase C (PKC) family, particularly those from the subgroup of 'novel' or nPKCs, such as PKC δ or PKC θ . This activation leads to the phosphorylation of Serine residues of IRS proteins, resulting in a decrease in insulin signaling [25, 26]. Additionally, an excess of

saturated fatty acids, such as palmitate, promotes ceramide synthesis, which prevents AKT translocation and activation, thereby attenuating insulin signaling. It can be considered that DAGs and ceramides play a crucial role in the development of skeletal muscle insulin resistance [27].

1.1.4 Exercise in the prevention and treatment of insulin resistance and T2D

Obesity is considered to be a major factor in the development of insulin resistance and the resulting T2D. The exact links between morbid obesity and its sequelae are not yet clear, but ectopic storage of fat in the liver and skeletal muscle is thought to be an important component in the development of insulin resistance [28]. Although caloric restriction can reduce body weight and improve insulin sensitivity, it can also lead to mitochondrial loss. Physical activity prevents this and thus improves insulin sensitivity through anabolic processes such as mitochondrial biogenesis and also through mitophagy, the selective degradation of dysfunctional mitochondria, ultimately leading to improved mitochondrial function [2, 29, 30].

In recent years, a significant correlation has been established between exercise training and the prevention of cardiovascular risk [31, 32]. During acute endurance training, muscular contraction increases the activity of AMPK (Adenosine monophosphate (AMP)-activated protein kinase) and, via the calcium influx from the endoplasmic reticulum, the activity of CAMKII (Ca^{2+} /calmodulin-dependent protein kinase II) and MAPK (mitogen-activated protein kinase). The activation of these essential components of cell metabolism then leads to an accelerated translocation of GLUT4 to the plasma membrane and thus to an increased uptake of glucose into the muscle cell [33, 34]. This process is insulin-independent, so that the contraction of the skeletal muscle leads to a reduction in hyperglycemia even if insulin resistance is already present. In addition, exercise also improves the insulin-dependent transport of glucose into the cell, i. e. it has an insulin-sensitizing effect [35]. This mechanism involves activation of early members of the insulin signaling cascade, such as the insulin receptor itself or its substrates (IRS1-4), as well as more distal components such as PDK1, the RabGAP proteins (Rab-GTPase-activating proteins) TBC1D1 and TBC1D4 (also known as AS160 = AKT substrate of 160 kDa). Glucose metabolism and insulin sensitivity in response to exercise are tightly controlled by a complex web of interacting and converging signals including a large number of posttranslational modifications [36].

One long-term positive effect of exercise on insulin sensitivity is the activation of nuclear transcription factors such PGC1 α (Peroxisome proliferator activated receptor-coactivator 1 alpha) and Nuclear respiratory factor-1 (NRF-1) by CaMKII and AMPK

signaling pathways [37]. The increased expression of these factors facilitates the transcription of mitochondrial proteins that promote mitochondrial biogenesis. An increase in mitochondrial density has been demonstrated to enhance the oxidative capacity of skeletal muscle, thereby facilitating the transportation of greater quantities of fatty acyl coenzyme A (FA-CoA) into the mitochondria for oxidation. This elevated FAO rate helps prevent the accumulation of bioactive fatty acid (FA) species, such as DAGs and ceramides and, as a consequence, improves insulin signaling [38]. Although controversially discussed in the literature, p38 MAPK also plays a role in contraction- and insulin-mediated glucose transport into skeletal muscle. Sharing the TAK1 (Transforming growth factor beta-activated kinase 1) upstream kinase with AMPK, some studies have suggested a beneficial impact of p38 MAPK on the expression levels of GLUT4 through the activation of the transcription factor MEF2 (Myocyte enhancer factor-2) [39, 40] and a reduction in stretch-induced glucose uptake following p38 MAPK inhibition [41, 42]. However, there is evidence that p38 MAPK has a negative impact on insulin-mediated glucose transport, while it may facilitate insulin-independent glucose uptake in conjunction with specific signaling molecules, such as adiponectin [43]. Another mechanism promoted by long-term training is the activation of the mTORC1/S6K (Mammalian target of rapamycin/serine kinase 6) signaling pathway, which leads to increased protein synthesis and subsequently increased muscle mass [44]. Elevated glycogen augments mTORC1-S6K1 signaling whereas AMPK deficiency leads to impaired contraction-induced muscle protein synthesis [45]. Figure 3 presents a summary of the pathways induced by acute and long-term muscle contraction.

However, the beneficial effects of exercise are highly dependent on various factors, including the species, tissue type, specific exercise regimen, and the time point of analysis (e.g. during, acutely post or long-term post) [46]. For example, combining endurance (aerobic) and resistance (anaerobic) exercise is considered more effective in preventing metabolic disorders than each training type alone [47]. Accordingly, research results from exercise studies even with only slightly different experimental designs vary considerably with regard to the statements made. Many, but by no means all studies describe increased gene expression levels of key factors related to insulin signaling, such as IR, IRS-1, PI3K, and GLUT4, as a long-term adaptation to regular physical activity [48-50].

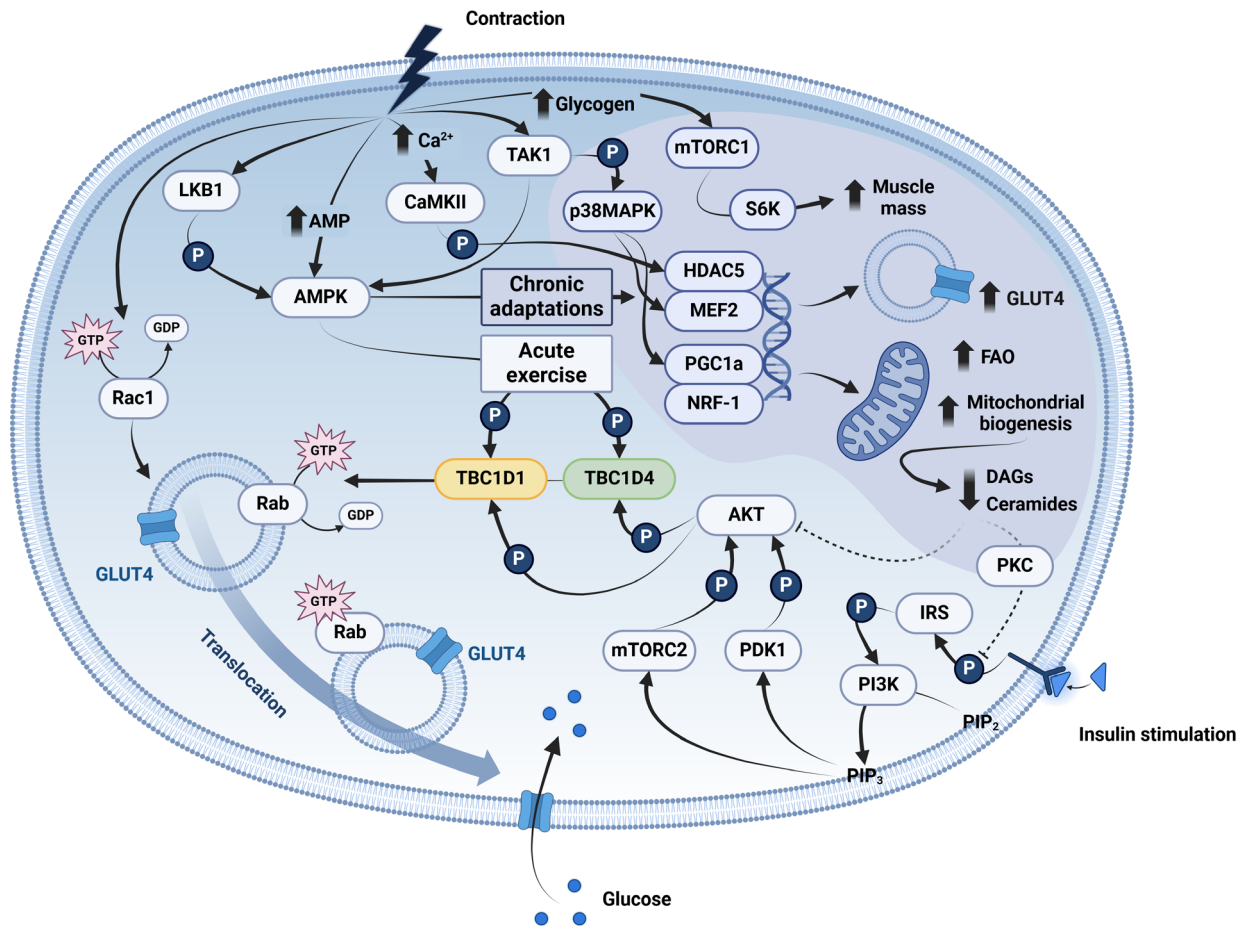


Figure 3: Impact of contraction on skeletal muscle insulin sensitivity. Skeletal muscle contraction increases the concentration of cytosolic Ca^{2+} , facilitating the activation of CaMKII (Ca^{2+} /calmodulin-dependent protein kinase II). The activation of AMPK (AMP-activated protein kinase) is triggered by an increase in AMP levels within the cell, as well as by phosphorylation events facilitated by LKB1 (Liver kinase B1). Several kinases, including AMPK, CaMKII, TAK1 (Transforming growth factor beta-activated kinase 1), and p38 MAPK (Mitogen-activated protein kinase), phosphorylate critical transcription factors, enhancing GLUT4 (*Slc2a4*) gene expression via phosphorylation of HDAC5 (Histone deacetylase 5) and MEF2 (Myocyte enhancer factor-2). Additionally, they activate PGC1 α (Peroxisome proliferator-activated receptor gamma coactivator 1-alpha) and NRF-1 (Nuclear respiratory factor 1), promoting mitochondrial biogenesis. The increase in fatty acid oxidation (FAO) results in reduced accumulation of toxic lipid species, such as ceramides and diacylglycerols (DAGs), which in turn leads to reduced activation of novel protein kinase C isoforms (nPKCs). This ultimately results in reduced serine phosphorylation and inhibition of insulin receptor substrate (IRS) proteins and AKT. The insulin signaling cascade is activated through autophosphorylation of the insulin receptor, leading to phosphorylation and activation of IRS (insulin receptor substrate) proteins. This, in turn, activates PI3K (Phosphatidylinositol 3-kinase), PDK1 (3-phosphoinositide-dependent protein kinase 1), and mTORC2 (mTOR Complex 2), with the latter two activating the serine-threonine kinase AKT. Both AKT and AMPK phosphorylate the RabGAPs (Rab-GTPase-activating proteins) TBC1D1 and TBC1D4. These are Rab-GTPase-activating proteins, also known as TBC1 (*tre-2/USP6*, *BUB2*, *cdc16*) domain family members 1 and 4 respectively. Phosphorylation of the RabGAPs results in their dissociation from downstream

Rab-GTPases. This leads to the accumulation of Rab-GTPases in their active, GTP-bound state, which facilitates the translocation of GLUT4-containing vesicles to the plasma membrane. Various signaling mechanisms have been described in parallel to AMPK for contraction-mediated glucose uptake into skeletal muscle, including the activation of the stretch-induced small Rho-GTPase Rac1 (reviewed in [51]). (Own illustration, created with Biorender.com)

Furthermore, it has been demonstrated that exercise training can enhance insulin signaling by reducing inflammation and oxidative stress, as pro-inflammatory cytokines and oxidative stress are major contributors to impaired insulin signaling [52]. However, although moderate physical activity has been shown to have a beneficial impact on the antioxidant status by reducing oxidative stress, intense exercise can lead to increased levels of oxidative stress in the short term. It is important to note that this increase in oxidative stress is only temporary and can lead to long-term benefits such as increased antioxidant capacity. Therefore, it is recommended to balance moderate and intense exercise for optimal health benefits. The impact of exercise on pro-inflammatory cytokine production is complex and varies depending on intensity and duration [52]. Interestingly, several studies report a phenomenon called "exercise non-response", which describes the variability with which individuals metabolically benefit from a given exercise program. However, these inter-individual differences in response are clearly dependent on a variety of factors, such as individual genetic predisposition, training intensities, volumes and types, and many others [53]. Given the increasing incidence of metabolic diseases worldwide and the goal of future personalized medicine, it is of utmost importance to understand the underlying links between individual genetic susceptibility and metabolic response to lifestyle factors such as diet and physical activity [54].

1.2 Rab-GTPase-activating proteins (RabGAPs) as key factors in glycemic control

1.2.1 Insulin- and contraction-dependent regulation of RabGAPs

The two serine/threonine-specific protein kinases AKT and AMPK are activated by different stimuli and pathways, and once activated, initiate complex signaling cascades in the cell. AKT is a crucial part of the insulin signaling pathway, while AMPK is activated in response to increased energy demands, such as during exercise [55]. Exercise increases energy expenditure in skeletal muscle, leading to an elevated AMP/ATP ratio. This supports AMPK phosphorylation at Thr172 by Liver kinase B1 (LKB1) [56, 57], thereby promoting its kinase activity through allosteric activation [58]. In addition

to LKB1 being the primary upstream kinase for AMPK, previous studies have demonstrated that AMPK can be activated not only through phosphorylation by LKB1, but also by Ca^{2+} /calmodulin-dependent protein kinase kinase (CaMKK) in response to calcium flux [59-61]. However, more recent data indicate that CaMKK does not directly regulate AMPK in skeletal muscle and previous reports on the impact of CaMKK on contraction-induced glucose uptake are likely due to off-target effects [62].

Both TBC1D4 and TBC1D1 contain a calmodulin-binding site (CBD). The exact regulatory function of this site has not yet been elucidated, but it is thought that the second messenger protein calmodulin is activated by increased intracellular Ca^{2+} levels and the resulting calmodulin/ Ca^{2+} complex activates CaMKII (Ca²⁺/calmodulin-dependent protein kinase II). In addition, the calmodulin/ Ca^{2+} complex may directly influence the cellular function of the RabGAPs, providing an AMPK-independent mechanism activated by muscle contraction [63]. Besides AMPK, LKB1 controls other AMPK-related kinases (ARKs) such as ARK5, SNF1-ARK (SNARK) and Salt-inducible kinase 1-3 (SIK1-3), which have been demonstrated or hypothesized to regulate RabGAP function [51]. Administering 5-Aminoimidazole-4-carboxamide ribonucleotide (AICAR), the most commonly used pharmacological AMPK activator, enhances glucose uptake into skeletal muscle, similar to the effects of exercise and muscle contraction [64-66]. Interestingly, while the stimulatory impact of AICAR on muscle glucose uptake is completely abolished in AMPK-deficient models, the inactivation or depletion of the AMPK subunits only reduced, but did not eliminate, contraction-induced glucose uptake in skeletal muscle [60, 67, 68]. This indicates the presence of multiple pathways, some dependent and some independent from AMPK that facilitate contraction-dependent glucose uptake in skeletal muscle. These apparently redundant mechanisms guarantee the correct operation of this evolutionarily preserved process that is crucial for survival. Figure 4 summarizes the regulatory pathways that induce contraction-mediated glucose uptake into skeletal muscle.

Both AKT and AMPK directly phosphorylate TBC1D1 and TBC1D4 in response to insulin, exercise and other stimuli, thereby enhancing GLUT4-mediated glucose transport [69, 70]. To date, numerous serine/threonine phosphorylation sites have been identified on TBC1D1 and TBC1D4. Nevertheless, only a limited number of these sites have been linked to a specific cellular function [71-73].

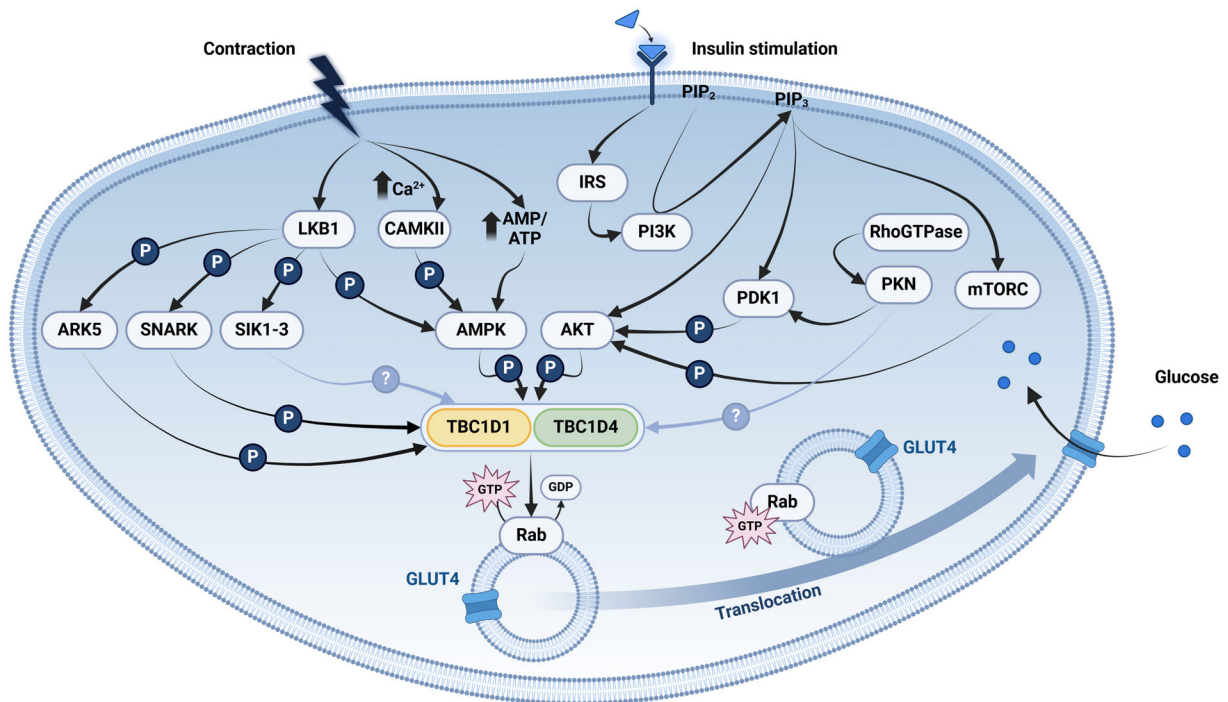


Figure 4: Insulin- and contraction-dependent regulation of RabGAPs. Intracellular signaling pathways that regulate glucose transporter 4 (GLUT4) translocation in skeletal muscle in response to insulin and contraction via the Rab-GTPase-activating proteins (RabGAPs) TBC1D1 and TBC1D4. Insulin activates AKT through the upstream regulators insulin receptor substrate (IRS), Phosphatidylinositol 3-kinase (PI3K), Mammalian target of rapamycin complex (mTORC), and 3-phosphoinositide-dependent protein kinase 1 (PDK1), which leads to the phosphorylation of TBC1D1 and TBC1D4 by AKT. Contraction activates liver kinase B1 (LKB1) and increases the AMP/ATP ratio, leading to the phosphorylation of TBC1D1 and TBC1D4 by AMPK (AMP-activated protein kinase). In addition to AMPK, other AMPK-related kinases (ARKs) controlled by LKB1, including ARK5, SNF1-ARK (SNARK) and Salt-inducible kinase 1-3 (SIK1-3), have been shown or speculated to regulate RabGAP function. Grey arrows indicate putative regulatory mechanisms. Once phosphorylated, TBC1D1 and TBC1D4 no longer inhibit the translocation of GLUT4-containing vesicles by inducing Rab-bound GTP hydrolysis, allowing for the incorporation of GLUT4 into the plasma membrane. PIP_{2/3}: Phosphatidylinositol-bis/trisphosphate, DAG: Diacylglycerol. Modified after [51]. (Own illustration, created with Biorender.com)

TBC1D1 and TBC1D4 belong to the family of RabGAPs and share a high degree of sequence homology. In fact, their functional GAP (GTPase-activating) domains are 79% identical and 91% similar (47% identical and 61% similar over their entire length) [74]. Figure 5 depicts the domain structure of the two RabGAPs.

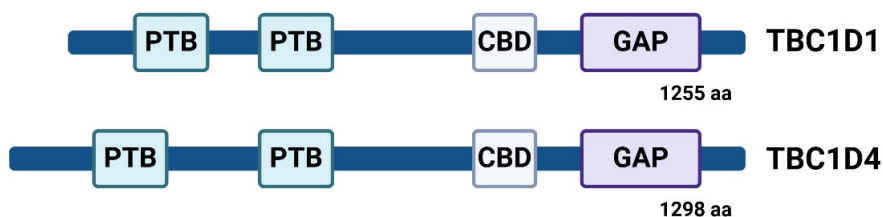


Figure 5: TBC1D1 and TBC1D4 domain structure (*Mus musculus*). The two RabGAPs TBC1D1 and TBC1D4 contain two N-terminal PTB (Phosphotyrosine-binding) domains, a Calmodulin-binding domain (CBD) and a catalytic TBC/GAP domain. Adapted from [71]. (Own illustration, created with Biorender.com)

It is noteworthy that in mice, there is a reciprocal expression pattern between TBC1D1 and TBC1D4 in different tissues. TBC1D1 is most highly expressed in skeletal muscle, with weaker expression in the hypothalamus and pancreatic beta cells. In contrast, TBC1D4 shows a broader, almost ubiquitous expression, with the highest levels found in adipose tissue, skeletal muscle, and the heart [75]. The two RabGAPs TBC1D1 and TBC1D4 represent important signaling junctions where insulin- and contraction-dependent signaling converges, and are therefore crucial master switches in the regulation of glucose transport in fat and muscle cells. Of note, only insulin-stimulated, but not contraction-stimulated glucose transport is impaired in skeletal muscle from insulin resistant or patients with diabetes [76]. As the signaling hub for both the insulin and contraction-stimulated pathways, the RabGAPs may determine which pathway is stimulated and which is inhibited. This complex regulatory mechanism is likely controlled through the phosphorylation of RabGAPs at specific serine or threonine sites. There is evidence for a differential role of TBC1D1 and TBC1D4 in exercise-related improvements of insulin sensitivity. TBC1D1 is thought to be the more relevant RabGAP isoform during contraction, while for TBC1D4, several studies have described an insulin-sensitizing effect post-exercise [77-79]. Deciphering the molecular mechanisms underlying insulin and contraction signaling pathways has the potential to contribute to prevention and treatment strategies for metabolic diseases in the future.

1.2.2 RabGAP-mediated control of GLUT4 translocation

The TBC1D family of proteins share a common feature, which is the presence of a functional Rab-GTPase-activating (GAP or TBC) domain. This domain binds to monomeric 21-kDa GTPases of the Rab family and inactivates them by stimulating their intrinsic GTPase activity [80]. In general, small Rab-GTPases are involved in the regulation of protein or vesicle transport within the cell. Of the more than 60 known isoforms of Rab-GTPases, several Rabs (e.g. Rab4, Rab8, Rab10, Rab11) have been

identified to play a role in the transport of GLUT4 vesicles [81]. Under basal conditions, RabGAPs are bound to the corresponding Rab-GTPases and catalyze their intrinsic GTPase hydrolysis activity, rendering them in an inactive, GDP-bound state. Phosphorylation of TBC1D1 and TBC1D4 by AKT, AMPK or other, as yet unknown, kinases at various serine and threonine residues does not result in a decrease in GAP activity, as initially assumed. Instead, it leads to changes in the subcellular localization of RabGAPs. This is presumably due to an interaction of the N-terminal PTB (phosphotyrosine-binding domains) with the insulin-regulated aminopeptidase IRAP, a resident protein of the GLUT4 storage vesicles [82]. Following phosphorylation of TBC1D1 and TBC1D4, the specific downstream Rab-GTPases no longer undergo enhanced GTP hydrolysis. This results in an increase in the GTP-bound form of Rab proteins, causing GLUT4-containing vesicles to migrate to the plasma membrane (Figure 6) [74].

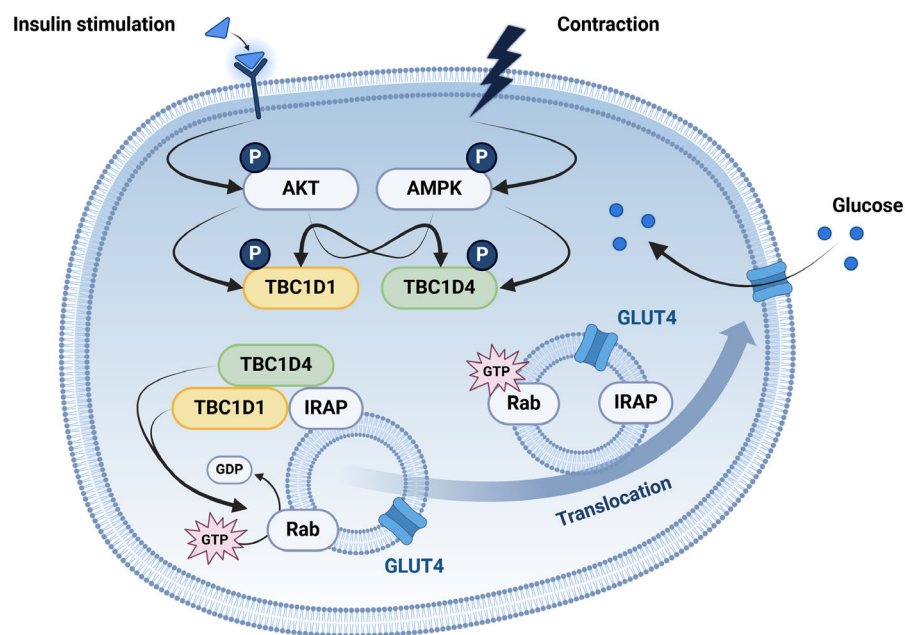


Figure 6: RabGAP-mediated GLUT4 translocation in response to insulin stimulation or skeletal muscle contraction. The resident protein IRAP interacts with TBC1D1 and TBC1D4 in a phosphorylation-dependent manner. Phosphorylation of the RabGAPs by upstream kinases, such as AKT or AMPK (AMP-activated protein kinase), prevents the recruitment of TBC1D1 and TBC1D4 to the Rab-GTPases located in GLUT4 vesicles. Dissociation of RabGAPs from downstream Rab-GTPases leads to the accumulation of Rab proteins in their active, GTP-bound state and enhances the translocation of GLUT4 vesicles to the cell surface. Adapted from [82, 83]. (Own illustration, created with Biorender.com)

1.2.3 Naturally occurring RabGAP gene variants

Several studies have shown that mutations in the *TBC1D1* or *TBC1D4* gene can lead to severe metabolic diseases in humans (Figure 7). A rare *TBC1D1* variant (R125W) was linked to an extreme form of familial obesity in two independent studies [84, 85]. Interestingly, this mutation does not affect the functional domain of the protein but one of the N-terminal phosphotyrosine-binding (PTB) domains that are thought to be important for protein-protein interactions and homo- or heterodimerization of RabGAPs [82, 86, 87]. Overexpression of the human R125W mutant in murine skeletal muscle resulted in a significantly decreased insulin-stimulated glucose transport [88]. Furthermore, our findings, in collaboration with the research group of Prof. Jeremy Tavaré (University of Bristol), revealed that the interaction between *TBC1D1* and its upstream kinase AMPK was hindered by the introduction of the R125W variant in murine skeletal muscle cells. Additionally, we observed a reduction in the phosphorylation of *TBC1D1*-Ser²³⁷, a crucial AMPK target site [89].

In accordance, previous work from our group led to the identification of an inactivating mutation in the *Tbc1d1* gene that protects mice from obesity and T2D. Our findings revealed that the Swiss Jim Lambert (SJL) inbred mouse strain harbors a naturally occurring nonsense mutation in the *Tbc1d1* gene, resulting in premature termination of translation and complete inactivation of the protein [90].

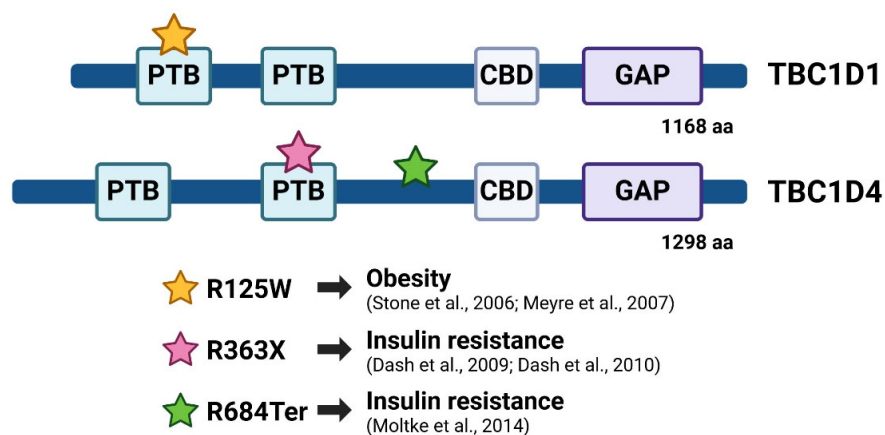


Figure 7: Gene variants identified in the human *TBC1D1* and *TBC1D4* genes. The two RabGAPs *TBC1D1* and *TBC1D4* contain two N-terminal PTB (Phosphotyrosine-binding) domains, a Calmodulin-binding domain (CBD) and a catalytic TBC/GAP domain. Adapted from [71, 81, 84, 85, 91, 92]. (Own illustration, created with Biorender.com)

Variants associated with metabolic disorders have also been identified in the human *TBC1D4* gene. In a patient suffering from *acanthosis nigrans*, an R363X premature stop mutation was described, which leads to severe insulin resistance. Overexpression of this mutant *TBC1D4* form in cultured adipocytes resulted in a significant decrease in

GLUT4-mediated glucose uptake. Interestingly, co-expression of this variant with the wildtype (WT) variant resulted in a dimerization of the two variants, indicating a dominant-negative effect of the R363X variant on TBC1D4 function [81, 91].

In addition, a *TBC1D4* p.Arg⁶⁸⁴Ter loss-of-function mutation was identified in genetically isolated Arctic populations, leading to markedly elevated postprandial blood glucose levels and a 10-fold increased risk of T2D in homozygous allele carriers. This mutation affects a TBC1D4 isoform specifically expressed in muscle cells and leads to a complete depletion of TBC1D4 protein in skeletal muscle and heart. In addition, GLUT4 protein abundance has been shown to be significantly reduced in these tissues [92]. The high allele frequency (17 %) of this mutation in the indigenous Greenlandic population indicates positive selection, probably due to traditional living conditions, especially high levels of physical activity and a low-carbohydrate but high-protein diet with unsaturated FAs (from fish and seal meat) [93]. Indeed, a randomized crossover study was recently conducted with homozygous carriers and homozygous non-carriers of the *TBC1D4* p.Arg⁶⁸⁴Ter variant. The results showed that a traditional diet slightly improved glycemic control and plasma lipid profile in Greenlandic Inuit compared to a Western diet [94, 95]. Moreover, we contributed to a study aiming to investigate whether physical activity is able to attenuate the effect of the *TBC1D4* p.Arg⁶⁸⁴Ter variant on postprandial hyperglycemia. The results obtained from this linear mixed model interaction analysis demonstrate a beneficial impact of daily physical activity on whole-body glycemia after an oral glucose load [96]. However, the molecular mechanisms underlying this enhanced response to exercise after deletion of TBC1D4 need to be further explored.

1.2.4 Investigation of RabGAP function using mouse models

Mice are the most widely used model animal in basic biomedical research. This is due on the one hand to their short generation time, on the other hand to the extensive transferability of physiological findings to humans and also the availability of a large number of manipulation and examination methods [97]. Over the past decade, a number of different mouse models have been developed to elucidate the specific function of TBC1D1 and/or TBC1D4 in substrate metabolism and glycemic control (Figure 8). We were the first to study a *Tbc1d1*-deficient mouse line that was generated by breeding as recombinant congenic strain (RCS) and presented substantially impaired insulin-stimulated glucose transport into skeletal muscle with concomitantly enhanced lipid utilization both *in vivo* and *ex vivo* in isolated skeletal muscles. Interestingly, GLUT4 protein but not mRNA expression was reduced in skeletal muscle

from *Tbc1d1*-deficient animals [90]. We concluded that TBC1D1 plays a key role as a master switch between glucose and lipid metabolism in skeletal muscle.

In 2012 and 2013, respectively, two independent working groups described the phenotype of conventional *Tbc1d4*-knockout mice (D4KO). These animals showed impaired insulin-stimulated glucose transport into the oxidative soleus muscle and adipocytes, while no changes were detected in the glycolytic *Extensor digitorum longus* (EDL) muscle. Fast oxidative fibers, also known as fast twitch or Type II fibers, primarily produce ATP through anaerobic glycolysis and contract relatively quickly. In contrast, slow-twitch or Type I fibers primarily utilize aerobic respiration (oxygen and glucose) to produce ATP and contract relatively slowly [98, 99]. The decreased glucose uptake in the D4KO mouse tissues was accompanied by a reduced abundance of GLUT4 protein in the respective tissue type. *In vivo*, however, D4KO mice showed little, if any, impairment of whole-body glycemia, at least when fed a standard chow diet [100, 101].

Recent studies have focused more on the characterization of knockin (KI) mice carrying amino acid exchanges at specific phosphorylation sites of TBC1D1 or TBC1D4. Both RabGAPs represent direct phosphorylation targets of both the AKT and the AMPK serine/ threonine kinases [72]. To date, at least 15 phosphorylation sites each have been described for TBC1D1 and TBC1D4, which are activated either by muscle contraction, insulin or AICAR depending on the study design [71]. For instance, a TBC1D1-Ser²³¹Ala KI mutation inactivating the primarily AMPK-sensitive TBC1D1-Ser²³¹ phosphorylation site resulted in the development of obesity, hyperglycemia, hyperinsulinemia, and hypercholesterolemia and eventually impaired insulin sensitivity [102]. Despite a reduction in glucose uptake and GLUT4 localization on the cell surface in skeletal muscle of mice with Ser²³¹Ala KI after AICAR stimulation, exercise did not have the same effect. This indicates the presence of additional pathways independent from AMPK in this process [67].

In analogy, one of the major insulin-responsive phosphorylation sites in TBC1D4, Thr⁶⁴⁹, was inactivated in a KI mouse model by a TBC1D4-Thr⁶⁴⁹Ala mutation. Thr⁶⁴⁹Ala KI mice showed decreased insulin sensitivity as well as decreased insulin-stimulated glucose transport and decreased cell surface GLUT4 content in skeletal muscle but not in adipocytes [103]. In the heart, the Thr⁶⁴⁹ phosphorylation site has been demonstrated to regulate the R-wave amplitude, a measure of ventricular function, without any association with general cardiac dysfunction [104]. Of note, neither contraction- nor AICAR-stimulated glucose transport was disturbed in Thr⁶⁴⁹Ala KI skeletal muscle [105].

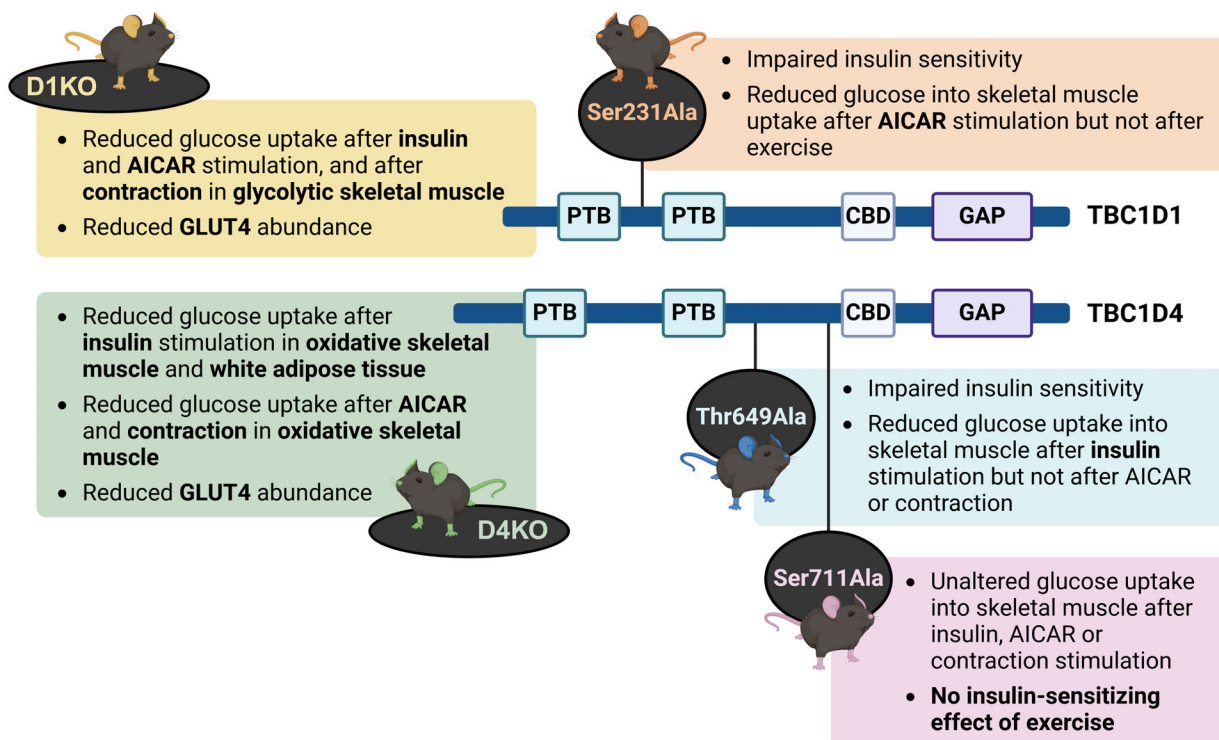


Figure 8: Genetically modified RabGAP mice and their phenotype regarding peripheral insulin sensitivity. D1KO: *Tbc1d1*-deficient mice (global knockout), D4KO: *Tbc1d4*-deficient mice (global knockout), PTB: Phosphotyrosine-binding domains, CBD: Ca⁺/calmodulin-binding domain. Adapted from [67, 77, 90, 100, 103, 106]. (Own illustration, created with Biorender.com)

Recently, another KI mouse model with a serine-to-alanine point mutation at TBC1D4 Ser⁷¹¹ was described. Ser⁷¹¹ is phosphorylated in response to both insulin and AMPK activation. While whole-body and muscle insulin sensitivity after exercise and contractions were improved in WT mice, the insulin-sensitizing effect of exercise was not detectable in TBC1D4-Ser⁷¹¹ KI mice. These findings provide genetic evidence that TBC1D4-Ser⁷¹¹ functions as a principal node for AMPK- and insulin-induced signaling, which mediates the impact of exercise and contractions on skeletal muscle glucose uptake by enhancing insulin sensitivity [77].

1.3 Objectives

The central aim of the studies summarized in this habilitation was to investigate how insulin and contraction signaling converge at the level of the RabGAPs. In order to study the dynamics of substrate partitioning and energy metabolism, we developed novel mouse models and assessed both the *in vivo* phenotype and the organ-specific substrate flux especially in skeletal muscle and adipose tissue. A more profound comprehension of the particular regulatory mechanisms governing insulin- and contraction-mediated glucose uptake into skeletal muscle may facilitate the development of novel prevention and treatment strategies for metabolic diseases.

The main objectives of the individual studies were to:

1. validate TBC1D1 as switch between glucose and lipid metabolism in skeletal muscle
2. investigate the impact of a combined depletion of TBC1D1 and TBC1D4 on whole-body glycemia and skeletal muscle and adipose tissue substrate utilization
3. investigate the relationship between TBC1D1, AMPK and contraction-mediated glucose uptake into skeletal muscle
4. investigate the specific role of TBC1D4 in contraction-mediated improvements of skeletal muscle insulin sensitivity
5. analyze the underlying mechanism of TBC1D1- and TBC1D4-dependent control of skeletal muscle lipid utilization
6. determine the specific contribution of AMPK, TBC1D1 and TBC1D4 on contraction-stimulated glucose uptake into skeletal muscle
7. investigate the physiological role of TBC1D4 in exercise-induced improvements of insulin sensitivity

2 Results

2.1 Conventional knockout of *Tbc1d1* in mice impairs insulin- and AICAR-stimulated glucose uptake in skeletal muscle

Original paper #1

Dokas J* and Chadt A*, Nolden T, Himmelbauer H, Zierath JR, Joost HG, Al-Hasani H (2013). Conventional knockout of *Tbc1d1* in mice impairs insulin- and AICAR-stimulated glucose uptake in skeletal muscle. *Endocrinology* 154(10):3502-14.

* Shared first authorship

<https://doi.org/10.1210/en.2012-2147>

Studying a RCS with an introgressed genomic fragment from the SJL inbred strain on a pure C57BL/6J genetic background we previously demonstrated a shift in skeletal muscle substrate utilization from glucose to FAs in mice carrying a loss-of-function variant of the *Tbc1d1* gene. However, a total of 19 protein-coding genes mapped within the critical region of the transferred genomic region [90]. Despite extensive sequencing and expression analyses, a contribution of one of these genes to the phenotype observed in *Tbc1d1*-deficient RCS mice [107] could not be 100% excluded at the time when these studies were performed. Thus, in order to provide direct functional evidence for a direct involvement of TBC1D1 in energy substrate metabolism, we generated conventional *Tbc1d1* knockout (KO) mice via the Cre-loxP technology. In analogy to the previously phenotyped RCS mouse strain, the conventional *Tbc1d1*-knockout mice (D1KO) demonstrated reduced body weight and elevated oxidative metabolism *in vivo*. Again phenocopying the observations from the RCS mouse model, intact skeletal muscles from D1KO mice displayed substantial impairments in both insulin- and AICAR-stimulated glucose uptake in glycolytic EDL muscle and an enhanced rate of FAO in oxidative Soleus muscle. The collected data presented the final proof for the direct relevance of TBC1D1 in skeletal muscle substrate metabolism [107].

2.2 Deletion of Both Rab-GTPase-Activating Proteins TBC1D1 and TBC1D4 in Mice Eliminates Insulin- and AICAR-Stimulated Glucose Transport

Original paper #2

Chadt A, Immisch A, de Wendt C, Springer C, Zhou Z, Stermann T, Holman GD, Loffing-Cueni D, Loffing J, Joost HG, Al-Hasani H (2015). Deletion of Both Rab-GTPase-Activating Proteins TBC1D1 and TBC1D4 in Mice Eliminates Insulin- and AICAR-Stimulated Glucose Transport. *Diabetes* 64(3):746-59

<https://doi.org/10.2337/db14-0368>

Previous investigations on *Tbc1d1*- or *Tbc1d4*-deficient mouse models (D1KO, D4KO) conducted by others [100, 101] and by our own research group [90, 107] revealed a discrepancy between the outcomes of physiological versus *ex vivo* analyses. Whereas there was clear evidence for severe disturbances of glucose transport into skeletal muscle and (only in D4KO) adipose tissue, D1KO and D4KO mice demonstrated only small if any impairments in whole-body glycemia. In addition, also insulin-, contraction- and AICAR-stimulated glucose uptake into skeletal muscle as well as insulin-stimulated glucose transport into adipocytes was only partially reduced in mice with a singular RabGAP deficiency. Due to the high sequence homology of the two RabGAPs [74] we postulated a compensatory action exerted by the respective remaining RabGAP as possible explanation for these observations. Thus, the new study aimed to analyze the impact of the combined inactivation of both TBC1D1 and TBC1D4 on energy metabolism by generating and characterizing double-deficient (D1/4KO) mice. Indeed, adversely to D1KO and D4KO mice, the D1/4KO mice displayed clear impairments in glucose, insulin and AICAR tolerance measured *in vivo*. Surprisingly, however, the decline in glucose uptake into skeletal muscle and adipose tissue was generally comparable to the effects previously seen in D1KO and D4KO mice. D1/4KO animals did not present stronger reductions in insulin- or AICAR-stimulated glucose uptake into intact skeletal muscles and isolated white adipocytes. The impairments, however, were independent from the respective tissue type. Whereas the disturbances in the single KO mice were apparently defined by their tissue-specific expression pattern, D1/4KO animals demonstrated reduced glucose uptake into all tissues measured. In accordance, also GLUT4 protein abundance (but not mRNA) was reduced by approximately 50% in all skeletal muscle types and the white adipose tissue (WAT) from D1/4KO mice. These results showed for the first time that TBC1D1 and TBC1D4

may exert complementary functions on physiological level but overlapping functions on the cellular level. Another important finding of this study was the fact the RabGAP deficiency seems to impair the retention of GLUT4 in intracellular vesicles in the basal state, as shown using cell surface labeling of GLUT4 [106].

2.3 AMPK and TBC1D1 Regulate Muscle Glucose Uptake After - But Not During - Exercise and Contraction

Original paper #3

Kjøbsted R, Roll JLW, Jørgensen NO, Birk JB, Foretz M, Viollet B, Chadt A, Al-Hasani H, Wojtaszewski JFP. (2019): "AMPK and TBC1D1 Regulate Muscle Glucose Uptake After - But Not During - Exercise and Contraction." *Diabetes*. 68(7):1427-1440. Impact factor 2019: 7.720

<https://doi.org/10.2337/db19-0050>

The beneficial effects of exercise on skeletal muscle insulin sensitivity have been well documented. The uptake of glucose by skeletal muscle is enhanced by physical activity, which is a key factor in maintaining healthy insulin levels. Although AMPK has been described for many years as a key regulator of contraction-mediated glucose uptake in skeletal muscle, data on the specific control kinetics have been conflicting [108]. In this study, we demonstrate that while glucose transport into skeletal muscle lacking AMPK was unaltered by exercise or contraction, it returned to resting levels in AMPK-deficient muscle at a notably faster rate than in wild-type muscle after the actual exercise or contraction stimulus. Furthermore, we found that skeletal muscle glucose uptake after contraction was positively correlated with TBC1D1 phosphorylation, and that *post* contraction glucose uptake was disturbed in *Tbc1d1*-deficient mice [109]. The data suggest that skeletal muscle glucose uptake is not a straightforward, single-step process but rather a complex, multi-step procedure involving different phases of time-resolved signaling mechanisms. A multitude of signaling factors may contribute to a single phase or multiple phases of this process. Activation of the AMPK-TBC1D1 signaling axis during exercise or contraction appears to be a crucial mechanism for maintaining glucose permeability in skeletal muscle following exercise or contraction, but not during the exercise or contraction itself. The perception of skeletal muscle glucose uptake in four dimensions may facilitate a more comprehensive understanding of inconsistencies in previously collected, current, and future data.

2.4 TBC1D4 is Necessary for Enhancing Muscle Insulin Sensitivity in Response to AICAR and Contraction

Original paper #4

Kjøbsted R, Chadt A, Jørgensen NO, Kido K, Larsen JK, de Wendt C, Al-Hasani H, Wojtaszewski JFP. (2019): "TBC1D4 is Necessary for Enhancing Muscle Insulin Sensitivity in Response to AICAR and Contraction." *Diabetes* 68(9):1756-1766. Impact factor 2019: 7.720

<https://doi.org/10.2337/db18-0769>

It has been demonstrated that a single session of exercise can markedly enhance skeletal muscle insulin sensitivity in both human and rodent subjects [110, 111]. It is noteworthy that these post-exercise improvements appear to be attributable to a synchronized increase in microvascular perfusion and GLUT4 translocation to the plasma membrane in response to insulin, rather than to persistently enhanced proximal insulin signaling [112-114]. These findings underscore the significance of distal insulin signaling and the regulation of GLUT4 translocation in elucidating the mechanistic basis of post-exercise insulin sensitization. Given these characteristics, RabGAPs such as TBC1D4 represent a promising avenue of investigation. Therefore, the objective of this study was to ascertain whether TBC1D4 is indispensable for augmenting muscle insulin sensitivity in response to AICAR and contraction. Our findings revealed that, in response to contraction and AICAR stimulation, the phosphorylation of AMPKa-Thr¹⁷² and its downstream targets exhibited a comparable increase in glycolytic skeletal muscle from wild-type and *Tbc1d4*-deficient mice. On the other hand, muscle from wild-type mice alone showed increased insulin-stimulated glucose absorption 3 hours after contraction or 6 hours after AICAR activation. These improvements in skeletal muscle insulin sensitivity in wild-type mice was associated to increased TBC1D4 (Thr⁶⁴⁹ and Ser⁷¹¹) phosphorylation. Notably, the phosphorylation status of TBC1D1 remained unaltered in this context, suggesting a specific function for TBC1D4 in regulating *post*-exercise insulin sensitivity in skeletal muscle [115].

2.5 The RabGAPs TBC1D1 and TBC1D4 Control Uptake of Long-Chain Fatty Acids Into Skeletal Muscle via Fatty Acid Transporter SLC27A4/FATP4

Original paper #5

Benninghoff T, Espelage L, Eickelschulte S, Zeinert I, Sinowenka I, Müller F, Schöndeling C, Batchelor H, Cames S, Zhou Z, Kotzka J, Chadt A#, Al-Hasani H (2020). The RabGAPs TBC1D1 and TBC1D4 Control Uptake of Long-Chain Fatty Acids Into Skeletal Muscle via Fatty Acid Transporter SLC27A4/FATP4. *Diabetes* 69(11):2281-2293.

Corresponding author

<https://doi.org/10.2337/db20-0180>

Most studies on the metabolic roles of the two RabGAPs TBC1D1 and TBC1D4 have been focused on their impact in the regulation of glucose transport into peripheral tissues. There is, however, also a strong contribution of lipid intermediates in the development of whole-body and skeletal muscle insulin resistance [116]. As we demonstrated in the past that depletion of one or even both RabGAPs leads not only to disturbances in skeletal muscle and adipose tissue glucose uptake but concomitantly also to enhanced lipid utilization both *in vivo* and in isolated skeletal muscle [90, 106, 117] and in beta cells [118], we sought to analyze the molecular mechanisms responsible for these findings and, in addition, to determine the responsible downstream targets of the two RabGAPs. Conducting knockdown experiments of *Tbc1d1* and *Tbc1d4*, respectively, in cultured murine C2C12 myotubes, we demonstrated that the two RabGAPs specifically control the uptake and oxidation of long-chain (LCFAs) but not short-chain fatty acids (SCFAs) independent from the saturation level. Moreover, we demonstrated that the RabGAPs control glucose and lipid utilization via an identical subset of Rab-GTPases, namely Rab8, Rab10 and Rab14. Further, analyzing D1KO and D4KO skeletal muscles, we showed that additional ablation of the FA transporter SLC27A4/FATP4 but not FAT/CD36 completely abrogated the enhanced lipid oxidation conferred by the RabGAP deficiency. In summary, our study showed for the first time that RabGAP-mediated control of skeletal muscle lipid metabolism converges with glucose metabolism at the level of downstream Rab-GTPases and involves regulated transport of LCFAs via SLC27A4/FATP4.

2.6 Contraction-Mediated Glucose Transport in Skeletal Muscle Is Regulated by a Framework of AMPK, TBC1D1/4, and Rac1

Original paper #6

de Wendt C*, Espelage L*, Eickelschulte S, Springer C, Toska L, Scheel A, Bedou AD, Benninghoff T, Cames S, Stermann T, Chadt A#, Al-Hasani H. (2021) Contraction-Mediated Glucose Transport in Skeletal Muscle Is Regulated by a Framework of AMPK, TBC1D1/4, and Rac1. *Diabetes* 70(12):2796-2809.

* Shared first authorship

Corresponding author

<https://doi.org/10.2337/db21-0587>

Both TBC1D1 and TBC1D4 have been described to be key regulators of skeletal muscle energy metabolism. As direct downstream targets of both AKT and AMPK, lack of the RabGAPs leads to severely impaired insulin- and AICAR-stimulated glucose transport into skeletal muscle. However, older studies performed in animals overexpressing a dominant-negative $\alpha 2$ -subunit of AMPK (AMPK-DN) in skeletal muscle demonstrated the presence of AMPK-independent mechanisms of contraction-mediated glucose uptake [119]. In order to investigate the cooperative AMPK-RabGAP signaling axis in the metabolic response to exercise and skeletal muscle contraction, we crossbred the existing D1KO, D4KO and D1/4KO mouse strains with AMPK-DN mice to generate a new mouse line deficient in one or both RabGAPs and carrying an inactivating variant of the AMPK. AMPK-DN mice demonstrated a reduced physical fitness during an acute treadmill training with additional aggravation due to *Tbc1d1*- or double but not *Tbc1d4* deficiency. As expected, glycolytic EDL and oxidative Soleus muscle reacted differently to the depletion of the respective RabGAP according to their expression pattern when analyzed *ex vivo* for contraction-stimulated glucose uptake. Strikingly, skeletal muscle depleted of active AMPK and both RabGAPs still displayed a residual contraction-stimulated glucose uptake, indicating additional regulators of this process. Only pharmacological inhibition of the small RhoGTPase Rac1, a known mediator of muscle stretching-induced glucose transport [120], in addition to the depletion of active AMPK and both RabGAPs completely abolished contraction-stimulated glucose transport into skeletal muscle. Our results emphasize the importance of the contraction-mediated glucose uptake process since it is obviously controlled by a large number of evolutionary conserved, partially redundant pathways.

Moreover, we provided a novel mechanistic link between the key players in this process [121].

2.7 Depletion of TBC1D4 improves the metabolic exercise response by overcoming genetically induced peripheral insulin resistance

Original paper #7

Springer C, Binsch C, Weide D, Toska L, Cremer AL, Backes H, Scheel AK, Espelage L, Kotzka J, Sill S, Kurowski A, Kim D, Karpinski S, Schnurr TM, Hansen T, Hartwig S, Lehr S, Cames S, Brüning JC, Lienhard M, Herwig R, Börno S, Timmermann B, Al-Hasani H, Chadt A (2024). Depletion of TBC1D4 improves the metabolic exercise response by overcoming genetically induced peripheral insulin resistance. *Diabetes* 12:db230463.

<https://doi.org/10.2337/db23-0463>

The RabGAP TBC1D4 represents a key signaling factor in the regulation of glucose transport into skeletal muscle and WAT, and thus plays a crucial role in the development of insulin resistance and T2D. In a previous collaborative study, we demonstrated that carriers of a loss-of-function variant in the human TBC1D4 gene exhibited particular sensitivity to increased daily activity by improving postprandial hyperglycemia [96]. In a subsequent study, we subjected *Tbc1d4*-deficient mice (D4KO) to a HFD and a moderate-intensity training regimen on treadmills. The exercise training resulted in significantly enhanced glucose and insulin tolerance, as well as augmented expression levels of markers indicative of mitochondrial activity and browning in WAT from D4KO animals. These improvements were significantly more pronounced in the D4KO animals compared to the WT animals. Furthermore, *in vivo* and *ex vivo* analyses of glucose uptake revealed increased glucose clearance in interscapular brown adipose tissue (iBAT) and WAT from trained D4KO mice, demonstrating a major role for adipose tissues in exercise-induced improvements in insulin sensitivity. The results of this study indicate that chronic exercise training may be an effective approach to overcoming genetically induced insulin resistance. In the future, gene variants in TBC1D4 may offer insights into precision medicine treatments as determinants of exercise response [122].

3 Conclusions

3.1 The two RabGAPs TBC1D1 and TBC1D4 represent molecular switches in skeletal muscle substrate utilization

Glucose and fat metabolism are closely linked both on a physiological and molecular level. Disorders of energy utilization are one of the most important characteristics in the development and progression of metabolic diseases [123]. At organ level, the precisely coordinated processes of glucose uptake and metabolism and FAO and storage in the skeletal muscle are of great importance for the entire organism. On the one hand, this is due to the large proportion of mass that the skeletal muscle takes up in relation to the body as a whole and, on the other, to its specific role in adapting to various metabolic demands, such as high postprandial blood glucose levels or a high demand for long-term energy during endurance sport [124]. Disruptions to this energy balance are characterized by so-called metabolic inflexibility, i. e. the inability of the tissue to adequately adjust to the corresponding metabolic requirements, and are strongly associated with the development of metabolic diseases. The molecular relationships that regulate the metabolic flexibility of the skeletal muscle are extremely complex and do not exist in isolation, but rather in close interaction with other organs [125].

TBC1D1 and TBC1D4, two key regulators of insulin and contraction-mediated glucose transport into skeletal muscle, and in the case of TBC1D4, insulin-stimulated glucose transport into adipocytes have been linked to human metabolic disorders, including obesity (TBC1D1) and insulin resistance and type 2 diabetes (TBC1D4) [81, 84, 85, 91, 92]. In two independent studies, we were able to show that the functions of TBC1D1 and TBC1D4 are not, as previously known (for TBC1D4) or at least suspected (for TBC1D1), restricted to the most distal signaling factor in insulin-stimulated GLUT4 translocation, but are also relevant in skeletal muscle lipid metabolism [90, 106]. Our findings indicate that the two RabGAPs represent molecular switches between skeletal muscle glucose and lipid metabolism as *Tbc1d1* (D1KO) and *Tbc1d4* (D4KO) knockout mice display severely impaired glucose uptake in response to insulin or the AMP mimetic AICAR with concomitant increase in lipid oxidation. Interestingly, a similar metabolic phenotype has been observed in mice with a deletion of GLUT4 in both adipocytes and muscle (amG4KO) [22]. It appears that complete (as in amG4KO mice) or partial depletion of GLUT4 (as in D1KO and D4KO mice), particularly in adipose tissue and skeletal muscle, promotes hepatic glucose uptake and lipid synthesis and leads to increased lipid utilization in peripheral tissues [23]. Indeed, we have shown that either single or combined RabGAP deficiency leads to elevated liver triglyceride

levels in D1KO, D4KO and D1/4KO mice, respectively [106]. It has been speculated that the increased FAO in peripheral tissues of amG4KO mice represents a compensatory mechanism for impaired glucose disposal in skeletal muscle and adipocytes [23]. However, our data suggest an independent regulation of glucose and lipid utilization in skeletal muscle by TBC1D1 and TBC1D4. The evidence is found in a dataset of isolated skeletal muscle after *ex vivo* measurements of insulin-stimulated glucose uptake and FAO (Figure 9).

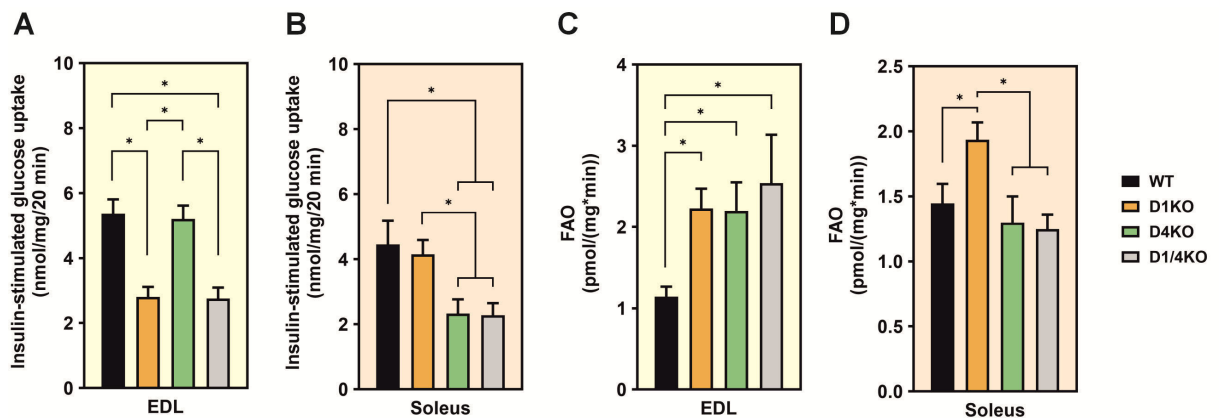


Figure 9: *Ex vivo* insulin-stimulated glucose uptake and FAO. *Ex vivo* insulin-stimulated glucose uptake (A, B) and FAO (C, D) in intact isolated glycolytic EDL (A, C) and oxidative Soleus (B, D) skeletal muscles from WT, D1KO, D4KO and D1/4KO mice. Adapted from [106]. (Own illustration)

While insulin-stimulated glucose uptake is impaired in RabGAP-deficient mice according to their expression pattern, with TBC1D1 being the predominant isoform in glycolytic and TBC1D4 the predominant isoform in oxidative skeletal muscle [126], TBC1D1 depletion results in increased FAO in both skeletal muscle types. In contrast, FAO is not affected in oxidative skeletal muscle of D4KO mice, despite the significantly reduced glucose uptake in this muscle type. Furthermore, knockout of both *Tbc1d1* and *Tbc1d4* does not have an additive effect on FAO, as the muscle from D1/4KO mice is similar to that from each individual knockout.

These data suggest that

- in glycolytic skeletal muscle TBC1D1 and TBC1D4 contribute equally to the effect on FAO,
- the same target(s) distal to both RabGAPs is / are likely to mediate the increased FAO,

- the increase in FAO is not directly related to impaired glucose uptake, as D4KO mice have normal glucose uptake but increased FAO in EDL muscle, and
- the influence of TBC1D1 and TBC1D4 deficiency is not additive, neither on glucose uptake nor on FAO.

3.2 TBC1D1 and TBC1D4 regulate both lipid and glucose metabolism in skeletal muscle via a distinct pool of downstream Rab-GTPases

Skeletal muscle insulin resistance is a crucial characteristic in the development of T2D. The negative association between intramyocellular fat content (IMCL) and insulin sensitivity in individuals with T2D suggests that the ectopic intracellular deposition of excess fat in skeletal muscle significantly contributes to impaired insulin sensitivity in this tissue [127, 128]. Recent reports suggest a strong association between IMCL content and the progression of early diabetes-related complications, such as microalbuminuria, cardiovascular disease risk, and cardiac autonomic neuropathy [129]. Although not all details of lipid-induced skeletal muscle insulin resistance have been clarified to date, differences in intracellular lipid compartmentalisation, storage, and metabolism provide possible explanatory models [130]. The process is centered around bioactive lipids, such as DAGs and ceramides [131-133]. DAGs can cause insulin resistance by recruiting and activating nPKCs when they accumulate in the cell membrane [134]. Alternatively, diacylglycerol transferases (DGAT) 1 and DGAT2 can convert them to triacylglycerol (TAG) and store them in lipid droplets, preventing interference with the insulin signaling cascade. Understanding the cellular function of critical regulators of lipid utilization in skeletal muscle may be valuable in future T2D prevention strategies.

While the two RabGAPs were previously described as key factors in skeletal muscle (TBC1D1 and TBC1D4) and adipose tissue (TBC1D4) glucose metabolism, we were the first to link the two signaling molecules to skeletal muscle lipid utilization as well [90, 106]. We have demonstrated that TBC1D1 and TBC1D4 have a reciprocal effect on glucose and FA metabolism in skeletal muscle. The increase in FAO occurs independently of any impairment in glucose uptake, indicating that the two processes are distinct from each other (Figure 9). It is important to note that our previous findings, which involved lentiviral overexpression of *Tbc1d1* in cultured muscle cells, suggest that RabGAP activity plays a role in this process as both uptake and oxidation of

LCFAs were significantly reduced by lentiviral overexpression of the WT *Tbc1d1* but not a GAP-inactive R941K mutant construct [90]. This indicates that Rab-GTPases downstream of TBC1D family proteins regulate FA uptake and oxidation in skeletal muscle [39]. Deletion of either RabGAP equally increases FAO, but deletion of both has no additive effect. This suggests the involvement of a single common Rab-GTPase or a pool of Rab-GTPases targeted by both RabGAPs [106]. The aim of our next study was to determine whether these Rab-GTPases are identical to the Rab-GTPases that control GLUT4 translocation, or if there is a distinct subset of Rab-GTPases that regulate FA uptake and/or oxidation. The Rab-GTPase family comprises more than 60 members in humans, which are involved in all aspects of membrane vesicle traffic [135, 136]. *In vitro*, six Rab proteins (Rab2a, Rab8a, Rab8b, Rab10, Rab14 and Rab28) have been identified as substrates for recombinant GAP domains of TBC1D1 and TBC1D4, all of which are associated with GLUT4 storage vesicles [74, 137, 138]. We demonstrated that the control of skeletal muscle lipid metabolism by RabGAP converges with glucose metabolism at the level of the downstream Rab-GTPases. Knockdown of a subset of the known RabGAP substrates, Rab8, Rab10 and Rab14 (but not Rab28), resulted in decreased LCFA uptake into skeletal muscle cells. Moreover, we can show a RabGAP-dependent control of LCFA but not SCFA uptake, strongly indicating a direct regulation of lipid transport via specialized FA transporters rather than a more indirect control of passive diffusion. Additionally, the two RabGAPs regulate LCFA import regardless of the degree of saturation [139]. Our data suggest that LCFA-specific metabolizing enzymes and/or transporters, such as FA translocase FAT/CD36 and FA transporters of the FATP protein family [140-142] may be involved in RabGAP-regulated FA uptake into skeletal muscle. Similar to the glucose transporter GLUT4, FAT/CD36 has been reported to traffic between intracellular compartments and the cell surface in response to insulin and contraction [143-145]. Furthermore, in cardiomyocytes, the translocation of FAT/CD36 to the plasma membrane has been demonstrated to be dependent on the expression levels of TBC1D4 and constitutively active Rab8a, Rab10, and Rab14 constructs [146]. It is noteworthy that also in adipocytes depletion of TBC1D4, but not TBC1D1, enhances the transport of LCFAs via FAT/CD36 translocation [147]. These data indicate a precise role for individual RabGAPs in the regulated transportation of FAs into different cell types. While both TBC1D1 and TBC1D4 play a role in regulating FA transport in skeletal muscle, with varying efficiencies for different fiber types, TBC1D4 appears to be the crucial control element in adipocytes and cardiomyocytes.

In our own study we have shown that the uptake of LCFAs in skeletal muscle was decreased in FAT/CD36 knockout mice, but was restored to normal levels in animals

that were double deficient in RabGAP-FAT/CD36. Moreover, the increase in FA transport observed in either *Tbc1d1* or *Tbc1d4* knockdown cells was completely eliminated by the combined knockdown of FA transporter 4 (Slc27a4/FATP4) and each of the RabGAPs [139]. In addition to FAT/CD36, FATP4 (and its close homologue FATP1) has been reported to facilitate the uptake of LCFAs into skeletal muscle. Its intrinsic acyl-CoA activity may contribute to its transport activity [148, 149]. Like FAT/CD36 and GLUT4, plasma membrane FATP4 increases in response to stimuli such as insulin and contraction in skeletal muscle [144, 149]. In human adipocytes, deficiency of TBC1D4 increased the uptake of LCFAs, which was accompanied by an increase in the abundance of both SLC27A4/FATP4 and FAT/CD36, particularly on the cell surface [150]. Figure 10 depicts the putative regulation of LCFA and glucose uptake into skeletal muscle via RabGAPs.

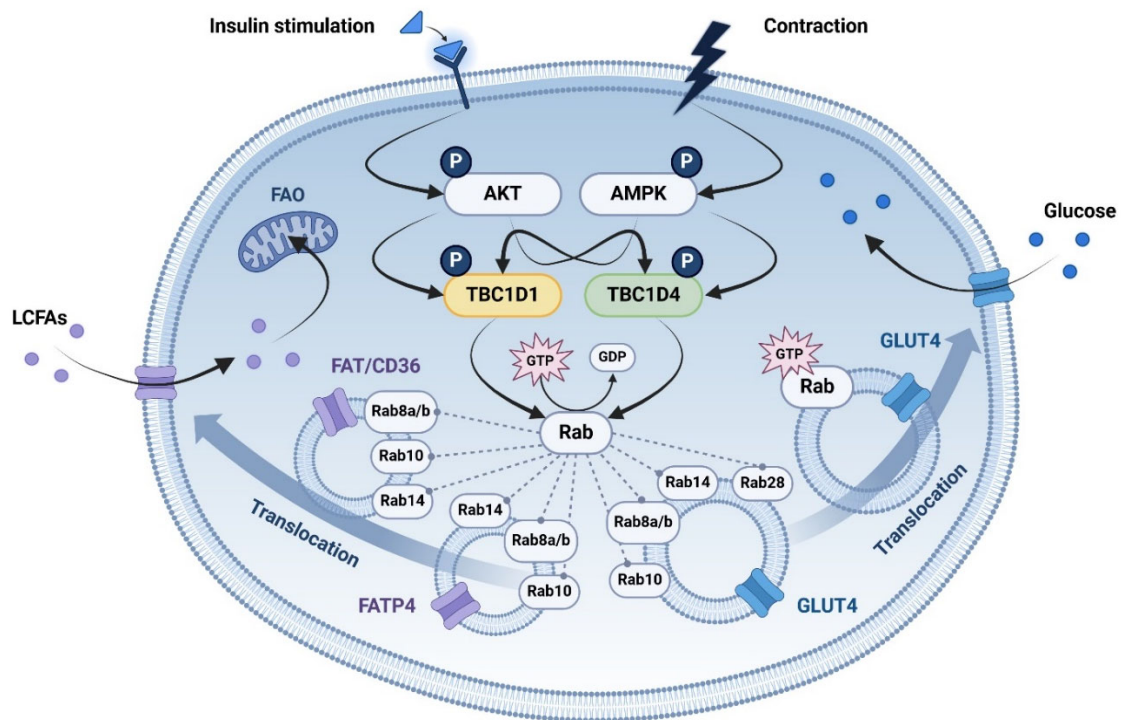


Figure 10: Putative regulation of long-chain fatty acid (LCFA) and glucose uptake into skeletal muscle via RabGAPs. FAO: Fatty acid oxidation, LCFAs: Long-chain fatty acids. Adapted from [82, 83, 138, 139]. (Own illustration, created with Biorender.com)

It is tempting to assume an analogue mechanism behind RabGAP-driven GLUT4 translocation and a similar translocation process of different FA transporters. However, there is some evidence for the involvement of different cellular localizations or storage compartments of the different transporters. GLUT4 has been demonstrated to derive from a dispersed vesicular storage compartment and early endosomes, both

fractionating in the light-microsomal (LDM) fraction [151]. Although both FATP1 and GLUT4 are increased on the plasma membrane after insulin stimulation, FATP1 is predominantly found in the high-density microsomal (HDM) and pellet fractions. This suggests that these two transporters originate from different compartments. In contrast, FATP4 was predominantly identified in the nuclei/mitochondria/cytoskeletal pellet fractions and was barely detectable in the LDM and HDM fractions [149]. In the past, the presence of different storage compartments from which GLUT4 is recruited in response to different stimuli, such as insulin and muscle contraction, has also been suggested [152, 153]. The question of whether there are stimulus-specific GLUT4 storage compartments in the cell has not yet been conclusively answered. It can be speculated that at least part of the reason why defective muscle GLUT4 trafficking in T2D is relatively specific to insulin action, whereas exercise-modulated GLUT4 translocation to the cell surface is unaffected, may be that insulin resistance involves defective trafficking of GLUT4 selectively into insulin-responsive GSVs [154, 155].

The literature presents a controversial discussion on whether the abundance of RabGAPs also affects the expression levels of the FA transporters FAT/CD36 and/or FATP4. Depletion of *Tbc1d4* in cultured L6 myotubes led to an increase in *Cd36* expression levels. In a separate study examining native skeletal muscle, transient overexpression of *Tbc1d1* resulted in decreased palmitate oxidation, but did not affect the abundance of FAT/CD36 protein [156-158]. In our own study FATP4, but not FAT/CD36 protein abundance was elevated in either glycolytic or oxidative skeletal muscle from D1KO and D4KO mice, respectively [139]. The findings are contradictory to the reports on the glucose transporter GLUT4, which consistently show a decrease in the abundance of GLUT4 protein due to RabGAP deficiency [90, 100, 101, 106, 159]. Regarding GLUT4, protein abundance is consistently reduced in accordance with the predominant RabGAP in a given tissue. For example, TBC1D1 is predominant in glycolytic skeletal muscle, while TBC1D4 is predominant in oxidative skeletal muscle, the heart, and adipose tissue [126]. It is possible that there are also differences in the impact of a specific RabGAP depletion on the protein abundance of FA transporters, depending on the tissue type being investigated. Another possible reason for the contrasting findings could be the presence of at least four different FA transporters in skeletal muscle that have been shown to be responsive to insulin and/or muscle contraction (FAT/CD36, FABPpm, FATP1 and FATP4 [160]). In contrast, only one glucose transporter, GLUT4, is known to acutely translocate to the cell surface in response to these stimuli. The various FA transporters may have partially overlapping functions. Therefore, detecting missorting mediated by RabGAP, as described for GLUT4 [161], may be technically challenging. It is currently unclear whether RabGAPs

directly regulate the oxidation of FA or if their function is limited to facilitating FA transport into the cell.

These data suggest that

- **TBC1D1 and TBC1D4 control the uptake of both saturated and unsaturated LCFAs into skeletal muscle cells through a Rab-GTPase-dependent mechanism,**
- **RabGAP-mediated control of skeletal muscle lipid metabolism converges with glucose metabolism at the level of the downstream Rab-GTPases and involves regulated transport of LCFAs via FATP4, and**
- **control over FA uptake by RabGAPs may involve changes in protein abundance of certain FA transporters as well as regulation of cellular translocation. This is presumably dependent on the RabGAP isoform, tissue type, and respective FA transporter.**

3.3 Insulin and contraction signaling in skeletal muscle converge at the level of the two RabGAPs TBC1D1 and TBC1D4

Physical activity has long been recognized as an effective tool in preventing and treating metabolic diseases [162]. Exercise has long-term positive effects on insulin sensitivity through the activation of PGC1 α , a transcription factor that stimulates mitochondrial biogenesis [163]. Additionally, long-term training promotes the activation of the mTORC1/S6K signaling pathway, leading to increased protein synthesis and subsequently, increased muscle mass [164]. During acute exercise training, muscular contraction increases the activity of AMPK by phosphorylation through its upstream kinase LKB1 [165]. In addition, the activity of CAMKII and MAPK (Mitogen-activated protein kinase) increase through calcium influx from the endoplasmic reticulum in response to muscle contraction [166, 167]. The activation of essential components of cell metabolism accelerates the translocation of GLUT4 to the plasma membrane, resulting in increased glucose uptake into the muscle cell. This process is insulin-independent, meaning that skeletal muscle contraction reduces hyperglycemia even in the insulin resistant state [76]. In addition, exercise also improves insulin-dependent glucose transport into the cell, on the one hand by activating early members of the insulin signaling cascade, such as the IR itself or its substrates (IRS1-4). On the other

hand, this mechanism also involves more distal components, such as PDK1, the RabGAP proteins TBC1D1 and TBC1D4 and various PKC isoforms [168].

In fact, the RabGAPs TBC1D1 and TBC1D4 act as convergence hubs between insulin and contraction signaling in skeletal muscle glucose uptake. AKT and AMPK directly phosphorylate these two factors at multiple residues, transmitting the signal to the facilitative GLUT4 glucose transporter. This process triggers the translocation of GLUT4 to the plasma membrane [71, 72]. In their function as key factors of insulin and contraction-mediated glucose uptake in skeletal muscle, TBC1D1 and TBC1D4 have been subjects of a whole series of studies on the molecular mechanisms behind exercise-mediated insulin sensitivity.

As we demonstrated in particular in our collaborative projects with the research group of Prof. Jørgen Wojtaszewski (University of Copenhagen, Denmark), it is important to perceive uptake of glucose by skeletal muscle as a multifaceted process that involves several stages of time-resolved signaling pathways, rather than a simple, one-step process. It seems that TBC1D1 and TBC1D4 play distinct roles in this process, the distinction between which can only be determined through time-resolved studies. While TBC1D1 appears to be a crucial regulator of contraction-stimulated glucose uptake following the muscle contraction period, TBC1D4 seems to exert a more pronounced influence on the insulin-sensitizing effect of acute exercise [109, 115]. Most studies do not discriminate glucose uptake during and immediately after muscle contraction since the measured uptake time often consists of a contraction period followed by at least some minutes of post-contraction glucose uptake. Furthermore, numerous studies have concentrated on RabGAP phosphorylation as a means of assessing efficient glucose transport. Nevertheless, the specific functions of only a limited number of the identified phosphorylation sites have thus far been elucidated, and the scope of investigation is constrained by the availability of specific antibodies [51]. It is important to consider these limitations when evaluating skeletal muscle glucose uptake.

We demonstrated that contraction-mediated glucose uptake into skeletal muscle via TBC1D1 and TBC1D4 involves regulators other than AMPK as, at least in the oxidative soleus muscle, AICAR-but not contraction-stimulated glucose uptake is abolished upon *Tbc1d4*-deficiency (Figure 11).

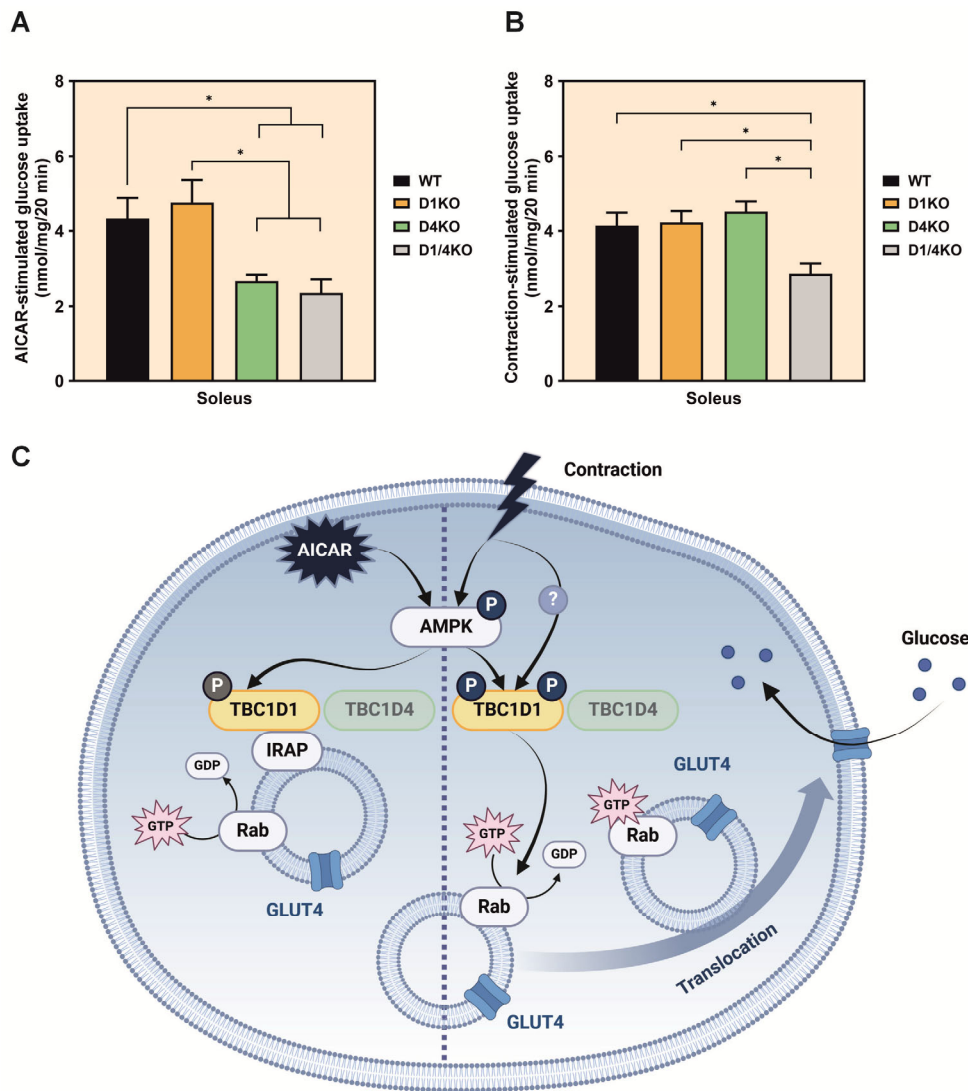


Figure 11: AICAR versus contraction signaling in *Tbc1d4*-deficient skeletal muscle. *Ex vivo* AICAR- (A) and contraction- (B) stimulated glucose uptake in intact isolated oxidative Soleus skeletal muscles from WT, D1KO, D4KO and D1/4KO mice. AICAR: 5-Aminoimidazole-4-carboxamide ribonucleotide. Adapted from [106, 121]. (Own illustration, C: Created with Biorender.com)

These findings suggest that contraction facilitates glucose uptake into skeletal muscle from D4KO mice via compensatory activation of TBC1D1, presumably via contraction- but not AMPK-responsive phosphorylation sites. The low abundance of TBC1D1 protein in oxidative skeletal muscle may explain why AICAR-mediated AMPK activation does not have the same effect. However, this model would account for the significantly reduced contraction-stimulated glucose uptake in skeletal muscle from D1/4KO mice, as there is no RabGAP exerting a compensatory function. The precise mechanisms behind the interaction between TBC1D1 and the contraction stimulus are currently under investigation.

Another interesting aspect of cellular exercise signaling is that already more than 20 years ago it was shown that the signal from muscle contraction to glucose uptake in

skeletal muscle is not exclusively mediated via AMPK. Indeed, overexpression of a dominant-negative subunit of AMPK in skeletal muscle completely abolished AICAR- but not contraction-stimulated glucose uptake in skeletal muscle [119]. Moreover, this effect was much more pronounced in the oxidative soleus than in the glycolytic EDL muscle.

The differences in response to skeletal muscle contraction between different muscle fiber types have long been recognized in the literature [169-172]. Deducing the translational potential of findings related to a specific muscle fiber type, such as our results on the differential expression pattern and function of individual RabGAPs in glycolytic EDL versus oxidative soleus muscle, is challenging due to the significant differences in the distribution of muscle fiber types between species. For example, mice have a higher proportion of fast twitch glycolytic fibers compared to humans. In contrast to humans, mice possess myosin heavy chain isoform type IIb fibers, which are absent in human muscle. Additionally, the soleus muscle in mice is one of the few oxidative muscles and lacks type IIb fibers [173]. However, in mice, the small Rho-GTPase Rac1 has emerged as a crucial factor in the AMPK-independent exercise signaling of skeletal muscle. Rac1 is activated by the mechanical stretching process that involves remodeling of the actin cytoskeleton [174, 175]. The knockout of *Rac1* in muscle results in a decrease in both *ex vivo* contraction-mediated and *in vivo* exercise-stimulated glucose uptake. However, it is interesting to note that it protects against HFD-induced insulin resistance in adipose tissue. [176, 177]. Rac1 and AMPK are responsible for the majority of glucose uptake in skeletal muscle following contraction. However, the exact response is dependent on the model system and the intensity of exercise or contraction used [120]. In the *ex vivo* situation, the combined inactivation of AMPK and Rac1 in skeletal muscle is sufficient to completely eliminate contraction-mediated glucose uptake in oxidative soleus muscle, but not in glycolytic EDL muscle.

Studies in mice have shown that the Rac1 protein is 40-50% more abundant in oxidative soleus muscles compared to glycolytic EDL and mixed gastrocnemius muscles. This suggests that Rac1 may play a more significant role in contraction-stimulated glucose uptake in these fibers. In both types of fiber, however, the activation of AMPK does not appear to be necessary or sufficient to activate Rac1, indicating that the activation of Rac1 due to exercise is independent of AMPK [177].

These data suggest the existence of an additional pathway that mediates contraction signaling in skeletal muscle glucose uptake, apart from AMPK and Rac1 activation, at least in glycolytic muscle fibers. A possible explanation is that there may be another contraction-sensitive kinase upstream from the RabGAPs. This kinase may facilitate the translocation of GLUT4 through the phosphorylation of TBC1D1 and/or TBC1D4.

In addition to the known LKB1 substrates, which have been referred to as 'AMPK-related kinases' (ARKs), other kinases such as PKCs may also play a role in this process [51]. To determine the specific contribution of each RabGAP and AMPK in contraction-stimulated glucose uptake into skeletal muscle, we generated and analyzed mice with *Tbc1d1*- (D1KO), *Tbc1d4*- (D4KO), combined *Tbc1d1/Tbc1d4*- (D1/4KO) deficiency and skeletal muscle-specific AMPK inactivation (AMPK-DN). Interestingly, deletion of both RabGAPs and inactivation of AMPK are sufficient to abolish contraction response (contraction vs. basal state) in oxidative soleus muscle, but not in glycolytic EDL muscle (Figure 12).

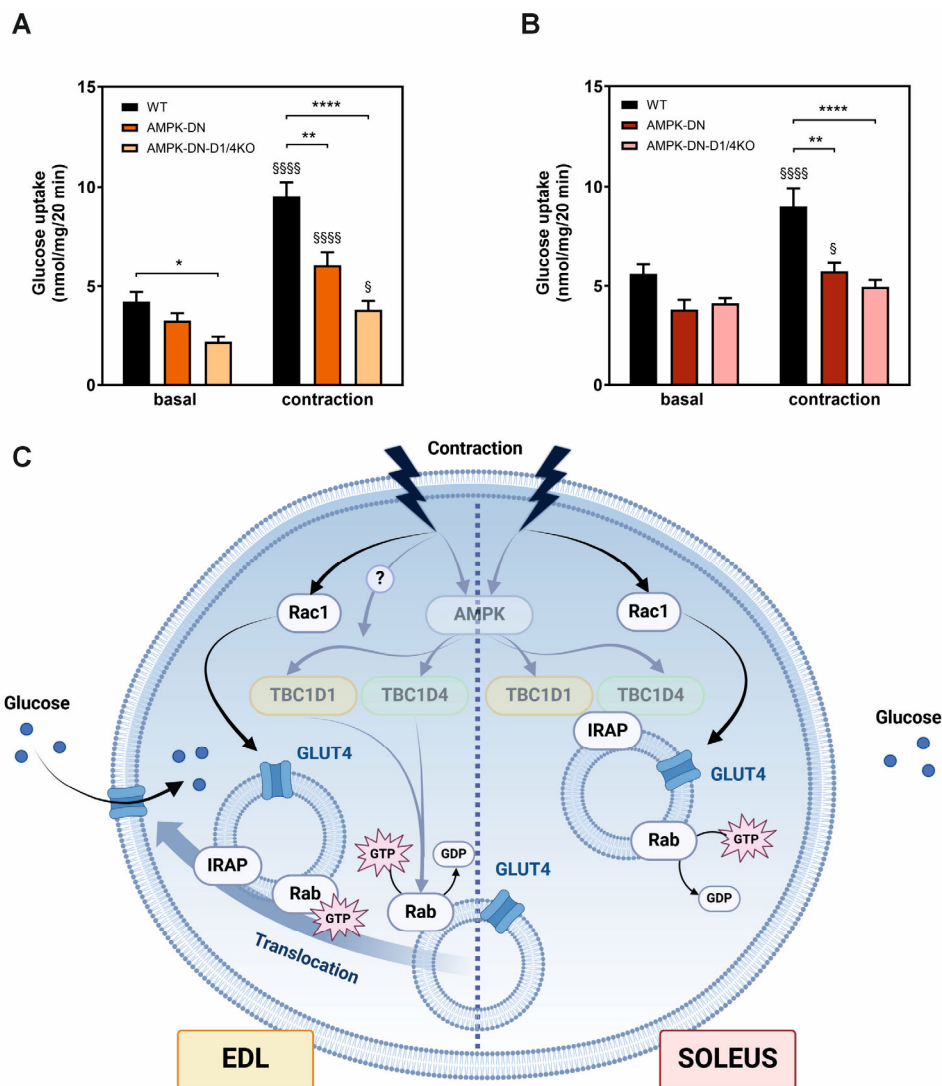


Figure 12: Deoxyglucose uptake in skeletal muscle from mice with combined depletion of AMPK activity and RabGAPs. *Ex vivo* deoxyglucose uptake in EDL (A) and Soleus (B) muscle +/- *ex vivo* electrical stimulation in a myograph chamber. D1KO: *Tbc1d1* deficiency, D4KO: *Tbc1d4* deficiency, D1/4KO: Combined *Tbc1d1/Tbc1d4* deficiency, AMPK-DN: Skeletal muscle-specific AMPK inactivation. Results are the mean \pm SEM of 7-11 experiments. * $p < 0.05$, ** $p < 0.01$, **** $p < 0.0001$, WT vs. DN vs. D1KO-DN vs. D4KO-DN vs. D1/4KO-DN by two-way ANOVA with Tukey correction; § $p < 0.05$, §§§§ $p < 0.0001$, § $P < 0.05$, basal vs. contracted by two-way ANOVA with Sidak correction. Adapted from [121]. (Own illustration, C: Created with Biorender.com)

The reason why Rac1 in the Soleus muscle is insufficient to mediate contraction-stimulated glucose uptake is unclear and indicates an interdependency with RabGAPs and/or AMPK that has not yet been elucidated. In glycolytic EDL muscle, either combined AMPK-Rac1 or RabGAP-Rac1 depletion or inactivation is required to completely abolish contraction-mediated glucose uptake (Figure 13).

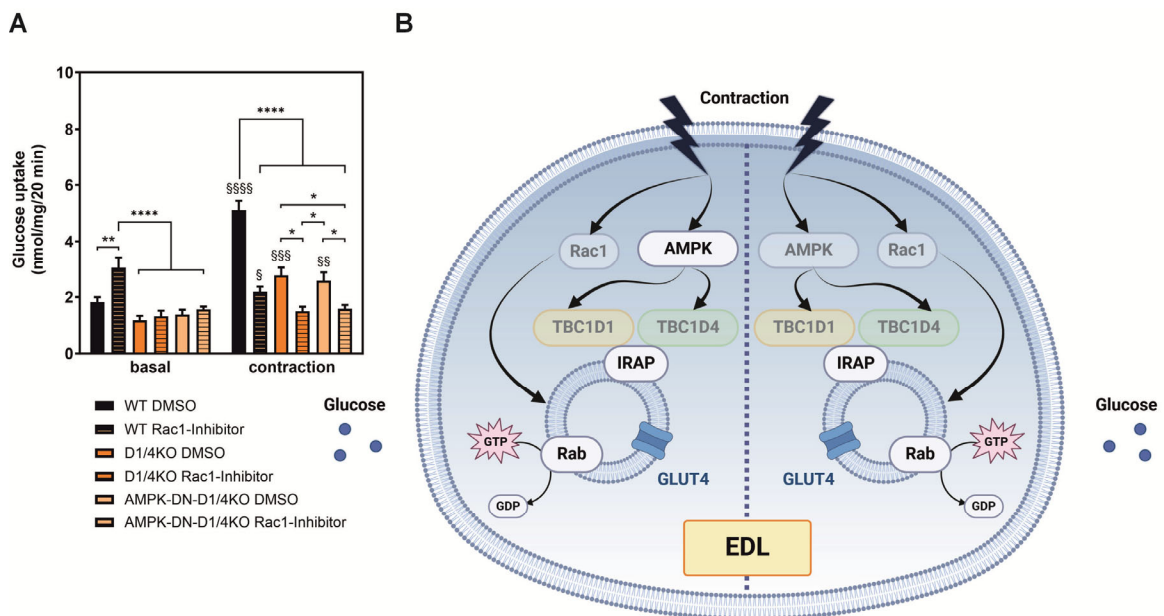


Figure 13: Deoxyglucose uptake in EDL muscle from mice with combined depletion of AMPK activity and RabGAPs and incubation with Rac1 inhibitor. (A) *Ex vivo* ^3H -DOG (deoxyglucose) uptake in intact isolated EDL muscle was determined using a myograph chamber after preincubation with either a Rac1 inhibitor or DMSO as vehicle control. $n = 5-10$. Data are mean \pm SEM. * $p < 0.05$, ** $p < 0.01$, **** $p < 0.0001$, WT vs. D1/4KO vs. AMPK-DN-D1/4KO by two-way ANOVA with Tukey correction; § $p < 0.05$, §§ $p < 0.01$, §§§ $p < 0.001$, §§§§ $p < 0.0001$, basal vs. contracted by two-way ANOVA with Sidak correction. Adapted from [121]. (Own illustration, B: Created with Biorender.com)

It is worth noting that there is no alternative AMPK-dependent pathway that circumvents the two RabGAPs. Therefore, it appears that TBC1D1 and TBC1D4 exclusively facilitate AMPK-mediated contraction signaling in the investigated skeletal muscle types.

The following conclusions can be drawn from these data:

- **There are several mechanisms that ensure proper functioning of skeletal muscle glucose uptake during contraction, highlighting the evolutionary significance of this pathway.**
- **AMPK, Rac1, and the two RabGAPs play crucial roles in contraction-mediated glucose uptake into skeletal muscle. However, the exact contribution of each compound depends on the muscle fiber type.**

- **There is evidence for an additional signaling pathway through muscle contraction via the RabGAPs in murine glycolytic muscle, presumably by an as-yet-unknown upstream kinase.**

3.4 Skeletal muscle insulin resistance induced by TBC1D4 depletion can be overcome by moderate exercise endurance training

We and others have previously demonstrated a critical role for both RabGAPs in skeletal muscle contraction signaling [106, 121, 126]. As described above, TBC1D1 and TBC1D4 appear to exert their specific function depending on the type of skeletal muscle fiber type, at least in mice. Subsequently, our research team concentrated on the physiological implications of RabGAP deficiency on exercise metabolism. In collaboration with the research group of Prof. Torben Hansen (Novo Nordisk Foundation Center for Basic Metabolic Research, Copenhagen, Denmark), we demonstrated that individuals homozygous for a previously identified TBC1D4 loss-of-function mutation exhibited enhanced benefits from increased levels of daily physical activity, with improvements observed in whole-body glycemia [96].

In our subsequent study, we observed that global *Tbc1d4*-deficient (D4KO) mice exhibited a similar improvement in whole-body glycemia following a moderate endurance training on treadmills (Figure 14). Indeed, D4KO mice exhibited a more pronounced benefit from the training than WT littermates. The rationale for this observation is presumed to be the low intensity of the exercise regimen, which, in contrast to the D4KO mice, was evidently insufficient to induce significant improvements in glycemic control in the WT mice, which is consistent with findings from other laboratories [178, 179]. Indeed, the outcomes of our study align with those of the human study in that our moderate-intensity exercise protocol reflects a more active lifestyle than a rigorous and frequent high-intensity exercise program, which may not be feasible for many individuals. It was somewhat unexpected that the enhanced insulin sensitivity observed in trained D4KO mice was associated with only a modestly enhanced skeletal muscle insulin sensitivity in D4KO mice, and not with a full rescue of the initial impairment. In contrast, both insulin-stimulated glucose uptake and GLUT4 abundance were substantially increased in WAT from trained D4KO mice. It appears that there is either a direct or indirect impact of regular physical activity on adipose tissue insulin sensitivity in the *Tbc1d4*-deficient state. Previous studies have

demonstrated a correlation between impairments in insulin-stimulated glucose uptake into both skeletal muscle and adipocytes and reduced protein abundance and/or translocation defects of the insulin-responsive GLUT4 in *Tbc1d4*-deficient oxidative skeletal muscle and adipocytes [100, 101, 106, 161]. Although adipose tissue accounts for less than 10% of whole-body glucose uptake, studies in adipocyte-specific GLUT4 knockout mice demonstrated the significant role of this tissue in maintaining healthy glucose homeostasis. These mice developed marked muscular and hepatic insulin resistance and became severely diabetic [21, 180].

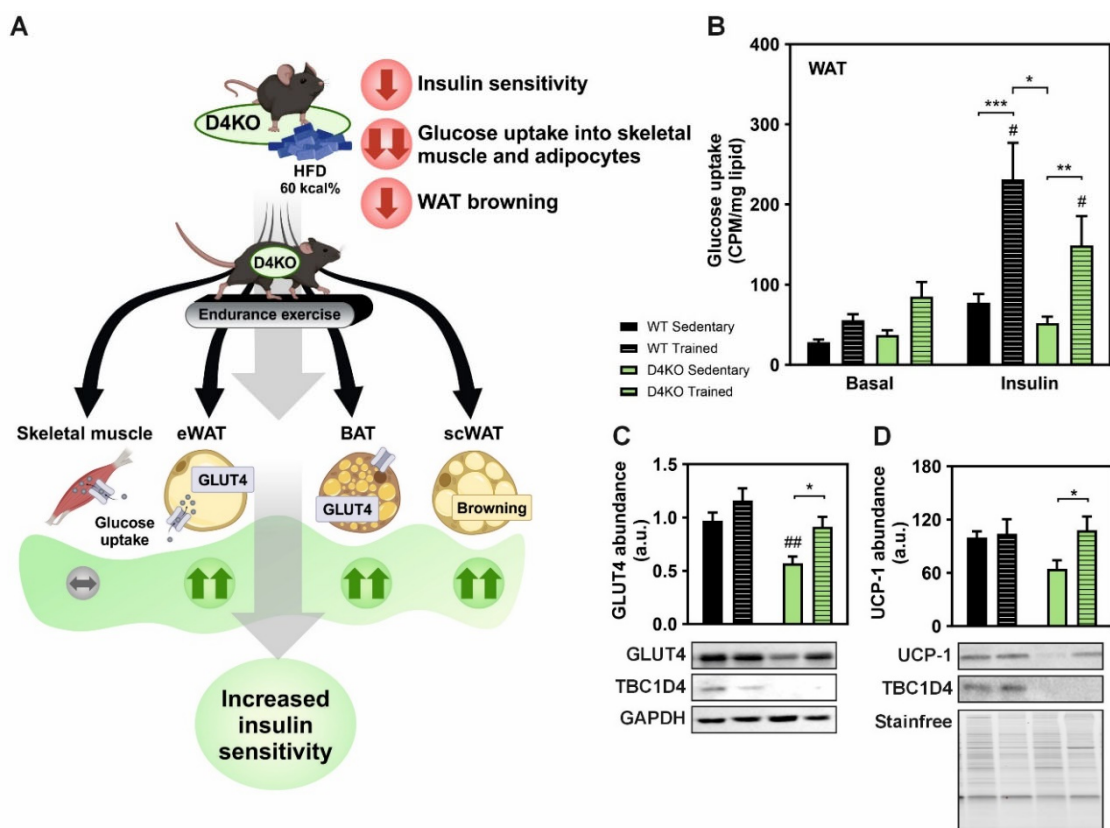


Figure 14: Improved adipose tissue insulin sensitivity in *Tbc1d4*-deficient mice following chronic treadmill training. (A) Disturbed insulin sensitivity in skeletal muscle and white adipose tissue is improved by moderate endurance exercise in *Tbc1d4*-deficient mice (D4KO). (B) Insulin-stimulated ¹⁴C-glucose uptake into isolated white adipocytes (WAT) from sedentary and trained wildtype (WT) and *Tbc1d4*-deficient (D4KO) mice, respectively. (C and D) GLUT4 and UCP-1 (Uncoupling protein-1) abundance in white adipose tissue from sedentary and trained WT and D4KO mice. eWAT: Epididymal white adipose tissue, scWAT: Subcutaneous white adipose tissue, BAT: Brown adipose tissue, HFD: High-fat diet. Adapted from [122]. (Own illustration, A: Created with Biorender.com)

The results of the mouse exercise study indicate that the expression of genes involved in oxidative metabolism and mitochondrial biogenesis and activity is increased in both skeletal muscle and adipose tissue from D4KO mice following training. In particular, transcriptome analysis and subsequent targeted validation via quantitative polymerase chain reaction (qPCR) and Western blot analysis demonstrated a reduced expression

of oxidative markers in D4KO adipose tissue in the sedentary state that was elevated to the WT level as a result of the treadmill training. Furthermore, decreased body fat content, reduced skeletal muscle total FA and MUFA (monounsaturated fatty acid) content, as well as reduced SCD1 (Stearoyl-CoA desaturase-1) activity in trained D4KO mice, indicate that regular physical activity may support the function of TBC1D4 as a molecular switch between lipid and glucose metabolism. Exercise training may have a multiplying effect on the stimulatory impact of a *Tbc1d4*-deficiency on FAO *per se*.

The relationship between the improvements in GLUT4 abundance and insulin-stimulated glucose uptake and the enhanced mitochondrial metabolism in adipose tissue from trained D4KO mice remains unclear. It is possible that these are two distinct processes, each resulting in enhanced insulin sensitivity, or that they are causally related. Other studies yielded disparate results regarding the effects of exercise training on the phenomenon of "browning," the increase in adipose tissue mitochondrial biogenesis and/ or activity, and related positive effects on insulin sensitivity. While some studies indicate that browning in adipocytes contributes to improvements in glucose tolerance, either by enhancing cellular energy expenditure or by secreting circulating factors with beneficial effects in other organs such as skeletal muscle or the liver [181, 182], others demonstrate a decoupling of these processes with no changes in insulin sensitivity despite increased browning of adipose cells [183]. In particular, it should be noted that not all studies demonstrating beneficial effects of exercise training on the activation of proteins of the insulin signaling pathway in adipose tissue also provide functional evidence such as the assessment of glucose uptake [184, 185]. The phenomenon of browning was initially described and investigated in the context of cold ambient temperatures. The assumption that maintaining mice at room temperature induces chronic cold stress due to their accelerated metabolism makes it challenging to interpret rodent browning studies for translational purposes [186, 187]. Nevertheless, the browning of adipose tissue has been demonstrated to be influenced by a multitude of factors, including cold exposure, physical activity, nutrition, and pharmacological intervention in both rodents and humans. Consequently, elucidating the underlying mechanisms of this process may provide valuable insights that could inform future disease prevention and treatment strategies for obesity and T2D [188]. TBC1D4 (and potentially TBC1D1) may represent promising targets for future precision medicine approaches, as they function as central hubs between skeletal muscle glucose and lipid metabolism.

The following conclusions can be drawn from these data:

- **Increased physical activity can ameliorate impaired whole-body insulin sensitivity observed in *Tbc1d4*-deficient mice and TBC1D4 loss-of-function allele carriers.**
- **In mice, the improvements in whole-body glycemia observed following moderate exercise training are facilitated by enhanced insulin sensitivity and browning in white adipose tissue.**
- **Further studies will focus on the underlying mechanisms of this presumed skeletal muscle-adipose tissue crosstalk and the cellular response to exercise training in the various tissues.**

In conclusion, our data offer a more profound understanding of the energy flux of skeletal muscle, particularly with regard to substrate partitioning and insulin sensitivity. Further research could include population-wide screenings for as yet unknown gene variants in the two RabGAPs, with a view to developing personalized prevention or treatment strategies.

4 References

1. American Diabetes Association Professional Practice Committee, 2. *Diagnosis and Classification of Diabetes: Standards of Care in Diabetes-2024*. Diabetes Care, 2024. **47**(Suppl 1): p. S20-S42.
2. Handy, R.M. and G.P. Holloway, *Insights into the development of insulin resistance: Unraveling the interaction of physical inactivity, lipid metabolism and mitochondrial biology*. Front Physiol, 2023. **14**: p. 1151389.
3. International Diabetes Federation, *IDF Diabetes Atlas 2021. 10th edition*.
4. Sims, E.A., et al., *Endocrine and metabolic effects of experimental obesity in man*. Recent Prog Horm Res, 1973. **29**: p. 457-96.
5. Chadt, A., et al., *Molecular links between Obesity and Diabetes: "Diabesity"*, in *Endotext*, L.J. De Groot, et al., Editors. 2000: South Dartmouth (MA).
6. Galicia-Garcia, U., et al., *Pathophysiology of Type 2 Diabetes Mellitus*. Int J Mol Sci, 2020. **21**(17).
7. Stumvoll, M., B.J. Goldstein, and T.W. van Haefen, *Type 2 diabetes: principles of pathogenesis and therapy*. Lancet, 2005. **365**(9467): p. 1333-46.
8. Kahn, S.E., R.L. Hull, and K.M. Utzschneider, *Mechanisms linking obesity to insulin resistance and type 2 diabetes*. Nature, 2006. **444**(7121): p. 840-6.
9. DeFronzo, R.A. and D. Tripathy, *Skeletal muscle insulin resistance is the primary defect in type 2 diabetes*. Diabetes Care, 2009. **32 Suppl 2**(Suppl 2): p. S157-63.
10. Smith, U. and B.B. Kahn, *Adipose tissue regulates insulin sensitivity: role of adipogenesis, de novo lipogenesis and novel lipids*. J Intern Med, 2016. **280**(5): p. 465-475.
11. Batista, T.M., N. Haider, and C.R. Kahn, *Defining the underlying defect in insulin action in type 2 diabetes*. Diabetologia, 2021. **64**(5): p. 994-1006.
12. Goodpaster, B.H. and L.M. Sparks, *Metabolic Flexibility in Health and Disease*. Cell Metab, 2017. **25**(5): p. 1027-1036.
13. Kelley, D.E., *Skeletal muscle fat oxidation: timing and flexibility are everything*. J Clin Invest, 2005. **115**(7): p. 1699-702.
14. Al-Hasani, H., et al., *Roles of the N- and C-termini of GLUT4 in endocytosis*. J Cell Sci, 2002. **115**(Pt 1): p. 131-40.
15. Liu, P., et al., *PtdIns(3,4,5)P3-Dependent Activation of the mTORC2 Kinase Complex*. Cancer Discov, 2015. **5**(11): p. 1194-209.
16. Watson, R.T., M. Kanzaki, and J.E. Pessin, *Regulated membrane trafficking of the insulin-responsive glucose transporter 4 in adipocytes*. Endocr Rev, 2004. **25**(2): p. 177-204.
17. Saltiel, A.R., *Insulin signaling in health and disease*. J Clin Invest, 2021. **131**(1).
18. Satoh, T., *Rho GTPases in insulin-stimulated glucose uptake*. Small GTPases, 2014. **5**: p. e28102.
19. Tunduguru, R. and D.C. Thurmond, *Promoting Glucose Transporter-4 Vesicle Trafficking along Cytoskeletal Tracks: PAK-Ing Them Out*. Front Endocrinol (Lausanne), 2017. **8**: p. 329.
20. Zisman, A., et al., *Targeted disruption of the glucose transporter 4 selectively in muscle causes insulin resistance and glucose intolerance*. Nat Med, 2000. **6**(8): p. 924-8.
21. Abel, E.D., et al., *Adipose-selective targeting of the GLUT4 gene impairs insulin action in muscle and liver*. Nature, 2001. **409**(6821): p. 729-33.
22. Kotani, K., et al., *GLUT4 glucose transporter deficiency increases hepatic lipid production and peripheral lipid utilization*. J Clin Invest, 2004. **114**(11): p. 1666-75.
23. Bickel, P.E., *Metabolic fuel selection: the importance of being flexible*. J Clin Invest, 2004. **114**(11): p. 1547-9.
24. Pei, J., B. Wang, and D. Wang, *Current Studies on Molecular Mechanisms of Insulin Resistance*. J Diabetes Res, 2022. **2022**: p. 1863429.
25. Li, M., et al., *Role of PKCdelta in Insulin Sensitivity and Skeletal Muscle Metabolism*. Diabetes, 2015. **64**(12): p. 4023-32.
26. Li, Y., et al., *Protein kinase C Theta inhibits insulin signaling by phosphorylating IRS1 at Ser(1101)*. J Biol Chem, 2004. **279**(44): p. 45304-7.
27. Gilbert, M., *Role of skeletal muscle lipids in the pathogenesis of insulin resistance of obesity and type 2 diabetes*. J Diabetes Investig, 2021. **12**(11): p. 1934-1941.
28. Wu, S., et al., *Tissue-specific mechanisms of fat metabolism that focus on insulin actions*. J Adv Res, 2022.

29. Toledo, F.G., et al., *Mitochondrial capacity in skeletal muscle is not stimulated by weight loss despite increases in insulin action and decreases in intramyocellular lipid content*. *Diabetes*, 2008. **57**(4): p. 987-94.
30. Guan, Y., J.C. Drake, and Z. Yan, *Exercise-Induced Mitophagy in Skeletal Muscle and Heart*. *Exerc Sport Sci Rev*, 2019. **47**(3): p. 151-156.
31. Iaccarino, G., et al., *Modulation of Insulin Sensitivity by Exercise Training: Implications for Cardiovascular Prevention*. *J Cardiovasc Transl Res*, 2021. **14**(2): p. 256-270.
32. Ashcroft, S.P., et al., *Exercise induces tissue-specific adaptations to enhance cardiometabolic health*. *Cell Metab*, 2024. **36**(2): p. 278-300.
33. Sylow, L., et al., *The many actions of insulin in skeletal muscle, the paramount tissue determining glycemia*. *Cell Metab*, 2021. **33**(4): p. 758-780.
34. Benchoula, K., A. Mediani, and W.E. Hwa, *The functions of Ca(2+)/calmodulin-dependent protein kinase II (CaMKII) in diabetes progression*. *J Cell Commun Signal*, 2023. **17**(1): p. 25-34.
35. Kjobsted, R., J.F. Wojtaszewski, and J.T. Treebak, *Role of AMP-Activated Protein Kinase for Regulating Post-exercise Insulin Sensitivity*. *Exp Suppl*, 2016. **107**: p. 81-126.
36. Stocks, B. and J.R. Zierath, *Post-translational Modifications: The Signals at the Intersection of Exercise, Glucose Uptake, and Insulin Sensitivity*. *Endocr Rev*, 2022. **43**(4): p. 654-677.
37. Lira, V.A., et al., *PGC-1alpha regulation by exercise training and its influences on muscle function and insulin sensitivity*. *Am J Physiol Endocrinol Metab*, 2010. **299**(2): p. E145-61.
38. Hawley, J.A. and S.J. Lessard, *Mitochondrial function: use it or lose it*. *Diabetologia*, 2007. **50**(4): p. 699-702.
39. Zetser, A., E. Gredinger, and E. Bengal, *p38 mitogen-activated protein kinase pathway promotes skeletal muscle differentiation. Participation of the Mef2c transcription factor*. *J Biol Chem*, 1999. **274**(8): p. 5193-200.
40. Zhao, M., et al., *Regulation of the MEF2 family of transcription factors by p38*. *Mol Cell Biol*, 1999. **19**(1): p. 21-30.
41. Chambers, M.A., et al., *Stretch-stimulated glucose uptake in skeletal muscle is mediated by reactive oxygen species and p38 MAP-kinase*. *J Physiol*, 2009. **587**(Pt 13): p. 3363-73.
42. Somwar, R., et al., *Activation of p38 mitogen-activated protein kinase alpha and beta by insulin and contraction in rat skeletal muscle: potential role in the stimulation of glucose transport*. *Diabetes*, 2000. **49**(11): p. 1794-800.
43. Bengal, E., S. Aviram, and T. Hayek, *p38 MAPK in Glucose Metabolism of Skeletal Muscle: Beneficial or Harmful?* *Int J Mol Sci*, 2020. **21**(18).
44. Bodine, S.C., *The role of mTORC1 in the regulation of skeletal muscle mass*. *Fac Rev*, 2022. **11**: p. 32.
45. Knudsen, J.R., et al., *Contraction-regulated mTORC1 and protein synthesis: Influence of AMPK and glycogen*. *J Physiol*, 2020. **598**(13): p. 2637-2649.
46. Egan, B. and J.R. Zierath, *Exercise metabolism and the molecular regulation of skeletal muscle adaptation*. *Cell Metab*, 2013. **17**(2): p. 162-84.
47. Sigal, R.J., et al., *Effects of aerobic training, resistance training, or both on glycemic control in type 2 diabetes: a randomized trial*. *Ann Intern Med*, 2007. **147**(6): p. 357-69.
48. Ren, J.M., et al., *Exercise induces rapid increases in GLUT4 expression, glucose transport capacity, and insulin-stimulated glycogen storage in muscle*. *J Biol Chem*, 1994. **269**(20): p. 14396-401.
49. Kim, Y., et al., *Effects of endurance training on gene expression of insulin signal transduction pathway*. *Biochem Biophys Res Commun*, 1995. **210**(3): p. 766-73.
50. Ojuka, E.O., V. Goyaram, and J.A. Smith, *The role of CaMKII in regulating GLUT4 expression in skeletal muscle*. *Am J Physiol Endocrinol Metab*, 2012. **303**(3): p. E322-31.
51. Peifer-Weiss, L., H. Al-Hasani, and A. Chadt, *AMPK and Beyond: The Signaling Network Controlling RabGAPs and Contraction-Mediated Glucose Uptake in Skeletal Muscle*. *Int J Mol Sci*, 2024. **25**(3).
52. Almuraikhy, S., et al., *Molecular regulators of exercise-mediated insulin sensitivity in non-obese individuals*. *J Cell Mol Med*, 2024. **28**(1): p. e18015.
53. Bohm, A., et al., *Exercise and diabetes: relevance and causes for response variability*. *Endocrine*, 2016. **51**(3): p. 390-401.
54. Collins, K.A., et al., *Differential Effects of Amount, Intensity, and Mode of Exercise Training on Insulin Sensitivity and Glucose Homeostasis: A Narrative Review*. *Sports Med Open*, 2022. **8**(1): p. 90.
55. Taniguchi, C.M., B. Emanuelli, and C.R. Kahn, *Critical nodes in signalling pathways: insights into insulin action*. *Nat Rev Mol Cell Biol*, 2006. **7**(2): p. 85-96.

56. Hawley, S.A., et al., *Complexes between the LKB1 tumor suppressor, STRAD alpha/beta and MO25 alpha/beta are upstream kinases in the AMP-activated protein kinase cascade.* J Biol, 2003. **2**(4): p. 28.
57. Sakamoto, K., et al., *Deficiency of LKB1 in skeletal muscle prevents AMPK activation and glucose uptake during contraction.* EMBO J, 2005. **24**(10): p. 1810-20.
58. Oakhill, J.S., J.W. Scott, and B.E. Kemp, *AMPK functions as an adenylate charge-regulated protein kinase.* Trends Endocrinol Metab, 2012. **23**(3): p. 125-32.
59. Hawley, S.A., et al., *Calmodulin-dependent protein kinase kinase-beta is an alternative upstream kinase for AMP-activated protein kinase.* Cell Metab, 2005. **2**(1): p. 9-19.
60. Hurley, R.L., et al., *The Ca²⁺/calmodulin-dependent protein kinase kinases are AMP-activated protein kinase kinases.* J Biol Chem, 2005. **280**(32): p. 29060-6.
61. Woods, A., et al., *Ca²⁺/calmodulin-dependent protein kinase kinase-beta acts upstream of AMP-activated protein kinase in mammalian cells.* Cell Metab, 2005. **2**(1): p. 21-33.
62. Negoita, F., et al., *CaMKK2 is not involved in contraction-stimulated AMPK activation and glucose uptake in skeletal muscle.* Mol Metab, 2023. **75**: p. 101761.
63. Kramer, H.F., et al., *Calmodulin-binding domain of AS160 regulates contraction- but not insulin-stimulated glucose uptake in skeletal muscle.* Diabetes, 2007. **56**(12): p. 2854-62.
64. Merrill, G.F., et al., *AICA riboside increases AMP-activated protein kinase, fatty acid oxidation, and glucose uptake in rat muscle.* Am J Physiol, 1997. **273**(6): p. E1107-12.
65. Bergeron, R., et al., *Effect of AMPK activation on muscle glucose metabolism in conscious rats.* Am J Physiol, 1999. **276**(5): p. E938-44.
66. Hayashi, T., et al., *Evidence for 5' AMP-activated protein kinase mediation of the effect of muscle contraction on glucose transport.* Diabetes, 1998. **47**(8): p. 1369-73.
67. Chen, Q., et al., *A Tbc1d1 (Ser231Ala)-knockin mutation partially impairs AICAR- but not exercise-induced muscle glucose uptake in mice.* Diabetologia, 2017. **60**(2): p. 336-345.
68. Jensen, T.E., et al., *AMPK alpha1 activation is required for stimulation of glucose uptake by twitch contraction, but not by H₂O₂, in mouse skeletal muscle.* PLoS One, 2008. **3**(5): p. e2102.
69. Kramer, H.F., et al., *Distinct signals regulate AS160 phosphorylation in response to insulin, AICAR, and contraction in mouse skeletal muscle.* Diabetes, 2006. **55**(7): p. 2067-76.
70. Chavez, J.A., et al., *Inhibition of GLUT4 translocation by Tbc1d1, a Rab GTPase-activating protein abundant in skeletal muscle, is partially relieved by AMP-activated protein kinase activation.* J Biol Chem, 2008. **283**(14): p. 9187-95.
71. Espelage, L., H. Al-Hasani, and A. Chadt, *RabGAPs in skeletal muscle function and exercise.* J Mol Endocrinol, 2020. **64**(1): p. R1-R19.
72. Mafakheri, S., A. Chadt, and H. Al-Hasani, *Regulation of RabGAPs involved in insulin action.* Biochem Soc Trans, 2018. **46**(3): p. 683-690.
73. Cartee, G.D., *Roles of TBC1D1 and TBC1D4 in insulin- and exercise-stimulated glucose transport of skeletal muscle.* Diabetologia, 2015. **58**(1): p. 19-30.
74. Roach, W.G., et al., *Substrate specificity and effect on GLUT4 translocation of the Rab GTPase-activating protein Tbc1d1.* Biochem J, 2007. **403**(2): p. 353-8.
75. Sakamoto, K. and G.D. Holman, *Emerging role for AS160/TBC1D4 and TBC1D1 in the regulation of GLUT4 traffic.* Am J Physiol Endocrinol Metab, 2008. **295**(1): p. E29-37.
76. Richter, E.A. and M. Hargreaves, *Exercise, GLUT4, and skeletal muscle glucose uptake.* Physiol Rev, 2013. **93**(3): p. 993-1017.
77. Kjobsted, R., et al., *TBC1D4-S711 Controls Skeletal Muscle Insulin Sensitization After Exercise and Contraction.* Diabetes, 2023. **72**(7): p. 857-871.
78. Maarbjerg, S.J., L. Sylow, and E.A. Richter, *Current understanding of increased insulin sensitivity after exercise - emerging candidates.* Acta Physiol (Oxf), 2011. **202**(3): p. 323-35.
79. Treebak, J.T., et al., *Potential role of TBC1D4 in enhanced post-exercise insulin action in human skeletal muscle.* Diabetologia, 2009. **52**(5): p. 891-900.
80. Zaid, H., et al., *Insulin action on glucose transporters through molecular switches, tracks and tethers.* Biochem J, 2008. **413**(2): p. 201-15.
81. Dash, S., et al., *A truncation mutation in TBC1D4 in a family with acanthosis nigricans and postprandial hyperinsulinemia.* Proc Natl Acad Sci U S A, 2009. **106**(23): p. 9350-5.
82. Mafakheri, S., et al., *AKT and AMP-activated protein kinase regulate TBC1D1 through phosphorylation and its interaction with the cytosolic tail of insulin-regulated aminopeptidase IRAP.* J Biol Chem, 2018. **293**(46): p. 17853-17862.
83. Eickelschulte, S., et al., *AKT/AMPK-mediated phosphorylation of TBC1D4 disrupts the interaction with insulin-regulated aminopeptidase.* J Biol Chem, 2021. **296**: p. 100637.

84. Meyre, D., et al., *R125W coding variant in TBC1D1 confers risk for familial obesity and contributes to linkage on chromosome 4p14 in the French population*. Hum Mol Genet, 2008. **17**(12): p. 1798-802.
85. Stone, S., et al., *TBC1D1 is a candidate for a severe obesity gene and evidence for a gene/gene interaction in obesity predisposition*. Hum Mol Genet, 2006. **15**(18): p. 2709-20.
86. Woo, J.R., et al., *The carboxy-terminal region of the TBC1D4 (AS160) RabGAP mediates protein homodimerization*. Int J Biol Macromol, 2017. **103**: p. 965-971.
87. Park, S., et al., *Affinity between TBC1D4 (AS160) phosphotyrosine-binding domain and insulin-regulated aminopeptidase cytoplasmic domain measured by isothermal titration calorimetry*. BMB Rep, 2012. **45**(6): p. 360-4.
88. An, D., et al., *TBC1D1 regulates insulin- and contraction-induced glucose transport in mouse skeletal muscle*. Diabetes, 2010. **59**(6): p. 1358-65.
89. Thomas, E.C., et al., *Isoform-specific AMPK association with TBC1D1 is reduced by a mutation associated with severe obesity*. Biochem J, 2018. **475**(18): p. 2969-2983.
90. Chadt, A., et al., *Tbc1d1 mutation in lean mouse strain confers leanness and protects from diet-induced obesity*. Nat Genet, 2008. **40**(11): p. 1354-9.
91. Dash, S., et al., *Analysis of TBC1D4 in patients with severe insulin resistance*. Diabetologia, 2010. **53**(6): p. 1239-42.
92. Moltke, I., et al., *A common Greenlandic TBC1D4 variant confers muscle insulin resistance and type 2 diabetes*. Nature, 2014. **512**(7513): p. 190-3.
93. Grarup, N., et al., *Diabetes in Population Isolates: Lessons from Greenland*. Rev Diabet Stud, 2015. **12**(3-4): p. 320-9.
94. Moller, G., et al., *The role of a traditional and western diet on glucose homeostasis in Greenlandic Inuit carriers and non-carriers of type 2 diabetes variant in the TBC1D4 gene: A protocol for a randomized clinical trial*. Contemp Clin Trials Commun, 2021. **21**: p. 100734.
95. Lewis, J.I., et al., *The effect of traditional diet on glucose homeostasis in carriers and non-carriers of a common TBC1D4 variant in Greenlandic Inuit: a randomised crossover study*. Br J Nutr, 2023: p. 1-14.
96. Schnurr, T.M., et al., *Physical activity attenuates postprandial hyperglycaemia in homozygous TBC1D4 loss-of-function mutation carriers*. Diabetologia, 2021. **64**(8): p. 1795-1804.
97. Kleinert, M., et al., *Animal models of obesity and diabetes mellitus*. Nat Rev Endocrinol, 2018. **14**(3): p. 140-162.
98. Blaauw, B., S. Schiaffino, and C. Reggiani, *Mechanisms modulating skeletal muscle phenotype*. Compr Physiol, 2013. **3**(4): p. 1645-87.
99. Pette, D. and C. Spamer, *Metabolic properties of muscle fibers*. Fed Proc, 1986. **45**(13): p. 2910-4.
100. Lansey, M.N., et al., *Deletion of Rab GAP AS160 modifies glucose uptake and GLUT4 translocation in primary skeletal muscles and adipocytes and impairs glucose homeostasis*. Am J Physiol Endocrinol Metab, 2012. **303**(10): p. E1273-86.
101. Wang, H.Y., et al., *AS160 deficiency causes whole-body insulin resistance via composite effects in multiple tissues*. Biochem J, 2013. **449**(2): p. 479-89.
102. Chen, L., et al., *Disruption of the AMPK-TBC1D1 nexus increases lipogenic gene expression and causes obesity in mice via promoting IGF1 secretion*. Proc Natl Acad Sci U S A, 2016. **113**(26): p. 7219-24.
103. Chen, S., et al., *Mice with AS160/TBC1D4-Thr649Ala knockin mutation are glucose intolerant with reduced insulin sensitivity and altered GLUT4 trafficking*. Cell Metab, 2011. **13**(1): p. 68-79.
104. Quan, C., et al., *PKB-Mediated Thr649 Phosphorylation of AS160/TBC1D4 Regulates the R-Wave Amplitude in the Heart*. PLoS One, 2015. **10**(4): p. e0124491.
105. Ducommun, S., et al., *Thr649Ala-AS160 knock-in mutation does not impair contraction/AICAR-induced glucose transport in mouse muscle*. Am J Physiol Endocrinol Metab, 2012. **302**(9): p. E1036-43.
106. Chadt, A., et al., *"Deletion of both Rab-GTPase-activating proteins TBC1D1 and TBC1D4 in mice eliminates insulin- and AICAR-stimulated glucose transport [corrected]*. Diabetes, 2015. **64**(3): p. 746-59.
107. Dokas, J., et al., *Tbc1d1 deletion suppresses obesity in leptin-deficient mice*. Int J Obes (Lond), 2016. **40**(8): p. 1242-9.
108. Kjobsted, R., et al., *AMPK in skeletal muscle function and metabolism*. FASEB J, 2018. **32**(4): p. 1741-1777.
109. Kjobsted, R., et al., *AMPK and TBC1D1 Regulate Muscle Glucose Uptake After, but Not During, Exercise and Contraction*. Diabetes, 2019. **68**(7): p. 1427-1440.

110. Richter, E.A., et al., *Muscle glucose metabolism following exercise in the rat: increased sensitivity to insulin*. J Clin Invest, 1982. **69**(4): p. 785-93.
111. Wojtaszewski, J.F., et al., *Insulin signaling in human skeletal muscle: time course and effect of exercise*. Diabetes, 1997. **46**(11): p. 1775-81.
112. Sjoberg, K.A., et al., *Exercise Increases Human Skeletal Muscle Insulin Sensitivity via Coordinated Increases in Microvascular Perfusion and Molecular Signaling*. Diabetes, 2017. **66**(6): p. 1501-1510.
113. Hansen, P.A., et al., *Increased GLUT-4 translocation mediates enhanced insulin sensitivity of muscle glucose transport after exercise*. J Appl Physiol (1985), 1998. **85**(4): p. 1218-22.
114. Wojtaszewski, J.F., et al., *Insulin signaling and insulin sensitivity after exercise in human skeletal muscle*. Diabetes, 2000. **49**(3): p. 325-31.
115. Kjobsted, R., et al., *TBC1D4 Is Necessary for Enhancing Muscle Insulin Sensitivity in Response to AICAR and Contraction*. Diabetes, 2019. **68**(9): p. 1756-1766.
116. Park, S.S. and Y.K. Seo, *Excess Accumulation of Lipid Impairs Insulin Sensitivity in Skeletal Muscle*. Int J Mol Sci, 2020. **21**(6).
117. Dokas, J., et al., *Conventional knockout of Tbc1d1 in mice impairs insulin- and AICAR-stimulated glucose uptake in skeletal muscle*. Endocrinology, 2013. **154**(10): p. 3502-14.
118. Stermann, T., et al., *Deletion of the RabGAP TBC1D1 Leads to Enhanced Insulin Secretion and Fatty Acid Oxidation in Islets From Male Mice*. Endocrinology, 2018. **159**(4): p. 1748-1761.
119. Mu, J., et al., *A role for AMP-activated protein kinase in contraction- and hypoxia-regulated glucose transport in skeletal muscle*. Mol Cell, 2001. **7**(5): p. 1085-94.
120. Sylow, L., et al., *Rac1 and AMPK Account for the Majority of Muscle Glucose Uptake Stimulated by Ex Vivo Contraction but Not In Vivo Exercise*. Diabetes, 2017. **66**(6): p. 1548-1559.
121. de Wendt, C., et al., *Contraction-Mediated Glucose Transport in Skeletal Muscle Is Regulated by a Framework of AMPK, TBC1D1/4, and Rac1*. Diabetes, 2021. **70**(12): p. 2796-2809.
122. Springer, C., et al., *Depletion of TBC1D4 improves the metabolic exercise response by overcoming genetically induced peripheral insulin resistance*. Diabetes, 2024.
123. Colosimo, S., et al., *Insulin resistance and metabolic flexibility as drivers of liver and cardiac disease in T2DM*. Diabetes Res Clin Pract, 2023. **206**: p. 111016.
124. Smith, R.L., et al., *Metabolic Flexibility as an Adaptation to Energy Resources and Requirements in Health and Disease*. Endocr Rev, 2018. **39**(4): p. 489-517.
125. Xourafa, G., M. Korbmacher, and M. Roden, *Inter-organ crosstalk during development and progression of type 2 diabetes mellitus*. Nat Rev Endocrinol, 2024. **20**(1): p. 27-49.
126. Szekeres, F., et al., *The Rab-GTPase-activating protein TBC1D1 regulates skeletal muscle glucose metabolism*. Am J Physiol Endocrinol Metab, 2012. **303**(4): p. E524-33.
127. Li, Y., et al., *Skeletal intramyocellular lipid metabolism and insulin resistance*. Biophys Rep, 2015. **1**: p. 90-98.
128. Savage, D.B., K.F. Petersen, and G.I. Shulman, *Disordered lipid metabolism and the pathogenesis of insulin resistance*. Physiol Rev, 2007. **87**(2): p. 507-20.
129. Schon, M., et al., *Intramyocellular Triglyceride Content During the Early Course of Type 1 and Type 2 Diabetes*. Diabetes, 2023. **72**(10): p. 1483-1492.
130. Kahn, D., et al., *Subcellular localisation and composition of intramuscular triacylglycerol influence insulin sensitivity in humans*. Diabetologia, 2021. **64**(1): p. 168-180.
131. Lair, B., et al., *Novel Insights and Mechanisms of Lipotoxicity-Driven Insulin Resistance*. Int J Mol Sci, 2020. **21**(17).
132. Sokolowska, E. and A. Blachnio-Zabielska, *The Role of Ceramides in Insulin Resistance*. Front Endocrinol (Lausanne), 2019. **10**: p. 577.
133. Ritter, O., T. Jelenik, and M. Roden, *Lipid-mediated muscle insulin resistance: different fat, different pathways?* J Mol Med (Berl), 2015. **93**(8): p. 831-43.
134. Kolczynska, K., et al., *Diacylglycerol-evoked activation of PKC and PKD isoforms in regulation of glucose and lipid metabolism: a review*. Lipids Health Dis, 2020. **19**(1): p. 113.
135. Stenmark, H. and V.M. Olkkonen, *The Rab GTPase family*. Genome Biol, 2001. **2**(5): p. REVIEWS3007.
136. Pfeffer, S.R., *Rab GTPases: master regulators that establish the secretory and endocytic pathways*. Mol Biol Cell, 2017. **28**(6): p. 712-715.
137. Miinea, C.P., et al., *AS160, the Akt substrate regulating GLUT4 translocation, has a functional Rab GTPase-activating protein domain*. Biochem J, 2005. **391**(Pt 1): p. 87-93.
138. Zhou, Z., et al., *Rab28 is a TBC1D1/TBC1D4 substrate involved in GLUT4 trafficking*. FEBS Lett, 2017. **591**(1): p. 88-96.

139. Benninghoff, T., et al., *The RabGAPs TBC1D1 and TBC1D4 Control Uptake of Long-Chain Fatty Acids Into Skeletal Muscle via Fatty Acid Transporter SLC27A4/FATP4*. *Diabetes*, 2020. **69**(11): p. 2281-2293.
140. Nickerson, J.G., et al., *Greater transport efficiencies of the membrane fatty acid transporters FAT/CD36 and FATP4 compared with FABPpm and FATP1 and differential effects on fatty acid esterification and oxidation in rat skeletal muscle*. *J Biol Chem*, 2009. **284**(24): p. 16522-30.
141. Glatz, J.F., J.J. Luiken, and A. Bonen, *Membrane fatty acid transporters as regulators of lipid metabolism: implications for metabolic disease*. *Physiol Rev*, 2010. **90**(1): p. 367-417.
142. Glatz, J.F.C., M. Nabben, and J. Luiken, *CD36 (SR-B2) as master regulator of cellular fatty acid homeostasis*. *Curr Opin Lipidol*, 2022. **33**(2): p. 103-111.
143. Luiken, J.J., et al., *Insulin induces the translocation of the fatty acid transporter FAT/CD36 to the plasma membrane*. *Am J Physiol Endocrinol Metab*, 2002. **282**(2): p. E491-5.
144. Jain, S.S., et al., *Additive effects of insulin and muscle contraction on fatty acid transport and fatty acid transporters, FAT/CD36, FABPpm, FATP1, 4 and 6*. *FEBS Lett*, 2009. **583**(13): p. 2294-300.
145. Steinbusch, L.K., et al., *Subcellular trafficking of the substrate transporters GLUT4 and CD36 in cardiomyocytes*. *Cell Mol Life Sci*, 2011. **68**(15): p. 2525-38.
146. Samovski, D., et al., *Insulin and AMPK regulate FA translocase/CD36 plasma membrane recruitment in cardiomyocytes via Rab GAP AS160 and Rab8a Rab GTPase*. *J Lipid Res*, 2012. **53**(4): p. 709-17.
147. Miklosz, A., et al., *Does TBC1D4 (AS160) or TBC1D1 Deficiency Affect the Expression of Fatty Acid Handling Proteins in the Adipocytes Differentiated from Human Adipose-Derived Mesenchymal Stem Cells (ADMSCs) Obtained from Subcutaneous and Visceral Fat Depots?* *Cells*, 2021. **10**(6).
148. Coe, N.R., et al., *The fatty acid transport protein (FATP1) is a very long chain acyl-CoA synthetase*. *J Biol Chem*, 1999. **274**(51): p. 36300-4.
149. Stahl, A., et al., *Insulin causes fatty acid transport protein translocation and enhanced fatty acid uptake in adipocytes*. *Dev Cell*, 2002. **2**(4): p. 477-88.
150. Miklosz, A., et al., *RabGAP AS160/TBC1D4 deficiency increases long-chain fatty acid transport but has little additional effect on obesity and metabolic syndrome in ADMSCs-derived adipocytes of morbidly obese women*. *Front Mol Biosci*, 2023. **10**: p. 1232159.
151. Holman, G.D. and I.V. Sandoval, *Moving the insulin-regulated glucose transporter GLUT4 into and out of storage*. *Trends Cell Biol*, 2001. **11**(4): p. 173-9.
152. Ploug, T., et al., *Analysis of GLUT4 distribution in whole skeletal muscle fibers: identification of distinct storage compartments that are recruited by insulin and muscle contractions*. *J Cell Biol*, 1998. **142**(6): p. 1429-46.
153. Lauritzen, H.P., *Insulin- and contraction-induced glucose transporter 4 traffic in muscle: insights from a novel imaging approach*. *Exerc Sport Sci Rev*, 2013. **41**(2): p. 77-86.
154. Kennedy, J.W., et al., *Acute exercise induces GLUT4 translocation in skeletal muscle of normal human subjects and subjects with type 2 diabetes*. *Diabetes*, 1999. **48**(5): p. 1192-7.
155. Klip, A., T.E. McGraw, and D.E. James, *Thirty sweet years of GLUT4*. *J Biol Chem*, 2019. **294**(30): p. 11369-11381.
156. Miklosz, A., et al., *The Effects of AS160 Modulation on Fatty Acid Transporters Expression and Lipid Profile in L6 Myotubes*. *Cell Physiol Biochem*, 2016. **38**(1): p. 267-82.
157. Maher, A.C., et al., *TBC1D1 reduces palmitate oxidation by inhibiting beta-HAD activity in skeletal muscle*. *Am J Physiol Regul Integr Comp Physiol*, 2014. **307**(9): p. R1115-23.
158. Miklosz, A., et al., *Challenging of AS160/TBC1D4 Alters Intracellular Lipid milieu in L6 Myotubes Incubated With Palmitate*. *J Cell Physiol*, 2017. **232**(9): p. 2373-2386.
159. Hargett, S.R., N.N. Walker, and S.R. Keller, *Rab GAPs AS160 and Tbc1d1 play nonredundant roles in the regulation of glucose and energy homeostasis in mice*. *Am J Physiol Endocrinol Metab*, 2016. **310**(4): p. E276-88.
160. Jain, S.S., et al., *Fatty acid transport and transporters in muscle are critically regulated by Akt2*. *FEBS Lett*, 2015. **589**(19 Pt B): p. 2769-75.
161. Xie, B., et al., *The Inactivation of RabGAP Function of AS160 Promotes Lysosomal Degradation of GLUT4 and Causes Postprandial Hyperglycemia and Hyperinsulinemia*. *Diabetes*, 2016. **65**(11): p. 3327-3340.
162. Qiu, Y., et al., *Exercise sustains the hallmarks of health*. *J Sport Health Sci*, 2023. **12**(1): p. 8-35.
163. Jornayvaz, F.R. and G.I. Shulman, *Regulation of mitochondrial biogenesis*. *Essays Biochem*, 2010. **47**: p. 69-84.
164. Yoon, M.S., *mTOR as a Key Regulator in Maintaining Skeletal Muscle Mass*. *Front Physiol*, 2017. **8**: p. 788.

165. Koh, H.J., J. Brandauer, and L.J. Goodyear, *LKB1 and AMPK and the regulation of skeletal muscle metabolism*. *Curr Opin Clin Nutr Metab Care*, 2008. **11**(3): p. 227-32.
166. Witczak, C.A., et al., *CaMKII regulates contraction- but not insulin-induced glucose uptake in mouse skeletal muscle*. *Am J Physiol Endocrinol Metab*, 2010. **298**(6): p. E1150-60.
167. Kuo, I.Y. and B.E. Ehrlich, *Signaling in muscle contraction*. *Cold Spring Harb Perspect Biol*, 2015. **7**(2): p. a006023.
168. Stanford, K.I. and L.J. Goodyear, *Exercise and type 2 diabetes: molecular mechanisms regulating glucose uptake in skeletal muscle*. *Adv Physiol Educ*, 2014. **38**(4): p. 308-14.
169. Sher, J. and C. Cardasis, *Skeletal muscle fiber types in the adult mouse*. *Acta Neurol Scand*, 1976. **54**(1): p. 45-56.
170. Manttari, S. and M. Jarvilehto, *Comparative analysis of mouse skeletal muscle fibre type composition and contractile responses to calcium channel blocker*. *BMC Physiol*, 2005. **5**(1): p. 4.
171. Wu, H., et al., *Transcriptional analysis of mouse skeletal myofiber diversity and adaptation to endurance exercise*. *J Muscle Res Cell Motil*, 2003. **24**(8): p. 587-92.
172. Lee, S.M., et al., *Muscle fiber type-dependence effect of exercise on genomic networks in aged mice models*. *Aging (Albany NY)*, 2022. **14**(8): p. 3337-3364.
173. Augusto, V., C.R. Padovani, and G.E.R.J.J.o.M.S. Campos, *Skeletal muscle fiber types in C57BL6J mice*. 2017. **21**(2): p. 0-0.
174. Sylow, L., et al., *Rac1 governs exercise-stimulated glucose uptake in skeletal muscle through regulation of GLUT4 translocation in mice*. *J Physiol*, 2016. **594**(17): p. 4997-5008.
175. Sylow, L., et al., *Stretch-stimulated glucose transport in skeletal muscle is regulated by Rac1*. *J Physiol*, 2015. **593**(3): p. 645-56.
176. Raun, S.H., et al., *Rac1 muscle knockout exacerbates the detrimental effect of high-fat diet on insulin-stimulated muscle glucose uptake independently of Akt*. *J Physiol*, 2018. **596**(12): p. 2283-2299.
177. Sylow, L., et al., *Rac1--a novel regulator of contraction-stimulated glucose uptake in skeletal muscle*. *Exp Physiol*, 2014. **99**(12): p. 1574-80.
178. E, L., et al., *Effect of exercise on mouse liver and brain bioenergetic infrastructures*. *Exp Physiol*, 2013. **98**(1): p. 207-19.
179. Chen, W., et al., *Moderate intensity treadmill exercise alters food preference via dopaminergic plasticity of ventral tegmental area-nucleus accumbens in obese mice*. *Neurosci Lett*, 2017. **641**: p. 56-61.
180. Reitman, M.L. and O. Gavrilova, *A-ZIP/F-1 mice lacking white fat: a model for understanding lipotrophic diabetes*. *Int J Obes Relat Metab Disord*, 2000. **24 Suppl 4**: p. S11-4.
181. Chouchani, E.T., L. Kazak, and B.M. Spiegelman, *New Advances in Adaptive Thermogenesis: UCP1 and Beyond*. *Cell Metab*, 2019. **29**(1): p. 27-37.
182. Poher, A.L., et al., *Ectopic UCP1 Overexpression in White Adipose Tissue Improves Insulin Sensitivity in Lou/C Rats, a Model of Obesity Resistance*. *Diabetes*, 2015. **64**(11): p. 3700-12.
183. Mossenbock, K., et al., *Browning of white adipose tissue uncouples glucose uptake from insulin signaling*. *PLoS One*, 2014. **9**(10): p. e110428.
184. de Las Heras, N., et al., *Chronic Exercise Improves Mitochondrial Function and Insulin Sensitivity in Brown Adipose Tissue*. *Front Physiol*, 2018. **9**: p. 1122.
185. Barbosa, M.A., et al., *Physical training improves thermogenesis and insulin pathway, and induces remodeling in white and brown adipose tissues*. *J Physiol Biochem*, 2018. **74**(3): p. 441-454.
186. Wong, C.P., et al., *Cold stress during room temperature housing alters skeletal response to simulated microgravity (hindlimb unloading) in growing female C57BL6 mice*. *Biochimie*, 2023. **210**: p. 61-70.
187. Hylander, B.L. and E.A. Repasky, *Thermoneutrality, Mice, and Cancer: A Heated Opinion*. *Trends Cancer*, 2016. **2**(4): p. 166-175.
188. Scheel, A.K., L. Espelage, and A. Chadt, *Many Ways to Rome: Exercise, Cold Exposure and Diet-Do They All Affect BAT Activation and WAT Browning in the Same Manner?* *Int J Mol Sci*, 2022. **23**(9).

5 Abbreviations

aG4KO	Knockout of the <i>Slc2a4</i> (GLUT4) gene specifically in adipocytes
amG4KO	Knockout of the <i>Slc2a4</i> (GLUT4) gene specifically in adipocytes and skeletal muscle
AICAR	5-Aminoimidazole-4-carboxamide ribonucleotide
AKT	= Protein kinase B (PKB)
AMPK	Adenosine monophosphate-activated protein kinase
AMPK-DN	Skeletal muscle-specific AMPK inactivation (overexpression of a DN = dominant negative AMPK α subunit)
ARK	AMPK-related kinase
AS160	Akt substrate of 160 kDa, = TBC1D4
BAT	Brown adipose tissue
CaMKK	Ca ²⁺ /calmodulin-dependent protein kinase kinase
CaMKII	Ca ²⁺ /calmodulin-dependent protein kinase II
CBD	Calmodulin-binding domain
Cbl	Casitas B-lineage lymphoma
CVD	Cardiovascular disease
D1KO	<i>Tbc1d1</i> -knockout (mouse)
D1/4KO	<i>Tbc1d1/Tbc1d4</i> -knockout (mouse)
D4KO	<i>Tbc1d4</i> -knockout (mouse)
DAG	Diacylglycerol
DGAT	Diacylglycerol transferase
EDL	<i>Extensor digitorum longus</i>
FA	Fatty acid
FABPpm	Fatty acid binding protein
FA-CoA	Fatty acyl coenzyme A
FAO	Fatty acid oxidation
FATP	Fatty acid transport protein
GAP domain	GTPase-activating domain
GLUT4	Glucose transporter type 4
GSV	GLUT4 storage vesicle
HDAC	Histone deacetylase
HDM fraction	High density microsomal
HFD	High-fat diet
iBAT	Interscapular brown adipose tissue
IMCL	Intramyocellular fat content
IR	Insulin receptor
IRAP	Insulin-regulated aminopeptidase
IRS	Insulin receptor substrate
KI	Knockin (mouse)

KO	Knockout (mouse)
LCFA	Long-chain fatty acid
LDM fraction	Light-density microsomal fraction
LKB1	Liver kinase B1
MAPK	Mitogen-activated protein kinase
MEF2	Myocyte enhancer factor-2
mG4KO	Knockout of the <i>Slc2a4</i> (GLUT4) gene specifically in skeletal muscle
mTORC1/S6K	Mammalian target of rapamycin complex 1/serine kinase 6
mTORC2	Mammalian target of rapamycin complex 2
MUFA	Monounsaturated fatty acid
nPKC	“novel” Protein kinase C isoform
NRF-1	Nuclear respiratory factor-1
PGC1α	Peroxisome proliferator activated receptor-coactivator 1 alpha
PDK1	3-phosphoinositide-dependent protein kinase 1
PH	Pleckstrin homology
PI3K	Phosphatidylinositol-3 kinase
PIP₂	Phosphatidylinositol 4,5-bisphosphate
PIP₃	Phosphatidylinositol 3,4,5-trisphosphate
PKB	Protein kinase B (= AKT)
PKC	Protein kinase C
PTB domain	Phosphotyrosine-binding domain
RabGAP	Rab-GTPase-activating protein
RCS	Recombinant-congenic strain
SCD1	Stearoyl-CoA desaturase-1
SCFA	Short-chain fatty acid
SIK	Salt-inducible kinase
SJL	Swiss Jim Lambert
SNARK	SNF1-ARK (SNF = Sucrose non-fermenting)
TAG	Triacylglycerol
TAK1	Transforming growth factor beta-activated kinase 1
TBC1D1	(Tre-2/USP6, BUB2, Cdc16) Domain Family, Member 1
TBC1D4	(Tre-2/USP6, BUB2, Cdc16) Domain Family, Member 4
T2D	Type 2 diabetes
UCP-1	Uncoupling Protein 1
WAT	White adipose tissue
WT	Wildtype

6 Acknowledgments

I would like to express my gratitude to my supervisor and mentor, Professor Hadi Al-Hasani, Director of the Institute for Clinical Biochemistry and Pathobiochemistry at the German Diabetes Center. I am grateful to him for sharing his expertise and providing me with all the necessary facilities for our research, for his continuous scientific guidance, for his enthusiasm and encouragement, and most of all for his optimism and belief that the next experiment would succeed when I lacked the necessary confidence in my abilities or my luck or both.

I would like to thank all colleagues and collaboration partners from the included papers for their constructive feedback and inconvenient questions throughout the project. I would also like to express my gratitude to my colleagues at the DIfE and the DDZ who have provided invaluable support and assistance on countless occasions over the years, enabling me to remain engaged in research to this day. Special thanks to Ulrike Bernhardt, Tanja Dreja, Verena Behrens, Carolin Borchert, Diana Schulze, Deike Hesse, Susanne Neschen, Reinhart Kluge, Ines Grüner, Brigitte Rischke, Annette Schober, Angelika Horrigs, Ilka Römer, Antonia Osmers, Jennifer Schwettmann, Stefan Lehr, Sonja Hartwig, Anette Kurowski, Heidrun Podini, Anke Brumloop, Dagmar Grittner, Birgit Knobloch, Carina Heitmann, Delia Bahn, Kálmán Bódis, Alexander Strom, Bengt Belgardt, Sandra Cames and Nicole Krause for support, guidance and fun.

I would also like to thank all the dedicated PhD, MSc, BSc and MD students who have invested their energy and time into the projects over the years, driving them forward continuously through their curiosity and questioning of so-called well-known facts.

Most importantly, I'd like to thank my family, Julian, Jaromir and Marika, for their endless love and support, without which none of this would have been possible. They've been a constant source of strength for me over the years. Ultimately, they're very supportive of my research, even if they have to share me with it. You're the best!

7 Original publications

Permission for reuse has been obtained from the respective publishing houses where required.

Conventional knockout of *Tbc1d1* in mice impairs insulin- and AICAR-stimulated glucose uptake in skeletal muscle

Janine Dokas^{1*}, Alexandra Chadt^{2*}, Tobias Nolden^{3,#}, Heinz Himmelbauer^{3,4,5}, Juleen R. Zierath^{6,7}, Hans-Georg Joost¹, Hadi Al-Hasani^{2,8¶}

¹German Institute for Human Nutrition, Potsdam, Germany; ²German Diabetes Center, Leibniz Center for Diabetes Research at the Heinrich-Heine-University Düsseldorf, Germany; ³Max Planck Institute for Molecular Genetics, Berlin, Germany; ⁴Centre for Genomic Regulation (CRG), Barcelona, Spain; ⁵Universitat Pompeu Fabra (UPF), Barcelona, Spain; ⁶Department of Molecular Medicine and Surgery, Karolinska Institutet, Stockholm, Sweden; ⁷Department of Physiology and Pharmacology, Karolinska Institutet, Stockholm, Sweden; ⁸German Center for Diabetes Research (DZD).

In the obesity-resistant SJL mouse strain, we previously identified a naturally occurring loss-of-function mutation in the gene for *Tbc1d1*. Characterization of recombinant inbred mice that carried the *Tbc1d1*^{SJL} allele on a C57BL/6J background indicated that loss of TBC1D1 protects from obesity, presumably by increasing the use of fat as energy source. To provide direct functional evidence for an involvement of TBC1D1 in energy substrate metabolism, we generated and characterized conventional *Tbc1d1* knockout mice. TBC1D1-deficient mice showed moderately reduced body weight, decreased respiratory quotient and an elevated resting metabolic rate. Ex vivo analysis of intact isolated skeletal muscle revealed a severe impairment in insulin- and AICAR-stimulated glucose uptake in glycolytic *extensor digitorum longus* (EDL) muscle and a substantially increased rate of fatty acid oxidation in oxidative *soleus* muscle. Our results provide direct evidence that TBC1D1 plays a major role in glucose and lipid utilization, and energy substrate preference in skeletal muscle.

In mice, susceptibility for obesity and diabetes is genetically determined and strain-dependent (1–4). In a cross breeding experiment with obesity-prone NZO mice and obesity-resistant SJL mice, we previously identified *Nob1*, a major quantitative trait locus (QTL) on chromosome 5 that was linked to body weight and fat mass (5). Characterization of a recombinant inbred mouse strain (B6.SJL.RCS.*Nob1.10*) that carried a 10 Mbp fragment (Chr. 5; 64.3–73.15 Mbp) of the critical QTL region from the SJL strain on a C57BL/6J background revealed that *Nob1* represents an obesity suppressor: mice carrying the *Nob1.10*^{SJL} allele showed reduced body weight and reduced adiposity (6). Moreover, B6.SJL.RCS.*Nob1.10*^{SJL} mice showed altered substrate preference in skeletal muscle, resulting in increased fatty acid oxidation and decreased insulin-stimulated glucose uptake. Further molec-

ular analysis of the critical QTL region in these mice revealed a SJL-specific loss-of-function mutation in the gene for *Tbc1d1*, leading to the complete loss of the protein (6). TBC1D1, a Rab-GTPase-activating protein, is closely related to the insulin signaling protein AS160 (TBC1D4) and is predominantly expressed in skeletal muscle. Both TBC1D1 and TBC1D4 have been implicated to play important roles in the regulation of glucose transport (7–9). Furthermore, TBC1D1 is involved in the regulation of lipid utilization in skeletal muscle, where the mutation in the gene may protect against obesity in mice (6). As a result, the mutated *Tbc1d1* was considered as the most likely candidate gene for the *Nob1* QTL.

Nevertheless, the 10 Mbp recombinant congenic donor fragment contained additional alleles from SJL, in addition to the mutated *Tbc1d1*^{SJL} gene that were transferred

ISSN Print 0013-7227 ISSN Online 1945-7170

Printed in U.S.A.

Copyright © 2013 by The Endocrine Society

Received November 20, 2012. Accepted July 18, 2013.

Abbreviations: AICAR, Aminoimidazole carboxamide ribonucleotide; EDL, Extensor digitorum longus; RMR, Resting metabolic rate

onto the C57BL/6J background: 49 protein coding genes, 4 pseudogenes, and one microRNA gene (Supplementary Table 1). In our previous study, we performed sequence analysis of 19 genes in the *Nob1* peak region and identified *Tbc1d1* as the only gene in the region with a SJL-specific variation in the coding region (6). Therefore, other, yet unknown SJL-specific gene variants might have contributed to the phenotype of B6.SJL.RCS.*Nob1.10* mice. The aim of the present study was to provide direct evidence for an involvement of TBC1D1 in glucose and lipid utilization in skeletal muscle and whole body energy homeostasis. Furthermore, we investigated whether disruption of *Tbc1d1* may represent the causal defect underlying the *Nob1* QTL. To confirm the effect of *Tbc1d1* deletion on body weight, body composition and fuel utilization, we generated a conventional *Tbc1d1* knockout mouse by gene trap technology (10). Our results provide direct evidence that TBC1D1 deficiency reduces body weight, impairs glucose utilization and increases lipid oxidation in skeletal muscle.

Materials and Methods

Materials. Radiochemicals were purchased from American Radiolabeled Chemicals, St. Louis, USA ([9,10(n)-³H] palmitic acid, 1 mCi/ml; 2-[1,2-³H(N)] deoxy-D-glucose, 1 mCi/ml) and from Hartmann Analytic, Braunschweig, Germany ([1-¹⁴C]-D-Mannitol, 0.1 mCi/ml). Human recombinant insulin Actrapid HM Penfill from Novo Nordisk Pharma GmbH (Mainz, Germany) was used throughout the experiments. AICAR (Aminoimidazole carboxamide ribonucleotide) was purchased from Enzo Life Sciences, Lörrach, Germany.

Experimental animals. For generation of *Tbc1d1* knockout mice, the gene-trap method was used. An embryonic stem cell (ESC) clone (E140H06) with a Sv129P2 genetic background (E14TG2a.4) was obtained from the German Gene Trap Consortium (Helmholtz Zentrum, München, Germany). ES cells were injected into blastocysts, which were implanted into pseudopregnant females. Chimeric males were mated with female C57BL/6J mice and F1 offspring carrying the transgene were backcrossed 5–10 times onto C57BL/6J background to receive a breeding colony. Animals were kept in accordance with the NIH guidelines for the care and use of laboratory animals and all experiments were approved by the Ethics Committee of the State Ministry of Agriculture, Nutrition and Forestry (States of Brandenburg and North Rhine-Westphalia, Germany). Three to six mice per cage (macrolon type III) were housed at a temperature of 22°C and a 12 h light-dark cycle (lights on at 6 a.m.). After weaning at the age of 19–21 d, animals received either a standard chow with 19% (wt/wt) protein (23 cal%), 3.3% fat (8 cal%) and 54.1% carbohydrates (69 cal%) containing 3.06 kcal/g energy (V153x R/M-H, Ssniff, Soest, Germany) or a high-fat diet with 26.2% (wt/wt) protein (20 cal%), 34.9% fat (60 cal%) and 26.3% carbohydrates (20 cal%) containing 5.24 kcal/g energy (D12492, Research Diets, New Brunswick, USA). Animals had

access to food and water ad libitum. **Genotyping** – Isolation of DNA from mouse tail tips was performed with the InViSorb Genomic DNA Kit II (Invitex, Berlin, Germany). Genotyping of mice was performed by PCR with three primers (Fwd: 5'-CAG GTG CCT GTT CAC TTC AA-3', Rev1: 5'-AAG TCT CCA GCG TCT GCT TC-3', Rev2: 5'-ATT CAG GCT GCG CAA CTG TTG GG-3').

RNA extraction and cDNA synthesis. Total RNA was extracted from *soleus* muscle with QIAzol and the RNeasy Mini Kit (Qiagen, Hilden, Germany) according to the manufacturer's guidelines. cDNA was transcribed from 2 µg of total RNA using GoScript Reverse Transcriptase (Promega, Mannheim, Germany) and random primers p(dN)₆ (Roche, Mannheim, Germany).

Quantitative real-time PCR. Quantitative real-time PCR was performed using a SYBR Green Master Mix (Applied Biosystems, Foster City, USA) and primers for *Tbc1d1* (P1: 5'-CTC AGC CCG GAG TTC TGA-3' (exon 1), P2: 5'-GAT GCT TCC TCG CTG TGA AT-3' (exon 2)), and for *Actb* (Fwd: 5'-GCC AAC CGT GAA AAG ATG AC-3', Rev: 5'-TAC GAC CAG AGG CAT ACA G-3') as endogenous control. Relative ratios of mtDNA to nuclear DNA were determined with primers for the mitochondrial *Nd2* gene (Fwd: 5'-AGG GAT CCC ACT GCA CAT AG-3', Rev: 5'-TGA GGG ATG GGT TGT AAG GA-3') and nuclear-encoded *18S rRNA* gene (Fwd: 5'-TGA GGC CAT GAT TAA GAG GG-3', Rev: 5'-AAGAAT TTC ACC TCT AGC GGC-3'). *Cpt1b* (Mm00487200_m1) was measured by TaqMan PCR with as *eEF2* endogenous control. The analyses were performed with the Applied Biosystems 7500 Fast Real-Time PCR-System (Applied Biosystems, Foster City, USA). Data were normalized according to the Δ Ct method (11).

Analysis of body weight, body composition and body length. Body weight was measured with an electronic scale (Sartorius, Göttingen, Germany), body composition (body fat and lean mass) was analyzed with a nuclear magnetic resonance spectrometer (Bruker-Minispes NMR-Analyzer mq10, Bruker Optics, Ettlingen, Germany). Body length was determined by measuring the nose-to-anus length.

Indirect calorimetry. Animals were placed in individual cages and respiratory quotient (RQ) and energy expenditure (EE) were measured after an adaption phase of 24 h by indirect calorimetry (Hartmann & Braun, Frankfurt, Germany). The flow rate was 0.5 l/min and rates of oxygen consumption ($\dot{V}O_2$) and carbon dioxide production ($\dot{V}CO_2$) were monitored for 23 h at 22°C. Animals had free access to water. Food was removed during daytime (6 a.m. – 6 p.m.). The RQ represents the quotient of $\dot{V}CO_2/\dot{V}O_2$, total energy expenditure (TEE) was calculated with the equation $TEE = 16.17 \dot{V}O_2 + 5.03 \dot{V}CO_2 + 5.98 N$, where N is excreted nitrogen and was set 0.1 g/d. The 15 lowest values represent the resting metabolic rate (RMR). Whole body carbohydrate and fat oxidation rates (g/min) were calculated using the following equations: carbohydrate oxidation rate = $4.585 \times \dot{V}CO_2$ (l/min) - $3.226 \times \dot{V}O_2$ (l/min); fat oxidation rate = $1.695 \times \dot{V}O_2$ (l/min) - $1.701 \times \dot{V}CO_2$ (l/min) (12).

Blood parameters. Blood glucose was determined with a glu-

cometer (Contour, Bayer, Leverkusen, Germany). Plasma insulin and plasma IGF-1 were measured with ELISA (Insulin Mouse Ultrasensitive ELISA, Alpco, Salem, USA; DuoSet ELISA Development System, R&D Systems, Abington, UK). Plasma ketone bodies were measured with the Autokit Total Ketone Bodies, free fatty acids with the NEFA-HR (2) system (both Wako Chemicals, Neuss, Germany). Triglycerides were determined with the Serum Triglyceride Determination Kit (Sigma-Aldrich, Steinheim, Germany). All plasma parameters were determined according to the manufacturer's guidelines.

Glucose tolerance test. Animals were kept individually and were fasted for 16 h before the experiment. Sterile glucose (2 g/kg body weight, 20% solution) was injected intraperitoneally. Blood samples were taken at 0, 15, 30, 60 and 120 min from the tail tip and glucose and insulin levels were determined as described above.

Liver triglycerides. 30 mg liver tissue was homogenized in 1 ml 10 mM sodium phosphate buffer containing 1% polyoxyethylene 10 tridecylethan and 1 mM EDTA using a Tissue Lyser (Qiagen, Hilden, Germany). The homogenate was incubated at 70°C for 5 min and centrifuged at 16,000 rcf for 10 min. The supernatant was used to measure liver triglycerides with the (TRIGS)-Kit (Randox, Crumlin, UK).

Analysis of glucose uptake and fatty acid oxidation in isolated skeletal muscles. *Extensor digitorum longus* (EDL) muscles were removed from anesthetized mice and incubated for 30 min at 30°C in vials containing preoxygenated (95% O₂/ 5% CO₂) Krebs-Henseleit buffer (KHB) containing 5 mM HEPES and supplemented with 5 mM glucose and 15 mM mannitol. All incubation steps were conducted under continuous gassing (95% O₂/ 5% CO₂) at 30°C and slight agitation. After recovery, muscles were transferred to new vials and incubated for 30 min in KHB/ 5 mM HEPES/ 15 mM mannitol/ 5 mM glucose under basal condition or in the presence of 120 nM insulin (Actrapid, Novo Nordisk, Mainz, Germany) or 2 mM AICAR (Enzo Life Sciences, Lörrach, Germany), respectively throughout the duration of the experiment. Muscles were then transferred to new vials containing preoxygenated KHB supplemented with AICAR or insulin and 15 mM mannitol and incubated for 10 min. Thereafter, muscles were transferred to new vials containing preoxygenated KHB supplemented with 1 mM [³H] 2-deoxy-glucose (2.5 mCi/ml) and 19 mM [¹⁴C]mannitol (0.7 mCi/ml) for 20 min. Muscles were immediately frozen in liquid nitrogen and stored at -80°C for subsequent signal transduction analysis. Cleared protein lysates were used to determine incorporated radioactivity by scintillation counting. To assess palmitate oxidation, *soleus* muscles were incubated in pregassed KHB containing 15 mM mannitol, 5 mM glucose, 3.5% fatty acid-free BSA, 4 mCi/ml [³H]palmitate and 600 μM unlabeled palmitate with or without 2 mM AICAR at 30°C for 2 h. After absorption of fatty acids to activated charcoal, fatty acid oxidation was determined by scintillation measurement of tritiated water.

Mitochondrial enzyme activity. The activity of citrate synthase (CS) was determined in soleus muscle homogenates using a citrate synthase assay kit (CS0720, Sigma-Aldrich) according to the manufacturer's directions. Enzyme activity was deter-

mined in triplicate based on the formation of 5-thio-2-nitrobenzoic acid at 415 nm on a spectrophotometer (iMark, Bio-Rad, Hercules, CA, USA).

SDS-PAGE and Western Blot. Tissues were homogenized with cell lysis buffer containing 20 mM Tris, 150 mM NaCl, 1 mM EGTA, 1 mM EDTA, 1% (v/v) Triton-X-100, 1 mM Na₃VO₄, 1 mM β-glycerolphosphat, 1 mM NaF, 2.5 mM Na₄P₂O₇ and a proteinase inhibitor cocktail (Complete, Roche, Mannheim, Germany) and centrifuged for 10 min at 16,000 rcf at 4°C. Protein content was determined from the supernatant with the BCA Protein Assay Kit (Pierce, Rockford, USA) as described in the manual. Protein samples (20 μg) were separated by SDS-PAGE and transferred onto nitrocellulose or polyvinylidene fluoride membranes by immunoblot analysis. Antibodies against TBC1D1, GLUT4 and GLUT1 were described previously (6). Antibodies against TBC1D4/AS160 (07-741, Millipore, Temecula, USA), ACC (#3662), pACC (Ser79) (#3661), AKT (#9272), pAKT (Ser473) (#9271), AMPKα (#2603), pAMPK (Thr172) (#2535, Cell Signaling, Danvers, USA) and GAPDH (AM4300, Ambion, Austin, USA) were used at dilutions of 1:1000. HRP-conjugated rabbit-antimouse and goat-antirabbit IgG (Dianova, Hamburg, Germany) were used as secondary antibodies in a dilution of 1:20,000. Immunodetection was performed with ECL Western blot detection analysis system (GE Healthcare, Buckinghamshire, UK). For quantification protein levels were normalized to GAPDH.

Statistics. Data are reported as means ± SEM. Significant differences were determined by one-way or two-way ANOVA (post hoc test, Bonferroni multiple comparison test) or paired two-tailed Student's t test as indicated in the Figure legends. Values of *P* < .05 were considered statistically significant.

Results

Generation of a Null-allele *Tbc1d1* mouse

To generate a *Tbc1d1* knockout mouse, we obtained a mouse ESC line deficient in TBC1D1 from the German Gene Trap Consortium (clone E140H06; GGTC). The genomic locus of the genetrapp vector (rFlipROSAbeo) insertion site as supplied by GGTC was verified by PCR and sequencing of genomic DNA isolated from trapped Sv129P2 ES cells. The genetrapp cassette containing an in-frame splice acceptor site followed by the coding sequence for a β-galactosidase/neomycin (β-Geo) fusion protein was located in intron 2 behind exon 3, which contains the TBC1D1 translation initiation codon (Figure 1A). Thus, the mutated *Tbc1d1* gene is predicted to yield a ~160 kDa fusion protein where 138 N-terminal amino acids of TBC1D1 are fused to β-galactosidase/neomycin (β-Geo). Chimeric males were then derived from genetrapp Sv129P2 ES cells and used to establish heterozygous wild-type/E140H06 founders; homozygous offspring were generated from heterozygous mating pairs. Genotypes were confirmed by PCR performed on gDNA isolated from

mouse tails (Figure 1B). We determined mRNA expression of *Tbc1d1* by quantitative Realtime PCR using a specific primer pair for the exon 1/exon2 junction in the *Tbc1d1* transcript (Figure 1A). Homozygous carriers of the trapped TBC1D1 (*Tbc1d1*^{-/-}) displayed reduced mRNA levels in skeletal muscle (Figure 1C) and other tissues (not shown). Consistently, β -galactosidase activity was undetected in sections of skeletal muscle and other tissues from these mice (not shown). Western Blot analysis of skeletal muscle (*M. extensor digitorum longus* (EDL), *M. soleus*) from *Tbc1d1*^{-/-} mice confirmed total loss of TBC1D1 protein, whereas the protein expression level of the related TBC1D4 was unaltered (Figure 1D-E and Supplementary Figure 1).

TBC1D1 depletion leads to decreased body weight, but no changes in glycemia

Male *Tbc1d1*^{-/-} mice and wildtype littermates were raised either on a standard diet (8% calories from fat) or a high-fat diet (60 kcal% fat), and body weight was measured at different time points between week 3 and week 15. Body composition was determined at week 15 by nuclear resonance spectroscopy (NMR). Body weight of standard diet-fed *Tbc1d1*^{-/-} mice was reduced compared to

the controls (Figure 2A). Animals of both genotypes gained substantially more weight when fed a high-fat diet, compared to standard diet (Figure 2A). However, *Tbc1d1*^{-/-} mice showed mildly reduced body weight compared to control littermates, which reached statistical significance at the latest time point (week 15; $P < .05$; Figure 2A). For *Tbc1d1*^{-/-} mice on a standard diet, the reduction in body weight was accompanied with decreased lean mass (Figure 2B), but fat mass was unaltered (Figure 2C). In contrast, *Tbc1d1*^{-/-} mice fed a high-fat diet also displayed reduced fat mass compared to the wildtype control mice (Figure 2C). Body length of mice (*Tbc1d1*^{+/+} vs. *Tbc1d1*^{-/-}: 9.9 ± 0.13 vs. 9.8 ± 0.07 cm; $n = 8-11$; $P = .932$), IGF-1 levels in plasma (*Tbc1d1*^{+/+} vs. *Tbc1d1*^{-/-}: 53.9 ± 4.3 vs. 58.9 ± 5.2 ng/ml; $n = 18-19$; $P = .508$) were not different between the genotypes. Plasma glucose and insulin levels, as well as glucose and insulin tolerance were determined in high-fat diet fed *Tbc1d1*^{-/-} mice and wild-type littermates. *Tbc1d1*^{-/-} mice showed normal postprandial plasma glucose levels (Figure 3A) and normal insulin levels in both fed and fasted states (not shown). Glucose tolerance was measured after an intraperitoneal injection of glucose in fasted animals raised on high-fat

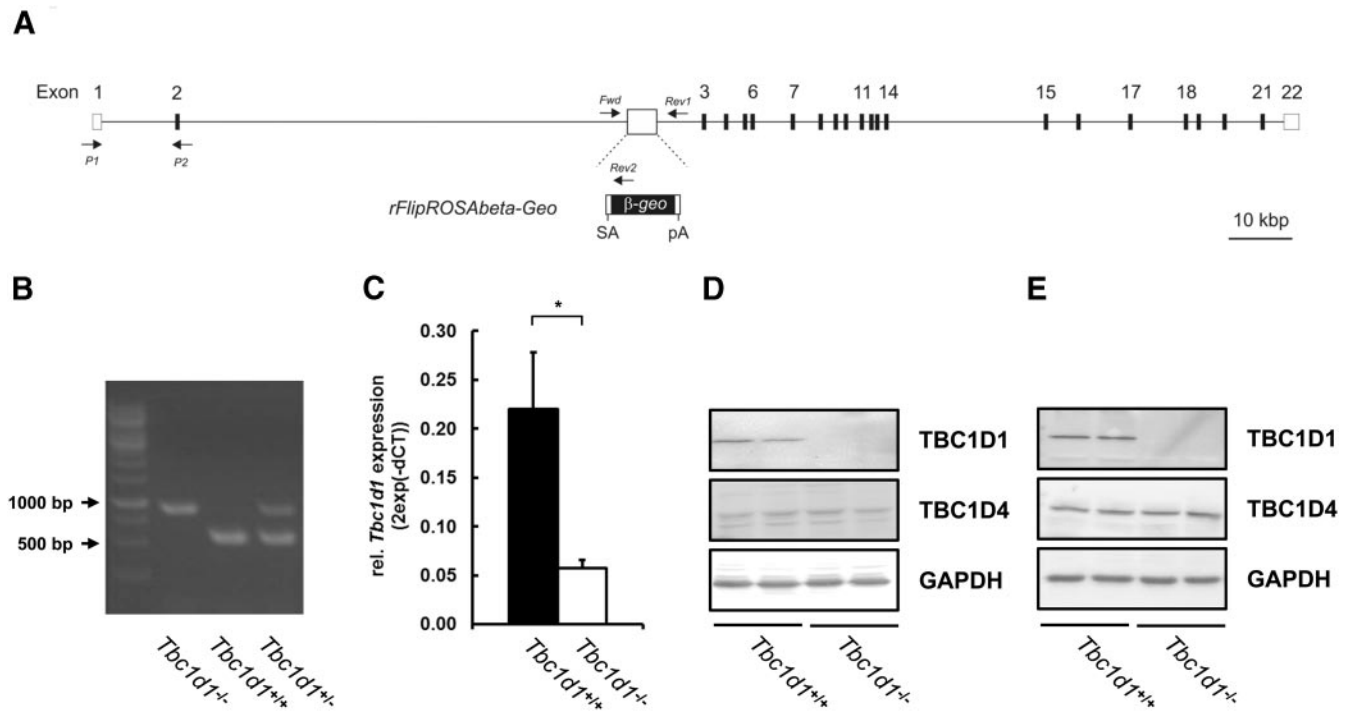


Figure 1. Targeted disruption of the *Tbc1d1* gene. A) A β -geo cassette containing a splice acceptor site (SA) and a polyadenylation signal (PA) was integrated into intron 2 of the *Tbc1d1* gene. Indicated are the primer positions used for genotyping (*Fwd*, *Rev1*, *Rev2*) and quantitative Realtime PCR (*P1*, *P2*); B) Genotyping of homozygous *Tbc1d1* knockout mice (*Tbc1d1*^{-/-}), wildtype littermate controls (*Tbc1d1*^{+/+}) and heterozygous allele carriers (*Tbc1d1*^{+/-}) using PCR primers indicated in A; C) Quantitative Realtime PCR of endogenous *Tbc1d1* in *M. tibialis anterior* (TA) skeletal muscle from *Tbc1d1*^{-/-} mice and controls. Data represent mean values, $n = 8 \pm$ SEM; D-E) Western Blot analysis of TBC1D1 and TBC1D4 in *soleus* (D) and *EDL* (E) muscles from *Tbc1d1*^{-/-} mice and controls. GAPDH expression was used as loading control. * $P < .05$ (Student's t test)

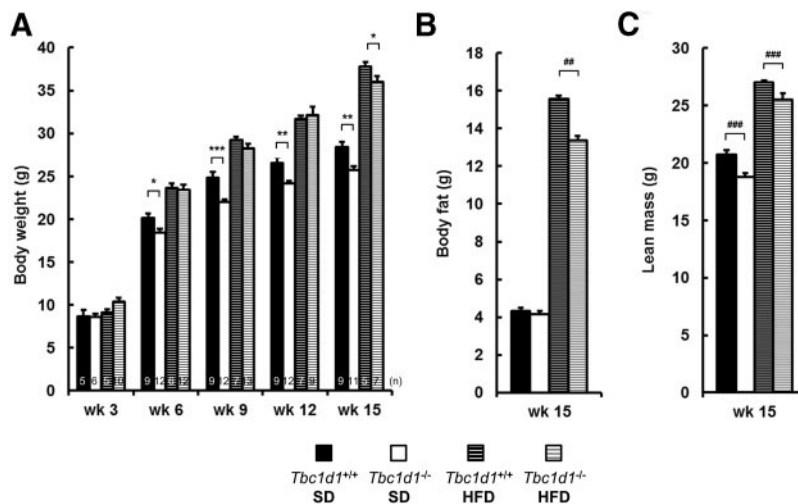


Figure 2. Body weight and body composition in *Tbc1d1* knockout mice. A) Body weight of male *Tbc1d1*^{-/-} mice and controls raised on either standard diet (SD) or high-fat diet (HFD); Data represent mean values, n = 5–13 ± SEM as indicated; B) Body fat mass and (C) lean mass of 15-wk old male *Tbc1d1*^{-/-} mice and controls as measured by nuclear magnetic resonance (NMR). Data represent mean values, n = 5–9 ± SEM as indicated; **P* < .05, ***P* < .01, and ****P* < .001 wildtype versus *Tbc1d1*^{-/-} (one-way ANOVA with post hoc Bonferroni Multiple comparison tests); ##*P* < .01, and ###*P* < .001 wildtype versus *Tbc1d1*^{-/-} (two-way ANOVA with post hoc Bonferroni Multiple comparison tests).

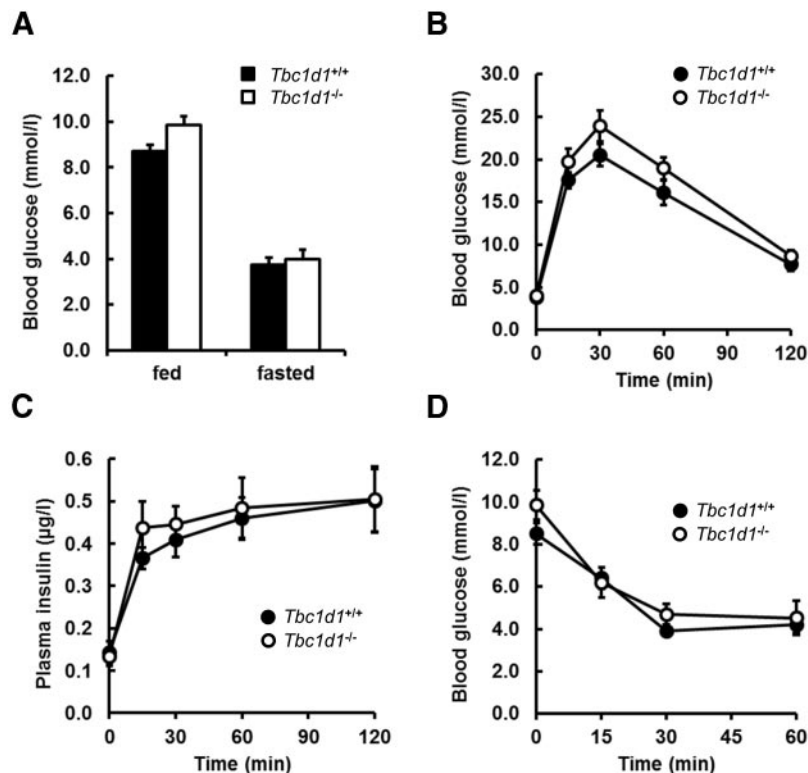


Figure 3. Blood glucose, insulin and glucose tolerance in *Tbc1d1* knockout mice. A) Blood glucose levels of 16-wk-old male *Tbc1d1*^{-/-} mice and controls raised on high-fat diet (HFD), determined in the postprandial and fasted state (16 h fasting o/n); B) Blood glucose and plasma insulin levels (C) during an intraperitoneal glucose tolerance test with 12-wk-old male *Tbc1d1*^{-/-} mice and controls raised on HFD; D) Blood glucose levels during an intraperitoneal insulin tolerance test in 12-wk-old male *Tbc1d1* knockout mice raised on HFD. Data represent mean values, n = 6–8 ± SEM; no significant differences were observed between genotypes (two-way ANOVA with post hoc Bonferroni Multiple comparison tests).

diet. Genotype dependent differences were not observed for blood glucose levels, as well as plasma insulin levels (Figure 3B and 3C). Likewise, insulin tolerance, analyzed in response to an intraperitoneal injection of insulin, was similar between *Tbc1d1*^{-/-} mice and wildtype littermates (Figure 3D).

TBC1D1 depletion increases fatty acid utilization and resting metabolic rate in vivo

We investigated whether inactivation of *Tbc1d1* alters energy homeostasis. At the age of 10 wk, the animals were placed in metabolic cages. Indirect calorimetry was conducted for 24 h and respiratory quotient, as well as energy expenditure were determined. On a standard diet, *Tbc1d1*^{-/-} mice and wildtype mice showed a similar respiratory quotient and energy expenditure, respectively (not shown). In contrast, respiratory quotient in both light and dark phase was reduced (Figure 4A and B) in high-fat diet fed *Tbc1d1*^{-/-} mice when compared to the controls (*Tbc1d1*^{+/+} vs. *Tbc1d1*^{-/-}: RQ_{24h}: 0.798 ± 0.006 vs. 0.782 ± 0.006; *P* < .05). Whole body carbohydrate oxidation rates were lower (Figure 4C) in *Tbc1d1*^{-/-} mice during both light (*Tbc1d1*^{+/+} vs. *Tbc1d1*^{-/-}: 0.461 ± 0.029 vs. 0.382 ± 0.023 mg/min; *P* < .05) and dark phase (1.027 ± 0.043 vs. 0.876 ± 0.041 mg/min; *P* < .05). Furthermore, whole body fat oxidation rates were increased (Figure 4D) in *Tbc1d1*^{-/-} mice during light (*Tbc1d1*^{+/+} vs. *Tbc1d1*^{-/-}: 0.572 ± 0.022 vs. 0.639 ± 0.022 mg/min; *P* < .05) and dark phase (0.540 ± 0.022 vs. 0.598 ± 0.013 mg/min; *P* < .05), respectively. While *Tbc1d1*^{-/-} mice showed moderately elevated total energy expenditure, which was not statistically significant when averaged over 24 h (Figure 4E), the resting metabolic rate (RMR) of

Tbc1d1^{-/-} mice was increased (*Tbc1d1*^{+/+} vs. *Tbc1d1*^{-/-}; RMR: 1.56 ± 0.01 vs. 1.63 ± 0.03 ; $P < .05$; Figure 4F).

TBC1D1 knockout mice display altered energy substrate utilization in skeletal muscle

TBC1D1 is predominantly expressed in skeletal muscle, with highest levels found in glycolytic fibers (6). To assess the effect of TBC1D1 deletion on energy substrate metabolism in skeletal muscle, we investigated both insulin-stimulated glucose uptake and fatty acid oxidation in intact isolated skeletal muscle of TBC1D1-deficient mice. EDL muscles from 16-wk-old male *Tbc1d1*^{-/-} mice and corresponding wildtype littermates were isolated and assayed for insulin- and AICAR-stimulated uptake of [³H]2-deoxyglucose as described in the methods section. *Tbc1d1*^{-/-} mice showed a substantially impaired 2-deoxyglucose uptake in the insulin-stimulated state (3.82 ± 0.24 vs. 7.35 ± 0.62 nmol/20 min; $P < 10^{-5}$, for *Tbc1d1*^{-/-} vs wildtype mice, respectively; Figure 5A). Likewise, AICAR-stimulated uptake of 2-deoxyglucose was markedly decreased in EDL muscles from *Tbc1d1*^{-/-} mice (3.56 ± 0.20 vs. 7.22 ± 0.73 nmol/20 min; $P < 10^{-3}$, for *Tbc1d1*^{-/-} vs. wildtype mice, respectively; Figure 5B). Sim-

ilar results for insulin-stimulated glucose uptake were obtained with isolated EDL muscle from high-fat fed mice (Supplementary Figure 2). We next investigated whether insulin or AMP kinase (AMPK) signaling were impaired in skeletal muscle from *Tbc1d1*^{-/-} mice, respectively. Basal and insulin (120 nM; 60 min) stimulated EDL muscle was homogenized, and AKT expression and phosphorylation of AKT^{Ser473} was analyzed by Western blot. AKT expression and phosphorylation, respectively was similar between genotypes (Figure 5C). In addition, basal and AICAR-stimulated (2 mM; 60 min) *soleus* muscle were homogenized, and both AMPK expression and phosphorylation of AMPK^{Thr172} was analyzed by Western blot. Quantitative assessment of replicate skeletal muscle samples revealed that neither expression nor phosphorylation of AMPK, respectively differed between genotypes (Figure 5D).

To further examine the mechanism for the reduced insulin-stimulated glucose uptake in skeletal muscle from *Tbc1d1*^{-/-} mice, EDL muscle from 16-wk-old male *Tbc1d1* knockout mice and wildtype mice were homogenized and the abundance of GLUT4 protein was determined by

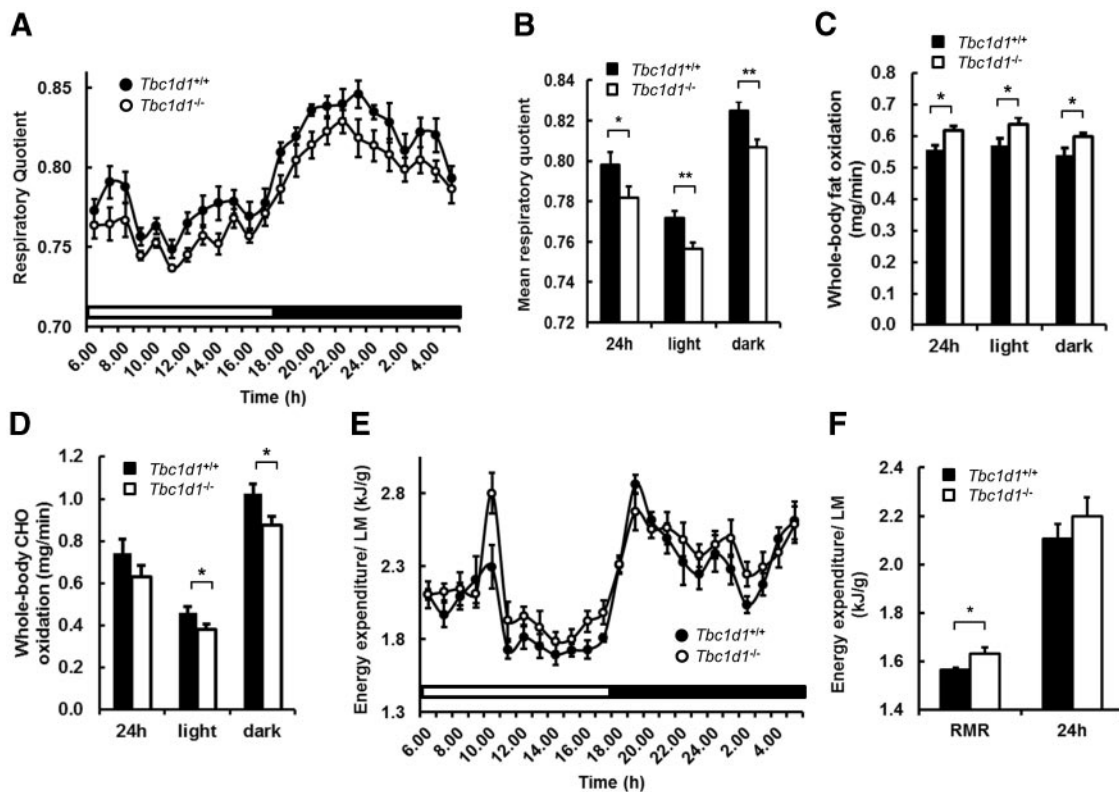


Figure 4. Respiratory quotient and energy expenditure of *Tbc1d1* knockout mice. A) Respiratory quotient of 10-wk-old male *Tbc1d1*^{-/-} mice and controls raised on high-fat diet (HFD), measured by indirect calorimetry over 24h; B) Mean values of respiratory quotients for 24h, light and dark phase, respectively; C, D) Estimated whole-body fat and carbohydrate (CHO) oxidation rates for 24h, light and dark phase, respectively; E) Energy expenditure of HFD-fed 10-wk-old male *Tbc1d1*^{-/-} mice and controls. Lean mass (LM) was determined by NMR; F) Resting metabolic rate (RMR) and mean 24h energy expenditure of HFD-fed 10-wk-old male *Tbc1d1*^{-/-} mice and controls; Data represent mean values, $n = 7-8 \pm$ SEM; * $P < .05$ and ** $P < .01$ wildtype vs. *Tbc1d1*^{-/-} (Student's t test).

Western blot analysis. GLUT4 protein abundance was reduced in *Tbc1d1*^{-/-} mice by approximately 50% (Figure 5E). In contrast, expression of the GLUT4-associated aminopeptidase IRAP (13) and GLUT1 were unaltered between *Tbc1d1* knockout and wildtype mice (Figure 5E,F).

To determine lipid utilization of skeletal muscle, *soleus* muscles from 16-wk-old male *Tbc1d1*^{-/-} mice and corresponding wildtype littermates were isolated and incubated with [³H]palmitate in the absence or presence of AICAR, and fatty oxidation was determined as described (6). Depletion of TBC1D1 increased fatty acid oxidation under basal conditions (3.29 ± 0.25 vs. 2.37 ± 0.20 pmol/min \times mg; $P < .001$; Figure 6A). Basal fatty acid oxidation in *soleus* muscle of *Tbc1d1*^{-/-} mice was increased to the level observed in AICAR-stimulated *soleus* muscle from wildtype mice. Moreover, AICAR-stimulated fatty acid oxidation was further enhanced in *Tbc1d1*^{-/-} mice (4.43 ± 0.32 vs. 3.28 ± 0.33 pmol/min \times mg; $P < .05$; Figure 6A), resulting in an almost 2-fold increase in fatty acid oxida-

tion over basal levels of control mice. Similarly, isolated *soleus* muscle from high-fat fed *Tbc1d1*^{-/-} mice showed elevated fatty acid oxidation (Supplementary Figure 2). Basal and AICAR (2 mM; 2 h) stimulated *soleus* muscles were then homogenized, and AMPK expression and phosphorylation of AMPK^{Thr172} was analyzed by Western blot. AICAR stimulation resulted in a robust increase in phosphorylation of AMPK^{Thr172} (Figure 6B), but neither expression nor phosphorylation of AMPK in response to AICAR (Figure 6C) differed between the two genotypes. We further analyzed expression and phosphorylation of Acetyl-CoA Carboxylase (ACC) by Western blot (Figure 6B). Neither expression nor phosphorylation of ACC (ACC^{Ser79}) in response to AICAR differed between the two genotypes (Figure 6D). Moreover, triglyceride levels of gastrocnemius muscle were not different in TBC1D1-deficient mice compared to control animals (Supplementary Figure 2). Likewise, mitochondrial DNA (mtDNA) copy number, citrate synthase (CS) enzyme activity and

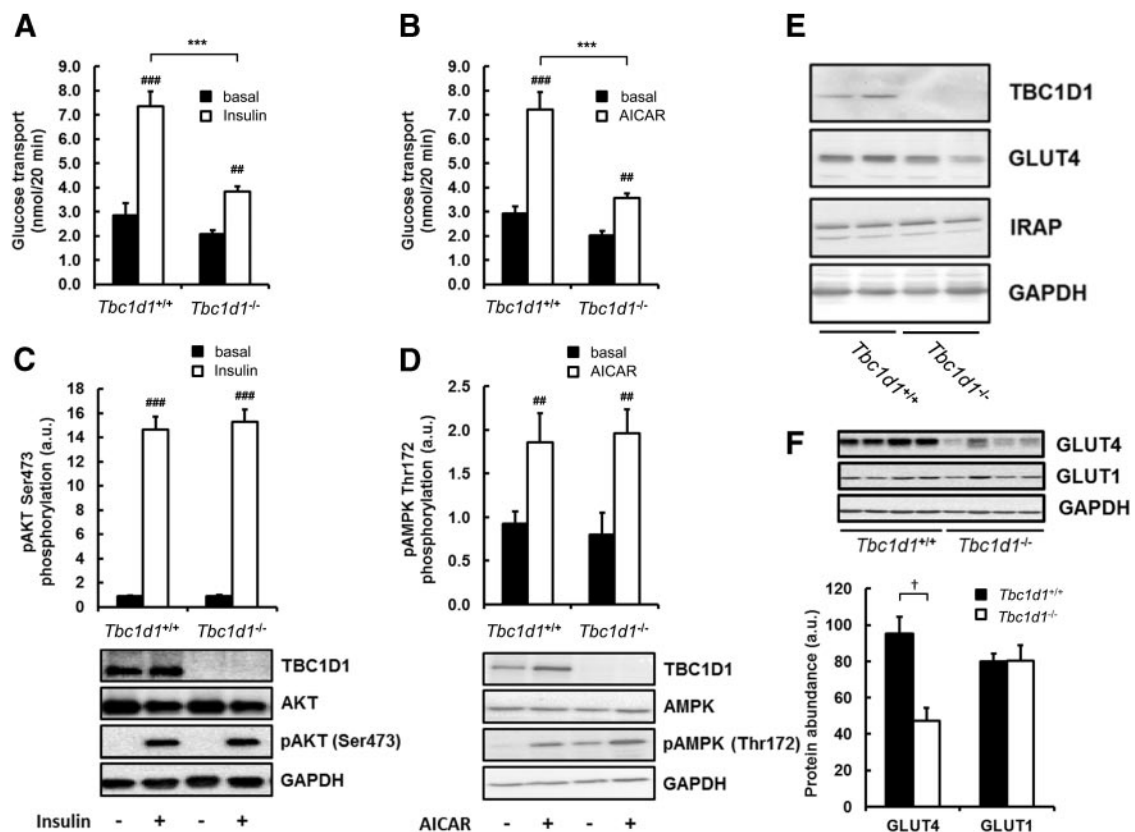


Figure 5. Ex vivo 2-deoxy-[³H]glucose uptake in skeletal muscle of *Tbc1d1* knockout mice. Intact *Extensor digitorum longus* (EDL) muscles from 16-wk-old standard diet (SD)-fed male *Tbc1d1*^{-/-} mice and controls were isolated and assayed for uptake of 2-deoxy-[³H]glucose as described in methods. Muscle lysates were then subjected to Western blot analysis. A) Basal and insulin-stimulated (120 nM) 2-deoxy-[³H]glucose uptake; B) basal and AICAR-stimulated (2 mM) 2-deoxy-[³H]glucose uptake. Data represent mean values, $n = 6-9 \pm$ SEMC) Genotype-dependent expression of TBC1D1, AKT, and basal and insulin-stimulated AKT (Ser473) phosphorylation; D) Genotype-dependent expression of TBC1D1, AMPK α , and basal and AICAR-stimulated AMPK (Thr172) phosphorylation; E) Genotype-dependent expression of TBC1D1, GLUT4 and IRAP; Data represent mean values, $n = 8 \pm$ SEM; F) Genotype-dependent expression of GLUT4 and GLUT1 in *M. tibialis anterior* (TA) lysates from 16-wk-old *Tbc1d1*^{-/-} mice and wild-type controls. Data represent mean values, $n = 4-5 \pm$ SEM; *** $P < .001$ wildtype vs. *Tbc1d1*^{-/-}; # $P < .05$, ## $P < .01$ and ### $P < .001$ basal vs. insulin or AICAR (two-way ANOVA with post hoc Bonferroni Multiple comparison tests); + $P < .01$ wildtype versus *Tbc1d1*^{-/-} (Student's t test).

expression of *Cpt1b* in soleus muscle were not different between the two genotypes (Supplementary Figure 3).

Contribution of TBC1D1 knockout to elevated hepatic triglycerides in SJL/J mice

Elevated fatty acid oxidation in skeletal muscle of SJL/J mice has been proposed to prevent fasting-induced hepatic steatosis in this mouse strain when fed a standard diet (14).

As SJL mice carry a naturally occurring loss-of-function mutation in *Tbc1d1*, we determined whether TBC1D1-deficiency accounts for the resistance of SJL/J mice to fasting-induced increases in hepatic triglyceride content. We therefore determined fasting liver triglycerides and circulating levels of lipids in standard diet-fed *Tbc1d1*-deficient SJL/J mice, and C57BL/6J mice with or without a functional *Tbc1d1*-gene, respectively. Consistent with previous findings (14), C57BL/6J mice displayed significantly higher levels of hepatic triglycerides, circulating triglycerides, free fatty acids and ketone bodies after 24-h fasting compared to fasted SJL/J mice, respectively (Figure 7A-D). However, *Tbc1d1*-deficient C57BL/6J mice displayed similar fasting levels of hepatic triglycerides, circulating triglycerides, free fatty acids and ketone bodies compared to wildtype littermates on a C57BL/6J background (Figure 7A-D).

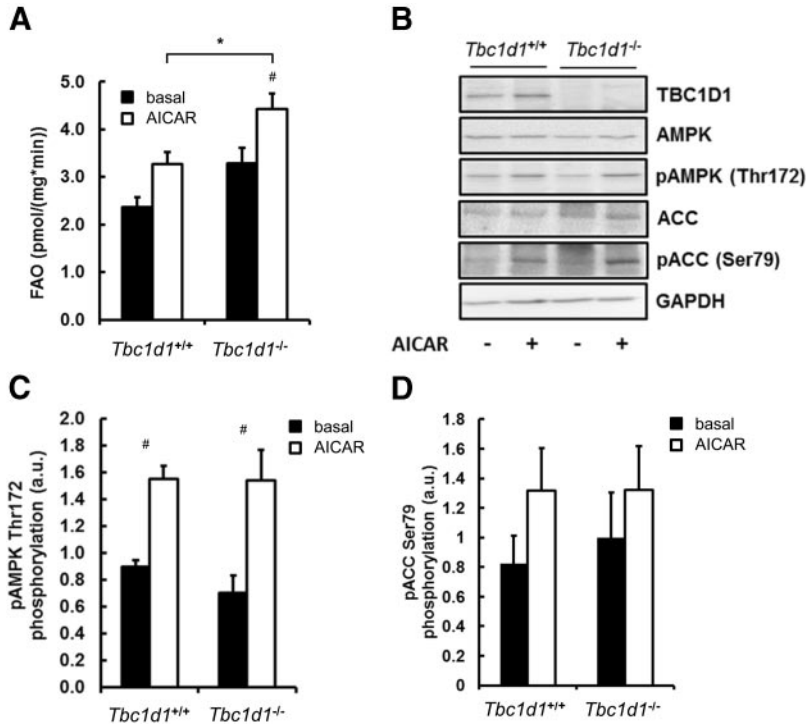


Figure 6. Ex vivo [³H]-palmitate oxidation in soleus muscle of *Tbc1d1* knockout mice. A) Intact soleus muscle from 16-wk-old SD-fed male *Tbc1d1*^{-/-} mice and controls was isolated and assayed for basal and AICAR (2 mM; 2 h) stimulated oxidation of radioactively labeled [³H]-palmitate as described in methods. Data represent mean values, n = 12–16 ± SEM; B) Quantitative Western blot analysis of TBC1D1, AMPK α and ACC protein expression, and (C, D) basal and AICAR-stimulated pAMPK (Thr172) and pACC (Ser79) phosphorylation in soleus lysates from 16-wk-old *Tbc1d1*^{-/-} mice and wild-type controls. Data represent mean values, n = 8 ± SEM; *P < .05 wildtype vs. *Tbc1d1*^{-/-}; #P < .05 basal vs. AICAR (two-way ANOVA with post hoc Bonferroni Multiple comparison tests).

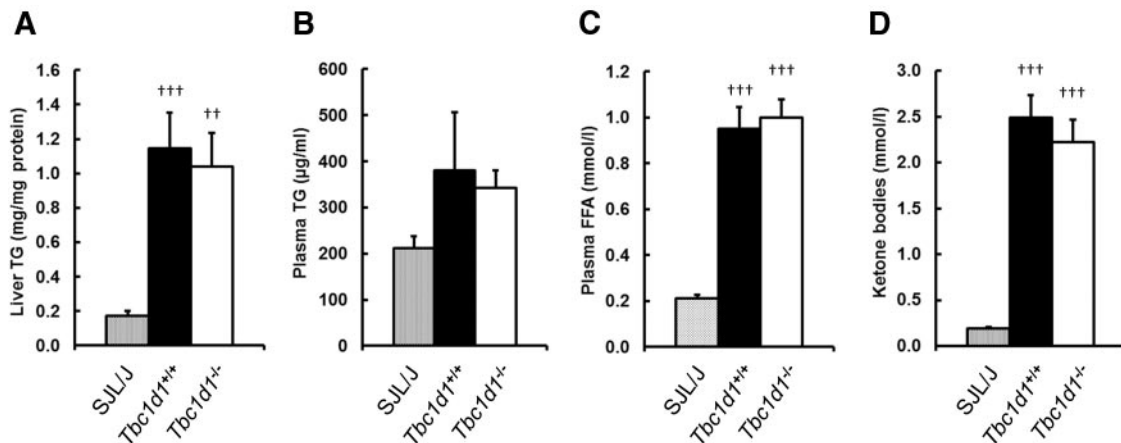


Figure 7. Fasting triglycerides, fatty acids and ketone bodies in *Tbc1d1* deficient mouse strains. Male 10–12 wk old standard diet (SD)-fed male SJL/J mice, *Tbc1d1*^{-/-} mice and wildtype littermate controls were fasted for 24 h before analysis of A) Liver triglycerides; B) plasma triglycerides; C) plasma free fatty acids (FFA); and D) ketone bodies as described in methods. Data represent mean values, n = 5–8 ± *Tbc1d1*^{-/-} SEM; +P < .05, ++P < .01 and +++P < .001 *Tbc1d1*^{+/+} and *Tbc1d1*^{-/-} vs. SJL/J mice. (one-way ANOVA with post hoc Bonferroni Multiple comparison tests).

Discussion

In this study, we generated and characterized a conventional *Tbc1d1* knockout mouse. Our results demonstrate a critical role of TBC1D1 in energy substrate metabolism in skeletal muscle and whole body energy homeostasis. Previously, we identified a naturally occurring mutation in *Tbc1d1* in the lean SJL mouse strain (6). In those mice, a 7 bp deletion in exon 18 (4047delACTCGCT in GenBank accession no. AK122445) results in a frameshift and premature termination of the protein. A recombinant inbred mouse line (B6.SJL.RCS.*Nob1.10*) that carried a 10 Mbp fragment from SJL (Chr. 5; 64.3 – 73.15 Mbp) including the mutated *Tbc1d1*^{SJL} allele on a C57BL/6J background showed reduced body weight, impaired glucose utilization and increased fat use in skeletal muscle, indicating a possible role of TBC1D1 in energy substrate preference. Interestingly, genetic evidence for linkage of a TBC1D1 variant (R125W) to obesity predisposition in human families has been provided (15, 16). However, as the 10 Mbp recombinant congenic donor fragment in *Tbc1d1*-deficient B6.SJL.RCS.*Nob1.10* mice contained numerous additional genes from SJL on a C57BL/6J background (Supplementary Table 1), some additional factors could possibly contribute to the phenotype of the mice. In fact, human linkage data also provided evidence for genetic interaction of TBC1D1 with an additional, yet unidentified human obesity predisposition locus at 4q34–35 implicating an important role for gene/gene interactions in TBC1D1-mediated obesity predisposition in humans (16).

We generated mutant mice by insertion of a β -geo gene trap cassette into the *Tbc1d1* gene. Homozygous carriers of the mutated locus displayed reduced levels of *Tbc1d1* mRNA and a complete lack of the protein, demonstrating that the gene trap mutagenesis resulted in generation of a null allele. The lower levels in *Tbc1d1* mRNA might be due to a reduction in mRNA stability of the trapped transcript. Consistently we were unable to detect significant levels of the TBC1D-LacZ fusion protein through β -galactosidase staining of skeletal muscle sections (data not shown). TBC1D1 deficiency only had a moderate effect on body weight. On a low fat diet *Tbc1d1*^{-/-} mice showed a decrease only in lean mass, whereas on a high-fat diet *Tbc1d1*^{-/-} mice displayed also reduced fat mass compared to the wildtype controls. This finding is consistent with our previous observation of reduced fat mass in high-fat diet-fed B6.SJL.RCS.*Nob1.10* mice (6), which indicates a strong influence of dietary fat on body composition of TBC1D1-deficient mice. Intriguingly, genetic variants of TBC1D1 have been associated previously with traits related to muscle growth and fat content in domesticated pigs and chicken (17–19), suggesting a possible evolution-

ary conserved role of TBC1D1 in regulating body composition in vertebrates. Consistent with our previous study of recombinant inbred mice lacking TBC1D1 we observed no changes in glucose and insulin tolerance of *Tbc1d1*^{-/-} animals, respectively (20). It is conceivable that compensatory mechanisms such as intact TBC1D4 signaling may counteract the effects of TBC1D1 deficiency on whole body glucose handling. We cannot exclude however that small effects of *Tbc1d1* deletion on glucose and insulin tolerance might have been masked by the overnight fasting protocol (21).

Indirect calorimetry revealed a decrease in the respiratory quotient of *Tbc1d1*^{-/-} mice fed high-fat, indicating an elevated use of lipids as energy source. Calculation of whole-body carbohydrate and fat utilization rates (12) confirm an increased rate of fat oxidation in *Tbc1d1*^{-/-} mice. Moreover, compared to wildtype controls, *Tbc1d1*^{-/-} mice display decreased carbohydrate oxidation rates. These findings are consistent with the genetic interaction of the *Nob1* QTL with dietary fat and the function of the *Nob1*^{SJL} allele as an obesity suppressor in high-fat diet fed mice (5, 6). In fact, *Tbc1d1*^{-/-} mice showed increased resting metabolic rate (RMR) that may in part explain the reduced body weight of the knockout animals. However, the molecular pathway that controls whole-body energy homeostasis in a TBC1D1-dependent fashion remains to be identified.

Intact isolated EDL muscle from *Tbc1d1*^{-/-} mice showed impaired insulin- and AICAR-stimulated 2-deoxyglucose uptake, and a substantial reduction in the abundance of GLUT4 protein (Figure 5). As both, protein abundance and signaling of AKT and AMPK were unaltered, the reduced glucose uptake in EDL muscle is likely the result of the decreased GLUT4 protein abundance in EDL muscle of *Tbc1d1*^{-/-} mice. A similar reduction in GLUT4 content and insulin-stimulated glucose uptake was also demonstrated in intact isolated EDL muscle from B6.SJL.RCS.*Nob1.10* mice (6). Unexpectedly however, insulin-stimulated glucose uptake in EDL muscle in vivo was moderately increased during an euglycemic hyperinsulinemic clamp (20). While the mechanism for the discrepancies between ex vivo and in vivo data is not known, one could speculate that systemic factors (e.g., hormones and/or metabolites) might overcome the intrinsic insulin resistance of glycolytic skeletal muscle to mediate improvements in insulin action in vivo. However, we were unable to detect corresponding changes in circulating hormones (i.e., insulin, leptin, resistin, adiponectin, PAI-1) or increased capillarization of skeletal muscle that might correlate with the elevated in vivo glucose uptake in EDL muscle (20). Interestingly, in TBC1D1-deficient B6.SJL.RCS.*Nob1.10* mice, hepatic insulin sensitivity was

enhanced whereas insulin-stimulated glucose uptake in soleus, gastrocnemius, diaphragm, heart muscle, white and brown adipose tissue and liver was not altered (20), indicating complex and tissue-selective effects of TBC1D1-deficiency on whole-body glucose handling. Nevertheless, TBC1D1 appears to play a metabolic role predominantly in skeletal muscle rather than in liver and adipose tissue since expression profiling studies indicate that TBC1D1 is mainly expressed in skeletal muscle and to a much lower extent in liver cells, brown and white adipose tissue (6, 20). Expression of genes involved in hepatic glucose and lipid metabolism in the liver and insulin-stimulated AKT^{Ser473} phosphorylation were unaltered between wildtype and TBC1D1-deficient mice (20).

In addition to the reduced glucose uptake in EDL muscle, both basal and AICAR-stimulated fatty acid oxidation was substantially increased in *soleus* muscle from *Tbc1d1*^{-/-} mice (Figure 6). However, protein abundance, as well as basal and AICAR-stimulated phosphorylation of AMPK was unaltered, indicating an elevated intrinsic capacity for fatty acid uptake and oxidation in *soleus* muscle from *Tbc1d1*^{-/-} animals. Thus, TBC1D1-deficiency causes altered energy substrate utilization in skeletal muscle where glucose uptake in the glycolytic EDL muscle is decreased and fatty acid oxidation in the oxidative *soleus* muscle is increased, resulting in elevated fat use and a decreased RQ.

Fatty acid metabolism is an important contributor to the pathogenesis of insulin resistance and type 2 diabetes (22, 23). Reduced lipid oxidation in skeletal muscle is associated with the development of insulin resistance and diabetes, whereas elevated fatty acid oxidation improves insulin action in skeletal muscle (24–27). Excess free fatty acids and incomplete fat oxidation have been implicated in the development of skeletal muscle insulin resistance (28, 29). The complex molecular pathways leading to lipid-induced insulin resistance in skeletal muscle are incompletely understood. Skeletal muscles from TBC1D1-deficient mice display a shift in energy substrate preference towards fat as fuel, while showing reduced glucose disposal and no apparent insulin resistance. Mitochondrial DNA (mtDNA) copy number and citric acid synthase activity were not altered, indicating that elevated mitochondrial capacity may not be the key contributing factor to the enhanced fatty acid oxidation in soleus muscle of *Tbc1d1*^{-/-} mice. In addition to established models with altered energy substrate preference (e.g., mice with altered activity of S6 kinases, fatty acid translocase (CD36), or peroxisome proliferator-activated receptor delta (30–32)), *Tbc1d1*^{-/-} animals may constitute a novel model to dissect the influence of altered glucose and lipid metabo-

lism in skeletal muscle on insulin sensitivity and glycemic control.

TBC1D1 and TBC1D4 are expressed in skeletal muscle and both proteins play roles in insulin-regulated translocation of the glucose transporter GLUT4 (7–9, 20, 33). The exact molecular function of TBC1D1 and TBC1D4 is unknown, but apparently requires the PTB domains, as well as the Rab-GAP domain activity (8, 34–37). The specificity of the GAP domains towards Rab-GTPases in vitro appears to be identical (8, 38). In humans, a nonsense mutation (R363X) in the related *TBC1D4* gene was associated with extreme postprandial hyperinsulinemia (39). In 3T3-L1 adipocytes, expression of a corresponding C-terminally truncated form of TBC1D4 reduced insulin-stimulated GLUT4 translocation in a dominant negative fashion, possibly via interaction of the N-terminal PTB domains with other proteins (39). *Tbc1d4* knockout mice display a complex phenotype that includes impaired glucose tolerance in female animals, as well as reduced glucose uptake in white adipose cells and *soleus* muscle, but not in EDL muscle, respectively (40). Interestingly, *Tbc1d4* knockout mice also showed a substantial reduction in GLUT4 protein in white adipose cells and *soleus* muscle, and a concomitant decrease in insulin-stimulated glucose uptake. TBC1D1 and TBC1D4 are both expressed in skeletal muscle, albeit at different ratios. TBC1D1 is the predominant form in glycolytic muscle, whereas TBC1D4 is more highly expressed in oxidative skeletal muscle, as well as in adipose cells, a cell type that does not express substantial amounts of TBC1D1 (6). Thus, knockout of either *Tbc1d1* or *Tbc1d4* appears to specifically reduce the abundance of GLUT4 protein in tissues where the respective TBC1D-family member is predominantly expressed, without altering abundance of GLUT4-vesicle resident proteins such as IRAP or VAMP2 (20, 40, 41). Interestingly, siRNA-mediated knockdown of *Tbc1d1* in 3T3-L1 adipocytes has been reported to increase GLUT1 protein levels through the mTOR pathway (42). However, in skeletal muscle ablation of TBC1D1 does not alter protein expression levels of GLUT1. Consistently, mice with reduced abundance of GLUT4 in both adipocytes and muscle show similar metabolic alterations as mice deficient in TBC1D1 or TBC1D4 (43). Because the mRNA levels of GLUT4 in skeletal muscle were unaltered in *Tbc1d1* and *Tbc1d4* knockout mice, respectively (6, 40), the reduction in glucose transporters is likely the result of a posttranslational event.

GLUT4 is considered a relatively stable protein which undergoes multiple translocation cycles between different membrane compartments before being eventually degraded, even in the absence of insulin (44, 45). The mechanism responsible for correct sorting of GLUT4 is not

completely understood but presumably involves Rab GTPases and accessory proteins found in GLUT4-containing vesicles (41, 46). Ablation of GLUT4 vesicle-associated proteins including sortilin (47), LDL receptor-related protein-1 (LRP1) (48), IRAP (49) and TUG (tether containing a UBX domain, for GLUT4) (50) has been shown to reduce cellular levels of GLUT4 protein due to missorting and degradation of the glucose transporters. Recent evidence suggests that impaired sorting of GLUT4-containing vesicles might lead to accelerated ubiquitin- and/or SUMO-dependent lysosomal degradation of GLUT4 through the ESCRT pathway (51–53). Also, overexpression of Rab-GTPases has been shown to result in missorting and enhanced degradation of recycling receptors such as the transferrin receptor and EGF receptor (54, 55). We speculate that impaired regulation of Rab GTPases downstream of TBC1D1 is responsible for aberrant sorting and subsequent degradation of GLUT4 in *Tbc1d1*^{-/-} mice.

The TBC1D1-deficient SJL mouse strain is protected from diet-induced obesity and type 2 diabetes, despite carrying strong diabetogenic alleles, (4, 5, 56, 57). Compared to other inbred mouse strains including C57BL/6J, SWR/J, AKR/J, FVB/NJ, and Sv129, SJL/J mice showed substantially lower fasting levels of free fatty acids, β -hydroxybutyrate and hepatic triglycerides (14). Furthermore, lower accumulation of triglycerides in the liver coincides with elevated fatty acid oxidation in skeletal muscle of SJL/J mice, indicating that fasting-induced hepatic steatosis can be prevented by increased fat use as an energy source (14). Thus it was hypothesized that elevated fatty acid oxidation in skeletal muscle of SJL mice is responsible for the lower fasting levels of free fatty acids and hepatic triglycerides in this strain when compared to C57BL/6J mice. We therefore investigated this hypothesis by analyzing the contribution of TBC1D1-deficiency to fasting-induced hepatic steatosis in *Tbc1d1* knockout animals on a C57BL/6J background. We confirmed that C57BL/6J mice and SJL/J mice differed largely in free fatty acids and hepatic triglyceride content in the fasted state (Figure 7). However, as *Tbc1d1*^{-/-} animals were not different from the wildtype controls in fasting levels of ketone bodies, free fatty acids, and circulating and hepatic triglycerides respectively, we can exclude a significant contribution of TBC1D1 in preventing fasting-induced hepatic steatosis in SJL mice. Thus, SJL/J mice may carry other strain-specific mutations besides the loss-of-function mutation in *Tbc1d1* that also contribute to the increased fatty acid oxidation in skeletal muscle, and to resistance to diet-induced obesity. Alternatively, increased fatty acid oxidation in muscle might not be sufficient to explain the protection from fasting-induced hepatic steatosis in SJL mice.

In summary, our results demonstrate that disruption of *Tbc1d1* in the SJL strain represents the causal defect underlying the *Nob1* QTL (5, 6, 57). We further show that TBC1D1 plays an important role in glucose and lipid utilization, energy substrate preference in skeletal muscle and whole body energy homeostasis.

Acknowledgments

We thank Carolin Borchert, Ines Grüner, Angelika Horrichs, Anne Karasinsky, Anette Kurowski, Diana Schulze, Annette Schober, and Elvira Steinmeyer for expert technical assistance and Ingo Voigt for blastocyst injection. This work was funded in part by grants from the Deutsche Forschungsgemeinschaft (GRK1208, AL452/4–1) and the EFSD/Lilly European Diabetes Research Program.

Address all correspondence and requests for reprints to: [¶]Institute for Clinical Biochemistry and Pathobiochemistry, German Diabetes Center, Leibniz Center for Diabetes Research at the Heinrich-Heine-University Düsseldorf, Auf'm Hennekamp 65, 40225 Düsseldorf, Germany, tel/fax +49–211-3382-240/430, al-hasani@hhu.de.

[#]Present address: Friedrich Loeffler Institute, Greifswald, Germany.

*Equal contribution.

Duality of interest: None of the authors has a duality of interest to declare.

This work was supported by .

References

1. Clee SM, Attie AD. The genetic landscape of type 2 diabetes in mice. *Endocrine reviews*. 2007;28:48–83.
2. Wuschke S, Dahm S, Schmidt C, Joost HG, Al-Hasani H. A meta-analysis of quantitative trait loci associated with body weight and adiposity in mice. *International journal of obesity*. 2007;31:829–841.
3. Schmidt C, Gonzaludo NP, Strunk S, Dahm S, Schuchhardt J, Kleijung F, Wuschke S, Joost HG, Al-Hasani H. A meta-analysis of QTL for diabetes-related traits in rodents. *Physiological genomics*. 2008;34:42–53.
4. West DB, Boozer CN, Moody DL, Atkinson RL. Dietary obesity in nine inbred mouse strains. *The American journal of physiology*. 1992;262:R1025–1032.
5. Plum L, Giesen K, Kluge R, Junger E, Linnartz K, Schurmann A, Becker W, Joost HG. Characterisation of the mouse diabetes susceptibility locus Nidd/SJL: islet cell destruction, interaction with the obesity QTL *Nob1*, and effect of dietary fat. *Diabetologia*. 2002;45:823–830.
6. Chadt A, Leicht K, Deshmukh A, Jiang LQ, Scherneck S, Bernhard U, Dreja T, Vogel H, Schmolz K, Kluge R, Zierath JR, Hultschig C, Hoeben RC, Schurmann A, Joost HG, Al-Hasani H. *Tbc1d1* mutation in lean mouse strain confers leanness and protects from diet-induced obesity. *Nature genetics*. 2008;40:1354–1359.
7. Sano H, Kane S, Sano E, Miinea CP, Asara JM, Lane WS, Garner CW, Lienhard GE. Insulin-stimulated phosphorylation of a Rab GTP-

- Pase-activating protein regulates GLUT4 translocation. *The Journal of biological chemistry*. 2003;278:14599–14602.
8. Roach WG, Chavez JA, Miinea CP, Lienhard GE. Substrate specificity and effect on GLUT4 translocation of the Rab GTPase-activating protein Tbc1d1. *The Biochemical journal*. 2007;403:353–358.
 9. An D, Toyoda T, Taylor EB, Yu H, Fujii N, Hirshman MF, Good-year LJ. TBC1D1 regulates insulin- and contraction-induced glucose transport in mouse skeletal muscle. *Diabetes*. 2010;59:1358–1365.
 10. Wiles MV, Vauti F, Otte J, Fuchtbauer EM, Ruiz P, Fuchtbauer A, Arnold HH, Lehrach H, Metz T, von Melchner H, Wurst W. Establishment of a gene-trap sequence tag library to generate mutant mice from embryonic stem cells. *Nature genetics*. 2000;24:13–14.
 11. Livak KJ, Schmittgen TD. Analysis of relative gene expression data using real-time quantitative PCR and the 2(-Delta Delta C(T)) Method. *Methods*. 2001;25:402–408.
 12. Peronnet F, Massicotte D. Table of nonprotein respiratory quotient: an update. *Canadian journal of sport sciences = Journal canadien des sciences du sport*. 1991;16:23–29.
 13. Keller SR, Scott HM, Mastick CC, Aebersold R, Lienhard GE. Cloning and characterization of a novel insulin-regulated membrane aminopeptidase from Glut4 vesicles. *The Journal of biological chemistry*. 1995;270:23612–23618.
 14. Guan HP, Goldstein JL, Brown MS, Liang G. Accelerated fatty acid oxidation in muscle averts fasting-induced hepatic steatosis in SJL/J mice. *The Journal of biological chemistry*. 2009;284:24644–24652.
 15. Meyre D, Farge M, Lecoer C, Proenca C, Durand E, Allegaert F, Tichet J, Marre M, Balkau B, Weill J, Delplanque J, Froguel P. R125W coding variant in TBC1D1 confers risk for familial obesity and contributes to linkage on chromosome 4p14 in the French population. *Human molecular genetics*. 2008;17:1798–1802.
 16. Stone S, Abkevich V, Russell DL, Riley R, Timms K, Tran T, Trem D, Frank D, Jammulapati S, Neff CD, Iliev D, Gress R, He G, Frech GC, Adams TD, Skolnick MH, Lanchbury JS, Gutin A, Hunt SC, Shattuck D. TBC1D1 is a candidate for a severe obesity gene and evidence for a gene/gene interaction in obesity predisposition. *Human molecular genetics*. 2006;15:2709–2720.
 17. Rubin CJ, Zody MC, Eriksson J, Meadows JR, Sherwood E, Webster MT, Jiang L, Ingman M, Sharpe T, Ka S, Hallbook F, Besnier F, Carlborg O, Bed'hom B, Tixier-Boichard M, Jensen P, Siegel P, Lindblad-Toh K, Andersson L. Whole-genome resequencing reveals loci under selection during chicken domestication. *Nature*. 2010;464:587–591.
 18. Fontanesi L, Galimberti G, Calo DG, Fronza R, Martelli PL, Scotti E, Colombo M, Schiavo G, Casadio R, Buttazzoni L, Russo V. Identification and association analysis of several hundred single nucleotide polymorphisms within candidate genes for back fat thickness in Italian Large White pigs using a selective genotyping approach. *Journal of animal science*. 2012;90:2450–2464.
 19. Fontanesi L, Colombo M, Tognazzi L, Scotti E, Buttazzoni L, Dall'Olio S, Davoli R, Russo V. The porcine TBC1D1 gene: mapping, SNP identification, and association study with meat, carcass and production traits in Italian heavy pigs. *Molecular biology reports*. 2011;38:1425–1431.
 20. Szekeres F, Chadt A, Tom RZ, Deshmukh AS, Chibalin AV, Bjornholm M, Al-Hasani H, Zierath JR. The Rab-GTPase-activating protein TBC1D1 regulates skeletal muscle glucose metabolism. *American journal of physiology Endocrinology and metabolism*. 2012;303:E524–533.
 21. Andrikopoulos S, Blair AR, Deluca N, Fam BC, Proietto J. Evaluating the glucose tolerance test in mice. *American journal of physiology Endocrinology and metabolism*. 2008;295:E1323–1332.
 22. Samuel VT, Petersen KF, Shulman GI. Lipid-induced insulin resistance: unravelling the mechanism. *Lancet*. 2010;375:2267–2277.
 23. Savage DB, Petersen KF, Shulman GI. Disordered lipid metabolism and the pathogenesis of insulin resistance. *Physiological reviews*. 2007;87:507–520.
 24. Kelley DE, Mokan M, Simoneau JA, Mandarino LJ. Interaction between glucose and free fatty acid metabolism in human skeletal muscle. *The Journal of clinical investigation*. 1993;92:91–98.
 25. Bruce CR, Hoy AJ, Turner N, Watt MJ, Allen TL, Carpenter K, Cooney GJ, Febbraio MA, Kraegen EW. Overexpression of carnitine palmitoyltransferase-1 in skeletal muscle is sufficient to enhance fatty acid oxidation and improve high-fat diet-induced insulin resistance. *Diabetes*. 2009;58:550–558.
 26. Kelley DE, Goodpaster B, Wing RR, Simoneau JA. Skeletal muscle fatty acid metabolism in association with insulin resistance, obesity, and weight loss. *The American journal of physiology*. 1999;277:E1130–1141.
 27. Kim JK, Gimeno RE, Higashimori T, Kim HJ, Choi H, Punreddy S, Mozell RL, Tan G, Stricker-Krongrad A, Hirsch DJ, Fillmore JJ, Liu ZX, Dong J, Cline G, Stahl A, Lodish HF, Shulman GI. Inactivation of fatty acid transport protein 1 prevents fat-induced insulin resistance in skeletal muscle. *The Journal of clinical investigation*. 2004;113:756–763.
 28. Roden M, Price TB, Perseghin G, Petersen KF, Rothman DL, Cline GW, Shulman GI. Mechanism of free fatty acid-induced insulin resistance in humans. *The Journal of clinical investigation*. 1996;97:2859–2865.
 29. Koves TR, Ussher JR, Noland RC, Slentz D, Mosedale M, Ilkayeva O, Bain J, Stevens R, Dyck JR, Newgard CB, Lopaschuk GD, Muoio DM. Mitochondrial overload and incomplete fatty acid oxidation contribute to skeletal muscle insulin resistance. *Cell metabolism*. 2008;7:45–56.
 30. Aguilar V, Alliouachene S, Sotiropoulos A, Sobering A, Arthea Y, Djouadi F, Miraux S, Thiaudiere E, Foretz M, Viollet B, Diolez P, Bastin J, Benit P, Rustin P, Carling D, Sandri M, Ventura-Clapier R, Pende M. S6 kinase deletion suppresses muscle growth adaptations to nutrient availability by activating AMP kinase. *Cell metabolism*. 2007;5:476–487.
 31. Lee CH, Olson P, Hevener A, Mehl I, Chong LW, Olefsky JM, Gonzalez FJ, Ham J, Kang H, Peters JM, Evans RM. PPARdelta regulates glucose metabolism and insulin sensitivity. *Proceedings of the National Academy of Sciences of the United States of America*. 2006;103:3444–3449.
 32. McFarlan JT, Yoshida Y, Jain SS, Han XX, Snook LA, Lally J, Smith BK, Glatz JF, Luiken JJ, Sayer RA, Tupling AR, Chabowski A, Holloway GP, Bonen A. In vivo, fatty acid translocase (CD36) critically regulates skeletal muscle fuel selection, exercise performance, and training-induced adaptation of fatty acid oxidation. *The Journal of biological chemistry*. 2012;287:23502–23516.
 33. Chavez JA, Roach WG, Keller SR, Lane WS, Lienhard GE. Inhibition of GLUT4 translocation by Tbc1d1, a Rab GTPase-activating protein abundant in skeletal muscle, is partially relieved by AMP-activated protein kinase activation. *The Journal of biological chemistry*. 2008;283:9187–9195.
 34. Eguez L, Lee A, Chavez JA, Miinea CP, Kane S, Lienhard GE, McGraw TE. Full intracellular retention of GLUT4 requires AS160 Rab GTPase activating protein. *Cell metabolism*. 2005;2:263–272.
 35. Tan SX, Ng Y, Burchfield JG, Ramm G, Lambright DG, Stockli J, James DE. The RabGAP TBC1D4/AS160 contains an atypical PTB domain that interacts with plasma membrane phospholipids to facilitate GLUT4 trafficking in adipocytes. *Molecular and cellular biology*. 2012;
 36. Koumanov F, Richardson JD, Murrow BA, Holman GD. AS160 phosphotyrosine-binding domain constructs inhibit insulin-stimulated GLUT4 vesicle fusion with the plasma membrane. *The Journal of biological chemistry*. 2011;286:16574–16582.
 37. Peck GR, Chavez JA, Roach WG, Budnik BA, Lane WS, Karlsson HK, Zierath JR, Lienhard GE. Insulin-stimulated phosphorylation of the Rab GTPase-activating protein TBC1D1 regulates GLUT4 translocation. *The Journal of biological chemistry*. 2009;284:30016–30023.
 38. Miinea CP, Sano H, Kane S, Sano E, Fukuda M, Peranen J, Lane WS,

- Lienhard GE. AS160, the Akt substrate regulating GLUT4 translocation, has a functional Rab GTPase-activating protein domain. *The Biochemical journal*. 2005;391:87–93.
39. Dash S, Sano H, Rochford JJ, Semple RK, Yeo G, Hyden CS, Soos MA, Clark J, Rodin A, Langenberg C, Druet C, Fawcett KA, Tung YC, Wareham NJ, Barroso I, Lienhard GE, O'Rahilly S, Savage DB. A truncation mutation in TBC1D4 in a family with acanthosis nigricans and postprandial hyperinsulinemia. *Proceedings of the National Academy of Sciences of the United States of America*. 2009;106:9350–9355.
40. Lansley MN, Walker NN, Hargrett SR, Stevens JR, Keller SR. Deletion of Rab GAP AS160 modifies glucose uptake and GLUT4 translocation in primary skeletal muscles and adipocytes and impairs glucose homeostasis. *American journal of physiology Endocrinology and metabolism*. 2012;
41. Kandror KV, Pilch PF. The sugar is sIRVed: sorting Glut4 and its fellow travelers. *Traffic*. 2011;12:665–671.
42. Zhou QL, Jiang ZY, Holik J, Chawla A, Hagan GN, Leszyk J, Czech MP. Akt substrate TBC1D1 regulates GLUT1 expression through the mTOR pathway in 3T3–L1 adipocytes. *The Biochemical journal*. 2008;411:647–655.
43. Kotani K, Peroni OD, Minokoshi Y, Boss O, Kahn BB. GLUT4 glucose transporter deficiency increases hepatic lipid production and peripheral lipid utilization. *The Journal of clinical investigation*. 2004;114:1666–1675.
44. Sargeant RJ, Paquet MR. Effect of insulin on the rates of synthesis and degradation of GLUT1 and GLUT4 glucose transporters in 3T3–L1 adipocytes. *The Biochemical journal*. 1993;290 (Pt 3):913–919.
45. Karylowski O, Zeigerer A, Cohen A, McGraw TE. GLUT4 is retained by an intracellular cycle of vesicle formation and fusion with endosomes. *Molecular biology of the cell*. 2004;15:870–882.
46. Bogan JS. Regulation of glucose transporter translocation in health and diabetes. *Annual review of biochemistry*. 2012;81:507–532.
47. Shi J, Kandror KV. Sortilin is essential and sufficient for the formation of Glut4 storage vesicles in 3T3–L1 adipocytes. *Developmental cell*. 2005;9:99–108.
48. Jedrychowski MP, Gartner CA, Gygi SP, Zhou L, Herz J, Kandror KV, Pilch PF. Proteomic analysis of GLUT4 storage vesicles reveals LRP1 to be an important vesicle component and target of insulin signaling. *The Journal of biological chemistry*. 2010;285:104–114.
49. Keller SR, Davis AC, Clairmont KB. Mice deficient in the insulin-regulated membrane aminopeptidase show substantial decreases in glucose transporter GLUT4 levels but maintain normal glucose homeostasis. *The Journal of biological chemistry*. 2002;277:17677–17686.
50. Yu C, Cresswell J, Loffler MG, Bogan JS. The glucose transporter 4-regulating protein TUG is essential for highly insulin-responsive glucose uptake in 3T3–L1 adipocytes. *The Journal of biological chemistry*. 2007;282:7710–7722.
51. Koumanov F, Pereira VJ, Whitley PR, Holman GD. GLUT4 Traffic through an ESCRT-III-Dependent Sorting Compartment in Adipocytes. *PLoS one*. 2012;7:e44141.
52. Giorgino F, de Robertis O, Laviola L, Montrone C, Perrini S, McCowen KC, Smith RJ. The sentrin-conjugating enzyme mUbc9 interacts with GLUT4 and GLUT1 glucose transporters and regulates transporter levels in skeletal muscle cells. *Proceedings of the National Academy of Sciences of the United States of America*. 2000;97:1125–1130.
53. Liu LB, Omata W, Kojima I, Shibata H. The SUMO conjugating enzyme Ubc9 is a regulator of GLUT4 turnover and targeting to the insulin-responsive storage compartment in 3T3–L1 adipocytes. *Diabetes*. 2007;56:1977–1985.
54. Matsui T, Itoh T, Fukuda M. Small GTPase Rab12 regulates constitutive degradation of transferrin receptor. *Traffic*. 2011;12:1432–1443.
55. Yang X, Zhang Y, Li S, Liu C, Jin Z, Wang Y, Ren F, Chang Z. Rab21 attenuates EGF-mediated MAPK signaling through enhancing EGFR internalization and degradation. *Biochemical and biophysical research communications*. 2012;421:651–657.
56. Scherneck S, Nestler M, Vogel H, Bluher M, Block MD, Berriel Diaz M, Herzig S, Schulz N, Teichert M, Tischer S, Al-Hasani H, Kluge R, Schurmann A, Joost HG. Positional cloning of zinc finger domain transcription factor Zfp69, a candidate gene for obesity-associated diabetes contributed by mouse locus Niddi/SJL. *PLoS genetics*. 2009;5:e1000541.
57. Plum L, Kluge R, Giesen K, Altmüller J, Ortlepp JR, Joost HG. Type 2 diabetes-like hyperglycemia in a backcross model of NZO and SJL mice: characterization of a susceptibility locus on chromosome 4 and its relation with obesity. *Diabetes*. 2000;49:1590–1596.

Alexandra Chadt,^{1,2} Anja Immisch,³ Christian de Wendt,¹ Christian Springer,¹ Zhou Zhou,¹ Torben Stermann,¹ Geoffrey D. Holman,⁴ Dominique Loffing-Cueni,⁵ Johannes Loffing,⁵ Hans-Georg Joost,^{2,3} and Hadi Al-Hasani^{1,2}



Deletion of Both Rab-GTPase-Activating Proteins TBC1D1 and TBC1D4 in Mice Eliminates Insulin- and AICAR-Stimulated Glucose Transport

DOI: 10.2337/db14-0368

The Rab-GTPase-activating proteins TBC1D1 and TBC1D4 (AS160) were previously shown to regulate GLUT4 translocation in response to activation of AKT and AMP-dependent kinase. However, knockout mice lacking either *Tbc1d1* or *Tbc1d4* displayed only partially impaired insulin-stimulated glucose uptake in fat and muscle tissue. The aim of this study was to determine the impact of the combined inactivation of *Tbc1d1* and *Tbc1d4* on glucose metabolism in double-deficient (D1/4KO) mice. D1/4KO mice displayed normal fasting glucose concentrations but had reduced tolerance to intraperitoneally administered glucose, insulin, and AICAR. D1/4KO mice showed reduced respiratory quotient, indicating increased use of lipids as fuel. These mice also consistently showed elevated fatty acid oxidation in isolated skeletal muscle, whereas insulin-stimulated glucose uptake in muscle and adipose cells was almost completely abolished. In skeletal muscle and white adipose tissue, the abundance of GLUT4 protein, but not GLUT4 mRNA, was substantially reduced. Cell surface labeling of GLUTs indicated that RabGAP deficiency impairs retention of GLUT4 in intracellular vesicles in the basal state. Our results show that TBC1D1 and TBC1D4 together play essential roles in insulin-stimulated glucose uptake and substrate preference in skeletal muscle and adipose cells.

In skeletal muscle and adipose cells, insulin stimulation leads to a rapid and reversible redistribution of GLUT4

from intracellular vesicles to the cell surface (1,2). The two related Rab-GTPase-activating proteins TBC1D1 and TBC1D4 (AS160) are phosphorylated in response to insulin, AMPK, and exercise/muscle contraction and have been implicated in important roles in regulating the translocation of GLUT4 (3–9). By positional cloning, we previously identified a naturally occurring loss-of-function mutation in *Tbc1d1* as an obesity suppressor in the lean, diabetes-resistant SJL mouse strain (10). In humans, mutations in *TBC1D4* (R363X) and *TBC1D1* (R125W) have been linked to severe postprandial hyperinsulinemia and obesity, respectively (11–13). TBC1D4 is found mainly in the heart, adipose tissue, and oxidative muscle fibers, whereas TBC1D1 is predominantly expressed in glycolytic skeletal muscle and is nearly absent from fat tissue (10,14,15). Both TBC1D1 and TBC1D4 display a similar domain architecture that includes two N-terminal phosphotyrosine-binding domains and a Rab-GTPase-activating (GAP) domain. The latter is believed to control the activation state of Rab-GTPases by converting them from the active guanosine triphosphate-bound state into the inactive guanosine diphosphate-bound state. Several lines of evidence suggest that the GAP domains in TBC1D1 and TBC1D4 directly regulate the activity of an overlapping set of Rab-GTPases, thereby controlling the subcellular targeting and transport activity of GLUT4 (7). So far, Rab2, Rab8b, Rab10, and Rab14 have been

¹German Diabetes Center, Leibniz Center for Diabetes Research, Heinrich-Heine-University, Düsseldorf, Germany

²German Center for Diabetes Research (DZD), Düsseldorf, Germany

³German Institute for Human Nutrition, Potsdam, Germany

⁴Department of Biology and Biochemistry, University of Bath, Bath, U.K.

⁵Institute of Anatomy, University of Zurich, Zurich, Switzerland

Corresponding author: Hadi Al-Hasani, hadi.al-hasani@ddz.uni-duesseldorf.de.

Received 3 March 2014 and accepted 16 September 2014.

This article contains Supplementary Data online at <http://diabetes.diabetesjournals.org/lookup/suppl/doi:10.2337/db14-0368/-/DC1>.

© 2015 by the American Diabetes Association. Readers may use this article as long as the work is properly cited, the use is educational and not for profit, and the work is not altered.

identified as substrates for recombinant GAP domains of TBC1D1 and TBC1D4 in vitro (4,16), but the significance of these findings for GLUT4 translocation in adipose and muscle cells in vivo remains to be further investigated. Moreover, the phosphotyrosine-binding domains may also be involved in TBC1D1/TBC1D4 signaling (17–19). Previous studies of isolated L6 muscle cells and 3L3-L1 adipocytes demonstrated that ablation of either *Tbc1d1* or *Tbc1d4*, or overexpression of mutated proteins, resulted in reduced insulin-stimulated translocation of GLUT4 (20–22). However, knockout mice lacking either *Tbc1d1* (15,23) or *Tbc1d4* (14,24) displayed only tissue-specific impairments of insulin-stimulated glucose uptake and rather minor alterations in glycemic control, indicating a substantial level of redundant expression and signaling.

The aim of this study was to determine the impact of the combined inactivation of *Tbc1d1* and *Tbc1d4* on glucose metabolism. Therefore, we characterized energy and substrate metabolism of *Tbc1d1/Tbc1d4* double-deficient mice. Our results demonstrate that both TBC1D1 and TBC1D4 operate in concert and play essential roles in insulin-stimulated glucose uptake and substrate preference in skeletal muscle.

RESEARCH DESIGN AND METHODS

Materials

Radiochemicals ([9,10(n)-³H]-palmitic acid; 2-[1,2-³H(N)]-deoxy-D-glucose, [1-¹⁴C]-D-mannitol, and [¹⁴C]-D-glucose [U]) were purchased from Hartmann Analytic (Braunschweig, Germany). Human recombinant insulin Actrapid HM Penfill from Novo Nordisk Pharma GmbH (Mainz, Germany) was used throughout the experiments. Collagenase (type I) was from Worthington Biochemical Corp. (Lakewood, NJ). AICAR was purchased from Enzo Life Sciences (Lörrach, Germany). Antibodies against TBC1D1 and GLUT4 were described previously (10). Antibodies against AKT, phospho-AKT (Ser473), AMPK α , phospho-AMPK (Thr172), and phosphoenolpyruvate carboxykinase 2 (PCK2), glycogen synthase, and glycogen synthase kinase 3 α were from Cell Signaling Technology (Danvers, MA). Antibodies against PCK1 were from Abcam (Cambridge, UK); antibodies against TBC1D4 were from Millipore (Temecula, CA); and GAPDH antibodies were from Ambion (Austin, TX). Antibodies against insulin-regulated aminopeptidase (IRAP) and GLUT1 were generous gifts from Dr. Susanna Keller (University of Virginia, Charlottesville, VA) and Dr. Annette Schürmann (German Institute of Human Nutrition, Potsdam, Germany), respectively.

Experimental Animals

Recombinant congenic *Tbc1d1*-deficient C57BL/6J mice (whole-body D1KO) were described previously (10). Mice with targeted deletion of *Tbc1d4* (whole-body D4KO) were obtained from Texas A&M Institute for Genomic Medicine (Houston, TX) and backcrossed to the D1KO strain using a microsatellite marker-assisted (“speed congenics”) selection (25). Heterozygous D1KO/

D4KO mice (>97.5% congenic with C57BL/6J) then were intercrossed to generate the four experimental genotypes: wild type (WT), D1KO, D4KO, and *Tbc1d1/Tbc1d4* double-deficient D1/4KO. Animals were kept in accordance with the National Institutes of Health guidelines for the care and use of laboratory animals, and all experiments were approved by the Ethics Committee of the State Ministry of Agriculture, Nutrition and Forestry (States of Brandenburg and North Rhine-Westphalia, Germany). Three to six mice per cage (Macrolon type III) were housed at a temperature of 22°C and a 12-h light–dark cycle (lights on at 6 A.M.) with ad libitum access to food and water. After weaning at the age of 19–21 days, animals received a standard chow with 19% (wt/wt) protein (23 cal%), 3.3% fat (8 cal%), and 54.1% carbohydrates (69 cal%) containing 3.06 kcal/g energy (V153 \times R/M-H; Ssniff, Soest, Germany).

Genotyping

DNA was isolated from mouse tail tips using the InViSorb Genomic DNA Kit II (Invitek, Berlin, Germany). Mice were genotyped by PCR with three primers for the *Tbc1d4* knockout (Fwd: 5'-AGTAGACTCAGAGTGGTCTTGG-3'; Rev-WT: 5'-GTCTTCCGACTCCATATTTGC-3'; Rev-KO: 5'-GCAGCGCATCGCCTTCTATC-3') and primers for D1KO mice, as described elsewhere (10).

RNA Extraction, cDNA Synthesis, and Quantitative Real-Time PCR

RNA was extracted and cDNA was synthesized as described previously (10). Real-time PCR was performed with a 7500 Fast Real-Time PCR System using TaqMan PCR probes (Applied Biosystems, Foster City, CA) for *Tbc1d1*, *Tbc1d4*, and *Slc2a4*, and data were normalized to *Actb* according to the Δ Ct method (26).

Analysis of Body Weight and Body Composition

Body weight was measured with an electronic scale (Sartorius, Göttingen, Germany). Body composition was analyzed with a nuclear magnetic resonance spectrometer (Echo MRI, Houston, TX).

Indirect Calorimetry

Animals were placed in individual cages and respiratory quotient (RQ) was measured by indirect calorimetry after a 24-h adaption phase, as described previously (23). Rates of oxygen consumption (V_{O_2}) and carbon dioxide production (V_{CO_2}) were monitored for 23 h at 22°C at a flow rate of 30 L/min. Animals had free access to water, and food was removed during the daytime (6 A.M. to 6 P.M.). Whole-body carbohydrate and fat oxidation rates (grams per minute) were calculated using the following equations: carbohydrate oxidation rate = $4.585 \times V_{CO_2}$ (L/min) – $3.226 \times V_{O_2}$ (L/min); fat oxidation rate = $1.695 \times V_{O_2}$ (L/min) – $1.701 \times V_{CO_2}$ (L/min) (27).

Tolerance Tests

For glucose tolerance tests (GTTs), sterile glucose (2 g/kg body weight, 20% solution) was injected intraperitoneally into fasted (16 h) animals. For insulin tolerance tests (ITTs) and AICAR tolerance tests (ATTs), nonfasted mice

were injected intraperitoneally either with insulin (1 IU/kg body weight) or AICAR (250 mg/kg body weight), and blood samples were taken from the tail tip at 0, 15, 30, 60 min (intraperitoneal ITT and ATT) and at 120 min (intraperitoneal GTT). Blood glucose was determined with a glucometer (Contour; Bayer, Leverkusen, Germany). Plasma insulin was measured with ELISA (Insulin Mouse Ultrasensitive ELISA; DRG, Marburg, Germany).

Determination of Free Fatty Acids, Triglycerides, and Glycogen

Frozen tissue (30 mg; liver and skeletal muscle) was pestled and analyzed using the Triglycerides (TRIGS) GPO-PAP Kit (Randox, Crumlin, UK) according to the manufacturer's guidelines. Muscle homogenates were tested negatively for adipocyte contamination (Supplementary Fig. 1). Glycogen content was determined using the amyloglucosidase method (28). Tissue homogenates were incubated with 30% potassium hydroxide (wt/vol) at 100°C for 30 min. Subsequently, samples were supplemented with acetic acid and an assay buffer containing sodium acetate and amyloglucosidase and incubated 3 h at 37°C. Glucose content then was measured enzymatically by a glucose oxidase-based colorimetric detection kit (Glucose liquidcolor; Human, Taunusstein, Germany) according to the manufacturer's instructions.

Analysis of Glucose Uptake in Adipocytes

Primary adipose cells were isolated by collagenase digestion of epididymal fat pads from 12- to 16-week-old male mice, and basal and insulin-stimulated uptake of [¹⁴C]glucose was performed as described elsewhere (29). Briefly, freshly isolated adipose cells (30) were incubated in Krebs-Ringer bicarbonate HEPES buffer (pH 7.4), 200 nmol/L adenosine containing 5% BSA with and without 120 nmol/L insulin for 30 min before measuring [¹⁴C]-glucose uptake. After 30 min, the cells were spun through dinonyl phthalate oil (Merck, Darmstadt, Germany) to remove excess label, and the cell-associated radioactivity was determined by measuring scintillation. The resulting counts were normalized to the lipid weight of the samples (29). Measurements were performed in quadruplicate.

Analysis of Glucose Uptake and Fatty Acid Oxidation in Isolated Skeletal Muscles

[³H]2-deoxyglucose uptake in intact isolated skeletal muscles was performed as described previously (10). Extensor digitorum longus (EDL) and soleus muscles were removed from anesthetized (500 mg/kg Avertin [2,2,2-tribromoethanol] via intraperitoneal injection) mice. Animals then were killed by heart puncture under anesthesia. Isolated muscles were incubated for 30 min at 30°C in vials containing preoxygenated (95% oxygen/5% carbon dioxide) Krebs-Henseleit buffer (KHB) containing 5 mmol/L HEPES and supplemented with 5 mmol/L glucose and 15 mmol/L mannitol. All incubation steps were conducted under continuous gassing (95% oxygen/5% carbon dioxide) at 30°C and slight agitation. After recovery, muscles were transferred to new vials and incubated for

30 min in KHB/5 mmol/L HEPES/15 mmol/L mannitol/5 mmol/L glucose under basal conditions or in the presence of 120 nmol/L insulin or 2 mmol/L AICAR, throughout the duration of the experiment. Then, muscles were incubated for 10 min in KHB/20 mmol/L mannitol under basal conditions or in the presence of 120 nmol/L insulin or 2 mmol/L AICAR before being transferred to radioactive glucose transport incubation. After 20 min of incubation in the presence of 1 mmol/L [³H]2-deoxy-glucose and 19 mmol/L [¹⁴C]mannitol, muscles were immediately frozen in liquid nitrogen and stored at -80°C. Cleared protein lysates were used to determine incorporated radioactivity by counting scintillation. The counts from [¹⁴C]mannitol were used to correct for the extracellular space.

To assess palmitate oxidation, EDL and soleus muscles were incubated in pregassed KHB containing 15 mmol/L mannitol, 5 mmol/L glucose, 3.5% fatty acid-free BSA, [³H]palmitate, and 600 μmol/L unlabeled palmitate with or without 2 mmol/L AICAR at 30°C for 2 h. After absorption of fatty acids into activated charcoal, fatty acid oxidation (FAO) was determined by measuring scintillation of tritiated water.

Cell Surface Photolabeling of GLUT4

Affinity photolabeling of GLUTs using the bio-LC-ATB-BGPA compound was performed as described previously (31). Following a 4-h fasting period, mice were anesthetized and EDL and soleus muscles were removed. Muscles were incubated in glass vials in preoxygenated KHB buffer containing 0.1% BSA, 2 mmol/L pyruvate, and 18 mmol/L mannitol for 30 min at 30°C. After recovery, 400 μmol/L bio-LC-ATB-BGPA was added and muscles were incubated with (120 nmol/L) or without insulin at 18°C for 8 min in the dark. After ultraviolet irradiation (6 min, 354 nm, 4°C), muscles were immediately frozen in liquid nitrogen. Recovery of photochemically biotinylated proteins from muscle lysates using streptavidin beads (Pierce, Rockford, IL) was performed as described (31), and total and labeled GLUT4 was determined by Western blot analysis.

SDS-PAGE and Western Blotting

Tissues were homogenized (20 mmol/L Tris, 150 mmol/L sodium chloride, 1 mmol/L EGTA, 1 mmol/L EDTA, 1% (v/v) Triton-X-100, 1 mmol/L sodium orthovanadate, 1 mmol/L β-glycerophosphate, 1 mmol/L sodium fluoride, 2.5 mmol/L sodium pyrophosphate tetrabasic, and a proteinase inhibitor and a phosphatase inhibitor cocktail (Complete and PhosSTOP; Roche, Mannheim, Germany) and centrifuged for 10 min at 16,000 relative centrifugal force at 4°C. Protein content of the supernatant was measured with the BCA Protein Assay Kit (Pierce). Immunoblotting and detection was performed with a ECL Western blot detection analysis system (GE Healthcare, Buckinghamshire, UK), as described previously (23).

Statistics

Data are reported as means ± SEMs. Significant differences were determined by one-way or two-way ANOVA (post hoc test, Bonferroni multiple comparison test) or paired

two-tailed Student *t* test, as indicated in the figure legends. *P* values <0.05 were considered statistically significant.

RESULTS

Tbc1d1/Tbc1d4 Double-Deficient Mice Show Only Marginal Differences in Body Weight and Body Fat

We crossbred mice deficient in *Tbc1d1* (whole-body D1KO) with conventional *Tbc1d4* knockout animals (whole-body D4KO) to yield *Tbc1d1/Tbc1d4* double-deficient (D1/4KO) mice on a C57BL/6J background. In all tissues analyzed, the abundance of TBC1D4 was not altered in *Tbc1d1*-deficient mice (Fig. 1A–C and Supplementary Fig. 2). Equally, TBC1D1 protein was not changed in mice deficient in *Tbc1d4* (Fig. 1A–C and Supplementary Fig. 2).

Male D1KO, D4KO, and D1/4KO mice and WT littermates were raised on a standard diet (8% calories from fat), and body weight and body composition were measured every 3 weeks until week 21. On a standard diet, D1KO, D4KO, and D1/4KO mice showed a lower body weight and a tendency toward reduced fat mass, whereas lean mass was not different compared with WT controls (Fig. 1D–F).

Tbc1d1/Tbc1d4 Double-Deficient Mice Show Impaired Glucose, Insulin, and AICAR Tolerance

Plasma glucose and insulin concentrations in standard-diet fed male D1KO, D4KO and D1/4KO mice and WT littermates were determined. D1KO and D4KO mice showed normal plasma glucose and insulin concentrations

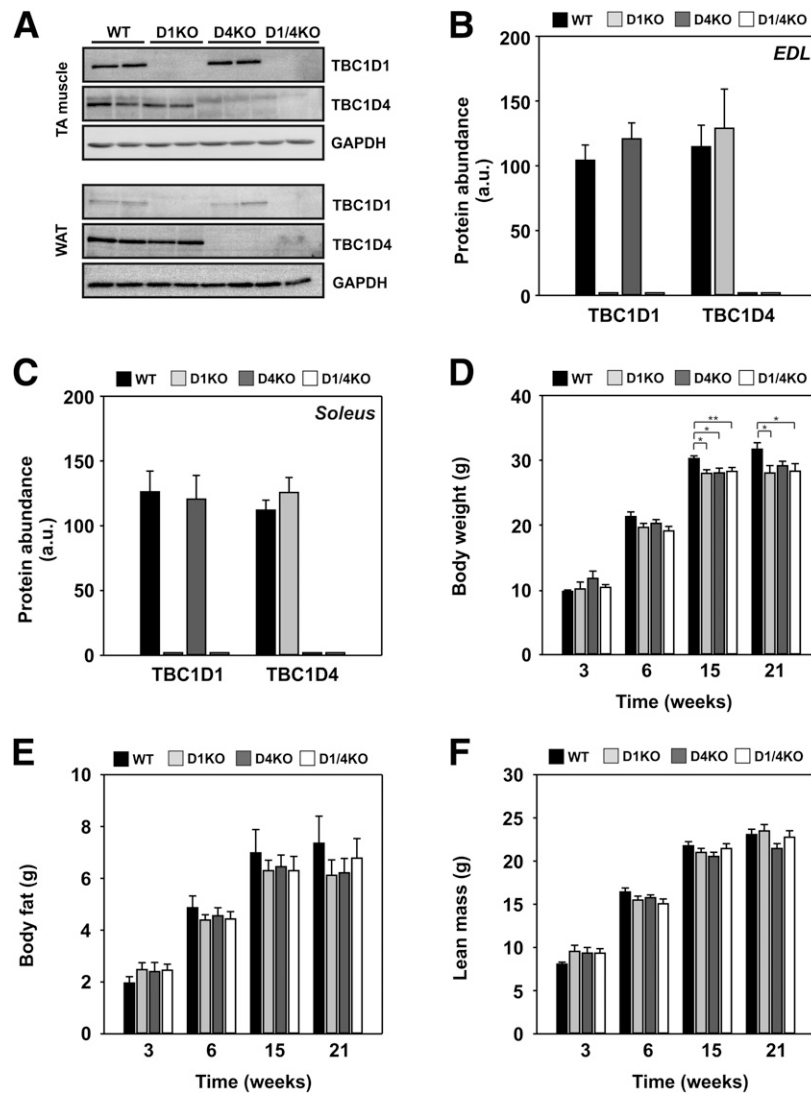


Figure 1—Disruption of *Tbc1d1* and *Tbc1d4* moderately reduces body weight. A: Western blot of TBC1D1 and TBC1D4 in tibialis anterior (TA) muscle and WAT from *Tbc1d1*-deficient (D1KO), *Tbc1d4*-deficient (D4KO), and double-deficient (D1/4KO) mice. Quantification of TBC1D1 and TBC1D4 protein abundance determined by Western blot analysis in glycolytic EDL muscle (B) and oxidative soleus muscle (C). Data are presented as mean \pm SEM ($n = 3$ –8). Body weight development (D), body fat development (E), and lean mass (F) in male D1KO, D4KO, and D1/4KO mice. Data are presented as mean \pm SEM ($n = 11$ –22). * $P < 0.05$, ** $P < 0.01$, WT vs. D1KO, D4KO, D1/4KO (one-way ANOVA). a.u., arbitrary units.

in both the postprandial and fasted states (Fig. 2A and B). In contrast, postprandial glucose concentrations were decreased in D1/4KO mice (WT vs. D1/4KO: 7.31 ± 0.18 vs. 6.34 ± 0.24 mmol/L; $P < 0.01$), whereas fasting glucose concentrations were normal. Moreover, fed and fasted plasma triglycerides as well as free fatty acids in plasma were not different between the genotypes (Supplementary Fig. 3). To investigate whole-body glycemic control of the animals, we performed intraperitoneal GTTs, ITTs, and ATTs. D1KO and D4KO mice showed normal blood glucose concentrations, as well as normal

plasma insulin concentrations during the intraperitoneal GTT (Fig. 2C and D). In contrast, D1/4KO mice displayed markedly impaired glucose tolerance, whereas insulin concentrations were normal (Fig. 2C and D). Similarly, D1KO and D4KO mice showed normal blood glucose concentrations in response to the intraperitoneal ITT, whereas D1/4KO mice displayed substantially impaired insulin tolerance (Fig. 2E). Last, D4KO mice retained normal blood glucose concentrations in response to intraperitoneal ATT, whereas both D1KO and D1/4KO mice had significantly impaired AICAR tolerance (Fig. 2F).

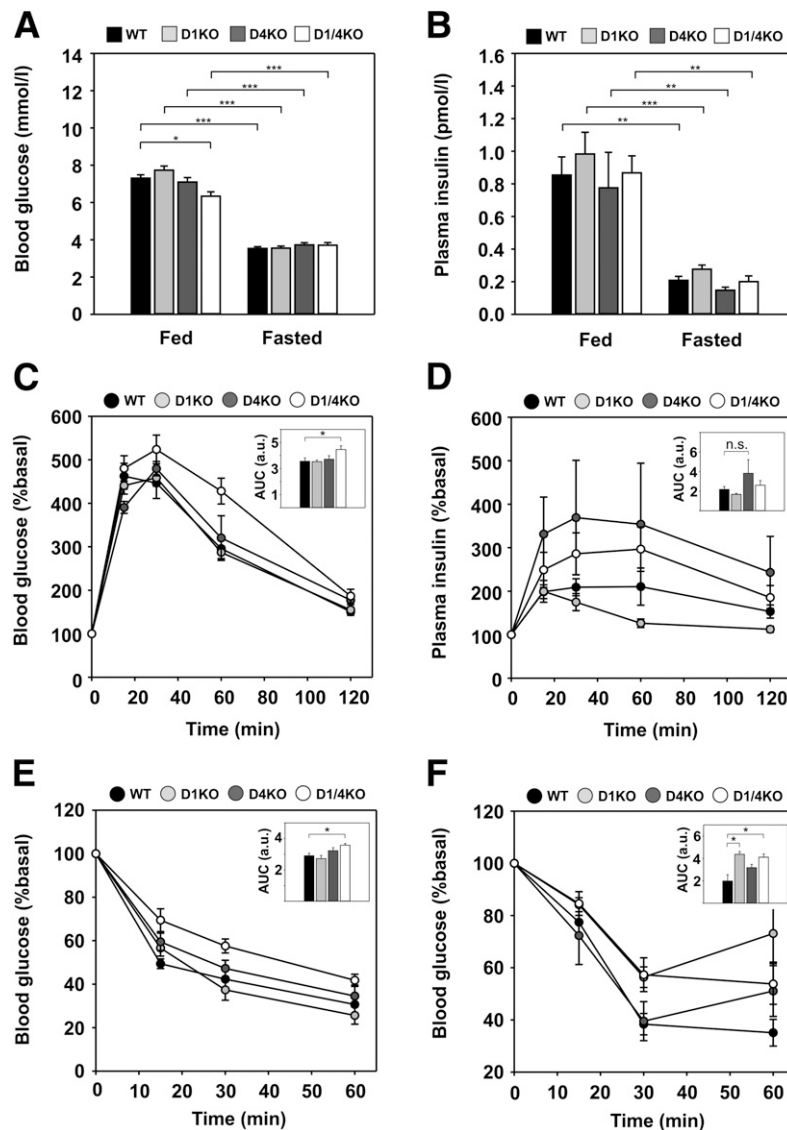


Figure 2—Deficiency in *Tbc1d1/Tbc1d4* impairs glucose, insulin, and AICAR tolerance. Blood glucose (A) and plasma insulin concentrations (B) in *Tbc1d1*-deficient (D1KO), *Tbc1d4*-deficient (D4KO), and double-deficient (D1/4KO) mice in the fed state and after 16 h of fasting. Data are presented as mean \pm SEM ($n = 13$ –27). * $P < 0.05$, ** $P < 0.01$, *** $P < 0.001$, fed vs. fasted (two-way ANOVA) and WT vs. D1/4KO (one-way ANOVA). Male mice aged 12–16 weeks were subjected to intraperitoneal tolerance tests for glucose (GTT), insulin (ITT), and AICAR (ATT). C: Blood glucose concentrations in D1KO, D4KO, and D1/4KO mice after intraperitoneal injection of glucose (2 mg/kg). D: Plasma insulin concentrations during intraperitoneal GTT. E: Blood glucose concentrations during intraperitoneal ITT (1 IU/kg). F: Blood glucose concentrations during intraperitoneal ATT (250 mg/kg). Data are presented as mean \pm SEM ($n = 8$ –16). * $P < 0.05$, WT vs. D1KO, D1/4KO (one-way ANOVA).

Tbc1d1/Tbc1d4 Depletion Increases FAO In Vivo

We investigated whole-body substrate utilization in male D1KO, D4KO and D1/4KO mice and WT littermates fed a standard diet. At the age of 13 weeks, animals were placed in metabolic cages and indirect calorimetry was conducted for 24 h. On a standard diet, D1KO, D4KO, and D1/4KO mice showed a substantial reduction in RQ compared with WT controls during the dark phase (Fig. 3A and B). Whole-body fat oxidation rates were increased substantially, whereas whole-body carbohydrate oxidation rates were significantly reduced only in D1/4KO mice (Fig. 3C and D).

Glucose Uptake Is Impaired in Skeletal Muscle from *Tbc1d1/Tbc1d4* Double-Deficient Mice

To determine the specific contribution of TBC1D1 and TBC1D4 to glucose uptake in skeletal muscle, EDL and soleus muscles from 16-week-old male mice were isolated and assayed for insulin- and AICAR-stimulated uptake of 2-deoxyglucose, as described in RESEARCH DESIGN AND METHODS. In glycolytic EDL muscle, basal 2-deoxyglucose uptake was not significantly different between the genotypes (Fig. 4A). In contrast, glucose uptake in response to insulin was substantially impaired in EDL muscles from D1KO and D1/4KO mice, whereas glucose uptake in EDL muscle from D4KO mice was normal (Fig. 4A). Similarly, AICAR-stimulated uptake of 2-deoxyglucose was markedly decreased in EDL muscles from D1KO and D1/4KO mice but not in EDL muscles from D4KO mice (Fig. 4B). In

oxidative soleus muscle, basal glucose uptake was also not different between the genotypes (Fig. 4C). However, insulin-stimulated glucose uptake was markedly reduced in soleus muscles from D4KO and D1/4KO mice, whereas glucose uptake in the soleus muscles from D1KO mice was normal (Fig. 4C). Again, AICAR-stimulated glucose uptake decreased correspondingly (Fig. 4D).

Glucose Uptake Is Impaired in White Adipose Tissue from *Tbc1d1/Tbc1d4* Double-Deficient Mice

We determined the impact of *Tbc1d1/Tbc1d4* deficiency on glucose uptake in isolated white adipose cells. Adipose cells from 16-week-old male mice were isolated by collagenase digestion and assayed for insulin-stimulated uptake of ^{14}C -D-glucose, as described in RESEARCH DESIGN AND METHODS. In basal adipose cells, glucose uptake was not different between the genotypes (Fig. 4E). However, insulin-stimulated glucose uptake was markedly reduced in adipose cells from D4KO and D1/4KO mice, whereas glucose uptake in cells from D1KO mice was normal (Fig. 4E).

Tbc1d1/Tbc1d4 Deficiency Has No Impact on AKT2 and AMPK Signaling

We next investigated whether insulin or AMPK signaling were impaired in skeletal muscle from D1KO, D4KO, and D1/4KO mice. Basal and insulin-stimulated (120 nmol/L; 60 min) EDL muscle was homogenized, and expression of AKT and phosphorylation of AKT^{Ser473} was analyzed by Western blotting. In addition, basal and AICAR-stimulated (2 mmol/L; 60 min) soleus muscle was homogenized, and

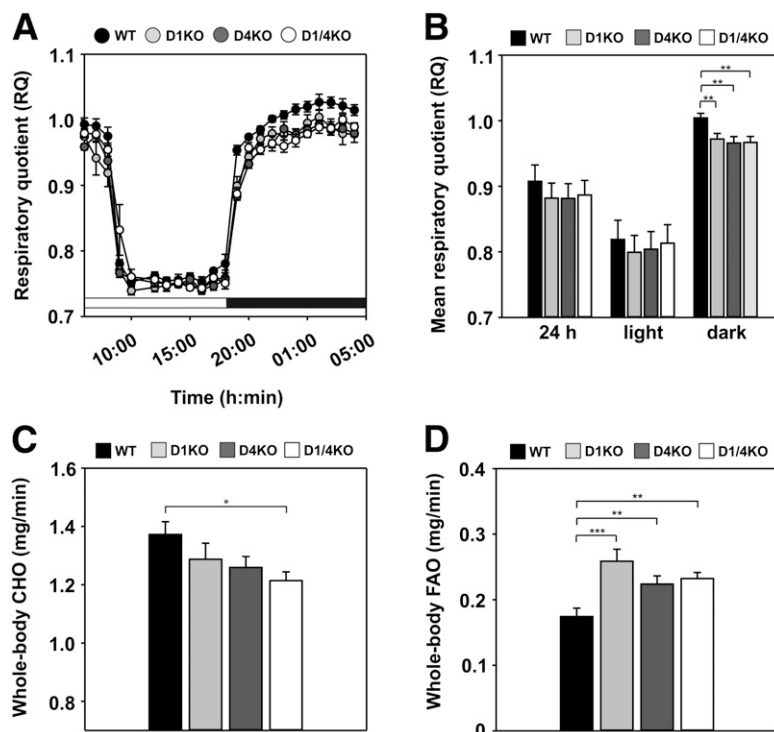


Figure 3—Deletion of *Tbc1d1* and *Tbc1d4* alters energy substrate preference. Male mice aged 12–16 weeks were subjected to indirect calorimetry. RQ (A), mean RQ (B), whole-body carbohydrate oxidation (CHO) (C) and whole-body FAO (D) in D1KO, D4KO, and D1/4KO mice. Data are presented as mean \pm SEM ($n = 8$ –11). * $P < 0.05$, ** $P < 0.01$, *** $P < 0.001$, WT vs. D1KO, D4KO, D1/4KO (one-way ANOVA).

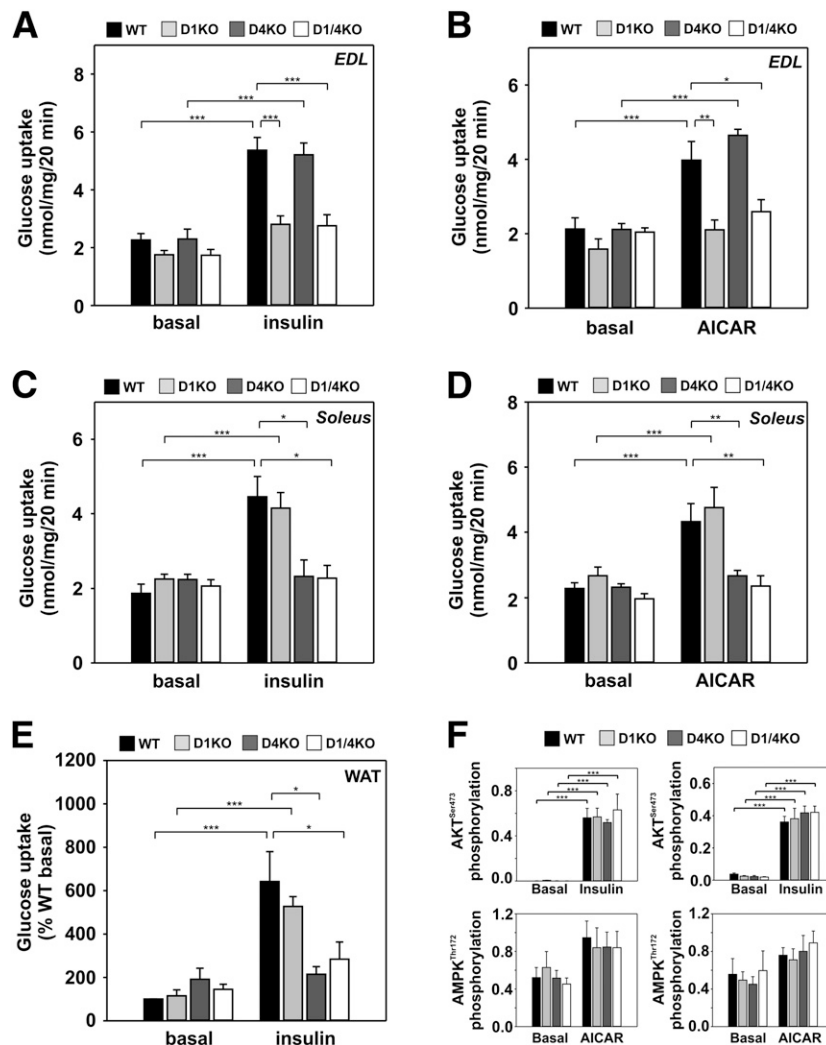


Figure 4—Lack of *Tbc1d1* and *Tbc1d4* impairs glucose uptake in skeletal muscle and adipose cells. Skeletal muscles and adipose cells from 16-week-old male mice and controls were isolated and assayed for glucose uptake. **A:** Insulin-stimulated [³H]-deoxyglucose uptake in EDL muscle from D1KO, D4KO, and D1/4KO mice ($n = 9-15$). **B:** AICAR-stimulated [³H]-deoxyglucose uptake in EDL muscle ($n = 6-11$). **C:** Insulin-stimulated [³H]-deoxyglucose uptake in isolated soleus muscle ($n = 6-9$). **D:** AICAR-stimulated [³H]-deoxyglucose uptake in isolated soleus muscle ($n = 6-11$). **E:** Insulin-stimulated [¹⁴C]-D-glucose (U) uptake in isolated adipocytes from epididymal WAT ($n = 4-6$). **F:** Quantification of Western blot analyses of AKT and AMPK phosphorylation in isolated EDL (left panel) and soleus muscles (right panel; $n = 4-6$) after ex vivo insulin and AICAR stimulation, respectively. Data are presented as mean \pm SEM. * $P < 0.05$, ** $P < 0.01$, *** $P < 0.001$, basal vs. insulin/AICAR (two-way ANOVA) and WT vs. D1KO, D4KO, D1/4KO (one-way ANOVA).

both expression of AMPK and phosphorylation of AMPK^{Thr172} were analyzed by Western blotting. Quantitative assessment of replicate skeletal muscle samples revealed that neither expression nor phosphorylation of AKT or AMPK differed between genotypes (Fig. 4F). Moreover, we found no evidence of compensatory changes in the phosphorylation of TBC1D1 and TBC1D4 (TBC1D1^{Ser237}, TBC1D4^{Thr588}, phospho (Ser/Thr)-AKT substrate phosphorylation) in insulin-stimulated skeletal muscle from knockout mice (Supplementary Fig. 4).

***Tbc1d1/Tbc1d4* Deficiency Results in Elevated FAO in Skeletal Muscle**

To determine the role of TBC1D1 and TBC1D4 in lipid utilization in skeletal muscle, EDL and soleus muscles from 16-week-old male mice were isolated and assayed for

basal and AICAR-stimulated oxidation of palmitate, as described in RESEARCH DESIGN AND METHODS. In glycolytic EDL muscle, basal palmitate oxidation was increased substantially (~twofold) in mice deficient in either *Tbc1d1*, *Tbc1d4*, or both (Fig. 5A). In intact isolated EDL muscle from control animals, AICAR stimulation led to a more than twofold increase in FAO (Fig. 5A). In contrast, in EDL muscle from D1KO, D4KO, and D1/4KO mice, the rates of FAO did not increase further in response to AICAR (Fig. 5A). In oxidative soleus muscle, basal palmitate oxidation was markedly increased (~1.4-fold) in mice deficient in *Tbc1d1*, whereas no changes in FAO were observed in mice lacking either *Tbc1d4* or in double-deficient mice (Fig. 5B). For AICAR-stimulated FAO in soleus muscle, no significant differences between the genotypes

were observed (Fig. 5B). The copy numbers of mitochondrial DNA in gastrocnemius muscle were not different between genotypes (Supplementary Fig. 5A). However, citric acid synthase activity was moderately elevated in gastrocnemius muscle from D1KO mice (Supplementary Fig. 5B).

Abundance of GLUT4 Is Reduced in Skeletal Muscle and White Adipose Tissue from *Tbc1d1/Tbc1d4*-Deficient Mice

In skeletal muscle, the mRNA levels for GLUT4 were not different between the genotypes (Supplementary Fig. 6). To further examine the mechanism of the reduced insulin- and AICAR-stimulated glucose uptake in skeletal muscle and adipose cells, tissues from 16-week-old male mice were homogenized, and the abundance of GLUT4 protein was determined by Western blot analysis. D1KO mice displayed the strongest reduction (~40–50%) in GLUT4 content in EDL and tibialis anterior muscle, whereas the abundance of GLUT4 was reduced by only ~30% in quadriceps muscle (Fig. 6A, B, and E). In D4KO mice, GLUT4 was reduced to ~75% in soleus muscle and to ~60% in white adipose tissue (WAT) (Fig. 6C and F). Correspondingly, D1/4KO mice showed reduced GLUT4 content in all tissues analyzed. The abundance of the GLUT4-associated aminopeptidase IRAP (32) also was significantly reduced in EDL and soleus muscle from D1/4KO mice (Supplementary Fig. 7).

RabGAP Deficiency Impairs Basal Retention of GLUT4 in Intracellular Vesicles

We investigated alterations in the subcellular distribution of GLUT4 using bio-LC-ATB-BGPA, a cell surface impermeant bis-glucose photolabeling reagent (31). Intact isolated EDL and soleus muscles from D1KO mice were incubated with bio-LC-ATB-BGPA in the absence or presence of insulin, as described in RESEARCH DESIGN AND METHODS. After ultraviolet irradiation to cross-link the photoactivated diazirine group of bio-LC-ATB-BGPA to cell surface-localized GLUTs, photolabeled GLUT4 was recovered from cell membranes using streptavidin-agarose and quantified by immunoblotting with GLUT4 antibodies.

Compared with the WT controls, the amount of photolabeled cell surface GLUT4 was significantly reduced in insulin-stimulated EDL muscles (Fig. 7A). In contrast, basal levels of photolabeled cell surface GLUT4 from *Tbc1d1*-deficient EDL muscles were not different from controls. In soleus muscle from D1KO mice, however, the levels of photolabeled GLUT4 were similar in the basal and insulin-stimulated states (Fig. 7B). When the amount of total GLUT4 is taken into account, the proportion of GLUT4 at the cell surface is increased in EDL but not in soleus muscle from D1KO mice (Fig. 7C and D). Similar changes occurred in D4KO mice (24).

Tbc1d1/Tbc1d4 Deficiency Reduces Glycogen and Increases Triglyceride Concentrations in the Liver

We investigated the impact of *Tbc1d1/Tbcd4* deficiency on the amount of triglycerides and glycogen in skeletal muscle and liver from mice fasted for 4 h. Hepatic glycogen concentrations were substantially decreased in D1KO, D4KO, and D1/4KO mice compared with WT controls (Fig. 8A). In contrast, fasting glycogen was increased in gastrocnemius (Fig. 8B) and quadriceps muscle (data not shown) of D1/4KO mice compared with WT controls. Abundance of glycogen synthase and phosphorylation (Ser⁶⁴¹) in liver and muscle were not significantly different between the genotypes (Supplementary Fig. 8). Also, no differences in the abundance of glycogen synthase kinase 3 α and phosphorylation (Ser²¹) were observed in liver and muscle (Supplementary Fig. 8). Hepatic triglyceride concentrations were increased in D1KO, D4KO, and D1/4KO mice (Fig. 8C), whereas triglycerides in muscle were not changed (Fig. 8D). Expressions of both forms of the gluconeogenic enzyme phosphoenolpyruvate carboxykinase (*Pck1* and *Pck2*) were increased in liver from D1KO, D4KO, and D1/4KO mice (Fig. 8E and F).

DISCUSSION

In this study we investigated the impact of the combined inactivation of *Tbc1d1* (D1KO) and *Tbc1d4* (D4KO) on glucose and lipid metabolism in *Tbc1d1/Tbc1d4* double-

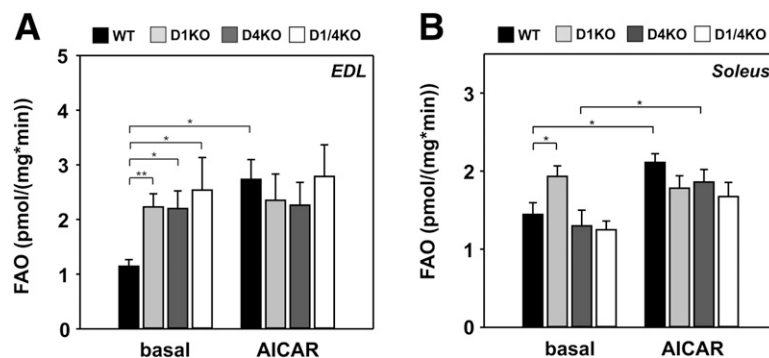


Figure 5—Deletion of *Tbc1d1* and *Tbc1d4* leads to elevated FAO in skeletal muscle. Skeletal muscles from 16-week-old male mice and controls were isolated and assayed for FAO, as described in Research Design and Methods. A: AICAR-stimulated ex vivo [³H]-palmitate oxidation in isolated EDL muscle from D1KO, D4KO, and D1/4KO mice. B: AICAR-stimulated ex vivo [³H]-palmitate oxidation in isolated soleus muscle from D1KO, D4KO, and D4KO mice. Data are presented as mean \pm SEM ($n = 7-8$). * $P < 0.05$, ** $P < 0.01$, basal vs. AICAR (two-way ANOVA) and WT vs. D1KO, D4KO, D1/4KO (one-way ANOVA).

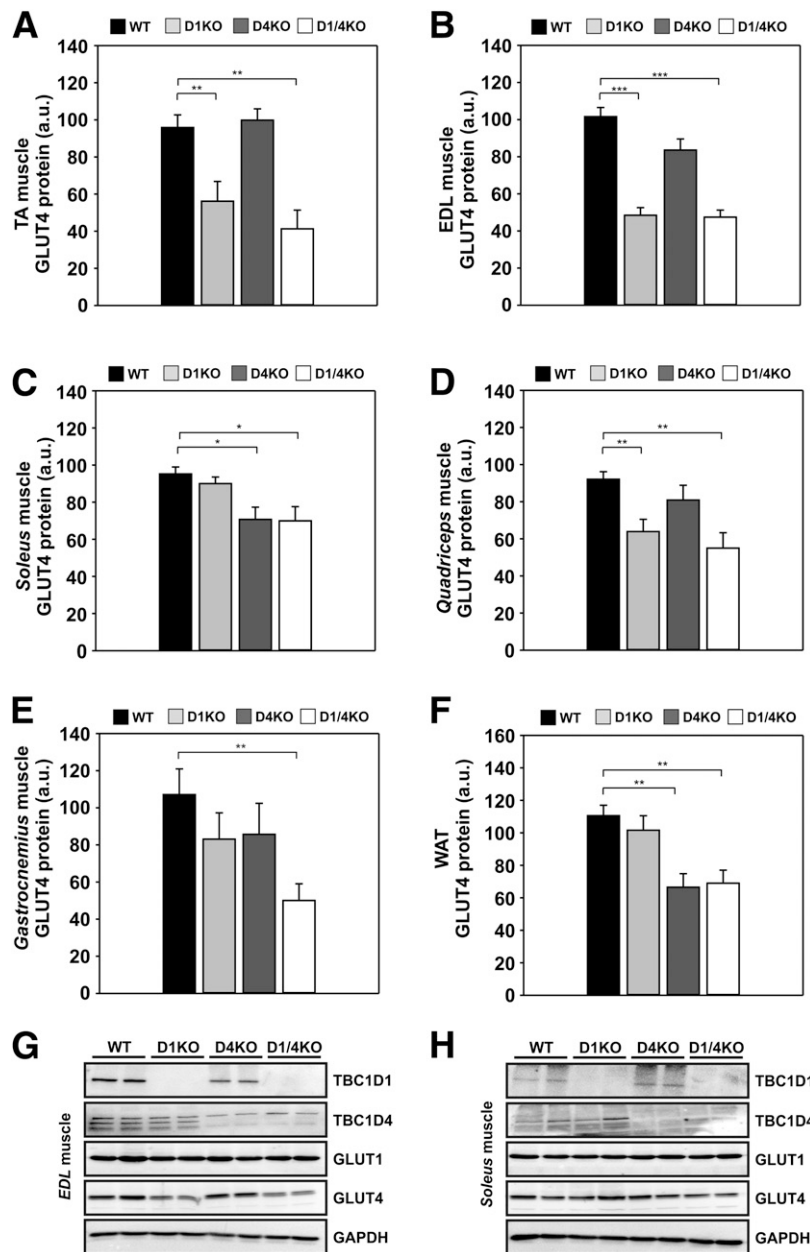


Figure 6—Deficiency in *Tbc1d1* and *Tbc1d4* reduced the abundance of GLUT4 in skeletal muscle and WAT. Abundance of the GLUT4 protein was determined by Western blot analysis of tissues from knockout mice and WT littermate controls. *A*: Tibialis anterior muscle. *B*: EDL muscle. *C*: Soleus muscle. *D*: Quadriceps muscle. *E*: Gastrocnemius muscle. *F*: WAT. Data are presented as mean \pm SEM ($n = 5-10$). * $P < 0.05$, ** $P < 0.01$, *** $P < 0.001$, WT vs. D1KO, D4KO, D1/4KO mice (one-way ANOVA). Representative Western blot analysis of TBC1D1, TBC1D4, GLUT1, and GLUT4 in EDL (*G*) and soleus muscle (*H*).

deficient (D1/4KO) mice. Our results demonstrate that both RabGAPs play critical roles in GLUT4 trafficking and glucose and lipid metabolism in muscle and adipose tissue.

On a standard diet, D1/4KO mice showed moderately reduced body weight and a trend toward reduced fat mass. Moreover, D1/4KO mice showed a reduced RQ, which resulted from a substantial increase in whole-body FAO and decreased use of carbohydrates as fuel. Both D1KO and D4KO mice displayed a similar reduction in body weight and RQ, suggesting that both *Tbc1d1* and *Tbc1d4* may contribute to energy substrate preference in

the animals. In a previous study, animals expressing a signaling-deficient *Tbc1d4*-(T642A) mutant (33) also displayed reduced body weight, whereas *Tbc1d4* knockout mice generated by Nestin-Cre/Lox-mediated deletion of the gene showed no significant change in body weight (14). In contrast, *Tbc1d1* deficiency substantially reduced body weight and RQ in obese mice fed a high-fat diet, indicating a possible interaction of the gene with dietary fat and/or obesity (10).

Similar to the single knockout mice, D1/4KO mice had normal fasting glucose concentrations. In contrast to

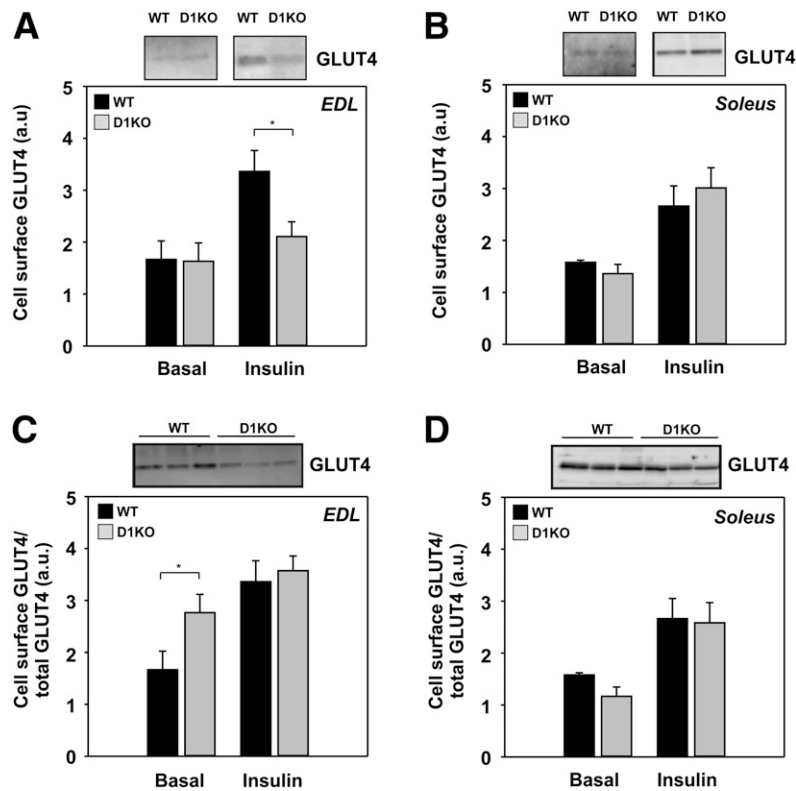


Figure 7—*Tbc1d1* deficiency leads to subcellular redistributions of GLUT4. Following a 4-h fasting period, mice were anesthetized and EDL and soleus muscles were removed. Muscles in the basal and insulin-stimulated states were cell surface labeled with impermeant Bio-LC-ATB-BGPA. Biotinylated proteins were recovered from muscle lysates using immobilized streptavidin beads and resolved by SDS-PAGE. Total and labeled cell surface GLUT4 were determined by Western blot analysis. The concentrations of cell surface GLUT4 then were compared without correction for total GLUT4 (EDL [A] and soleus [B]; bands show recovered biotinylated GLUT4) or with correction for total GLUT4 (EDL [C] and soleus [D]; bands show total GLUT4). Data are presented as mean \pm SEM ($n = 3-9$). * $P < 0.05$, WT vs. D1KO mice (two-tailed unpaired t test). a.u., arbitrary units.

D1KO and D4KO animals, however, D1/4KO mice displayed markedly impaired tolerance to glucose, insulin, and AICAR, indicating an important role of both RabGAPs in glucose disposal in vivo. Thus, the impact of a single RabGAP knockout on glycemic control (i.e., D1KO and D4KO) seems to be largely compensated for by the residual RabGAP activity of the functioning gene, whereas inactivation of both RabGAPs leads to a pronounced impairment of glucose disposal. Interestingly, D1KO mice had reduced AICAR tolerance compared with D4KO animals, indicating an increased relevance of TBC1D1 in the AICAR response. This might reflect tissue-specific differences in the abundance of RabGAP and/or sensitivity of the RabGAPs to AICAR. The reduced postprandial glucose concentrations in D1/4KO mice could be related to a proposed function of the RabGAPs in insulin secretion (34,35). However, we did not observe genotype-specific differences in circulating insulin concentrations.

In mice, *Tbc1d1* is predominantly expressed in glycolytic muscle fibers, whereas *Tbc1d4* is expressed more strongly in oxidative muscle and in adipose cells (14,23). Consistent with the tissue-specific expression profile of both RabGAPs, insulin-stimulated glucose uptake in

D1KO mice was substantially reduced in intact isolated EDL muscle but was normal in soleus muscle and isolated adipose cells. Conversely, D4KO mice showed severely impaired insulin-stimulated glucose uptake in soleus muscle and adipose cells, whereas glucose uptake was normal in EDL muscle. The combined ablation of both RabGAPs in D1/4KO mice essentially resulted in the elimination of insulin- and AICAR-stimulated glucose uptake in EDL and soleus muscle and in a substantial reduction of insulin-stimulated glucose uptake in adipose cells. However, in the double knockout mice, deletion of one of the RabGAPs (e.g., *Tbc1d1* in EDL, *Tbc1d4* in soleus and WAT) is sufficient to abolish insulin- and AICAR-stimulated glucose uptake without any further reduction in glucose transport in these tissues. In D1KO mice, GLUT4-associated glucose transport is clearly deficient in glycolytic muscle, yet GTT and ITT responses are normal. This suggests that glycolytic muscle types alone are not essential for maintaining whole animal glucose homeostasis, possibly because of background maintenance of TBC1D4 activity and normal glucose transport activity in nonglycolytic muscle. Consistent with these findings, previous studies of GLUT4-deficient

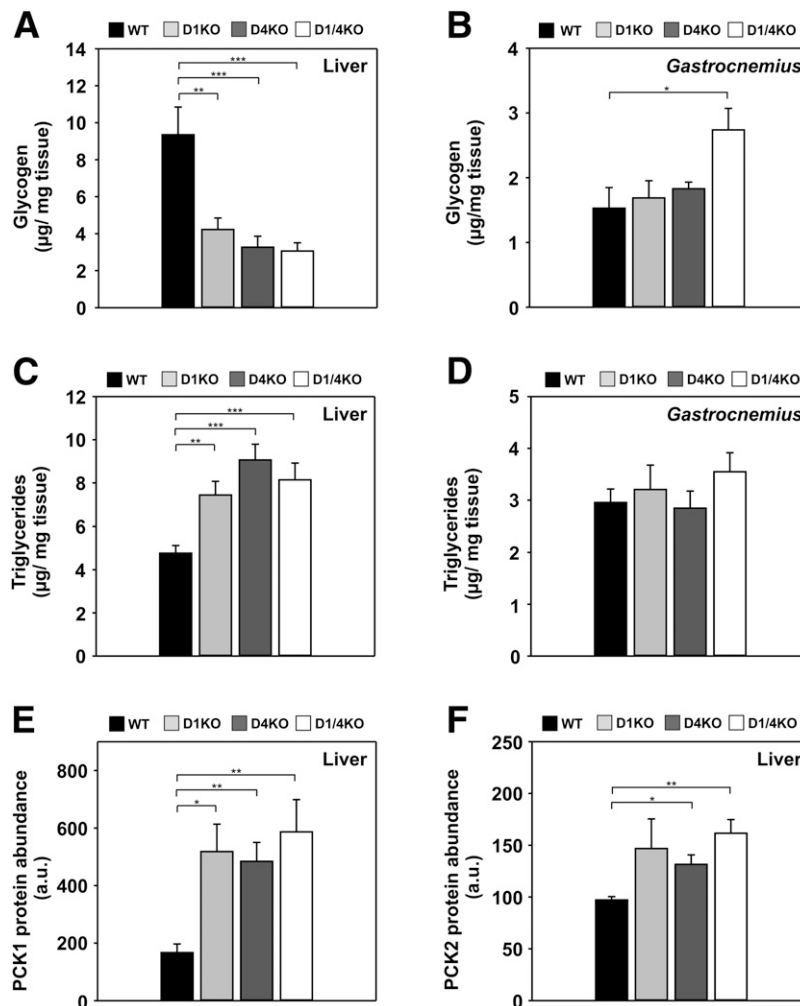


Figure 8—*Tbc1d1/Tbc1d4* deficiency reduces glycogen content and increases triglyceride concentrations and the abundance of PCK1 and PCK2 in the liver. Tissues from 16-week-old male mice were analyzed for triglyceride and glycogen content and for protein expression of PCK1 and PCK2 using Western blot. **A**: Glycogen content in liver ($n = 18$ – 24). **B**: Glycogen content in gastrocnemius muscle ($n = 7$). **C**: Hepatic triglyceride content ($n = 12$ – 19). **D**: Triglyceride content in gastrocnemius muscle ($n = 7$ – 13). Abundance of hepatic PCK1 (**E**) and PCK2 expression (**F**) ($n = 6$). Data are presented as mean \pm SEM. * $P < 0.05$, ** $P < 0.01$, *** $P < 0.001$, WT vs. D1KO, D4KO, D1/4KO mice (one-way ANOVA). a.u., arbitrary units.

mice also demonstrated substantial compensation for reduced glucose transport in muscle and adipose tissue by altering hepatic fuel metabolism and increasing utilization of fatty acids (36). Thus, taken together, *Tbc1d1* and *Tbc1d4* play an essential role in insulin- and AICAR-stimulated glucose uptake in both skeletal muscle and adipose cells.

The reduced glucose uptake in response to insulin and AICAR was paralleled by a considerable reduction in GLUT4 abundance in muscle and adipose cells. Because the mRNA levels of GLUT4 were unaltered in the knockout mice, the decrease in GLUTs is likely the result of posttranslational events and may reflect missorting of the protein, presumably caused by the altered function of one or more Rabs downstream of TBC1D1/TBC1D4 (14,23,24,37). Consistent with a defect in protein sorting, the abundance of the insulin-regulated aminopeptidase IRAP, a resident protein of GLUT4 vesicles (38,39), binding

partner of TBC1D4 (40), and potential regulator of GLUT4 sorting (41), also was significantly reduced in both EDL and soleus muscle from D1/4KO mice.

Previous studies showed that basal glucose transport is strongly correlated with the abundance of GLUT4 protein in adipose cells and skeletal muscle. Deletion of GLUT4 in these tissues led to a profound reduction in basal glucose transport, whereas overexpression of GLUT4 resulted in a substantial increase in basal uptake of glucose into the cells (42–45). In contrast, in skeletal muscle and adipose cells from D1KO, D4KO, and D1/4KO mice, basal glucose transport was normal despite substantially reduced abundance of cellular GLUT4 protein. Thus the dissociation of basal glucose transport and GLUT4 abundance in mice suggests that a lack of RabGAPs leads to a redistribution of GLUT4 from intracellular compartments to the cell surface in the basal state. We therefore investigated the

subcellular distribution of GLUT4 by cell surface photolabeling of the protein in EDL and soleus muscle from D1KO mice and compared the surface concentration with the total GLUT4 concentration. Consistent with the glucose transport data, the amount of basal cell surface GLUT4 in the EDL muscles of D1KO mice was comparable with that of WT mice despite a lower abundance of total GLUT4. Thus, in unstimulated D1KO cells, a higher proportion of GLUT4 was present on the cell surface. In the insulin-stimulated state, both glucose uptake and cell surface GLUT4 were equally reduced compared with concentrations in WT mice, indicating that the fraction of GLUT4 present on the plasma membrane in insulin-stimulated cells is relatively normal. Thus, while it is not known at what stage in GLUT4 trafficking TBC1D1 and TBC1D4 participate at the molecular level, our findings are consistent with the RabGAPs being involved in intracellular retention of GLUT4 vesicles in the basal state (22,46).

Consistent with the reduction in RQ, D1KO, D4KO, and D1/4KO mice exhibited elevated basal FAO in EDL muscle. In the oxidative soleus muscle, FAO was elevated only in D1KO mice and was not increased further by AICAR stimulation. Unexpectedly, soleus muscle from D1/4KO mice did not show increased FAO despite the lack of TBC1D1, indicating that additional factors that modulate lipid oxidation in this type of muscle might be involved. In contrast, D1KO, D4KO, and D1/4KO mice had equally increased levels of FAO in glycolytic EDL muscle, which also was not further increased by AICAR. Thus, in glycolytic muscle, inactivation of each RabGAP equally contributes to the elevated FAO. Moreover, elevation of FAO is not directly related to impaired glucose uptake because *Tbc1d4* knockouts have normal glucose uptake but increased FAO in EDL muscle. The mechanism responsible for the elevated FAO in glycolytic skeletal muscle of RabGAP-deficient mice remains to be clarified. We previously showed that knockdown *Tbc1d1* in cultured skeletal muscle cells also increases fatty acid uptake and FAO, whereas overexpression of the gene has the opposite effect (10). However, overexpression of a RabGAP-deficient mutant, *Tbc1d1*-R941K, had no effect on fatty acid uptake and FAO, indicating the involvement of Rab-GTPases in this process (10). Interestingly, knockout of both *Tbc1d1* and *Tbc1d4* did not exert additive effects on FAO in EDL muscle, which suggests that both RabGAPs may regulate the same downstream target.

RabGAP-deficient D1/4KO mice phenocopy adipose- and muscle-specific GLUT4 knockout mice; these animals show substantially reduced glucose uptake in response to insulin and increased use of lipids as an energy source (36). In fact, the reduced abundance of GLUT4 explains, at least in part, the decreased glucose uptake in response to a stimulus. The inability to use glucose in muscle and adipocytes is associated with elevated hepatic triglycerides and reduced hepatic glycogen content, whereas fasting glycogen concentrations in skeletal muscle tend to be increased. Although hepatic glycogen concentrations in

adipose- and muscle-specific GLUT4 knockout mice were not reported, conversion of glucose to fatty acids in the liver was substantially increased in these animals (36). Consistent with our data, muscle-specific GLUT4 knockout mice also displayed increased fasting glycogen content in skeletal muscle despite substantially reduced glucose uptake (47). A complex counterregulation of increased glycogen synthesis and decreased glycogen breakdown was proposed to explain this effect (47). We could not confirm a substantial increase in glycogen synthesis in skeletal muscle from fasted D1/4KO mice; however, the effect size might be larger in muscle completely lacking GLUT4. Thus, the mechanistic basis for the underlying tissue crosstalk remains to be further explored.

In summary, our results indicate that both RabGAPs play important roles in GLUT4 trafficking and glucose and lipid metabolism in muscle and adipose cells. So far, of the many Rab-GTPases previously associated with GLUT4-containing compartments (48,49), only Rab8, Rab10, and Rab14 were identified as substrates for both TBC1D1 and TBC1D4 in vitro; furthermore, they have been implicated in roles in trafficking of GLUT4 in vivo (50–53). Future studies investigating the specific contribution of the Rabs to the regulation of metabolic flexibility are required.

Acknowledgments. The authors thank Carolin Borchert, Diana Schulze, Ines Grüner, Angelika Horrigs, Anette Kurowski, Ilka Römer, Annette Schober, Antonia Osmers, and Jennifer Schwettmann for expert technical assistance, as well as Susanna Keller and Annette Schürmann for generously providing antibodies.

Funding. This work was supported by the Ministry of Science and Research of the State of North Rhine-Westphalia (MIWF NRW) and the German Federal Ministry of Health (BMG) and was funded in part by grants from the Deutsche Forschungsgemeinschaft (GRK1208, AL452/4-1), the German Academic Exchange Service (DAAD) (to G.D.H.), the EFS/Lilly European Diabetes Research Program, and the Swiss National Science Foundation (310000-122243/1, 310030-143929/1).

Duality of Interest. No conflicts of interest relevant to this article were reported.

Author Contributions. A.C. and H.A.-H. conceived the experiments, analyzed data, and wrote the manuscript. A.C., A.I., C.d.W., C.S., Z.Z., T.S., and D.L.-C. performed the experiments and analyzed data. A.C., G.D.H., J.L., H.-G.J., and H.A.-H. contributed to the discussion and reviewed and edited the manuscript. H.A.-H. is the guarantor of this work and, as such, had full access to all of the data in the study and takes responsibility for the integrity of the data and the accuracy of the data analysis.

References

- Leto D, Saltiel AR. Regulation of glucose transport by insulin: traffic control of GLUT4. *Nat Rev Mol Cell Biol* 2012;13:383–396
- Holman GD, Cushman SW. Subcellular localization and trafficking of the GLUT4 glucose transporter isoform in insulin-responsive cells. *Bioessays* 1994; 16:753–759
- Sano H, Kane S, Sano E, et al. Insulin-stimulated phosphorylation of a Rab GTPase-activating protein regulates GLUT4 translocation. *J Biol Chem* 2003;278:14599–14602
- Roach WG, Chavez JA, Miinea CP, Lienhard GE. Substrate specificity and effect on GLUT4 translocation of the Rab GTPase-activating protein Tbc1d1. *Biochem J* 2007;403:353–358

5. Kramer HF, Witczak CA, Fujii N, et al. Distinct signals regulate AS160 phosphorylation in response to insulin, AICAR, and contraction in mouse skeletal muscle. *Diabetes* 2006;55:2067–2076
6. Chen S, Murphy J, Toth R, Campbell DG, Morrice NA, Mackintosh C. Complementary regulation of TBC1D1 and AS160 by growth factors, insulin and AMPK activators. *Biochem J* 2008;409:449–459
7. Sakamoto K, Holman GD. Emerging role for AS160/TBC1D4 and TBC1D1 in the regulation of GLUT4 traffic. *Am J Physiol Endocrinol Metab* 2008;295:E29–E37
8. An D, Toyoda T, Taylor EB, et al. TBC1D1 regulates insulin- and contraction-induced glucose transport in mouse skeletal muscle. *Diabetes* 2010;59:1358–1365
9. Funai K, Cartee GD. Inhibition of contraction-stimulated AMP-activated protein kinase inhibits contraction-stimulated increases in PAS-TBC1D1 and glucose transport without altering PAS-AS160 in rat skeletal muscle. *Diabetes* 2009;58:1096–1104
10. Chadt A, Leicht K, Deshmukh A, et al. Tbc1d1 mutation in lean mouse strain confers leanness and protects from diet-induced obesity. *Nat Genet* 2008;40:1354–1359
11. Stone S, Abkevich V, Russell DL, et al. TBC1D1 is a candidate for a severe obesity gene and evidence for a gene/gene interaction in obesity predisposition. *Hum Mol Genet* 2006;15:2709–2720
12. Meyre D, Farge M, Lecoeur C, et al. R125W coding variant in TBC1D1 confers risk for familial obesity and contributes to linkage on chromosome 4p14 in the French population. *Hum Mol Genet* 2008;17:1798–1802
13. Dash S, Sano H, Rochford JJ, et al. A truncation mutation in TBC1D4 in a family with acanthosis nigricans and postprandial hyperinsulinemia. *Proc Natl Acad Sci U S A* 2009;106:9350–9355
14. Wang HY, Ducommun S, Quan C, et al. AS160 deficiency causes whole-body insulin resistance via composite effects in multiple tissues. *Biochem J* 2013;449:479–489
15. Szekeres F, Chadt A, Tom RZ, et al. The Rab-GTPase-activating protein TBC1D1 regulates skeletal muscle glucose metabolism. *Am J Physiol Endocrinol Metab* 2012;303:E524–E533
16. Miinea CP, Sano H, Kane S, et al. AS160, the Akt substrate regulating GLUT4 translocation, has a functional Rab GTPase-activating protein domain. *Biochem J* 2005;391:87–93
17. Hatakeyama H, Kanzaki M. Regulatory mode shift of Tbc1d1 is required for acquisition of insulin-responsive GLUT4-trafficking activity. *Mol Biol Cell* 2013;24:809–817
18. Koumanov F, Richardson JD, Murrow BA, Holman GD. AS160 phosphotyrosine-binding domain constructs inhibit insulin-stimulated GLUT4 vesicle fusion with the plasma membrane. *J Biol Chem* 2011;286:16574–16582
19. Tan SX, Ng Y, Burchfield JG, et al. The Rab GAPase-activating protein TBC1D4/AS160 contains an atypical phosphotyrosine-binding domain that interacts with plasma membrane phospholipids to facilitate GLUT4 trafficking in adipocytes. *Mol Cell Biol* 2012;32:4946–4959
20. Sun Y, Bilan PJ, Liu Z, Klip A. Rab8A and Rab13 are activated by insulin and regulate GLUT4 translocation in muscle cells. *Proc Natl Acad Sci U S A* 2010;107:19909–19914
21. Brewer PD, Romenskaia I, Kanow MA, Mastick CC. Loss of AS160 Akt substrate causes Glut4 protein to accumulate in compartments that are primed for fusion in basal adipocytes. *J Biol Chem* 2011;286:26287–26297
22. Eguez L, Lee A, Chavez JA, et al. Full intracellular retention of GLUT4 requires AS160 Rab GTPase activating protein. *Cell Metab* 2005;2:263–272
23. Dokas J, Chadt A, Nolden T, et al. Conventional knockout of Tbc1d1 in mice impairs insulin- and AICAR-stimulated glucose uptake in skeletal muscle. *Endocrinology* 2013;154:3502–3514
24. Lansey MN, Walker NN, Hargett SR, Stevens JR, Keller SR. Deletion of Rab GAP AS160 modifies glucose uptake and GLUT4 translocation in primary skeletal muscles and adipocytes and impairs glucose homeostasis. *Am J Physiol Endocrinol Metab* 2012;303:E1273–E1286
25. Wakeland E, Morel L, Achey K, Yui M, Longmate J. Speed congenics: a classic technique in the fast lane (relatively speaking). *Immunol Today* 1997;18:472–477
26. Livak KJ, Schmittgen TD. Analysis of relative gene expression data using real-time quantitative PCR and the 2(-Delta Delta C(T)) Method. *Methods* 2001;25:402–408
27. Péronnet F, Massicotte D. Table of nonprotein respiratory quotient: an update. *Can J Sport Sci* 1991;16:23–29
28. Passonneau JV, Lauderdale VR. A comparison of three methods of glycogen measurement in tissues. *Anal Biochem* 1974;60:405–412
29. Gliemann J, Rees WD, Foley JA. The fate of labelled glucose molecules in the rat adipocyte. Dependence on glucose concentration. *Biochim Biophys Acta* 1984;804:68–76
30. Al-Hasani H, Hinck CS, Cushman SW. Endocytosis of the glucose transporter GLUT4 is mediated by the GTPase dynamin. *J Biol Chem* 1998;273:17504–17510
31. Hashimoto M, Hatanaka Y, Yang J, Dhese J, Holman GD. Synthesis of biotinylated bis(D-glucose) derivatives for glucose transporter photoaffinity labelling. *Carbohydr Res* 2001;331:119–127
32. Keller SR, Scott HM, Mastick CC, Aebersold R, Lienhard GE. Cloning and characterization of a novel insulin-regulated membrane aminopeptidase from Glut4 vesicles. *J Biol Chem* 1995;270:23612–23618
33. Chen S, Wasserman DH, MacKintosh C, Sakamoto K. Mice with AS160/TBC1D4-Thr649Ala knockin mutation are glucose intolerant with reduced insulin sensitivity and altered GLUT4 trafficking. *Cell Metab* 2011;13:68–79
34. Rütli S, Arous C, Nica AC, Kanzaki M, Halban PA, Bouzakri K. Expression, phosphorylation and function of the Rab-GTPase activating protein TBC1D1 in pancreatic beta-cells. *FEBS Lett* 2014;588:15–20
35. Bouzakri K, Ribaux P, Tomas A, Parnaud G, Rickenbach K, Halban PA. Rab GTPase-activating protein AS160 is a major downstream effector of protein kinase B/Akt signaling in pancreatic beta-cells. *Diabetes* 2008;57:1195–1204
36. Kotani K, Peroni OD, Minokoshi Y, Boss O, Kahn BB. GLUT4 glucose transporter deficiency increases hepatic lipid production and peripheral lipid utilization. *J Clin Invest* 2004;114:1666–1675
37. Seixas E, Barros M, Seabra MC, Barral DC. Rab and Arf proteins in genetic diseases. *Traffic* 2013;14:871–885
38. Ross SA, Herbst JJ, Keller SR, Lienhard GE. Trafficking kinetics of the insulin-regulated membrane aminopeptidase in 3T3-L1 adipocytes. *Biochem Biophys Res Commun* 1997;239:247–251
39. Malide D, St-Denis JF, Keller SR, Cushman SW. Vp165 and GLUT4 share similar vesicle pools along their trafficking pathways in rat adipose cells. *FEBS Lett* 1997;409:461–468
40. Peck GR, Ye S, Pham V, et al. Interaction of the Akt substrate, AS160, with the glucose transporter 4 vesicle marker protein, insulin-regulated aminopeptidase. *Mol Endocrinol* 2006;20:2576–2583
41. Jordens I, Molle D, Xiong W, Keller SR, McGraw TE. Insulin-regulated aminopeptidase is a key regulator of GLUT4 trafficking by controlling the sorting of GLUT4 from endosomes to specialized insulin-regulated vesicles. *Mol Biol Cell* 2010;21:2034–2044
42. Al-Hasani H, Yver DR, Cushman SW. Overexpression of the glucose transporter GLUT4 in adipose cells interferes with insulin-stimulated translocation. *FEBS Lett* 1999;460:338–342
43. Zisman A, Peroni OD, Abel ED, et al. Targeted disruption of the glucose transporter 4 selectively in muscle causes insulin resistance and glucose intolerance. *Nat Med* 2000;6:924–928
44. Abel ED, Peroni O, Kim JK, et al. Adipose-selective targeting of the GLUT4 gene impairs insulin action in muscle and liver. *Nature* 2001;409:729–733
45. Ren JM, Marshall BA, Mueckler MM, McCaleb M, Amatruda JM, Shulman GI. Overexpression of Glut4 protein in muscle increases basal and

- insulin-stimulated whole body glucose disposal in conscious mice. *J Clin Invest* 1995;95:429–432
46. Ishikura S, Klip A. Muscle cells engage Rab8A and myosin Vb in insulin-dependent GLUT4 translocation. *Am J Physiol Cell Physiol* 2008;295:C1016–C1025
47. Kim YB, Peroni OD, Aschenbach WG, et al. Muscle-specific deletion of the Glut4 glucose transporter alters multiple regulatory steps in glycogen metabolism. *Mol Cell Biol* 2005;25:9713–9723
48. Stöckli J, Fazakerley DJ, James DE. GLUT4 exocytosis. *J Cell Sci* 2011;124:4147–4159
49. Kaddai V, Le Marchand-Brustel Y, Cormont M. Rab proteins in endocytosis and Glut4 trafficking. *Acta Physiol (Oxf)* 2008;192:75–88
50. Sun Y, Chiu TT, Foley KP, Bilan PJ, Klip A. Myosin Va mediates Rab8A-regulated GLUT4 vesicle exocytosis in insulin-stimulated muscle cells. *Mol Biol Cell* 2014;25:1159–1170
51. Chen Y, Wang Y, Zhang J, et al. Rab10 and myosin-Va mediate insulin-stimulated GLUT4 storage vesicle translocation in adipocytes. *J Cell Biol* 2012;198:545–560
52. Reed SE, Hodgson LR, Song S, et al. A role for Rab14 in the endocytic trafficking of GLUT4 in 3T3-L1 adipocytes. *J Cell Sci* 2013;126:1931–1941
53. Sadacca LA, Bruno J, Wen J, Xiong W, McGraw TE. Specialized sorting of GLUT4 and its recruitment to the cell surface are independently regulated by distinct Rabs. *Mol Biol Cell* 2013;24:2544–2557



AMPK and TBC1D1 Regulate Muscle Glucose Uptake After, but Not During, Exercise and Contraction

Rasmus Kjøbsted,¹ Julie L.W. Roll,¹ Nicolas O. Jørgensen,¹ Jesper B. Birk,¹ Marc Foretz,^{2,3,4} Benoit Viollet,^{2,3,4} Alexandra Chadt,^{5,6} Hadi Al-Hasani,^{5,6} and Jørgen F.P. Wojtaszewski¹

Diabetes 2019;68:1427–1440 | <https://doi.org/10.2337/db19-0050>

Exercise increases glucose uptake in skeletal muscle independently of insulin signaling. This makes exercise an effective stimulus to increase glucose uptake in insulin-resistant skeletal muscle. AMPK has been suggested to regulate muscle glucose uptake during exercise/contraction, but findings from studies of various AMPK transgenic animals have not reached consensus on this matter. Comparing methods used in these studies reveals a hitherto unappreciated difference between those studies reporting a role of AMPK and those that do not. This led us to test the hypothesis that AMPK and downstream target TBC1D1 are involved in regulating muscle glucose uptake in the immediate period after exercise/contraction but not during exercise/contraction. Here we demonstrate that glucose uptake during exercise/contraction was not compromised in AMPK-deficient skeletal muscle, whereas reversal of glucose uptake toward resting levels after exercise/contraction was markedly faster in AMPK-deficient muscle compared with wild-type muscle. Moreover, muscle glucose uptake after contraction was positively associated with phosphorylation of TBC1D1, and skeletal muscle from TBC1D1-deficient mice displayed impaired glucose uptake after contraction. These findings reconcile previous observed discrepancies and redefine the role of AMPK activation during exercise/contraction as being important for maintaining glucose permeability in skeletal muscle in the period after, but not during, exercise/contraction.

To meet the increased energy demand in skeletal muscle during exercise and contraction, glucose uptake is

markedly increased. After the cessation of exercise and contraction, energy demand decreases and muscle glucose uptake gradually returns to resting levels (1–5). Studies have shown that exercise/contraction uses mechanisms to increase muscle glucose uptake that are independent of those engaged upon insulin stimulation (6–8). It has been speculated that cellular feed-forward events secure the initial rise in glucose uptake upon initiation of exercise/contraction, whereas other events control glucose uptake during exercise/contraction based on cellular feedback signals (9). Along these lines, the reversal of glucose uptake after cessation of exercise/contraction is likely also a regulated process securing adequate cellular fuel supply in recovery. However, the nature of this process is still only weakly understood.

Skeletal muscle glucose uptake can be defined as a three-step process involving delivery, transport, and metabolism of glucose (10,11). During exercise, the glucose transport capacity is mainly determined by the representation of GLUT4 at the cell surface membrane that is regulated by both exo- and endocytotic processes (12). It is well known that pharmacological activation of the cellular energy sensor AMPK is sufficient to increase glucose uptake and GLUT4 representation at the cell surface membrane of skeletal muscle (13). An obvious extrapolation of these observations has been to assume that the AMPK activation seen in skeletal muscle during exercise/contractile activity (14,15) is regulating glucose uptake under these conditions as well. However, despite numerous studies, no consensus on the role of AMPK in regulating muscle glucose uptake during exercise/contractile activity has been reached (16).

¹Section of Molecular Physiology, Department of Nutrition, Exercise, and Sports, Faculty of Science, University of Copenhagen, Copenhagen, Denmark

²INSERM, U1016, Institut Cochin, Paris, France

³Centre National de la Recherche Scientifique (CNRS), UMR8104, Paris, France

⁴Université Paris Descartes, Sorbonne Paris Cité, Paris, France

⁵German Diabetes Center, Leibniz Center for Diabetes Research, Heinrich Heine University Düsseldorf, Medical Faculty, Düsseldorf, Germany

⁶German Center for Diabetes Research (DZD), München-Neuherberg, Germany

Corresponding author: Jørgen F.P. Wojtaszewski, jwojtaszewski@nxs.ku.dk

Received 16 January 2019 and accepted 12 April 2019

This article contains Supplementary Data online at <http://diabetes.diabetesjournals.org/lookup/suppl/doi:10.2337/db19-0050/-/DC1>.

© 2019 by the American Diabetes Association. Readers may use this article as long as the work is properly cited, the use is educational and not for profit, and the work is not altered. More information is available at <http://www.diabetesjournals.org/content/license>.

Going through the literature, we observed an unappreciated methodological difference between those studies reporting impairments in exercise/contraction-induced muscle glucose uptake by ablation of AMPK activity in skeletal muscle and those studies that did not. In the majority of studies reporting decreased muscle glucose uptake with contraction, the actual assessment of glucose uptake by muscle tracer accumulation took place either in the period during as well as in the period after contraction (17,18) or solely in the period after contraction (17,19–23). Moreover, studies have suggested that pharmacological agents activating AMPK increase muscle glucose uptake by slowing down GLUT4 endocytosis, whereas insulin and contraction increases glucose uptake by enhancing GLUT4 exocytosis (24–26). Inspired by these observations, we tested the hypothesis that the increase in glucose uptake during exercise/contractile activity occurs independently of AMPK, whereas AMPK becomes key for maintaining muscle glucose uptake in the period after exercise/contractile activity. Herein, using both conventional and conditional AMPK α 1 α 2 muscle-specific double-knockout (mdKO) mice as well as whole-body TBC1D1 KO mice, we demonstrate that AMPK is not necessary for contraction to increase muscle glucose uptake. In contrast, we provide evidence to support that AMPK regulates muscle glucose uptake in the immediate period after exercise/contraction and that this is likely mediated by phosphorylation of its downstream target TBC1D1. Collectively, these results redefine the biological role of AMPK and TBC1D1 signaling in the context of skeletal muscle glucose uptake.

RESEARCH DESIGN AND METHODS

Animals

All animal experiments were approved by the Danish Animal Experiments Inspectorate and complied with the EU convention for the protection of vertebrates used for scientific purposes. Animals used in this study were conventional and conditional (inducible) AMPK α 1 α 2 mdKO and recombinant congenic *TBC1D1*-deficient (whole-body TBC1D1 KO) female mice with corresponding wild-type (WT) littermates as controls (27–29). Mice (16 \pm 2 weeks [mean \pm SD]) were group housed at two animal facilities at the Department of Experimental Medicine and kept in a temperature- and humidity-controlled room on a 12:12 h light-dark cycle with free access to standard rodent chow and water.

Muscle Glucose Uptake After Exercise

All mice were acclimatized to treadmill running and subsequently subjected to a graded maximal running test as previously described (30). For muscle glucose uptake measurements after exercise, mice were fasted in single cages for 2 h before either performing a single bout of treadmill exercise (30 min, 10° incline, and 60% of maximal running speed) or resting as sedentary controls. Immediately after rest/exercise, mice were anesthetized by an intraperitoneal

injection of pentobarbital (9 mg/100 g body weight) and left to recover on a heating plate (30°C) for 30 min. Hereafter, a bolus of [3 H]2-deoxyglucose (12.3 MBq/kg body weight) dissolved in isotonic saline was administered retroorbitally. After 10 min, during which blood sampling was performed at time points 0, 5, and 10 min, tibialis anterior (TA) and extensor digitorum longus (EDL) muscles were rapidly dissected and frozen for analysis of muscle glucose uptake as previously described (31).

Muscle Glucose Uptake During and After In Situ Contraction

Glucose uptake in TA and EDL muscles during in situ contraction was determined as previously described (31). In short, an electrode was placed on the common peroneal nerve of one leg of anesthetized animals (intraperitoneal injection of pentobarbital, 9 mg/100 g body weight), after which electrical stimulation was applied for 10 min to initiate contraction of the TA and EDL muscles. The other leg served as a sham-operated control. Muscle glucose uptake during in situ contraction was determined by retro-orbital injection of [3 H]2-deoxyglucose as described above. For muscle glucose uptake measurements after in situ contraction, anesthetized and muscle-contracted animals were left to recover on a heating plate (30°C) for 30 or 60 min, after which muscle glucose uptake was determined as described above.

Insulin-Stimulated Glucose Uptake of Incubated Skeletal Muscle

Fed animals were anesthetized by an intraperitoneal injection of pentobarbital (10 mg/100 g body weight) before EDL muscles were isolated and suspended in incubation chambers containing Krebs-Ringer buffer (KRB) as previously described (31). In short, EDL muscles were incubated for 30 min in the absence or presence of 100 μ U/mL insulin, after which half of the muscles were transferred to new incubation chambers containing KRB for either 30 min or 1 h. 2-Deoxyglucose uptake was measured during a 10-min period after the respective incubation period by adding 1 mmol/L [3 H]2-deoxyglucose (0.028 MBq/mL) and 7 mmol/L [14 C]mannitol (0.0083 MBq/mL) to the incubation medium. 2-Deoxyglucose uptake was determined as previously described (31).

Glucose Uptake in Incubated Skeletal Muscle 2 h After Prior In Situ Contraction

After in situ contraction of a single mouse hind limb, EDL muscles from both legs were isolated and incubated in incubation chambers with KRB as described above. 2-Deoxyglucose uptake was measured during the last 10 min of the 2-h incubation period by adding 1 mmol/L [3 H]2-deoxyglucose (0.028 MBq/mL) and 7 mmol/L [14 C]mannitol (0.0083 MBq/mL) to the incubation medium. During the incubation period, KRB was replaced at time points 30, 60, and 90 min to minimize fluctuations in energy substrate content (pyruvate) of the KRB.

Muscle Processing, SDS-PAGE, and Western Blot Analyses

Muscles were homogenized as previously described (31,32), and lysates were collected and frozen in liquid nitrogen for subsequent analyses. The bicinchoninic acid method was used to determine total protein abundance in muscle lysates. Lysates were boiled in Laemmli buffer and subjected to SDS-PAGE and immunoblotting as previously described (31,32).

AMPK Activity

Heterotrimer-specific AMPK activity in skeletal muscle was determined by three consecutive immunoprecipitations as previously described (31,32).

Muscle Glycogen and Glucose-6-phosphate

Muscle glycogen was measured on muscle protein homogenate after acid hydrolysis as previously described (31). Muscle glucose-6-phosphate content was measured fluorometrically as described by Lowry and Passonneau (33).

Antibodies

Primary antibodies against pAMPK α -Thr172 (2531), pACC-Ser79/212 (3661), pTBC1D4-Thr642 (8881), pErk1/2-Thr202/Tyr204 (9101), pP38MAPK-Thr180/Tyr182 (9211), Erk1/2 (9102), P38MAPK (9212), GAPDH (2118), and TBC1D1 (4629) were from Cell Signaling Technology. Antibodies against pTBC1D1-Ser231 (07-2268) and TBC1D4 (AS160) (07-741) were from Millipore, and AMPK α 2 (SC-19131), hexokinase II (SC-6512), and GLUT4 (PA1-1065) antibodies were from Santa Cruz Biotechnology and Thermo Fisher Scientific, respectively. ACC protein was detected using horseradish peroxidase-conjugated streptavidin from Dako (P0397). AMPK α 1 protein were detected using antibody as previously described (30,34). Antibodies used for the AMPK activity assay were raised against AMPK γ 3 (provided by D.G. Hardie, University of Dundee, Scotland, U.K.), AMPK α 2 (SC-19131; Santa Cruz Biotechnology), and AMPK α 1 (purchased from GenScript, Jiangning, Nanjing, China).

Statistical Analyses

Statistical analyses were performed using SigmaPlot (version 13.0; SYSTAT, Erkrath, Germany). Data are presented as the means \pm SEM unless stated otherwise. Two-way ANOVA with and without repeated measures was used to assess statistical differences. In case of unequal variance (Fig. 1E and G), the two-sided Student *t* test was used to assess statistical difference between groups. The Student-Newman-Keuls test was used for post hoc testing. Correlation analyses were performed by calculating the Pearson product moment correlation. Statistical significance was defined as $P < 0.05$.

RESULTS

Glucose Uptake Is Decreased in AMPK-Deficient Muscle in Recovery From Exercise and Contraction

We have previously shown that glucose uptake during in vivo exercise is intact in skeletal muscle from conventional AMPK α 1 α 2 mdKO mice (30). However, when evaluating muscle glucose uptake 30 min after in vivo exercise,

we found that glucose uptake was significantly lower in skeletal muscle from AMPK α 1 α 2 mdKO mice compared with WT littermates (Fig. 1A). We next sought to demonstrate whether reductions in muscle glucose uptake after in vivo exercise were imitated in a well-controlled experimental setup using nerve stimulation to elicit in situ muscle contraction in anesthetized mice. Again, we found that glucose uptake during in situ contraction was similar in muscle of WT and AMPK α 1 α 2 mdKO mice, whereas glucose uptake was significantly decreased in skeletal muscle from AMPK α 1 α 2 mdKO mice compared with WT mice 30 min and 1 h after contraction (Fig. 1B). We confirmed this phenotype in skeletal muscle of the inducible AMPK α 1 α 2 mdKO model (Fig. 1C and Supplementary Fig. 1A), ensuring that the phenotype observed in the conventional AMPK α 1 α 2 mdKO model is unlikely to be associated with secondary adaptations caused by embryonic AMPK α 1 α 2 deletion. The in situ contraction protocol reduced glycogen content (Fig. 1D and E) and increased phosphorylation of Erk1/2 Thr202/Tyr204 and p38 MAPK Thr180/Tyr182 (Fig. 1F–H) in skeletal muscle to an extent that did not differ between genotypes. This indicates that the in situ contraction protocol induced comparable changes in skeletal muscle from WT and AMPK-deficient mice. Importantly, we found that muscle glucose uptake during recovery from submaximal insulin stimulation was not affected by acute loss of AMPK activity in skeletal muscle (Supplementary Fig. 1B), demonstrating that the diminished ability of AMPK-deficient mice to maintain elevated glucose uptake rates during recovery is confined to the contraction stimulus.

AMPK-Deficient Mice Exhibit Intact Capacity for Delivery, Transport, and Phosphorylation of Glucose in Skeletal Muscle

Muscle glucose uptake has been shown to depend on delivery, transport, and phosphorylation of glucose (10). Delivery of glucose to the muscle is dependent on the blood glucose concentration as well as blood flow, and transport and phosphorylation of glucose is dependent on GLUT4 and HKII protein abundance/activity, respectively. When measuring blood glucose concentrations, we did not detect differences between genotypes during and in recovery from in situ contraction (Fig. 2A and Supplementary Fig. 2A). Moreover, we found that the muscle protein abundance of GLUT4 and HKII was not compromised in AMPK α 1 α 2 mdKO muscle (Fig. 2B, C, and F) but slightly decreased in inducible AMPK α 1 α 2 mdKO muscle compared with WT muscle (Supplementary Fig. 2B and C). Interestingly, measurements of the glucose metabolite glucose-6-phosphate, an allosteric inhibitor of HKII activity, revealed decreased levels in muscle from AMPK α 1 α 2 mdKO mice compared with WT mice in the period after contraction (Fig. 2D). We suspect this to be a consequence of the observed decrease in glucose uptake. Collectively, these data suggest that the capacity to take up glucose into muscle is similar between genotypes and that HKII activity

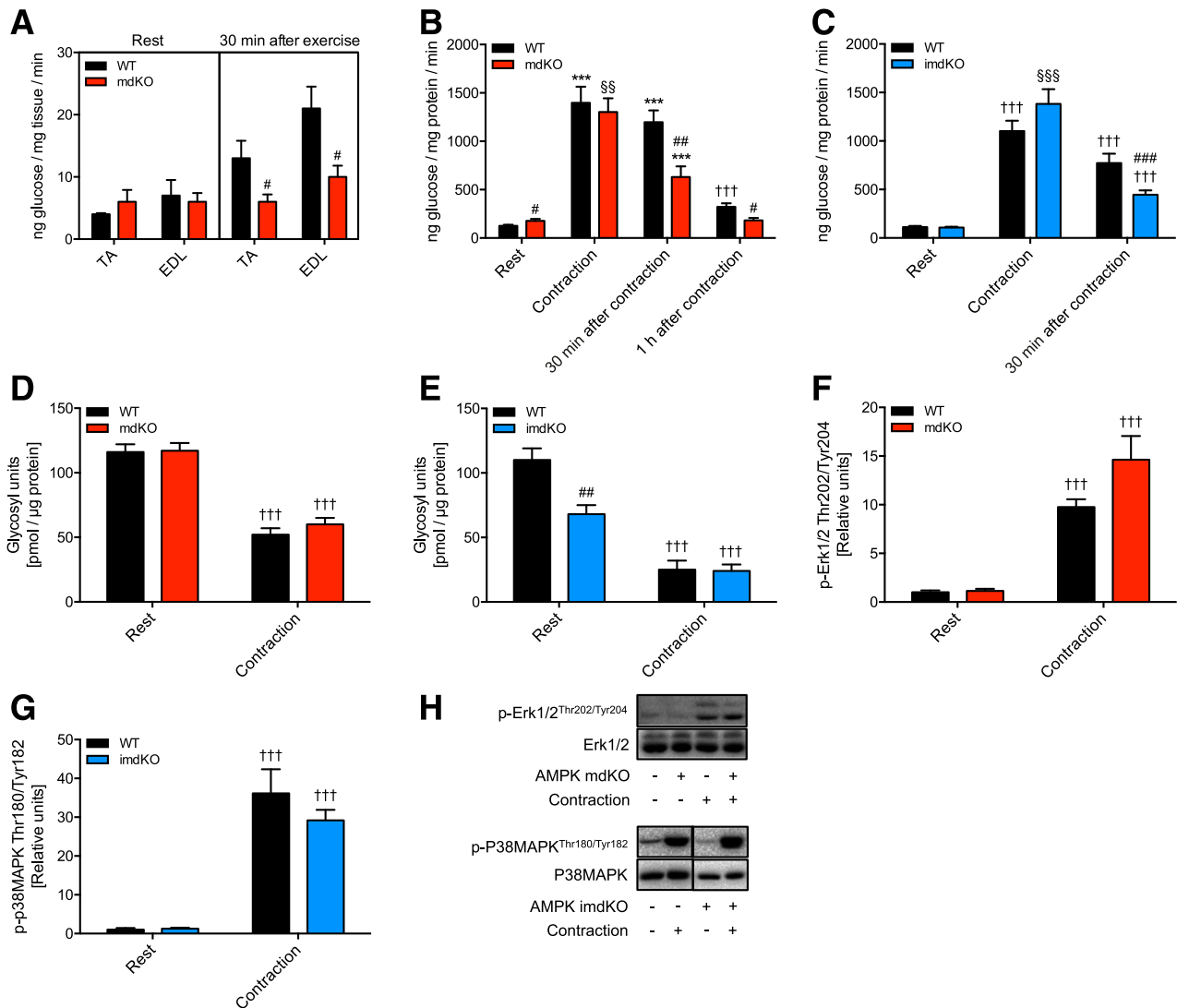


Figure 1—Glucose uptake in the period after exercise and contraction is decreased in AMPK-deficient skeletal muscle. **A:** In vivo glucose uptake in EDL and TA muscle from AMPK mdKO mice (red bars) and WT littermates (black bars) at rest and 30 min after treadmill exercise (rest, $n = 3$; exercise, $n = 6-9$). **B** and **C:** In vivo glucose uptake in TA muscle from AMPK mdKO mice, AMPK imdKO mice (blue bars), and WT littermates at rest, during in situ contraction, and 30 min and 1 h (only AMPK mdKO mice) after contraction (rest, $n = 9-23$; contraction, $n = 4-10$; 30 min after contraction, $n = 5-10$; 1 h after contraction, $n = 6$). **D** and **E:** Glycogen content in TA muscle from AMPK mdKO mice, AMPK imdKO mice, and WT littermates at rest and in response to 10 min in situ contraction (rest, $n = 9-20$; contraction, $n = 4-10$). **F** and **G:** Phosphorylation of Erk1/2 Thr202/Tyr204 (AMPK mdKO) and P38MAPK Thr180/Tyr182 (AMPK imdKO) in TA muscle from AMPK-deficient mice and WT littermates at rest and in response to 10 min in situ contraction (rest, $n = 9-20$; contraction, $n = 4-10$). **H:** Representative immunoblots. Significantly different from WT is indicated as follows: ### $P < 0.001$, ## $P < 0.01$, and # $P < 0.05$. Significantly different from rest and 1 h after contraction is indicated as follows: *** $P < 0.001$. Significantly different from rest, 30 min after contraction, and 1 h after contraction is indicated as follows: §§§ $P < 0.001$ and §§ $P < 0.01$. Significantly different from rest is indicated as follows: ††† $P < 0.001$. Statistical symbols presented in **A**, **D**, **F**, and **G** indicate main effect of intervention/genotype. Data in **A-G** are means \pm SEM.

and thus phosphorylation of glucose is likely not rate limiting for glucose uptake after contraction in AMPK-deficient muscle. To exclude that the reduced glucose uptake in AMPK-deficient muscle after in vivo exercise and in situ contraction was not due to a defect in glucose delivery, we measured glucose uptake in isolated and incubated EDL muscle from WT and AMPK α 1 α 2 mdKO mice. Compared with the rested muscle, we found that glucose uptake was still increased 2 h after in situ contraction in incubated muscle from WT mice, whereas

glucose uptake had returned to resting levels in prior contracted muscle from AMPK α 1 α 2 mdKO mice (Fig. 2E). Together this suggests that the mechanism responsible for maintaining elevated muscle glucose uptake after exercise/contraction is located at the intracellular level.

AMPK Activity in WT Muscle Reverses to Resting Levels 1 h After Contraction

Next we investigated whether the in situ contraction-induced increase in AMPK activity was maintained into

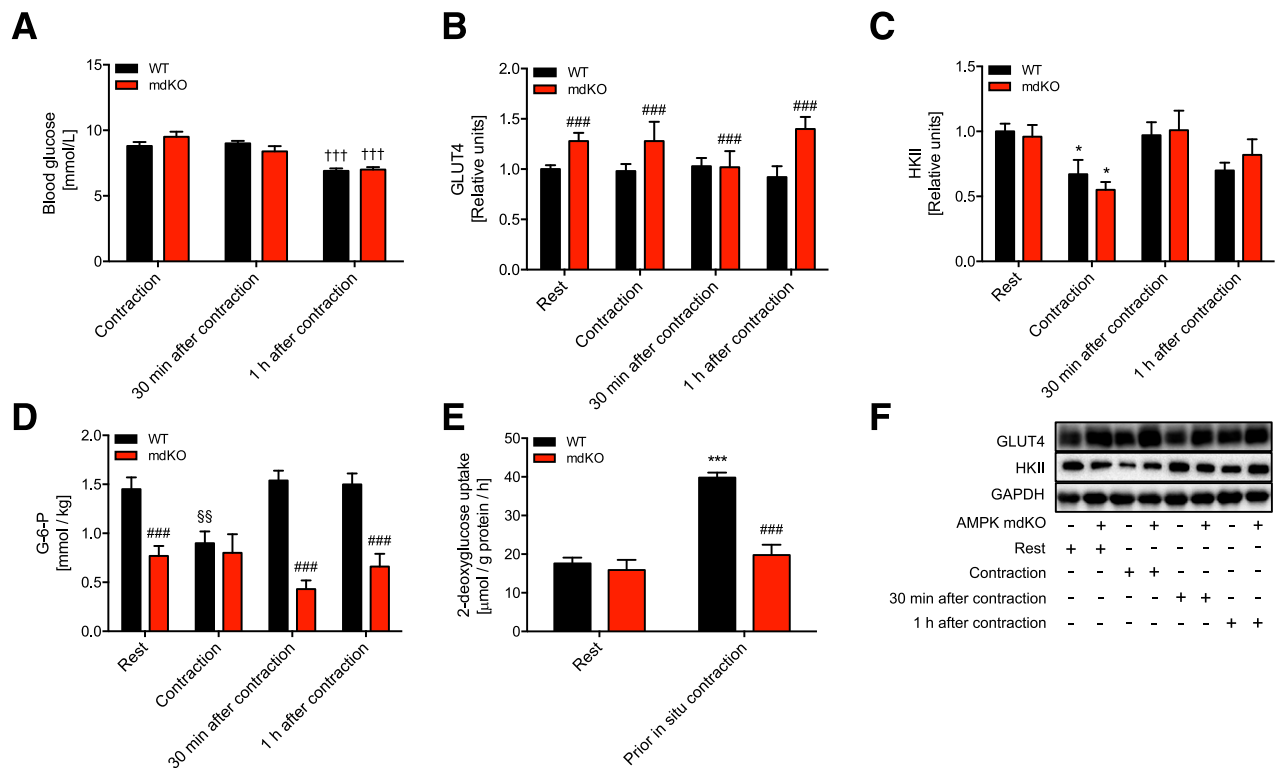


Figure 2—AMPK mdKO mice show normal capacity for glucose handling in skeletal muscle. **A:** Blood glucose concentration (mmol/L) in AMPK mdKO mice (red bars) and WT littermates (black bars) during, 30 min after, and 1 h after in situ contraction (contraction, $n = 15$ – 21 ; 30 min after contraction, $n = 24$ – 30 ; 1 h after contraction, $n = 18$). **B and C:** GLUT4 and HKII protein abundance in TA muscle from AMPK mdKO mice and WT littermates at rest, during in situ contraction, and 30 min and 1 h after contraction (rest, $n = 19$ – 23 ; contraction, $n = 5$ – 7 ; 30 min after contraction, $n = 8$ – 10 ; 1 h after contraction, $n = 6$). **D:** Glucose-6-phosphate (G-6-P) in TA muscle from AMPK mdKO mice and WT littermates at rest, during in situ contraction, and 30 min and 1 h after contraction ($n = 4$ – 6). **E:** Ex vivo glucose uptake in isolated and incubated EDL muscle from AMPK mdKO mice and WT littermates 2 h after rest or prior in situ contraction ($n = 3$ – 4). **F:** Representative immunoblots. Significantly different from WT is indicated as follows: $###P < 0.001$. Significantly different from contraction and 30 min after contraction is indicated as follows: $\dagger\dagger\dagger P < 0.001$. Significantly different from rest and 30 min after contraction is indicated as follows: $***P < 0.001$ and $*P < 0.05$. Significantly different from rest, 30 min after contraction, and 1 h after contraction is indicated as follows: $\S\S P < 0.01$. Statistical symbols presented in A–C indicate main effect of intervention/genotype. Data in A–E are means \pm SEM.

recovery, explaining greater glucose uptake in the period after contraction. We observed that the AMPK α 2 β 2 γ 3-, AMPK α 2 β γ 1-, and AMPK α 1 β γ 1-associated activity in WT muscle had returned to resting levels 1 h after contraction (Fig. 3A and Supplementary Fig. 3A and B). This was also mirrored by measurements of phosphorylated AMPK Thr172 and ACC Ser212 (Fig. 3B, C, and F and Supplementary Fig. 3C and D). Thus, although AMPK seems to be necessary for maintaining elevated muscle glucose uptake in recovery from exercise and contraction, the mismatch between AMPK activity and muscle glucose uptake 1 h after contraction indicates that one or several proteins regulated by AMPK and likely located closer to the GLUT4 recruitment event are responsible for maintaining higher rates of glucose uptake in skeletal muscle after exercise and contraction.

Glucose Uptake Is Decreased in TBC1D1-Deficient Muscle in Recovery From Contraction

Evidence indicates that AMPK-mediated glucose uptake involves phosphoregulation of TBC1D1, which has been

suggested to increase GLUT4 translocation to the muscle cell surface membrane (35). Interestingly, we found that phosphorylation of AMPK downstream target TBC1D1 Ser231 was increased 30 min and 1 h after in situ contraction (Fig. 3D–F). Moreover, these findings were positively correlated with glucose uptake in WT muscle but not in AMPK-deficient muscle (Fig. 3G and H and Supplementary Fig. 3E and F). In comparison, we did not observe associations between postcontraction glucose uptake and phosphorylation of Akt2 downstream target TBC1D4 Thr649 (Supplementary Fig. 3G and H). We also observed a small increase in phosphorylation of TBC1D1 Ser231 in skeletal muscle from AMPK-deficient mice after contraction. The reason for this is unclear, but it may be a consequence of AMPK-independent effects of contraction in muscle. Alternatively, contraction may lead to AMPK activation and thus phosphorylation of TBC1D1 in non-muscle cells that are present in the sample preparations of whole skeletal muscle tissue.

To support the possible role of an AMPK–TBC1D1 signaling axis regulating muscle glucose uptake after

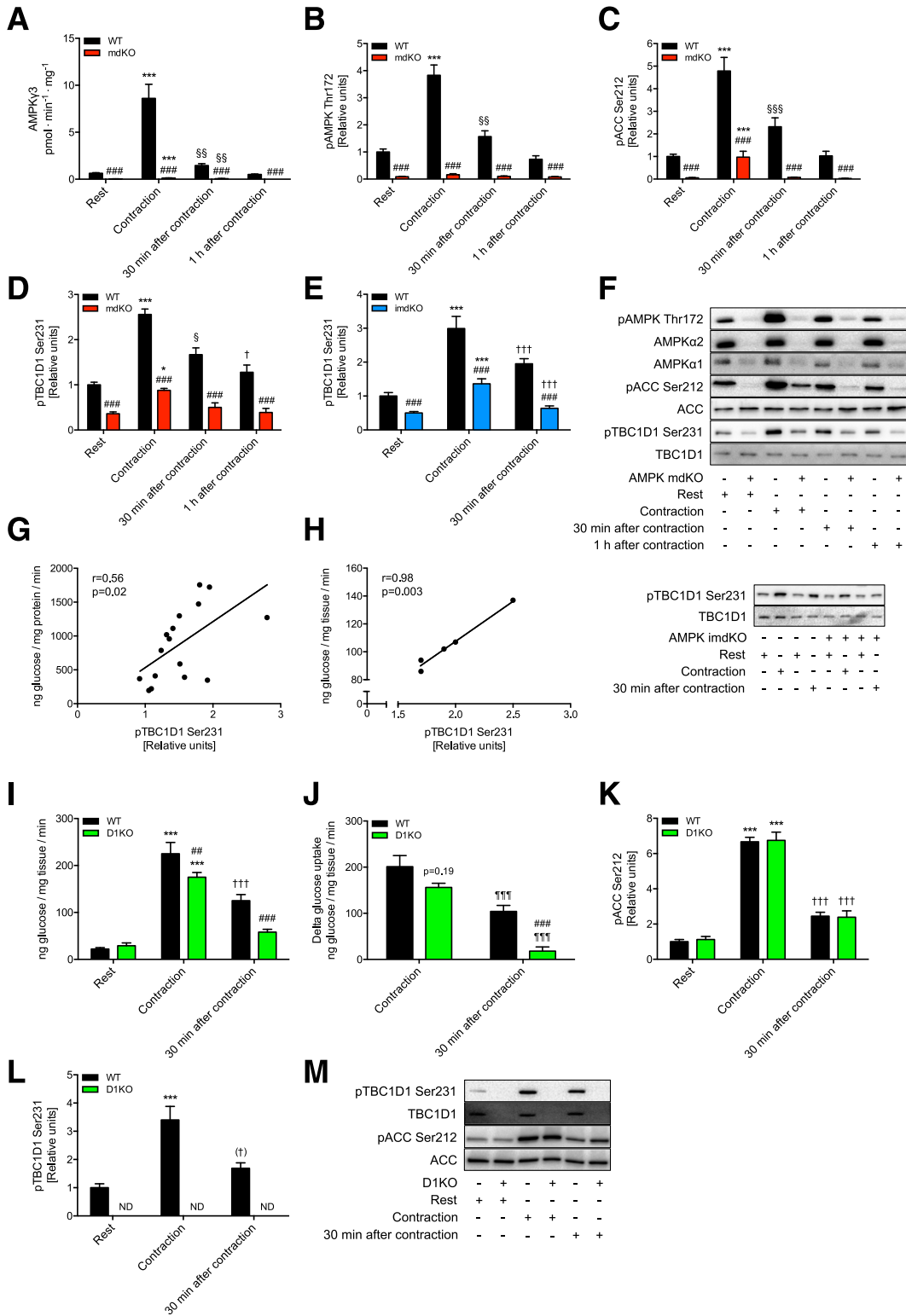


Figure 3—An AMPK-TBC1D1 signaling axis regulates muscle glucose uptake in the period after contraction. AMPK γ 3-associated activity (A) and phosphorylation of AMPK Thr172 (B), ACC Ser212 (C), and TBC1D1 Ser231 (D) in TA muscle from AMPK mdKO mice (red bars) and WT littermates (black bars) at rest, during in situ contraction, and 30 min and 1 h after contraction (rest, $n = 15$ –23; contraction, $n = 5$ –7; 30 min after contraction, $n = 4$ –10; 1 h after contraction, $n = 6$). E: Phosphorylation of TBC1D1 Ser231 in TA muscle from AMPK imdKO mice (blue bars) and WT littermates (black bars) at rest, during in situ contraction, and 30 min after contraction (rest, $n = 9$ –20; contraction, $n = 4$ –10; 30 min after contraction, $n = 5$ –10). F: Representative immunoblots for B–E. Pearson correlations between glucose uptake and phosphorylation of TBC1D1 Ser231 in TA muscle from WT littermates of AMPK mdKO (G) and AMPK imdKO mice (H) 30 min and 1 h after in situ contraction ($n = 16$ and $n = 6$, respectively). R and significance level are indicated in the respective panel. I: In vivo glucose uptake in TA muscle from TBC1D1 KO mice (green bars) and WT littermates (black bars) at rest, during in situ contraction, and 30 min after contraction (rest, $n = 11$ –12; contraction, $n = 6$; 30 min after contraction, $n = 5$ –6). J: The incremental increase (delta) in glucose uptake

contraction, we next investigated glucose uptake both during and after contraction in skeletal muscle from TBC1D1 KO mice. Compared with WT littermates, we found that the contraction-induced increase in glucose uptake reversed faster in skeletal muscle from TBC1D1 KO mice (Fig. 3I). This became even more apparent when calculating the incremental increase (delta values for individual paired muscles) in glucose uptake during and 30 min after contraction (Fig. 3J). Importantly, the contraction-induced increase in phosphorylation of ACC Ser212 was similar in skeletal muscle from both genotypes (Fig. 3K and M), indicating that KO of TBC1D1 does not compromise the ability of contraction to induce AMPK signaling in skeletal muscle. As expected, contraction only increased phosphorylation of TBC1D1 Ser231 in skeletal muscle from WT littermates (Fig. 3L and M). As previously reported (29), we found a ~50% reduction in GLUT4 protein abundance in skeletal muscle from TBC1D1 KO mice (Supplementary Fig. 3I), which likely accounts for the lesser increase in glucose uptake observed during *in situ* contraction (Fig. 3I).

The Majority of Studies Reporting Decreased Glucose Uptake in AMPK-Deficient Muscle During Exercise/Contractile Activity Measure Glucose Uptake in the Recovery Period

To the best of our knowledge, 19 studies, including the present one, have investigated glucose uptake in AMPK-deficient mouse skeletal muscle during exercise/contractile activity by radioactive glucose tracer accumulation. Intriguingly, 8 out of 10 studies reporting impaired contraction-induced glucose uptake in AMPK-deficient muscle actually measure glucose uptake in the period after contraction (Table 1). Such inconsistencies are also evident in studies reporting impaired contraction-induced glucose uptake in skeletal muscle from TBC1D1-deficient mouse models (Table 1). Collectively, these observations support the notion of an AMPK-TBC1D1 signaling axis regulating muscle glucose uptake in the period after exercise and contraction.

DISCUSSION

AMPK has long been known for its ability to regulate muscle glucose uptake based on numerous studies showing impaired glucose uptake in AMPK-deficient muscle when stimulated with pharmacological AMPK agonists (18,23,28,36,37). Since

AMPK is activated in skeletal muscle during exercise and contraction, common belief has been to assume that AMPK regulates muscle glucose uptake under these conditions as well. However, during the last 17 years, studies investigating the role of AMPK in regulating muscle glucose uptake during exercise and contraction have not been able to reach consensus.

To address this matter, we carefully examined whether the observed discrepancies in contraction-induced muscle glucose uptake between different AMPK-deficient mouse models were due to circumstances related to the timing of the uptake measurements. As a consequence, we performed measurements of muscle glucose uptake assessed by retroorbital injection of [³H]2-deoxyglucose during and after exercise/contraction in two mouse models with skeletal muscle AMPK deficiency. Using this approach, we now provide genetic evidence to support that AMPK regulates muscle glucose uptake after, rather than during, exercise/contraction. Based on these findings, we propose a model by which activation of AMPK in skeletal muscle during exercise acts to maintain a high glucose transport capacity in recovery from exercise. We propose that AMPK in this way secures a faster normalization of myocellular energy and fuel status after contractile activity.

As contraction acutely increases AMPK activity in skeletal muscle (14,31,38), we investigated whether this effect was maintained in recovery from contraction, potentially explaining our findings on glucose uptake. Interestingly, in WT skeletal muscle, we found that AMPK activity, as well as phosphorylation of AMPK Thr172 and ACC Ser212, had returned to resting levels 1 h after contraction, although glucose uptake was still increased compared with resting levels. In contrast, phosphorylation of the AMPK downstream target TBC1D1 was still increased 1 h after contraction, demonstrating that distinct signaling downstream of AMPK as well as glucose uptake are sustained for a long time during recovery even though AMPK activity is not. The reason for the apparent discrepancy between AMPK activity and downstream phosphorylation of TBC1D1 is unclear. We speculate that it relates to changes in phosphatase activity, altered cellular localization of TBC1D1, or time-based dynamics in protein phosphorylation. Studies in humans have also reported increased phosphorylation of TBC1D1 Ser231 in skeletal muscle as long as 30–180 min after the cessation of exercise (39,40). Interestingly, studies in rats and humans

(contraction/30 min after contraction values minus resting values) in TA muscle from TBC1D1 KO mice and WT littermates ($n = 5-6$). Phosphorylation of ACC Ser212 (K) and TBC1D1 Ser231 (L) in TA muscle from TBC1D1 KO mice and WT littermates at rest, during *in situ* contraction, and 30 min after contraction (rest, $n = 11-12$; contraction, $n = 6$; 30 min after contraction, $n = 5-6$). M: Representative immunoblots. Significantly different from WT is indicated as follows: ### $P < 0.001$ and ## $P < 0.01$. Significantly different from rest, 30 min after contraction, and 1 h after contraction is indicated as follows: *** $P < 0.001$ and * $P < 0.05$. Significantly different from rest and 1 h after contraction is indicated as follows: \$\$\$ $P < 0.001$, \$\$ $P < 0.01$, and \$ $P < 0.05$. Significantly different from rest is indicated as follows: ††† $P < 0.001$, †† $P < 0.05$, and (†) $P = 0.066$. Significantly different from contraction is indicated as follows: ¶¶¶ $P < 0.001$. Statistical symbols presented in A–C indicate main effect of intervention/genotype. Data in A–E and I–L are means \pm SEM. ND, not detectable.

Table 1—Overview of studies investigating exercise- and contraction-induced glucose uptake in AMPK- and TBC1D1-deficient mouse skeletal muscle by radioactive glucose tracer accumulation

Mouse model name	Target protein	Type of manipulation	Tissue specificity	Exercise/contraction-induced glucose uptake or clearance			Tracer uptake measurement	Period of C: contractile activity, T: tracer exposure (min)	Reference
				Background strain	Ex vivo	In situ			
LKB1 KO	LKB1	Loss of protein	Heart and skeletal muscle (MCK)	C57Bl/6	↓EDL	—	After contraction	C: 0–10 T: 10–20	19
LKB1 KO	LKB1	Loss of protein	Heart and skeletal muscle (MCK)	C57Bl/6	—	↓EDL	After contraction	C: 0–5 T: 20–30	19
LKB1 MKO	LKB1	Loss of protein	Heart and skeletal muscle (MCK)	FVB	↓EDL	—	After contraction	C: 0–10 T: 10–20	20
α1 KO	AMPKα1	Loss of protein	Whole body	C57Bl/6-Sv129	↓SOL	—	After contraction	C: 0–10 T: 10–20	21
α1α2 imdKO	AMPKα1 and AMPKα2	Loss of protein	Skeletal muscle (HSA)	C57Bl/6-Sv129	—	↓(TA, EDL)	After contraction	C: 0–10 T: 40–50	This study
α2 KD	AMPKα2	Loss of activity	Heart and skeletal muscle (MCK)	C57Bl/6	↓SOL	—	After contraction	C: 0–10 T: 10–20	21
α2 KD	AMPKα2	Loss of activity	Heart and skeletal muscle (MCK)	C57Bl/6	↓EDL	—	After contraction	C: 0–2 T: 12–32	22
α2 KD	AMPKα2	Loss of activity	Heart and skeletal muscle (MCK)	C57Bl/6	↓EDL	—	After contraction	C: 0–10 T: 10–30	23
α2 KD	AMPKα2	Loss of activity	Heart and skeletal muscle (MCK)	C57Bl/6	—	↓(EDL, SOL)	After contraction	C: 0–15° T: 25–45	23
TBC1D1 Nob1.10 ^{S/L}	TBC1D1	Loss of protein	Whole body	C57Bl/6	↓EDL ¹ , ↔SOL	—	After contraction	C: 0–10 T: 20–40	63
TBC1D1 Nob1.10 ^{S/L}	TBC1D1	Loss of protein	Whole body	C57Bl/6	—	↑TA ¹	After contraction	C: 0–10 T: 40–50	This study
α2ITG	AMPKα2	Loss of activity	Heart and skeletal muscle (MCK)	FVB	↓EDL ²	—	After contraction	C: 0–10 T: 10–20	48
MLKB1KO	LKB1	Loss of protein	Heart and skeletal muscle (MCK)	FVB	↓SOL	—	After contraction	C: 0–10 T: 10–20	17
α1α2 mdKO	AMPKα1 and AMPKα2	Loss of protein	Skeletal muscle (HSA)	C57Bl/6-Sv129	—	↓TA	After contraction	C: 0–10 T: 40–50 and 70–80	This study
α2 KO	AMPKα2	Loss of protein	Whole body	C57Bl/6	↔SOL ²	—	After contraction	C: 0–10 T: 10–20	21
α2ITG	AMPKα2	Loss of activity	Heart and skeletal muscle (MCK)	FVB	↔EDL ²	—	After contraction	C: 0–10 T: 10–20	47
γ3 KO	AMPKγ3	Loss of protein	Whole body	C57Bl/6	↔EDL ²	—	After contraction	C: 0–10 T: 10–20	37
TBC1D1 Ser231Ala	TBC1D1	Loss of function	Whole body	C57Bl/6	↔EDL	—	After contraction	C: 0–10 T: 10–20	64
α1α2 mdKO	AMPKα1 and AMPKα2	Loss of protein	Skeletal muscle (HSA)	C57Bl/6-Sv129	—	↓(TA, EDL)	After exercise	C: 0–30 T: 60–70	This study
MLKB1KO	LKB1	Loss of protein	Heart and skeletal muscle (MCK)	FVB	—	↓TA	During and after contraction	C: 0–15 T: 0–45	17

Continued on p. 1435

Table 1—Continued

Mouse model name	Target protein	Type of manipulation	Tissue specificity	Background strain	Exercise/contraction-induced glucose uptake or clearance			Tracer uptake measurement	Period of C: contractile activity, T: tracer exposure (min)	Reference
					Ex vivo	In situ	In vivo			
$\alpha 1$ KO	AMPK $\alpha 1$	Loss of protein	Whole body	C57Bl/6-Sv129	↔EDL, ↓SOL	—	—	During and after contraction	C: 0–10 T: 5–15	18
TBC1D1 4P mutant	TBC1D1	Loss of function	Skeletal muscle (OE by gene electrotransfer)	ICR	—	↓TA	—	During and after contraction	C: 0–15 T: 0–45	45
TBC1D1 4A mutant	TBC1D1	Loss of function	Skeletal muscle (OE by gene electrotransfer)	ICR	—	↓TA	—	During and after contraction	C: 0–15 T: 0–45	35
$\alpha 2$ ITG	AMPK $\alpha 2$	Loss of activity	Heart and skeletal muscle (MCK)	FVB	—	↔(EDL, TA, GAS) ²	—	During and after contraction	C: 0–15 T: 0–45	47
$\alpha 2$ KD	AMPK $\alpha 2$	Loss of activity	Heart and skeletal muscle (MCK)	C57Bl/6	↔(EDL, SOL)	—	—	During and after contraction	C: 0–10 T: 5–15	49
$\alpha 2$ KO	AMPK $\alpha 2$	Loss of protein	Whole body	C57Bl/6-Sv129	↔(EDL, SOL) ^{2,3}	—	—	During and after contraction	C: 0–10 T: 5–15	18
$\alpha 1\alpha 2$ imdKO	AMPK $\alpha 1$ and AMPK $\alpha 2$	Loss of protein	Skeletal muscle (HSA)	C57Bl/6-Sv129	—	↔(TA, EDL)	—	During contraction	C: 0–10 T: 0–10	This study
$\alpha 1\alpha 2$ mdKO	AMPK $\alpha 1$ and AMPK $\alpha 2$	Loss of protein	Skeletal muscle (HSA)	C57Bl/6-Sv129	↔(EDL, SOL) ³	—	—	During contraction	C: 0–10 T: 0–10	27
$\alpha 1\alpha 2$ mdKO	AMPK $\alpha 1$ and AMPK $\alpha 2$	Loss of protein	Skeletal muscle (HSA)	C57Bl/6-Sv129	—	↔TA	—	During contraction	C: 0–10 T: 0–10	This study
$\beta 2$ KO	AMPK $\beta 2$	Loss of protein	Whole body	C57Bl/6	↔EDL	—	—	During contraction	C: 0–20 T: 0–20	51
$\beta 2$ KO	AMPK $\beta 2$	Loss of protein	Whole body	C57Bl/6	↔EDL	—	—	During contraction	C: 0–20 T: 0–20	36
TBC1D1 <i>Nob1.10^{S/L}</i>	TBC1D1	Loss of protein	Whole body	C57Bl/6	—	↔TA ^{1,3}	—	During contraction	C: 0–10 T: 0–10	This study
LKB1 MKO	LKB1	Loss of protein	Heart and skeletal muscle (MCK)	FVB	↔EDL	—	—	During contraction	C: 0–10 T: 0–10	20
$\beta 1\beta 2$ M-KO	AMPK $\beta 1$ and AMPK $\beta 2$	Loss of protein	Heart and skeletal muscle (MCK)	C57Bl/6	↓(EDL, SOL) ⁴	—	—	During contraction	C: 0–10 T: 0–10	50
$\beta 1\beta 2$ M-KO	AMPK $\beta 1$ and AMPK $\beta 2$	Loss of protein	Heart and skeletal muscle (MCK)	C57Bl/6	↓(EDL, SOL) ⁴	—	—	During contraction	C: 0–10 T: 0–10	51
$\alpha 2$ KD	AMPK $\alpha 2$	Loss of activity	Heart and skeletal muscle (MCK)	C57Bl/6	↓(SOL, EDL) ⁷	—	—	During contraction	C: 0–10 T: 0–10	50
$\alpha 1\alpha 2$ mdKO	AMPK $\alpha 1$ and AMPK $\alpha 2$	Loss of protein	Skeletal muscle (HSA)	C57Bl/6-Sv129	—	↔(EDL, TA, GAS, SOL) ⁵	—	During exercise	C: 0–30 T: 0–30	30
$\alpha 2$ KD	AMPK $\alpha 2$	Loss of activity	Heart and skeletal muscle (MCK)	C57Bl/6	—	↔(QUAD, GAS)	—	During exercise	C: 0–30 T: 0–30	65
TBC1D1 KO	TBC1D1	Loss of protein	Whole body	C57Bl/6	—	↔R.QUAD, ↓W.QUAD ¹	—	During exercise	C: 0–20 T: 0–20	46

Continued on p. 1436

Table 1—Continued

Mouse model name	Target protein	Type of manipulation	Tissue specificity	Background strain	Exercise/contraction-induced glucose uptake or clearance			Tracer uptake measurement	Period of C: contractile activity, T: tracer exposure (min)	Reference
					Ex vivo	In situ	In vivo			
TBC1D1^{Ser231Ala}	TBC1D1	Loss of function	Whole body	C57Bl/6	—	—	↔-(QUAD, GAS)	During exercise	C: 0–35 T: 0–35	66
LKB1 MKO	LKB1	Loss of protein	Heart and skeletal muscle (MCK)	FVB	—	—	↔-(QUAD, EDL)	During exercise	C: 0–20 T: 0–20	20
α2 KD	AMPKα2	Loss of activity	Heart and skeletal muscle (MCK)	C57Bl/6	—	—	↔GAS	During exercise	C: 0–20 T: 0–20	50
α2 KD	AMPKα2	Loss of activity	Heart and skeletal muscle (MCK)	C57Bl/6	—	—	↓(SOL, SVL, GAS)^f	During exercise	C: 0–30 T: 5–30	67
β1β2M-KO	AMPKβ1 and AMPKβ2	Loss of protein	Heart and skeletal muscle (MCK)	C57Bl/6	—	—	↓(SOL, GAS)⁴	During exercise	C: 0–20 T: 0–20	51

The bold font indicates studies that support the hypothesis of AMPK being important for regulating muscle glucose uptake in the period after contraction and exercise. For some studies, information related to the study/model is important for the interpretation of data as this may help explain observed inconsistencies between defects in muscle glucose uptake and timing of uptake measurements. GAS, gastrocnemius; HSA, human skeletal actin; MCK, muscle creatine kinase; OE, overexpression; QUAD, quadriceps; R, red (oxidative); SOL, soleus; SVL, superficial vastus lateralis; KD, kinase dead; MKO, muscle-specific knockout; W, white (glycolytic). ¹These studies found decreased GLUT4 protein abundance in muscle from TBC1D1 KO mice compared with WT littermates that may account for the partial reduction in muscle glucose uptake observed during contraction and exercise. ²These studies reported that AMPKα1 activity and/or contraction-induced phosphorylation of ACC Ser212 were intact in skeletal muscle from the AMPK-deficient mice, which may preserve the ability to maintain elevated muscle glucose uptake in recovery from contraction. ³These studies showed that although the main effects of AMPK/TBC1D1 deficiency on muscle glucose uptake were present, the incremental increase (delta value) in contraction-induced muscle glucose uptake was not different between genotypes. ⁴This AMPK-deficient mouse model has drastically reduced mitochondrial content in skeletal muscle that may diminish muscle glucose uptake during contraction. ⁵This study reported that the exercise-induced glucose uptake in soleus muscle was significantly higher in the AMPK-deficient mouse model compared with WT littermates. However, this was likely due to elevated blood glucose concentrations in the AMPK-deficient mouse model during exercise. ⁶This study suggested that the observed decrease in glucose uptake/clearance in muscle from AMPK-deficient mice during exercise was likely due to impaired glucose delivery. ⁷These studies reported decreased force production in AMPK-deficient muscle compared with WT muscle that may account for the observed difference in muscle glucose uptake during contraction. ⁸This contraction protocol consisted of two 7-min in situ contraction periods with 1 min rest in between.

report that both phosphorylation of TBC1D1 and muscle glucose uptake return to pre-exercise levels 3–5 h in recovery from exercise (41–43). Collectively, these findings suggest that phosphorylation of TBC1D1 and glucose uptake decrease similarly in skeletal muscle after exercise but that these two measures may not always track with AMPK activity.

AMPK has been shown to target several proteins involved in regulating muscle glucose uptake, including TBC1D4 and PIKfyve (34,44). However, most evidence supports that AMPK-mediated phosphorylation of TBC1D1 (and not TBC1D4 and PIKfyve) facilitates AMPK-mediated effects on muscle glucose uptake (35,45). We found that phosphorylation of TBC1D1 is likely not important for regulating muscle glucose uptake during contraction, as phosphorylation of TBC1D1 was severely impaired in AMPK-deficient muscle even though contraction-induced glucose uptake was not. In contrast, we found that phosphorylation of TBC1D1 Ser231 in the period after contraction was positively associated with glucose uptake. Since this association was found in WT muscle only, this could indicate that AMPK phosphorylates TBC1D1 during exercise/contraction to secure muscle glucose uptake in the period after exercise/contraction. In support of this, we found that increased rates of glucose uptake in skeletal muscle after contraction were dependent on the presence of TBC1D1 as the contraction-induced increase in glucose uptake reversed faster in TBC1D1-deficient muscle compared with WT muscle. Because glycolytic skeletal muscle from TBC1D1 KO mice exhibits a loss in GLUT4 protein content (29), this likely accounts for the minor decrease in muscle glucose uptake observed during contraction. This is also supported by the observation that while exercise-induced glucose uptake is impaired in glycolytic quadriceps muscle from TBC1D1 KO mice, such a defect is not observed in oxidative quadriceps muscle, which expresses normal levels of GLUT4 protein content compared with muscle from WT littermates (46).

Going through the literature, we noticed that the majority of studies reporting impaired exercise/contraction-induced glucose uptake in AMPK-deficient muscle had unintentionally been measuring glucose uptake in recovery from exercise/contraction (Table 1), supporting the idea of AMPK being a regulator of muscle glucose uptake in the period after exercise/contraction. Nevertheless, some studies have reported intact contraction-induced glucose uptake in AMPK-deficient muscle although measurements of glucose uptake were performed in recovery (18,21,37,47–49), whereas others have reported impaired contraction-induced glucose uptake in AMPK-deficient muscle when measurements of glucose uptake were performed during contraction (50,51). These findings, however, may be related to incomplete KO of AMPK activity in skeletal muscle as KO of single catalytic subunits of AMPK has been shown to increase the activity of the remaining catalytic subunit during contractile activity (14). Also, secondary adaptations leading, for example, to reduced force production and reduced mitochondrial content in skeletal

muscle from AMPK-deficient mice may have masked the likely function of AMPK in regulating muscle glucose uptake after contraction (Table 1). We cannot ultimately rule out that AMPK may be necessary for regulating muscle glucose uptake during longer periods of exercise (>30 min) and contraction (>10 min) where the myocellular stress may be further elevated. However, measurements of skeletal muscle glucose uptake in AMPK kinase-dead mice and AMPK α 1 α 2 mdKO mice during longer periods of contraction (20 min) (52) and in vivo exercise (90 min) (J.R. Hingst, J.F.P.W., unpublished observations), respectively, argue against this idea.

Only a few studies have investigated whether TBC1D1 may be involved in regulating exercise/contraction-induced glucose uptake in skeletal muscle. Interestingly, two studies using gene electrotransfer into mouse TA muscle leading to overexpression of TBC1D1 mutated at several predicted AMPK phosphorylation sites report a 22% and 42% reduction in contraction-stimulated glucose uptake without a change in GLUT4 protein abundance between muscles transfected with control or mutated TBC1D1 (35,45). However, in both studies, muscle glucose uptake rates were measured as the combined uptake of glucose during (15 min) and after (30 min) contraction. Based on the findings presented here, this may suggest that the observed impairment in contraction-induced glucose uptake in skeletal muscle transfected with mutated TBC1D1 was due to measurements of glucose uptake rates in the recovery period from contraction.

If we permit translation of our observations in mice to human physiology, this may in fact bring some new aspects into former human observations. First, it has been shown that the activation of AMPK in human skeletal muscle in response to exercise (53–55) is not reversed immediately after exercise but is maintained above basal levels for a prolonged period of time. In some studies, this is evident from enhanced AMPK activity per se (40,54,56) and in other studies from enhanced AMPK downstream signaling (57,58). Thus, it would be expected that in muscle of humans, the sarcolemmal glucose transport capacity is maintained high in the period after exercise. Apparently this view conflicts with the observation that muscle glucose uptake quickly reverses to resting levels shortly after exercise (3,59). However, the reversal of glucose uptake is likely the result of a marked decrease in muscle perfusion (delivery) (60) rather than a decrease in sarcolemmal glucose permeability. This interpretation may be inferred from a study in which the muscular interstitial glucose concentration was measured in the period after exercise. Thus, several hours into recovery from one-legged exercise, the interstitial muscle glucose concentration was markedly lower in the prior exercised leg (~1.85 mmol/L) compared with the rested leg (~4.13 mmol/L) despite comparable blood flow to the two legs (61). Therefore we now propose that the maintained membrane glucose permeability in human skeletal muscle relates to elevated AMPK activity and downstream signaling in the recovery period from exercise. The enhanced glucose

permeability is thus favoring glucose uptake in previously exercised muscle once delivery of glucose (perfusion/plasma concentration) increases, for example, upon food intake and subsequent insulin release.

In conclusion, by measurements of muscle glucose uptake during and in recovery from exercise/contraction and careful evaluation of the literature, our findings provide new means of AMPK for the regulation of muscle glucose uptake. Our study seems to explain the large discrepancy that occurred in the aftermath of the seminal observation by Mu et al. (23) in 2001, indicating a role of AMPK in regulating muscle glucose uptake during contractile activity. Hence, it appears that the acute activation of AMPK in skeletal muscle during exercise/contraction acts to secure glucose uptake when the contractile activity ceases. This provides a mechanism by which a high glucose transport capacity is secured, favoring replenishment of muscle cellular energy stores after exercise/contraction. An important premise for this interpretation, if indeed AMPK functions to delay GLUT4 endocytosis in skeletal muscle (24), is that the stimuli leading to enhanced GLUT4 exocytosis prevail over GLUT4 endocytosis in regulating GLUT4 content at the cell surface membrane during exercise and contraction where AMPK activity is also elevated. Although debatable, such stimuli may include entry of extracellular Ca^{2+} as well as mechanical stress signaling (11,62). Together with our previous findings, revealing a role of AMPK in regulating muscle insulin sensitivity after exercise and contraction (31), the current study identifies AMPK as an important regulator of muscle glucose metabolism after, rather than during, exercise/contraction.

Acknowledgments. The authors thank Betina Bolmgren and Irene Bech Nielsen (Department of Nutrition, Exercise, and Sports, Faculty of Science, University of Copenhagen) for their skilled technical assistance. The authors also thank Dr. Peter Schjerling (Institute of Sports Medicine, Bispebjerg Hospital, University of Copenhagen) for genotyping the AMPK mdKO and imdKO mice, Karyn A. Esser (Department of Physiology, College of Medicine, University of Kentucky) for providing inducible human skeletal actin (HSA)-Cre transgenic mice, and Dr. Joachim Fentz (Department of Nutrition, Exercise, and Sports, Faculty of Science, University of Copenhagen) for his instrumental pilot experiments.

Funding. This work was supported by grants from the Danish Council for Independent Research, Medical Sciences (to J.F.P.W.), the Novo Nordisk Foundation (to J.F.P.W.), and the Lundbeck Foundation (to J.F.P.W.).

Duality of Interest. No potential conflicts of interest relevant to this article were reported.

Author Contributions. R.K. conceived and designed the research, performed the experiments, analyzed the data, and wrote the manuscript. J.L.W.R., N.O.J., and J.B.B. performed experiments and analyzed the data. M.F., B.V., A.C., and H.A.-H. provided founder mice for the study. J.F.P.W. conceived and designed the research and contributed to drafting the manuscript. All authors interpreted the results, contributed to the discussion, edited and revised the manuscript, and read and approved the final version of the manuscript. J.F.P.W. is the guarantor of this work and, as such, had full access to all the data in the study and takes responsibility for the integrity of the data and the accuracy of the data analysis.

Data Availability. The data and resources generated during and/or analyzed during the current study are available from the corresponding author on reasonable request.

Prior Presentation. Parts of this study were presented in abstract form at the 10th International Meeting on AMPK, Niagara-on-the-Lake, Ontario, Canada, 30 September–4 October 2018.

References

1. Ploug T, Galbo H, Vinten J, Jørgensen M, Richter EA. Kinetics of glucose transport in rat muscle: effects of insulin and contractions. *Am J Physiol* 1987;253:E12–E20
2. Young DA, Wallberg-Henriksson H, Sleeper MD, Holloszy JO. Reversal of the exercise-induced increase in muscle permeability to glucose. *Am J Physiol* 1987;253:E331–E335
3. Wojtaszewski JFP, MacDonald C, Nielsen JN, et al. Regulation of 5'AMP-activated protein kinase activity and substrate utilization in exercising human skeletal muscle. *Am J Physiol Endocrinol Metab* 2003;284:E813–E822
4. Richter EA, Mikines KJ, Galbo H, Kiens B. Effect of exercise on insulin action in human skeletal muscle. *J Appl Physiol* (1985) 1989;66:876–885
5. Wojtaszewski JFP, Hansen BF, Kiens B, Richter EA. Insulin signaling in human skeletal muscle: time course and effect of exercise. *Diabetes* 1997;46:1775–1781
6. Ploug T, Galbo H, Richter EA. Increased muscle glucose uptake during contractions: no need for insulin. *Am J Physiol* 1984;247:E726–E731
7. Richter EA, Ploug T, Galbo H. Increased muscle glucose uptake after exercise. No need for insulin during exercise. *Diabetes* 1985;34:1041–1048
8. Wojtaszewski JF, Higaki Y, Hirshman MF, et al. Exercise modulates post-receptor insulin signaling and glucose transport in muscle-specific insulin receptor knockout mice. *J Clin Invest* 1999;104:1257–1264
9. Richter EA, Hargreaves M. Exercise, GLUT4, and skeletal muscle glucose uptake. *Physiol Rev* 2013;93:993–1017
10. Wasserman DH, Kang L, Ayala JE, Fueger PT, Lee-Young RS. The physiological regulation of glucose flux into muscle in vivo. *J Exp Biol* 2011;214:254–262
11. Sylow L, Kleinert M, Richter EA, Jensen TE. Exercise-stimulated glucose uptake - regulation and implications for glycaemic control. *Nat Rev Endocrinol* 2017;13:133–148
12. Jaldin-Fincati JR, Pavarotti M, Frendo-Cumbo S, Bilan PJ, Klip A. Update on GLUT4 vesicle traffic: a cornerstone of insulin action. *Trends Endocrinol Metab* 2017;28:597–611
13. Kurth-Kraczek EJ, Hirshman MF, Goodyear LJ, Winder WW. 5' AMP-activated protein kinase activation causes GLUT4 translocation in skeletal muscle. *Diabetes* 1999;48:1667–1671
14. Trebak JT, Pehmøller C, Kristensen JM, et al. Acute exercise and physiological insulin induce distinct phosphorylation signatures on TBC1D1 and TBC1D4 proteins in human skeletal muscle. *J Physiol* 2014;592:351–375
15. Birk JB, Wojtaszewski JFP. Predominant alpha2/beta2/gamma3 AMPK activation during exercise in human skeletal muscle. *J Physiol* 2006;577:1021–1032
16. Kjøbsted R, Hingst JR, Fentz J, et al. AMPK in skeletal muscle function and metabolism. *FASEB J* 2018;32:1741–1777
17. Koh H-J, Toyoda T, Fujii N, et al. Sucrose nonfermenting AMPK-related kinase (SNARK) mediates contraction-stimulated glucose transport in mouse skeletal muscle. *Proc Natl Acad Sci U S A* 2010;107:15541–15546
18. Jørgensen SB, Viollet B, Andreelli F, et al. Knockout of the alpha2 but not alpha1 5'-AMP-activated protein kinase isoform abolishes 5-aminoimidazole-4-carboxamide-1-beta-4-ribofuranosidebut not contraction-induced glucose uptake in skeletal muscle. *J Biol Chem* 2004;279:1070–1079
19. Sakamoto K, McCarthy A, Smith D, et al. Deficiency of LKB1 in skeletal muscle prevents AMPK activation and glucose uptake during contraction. *EMBO J* 2005;24:1810–1820
20. Jeppesen J, Maarbjerg SJ, Jordy AB, et al. LKB1 regulates lipid oxidation during exercise independently of AMPK. *Diabetes* 2013;62:1490–1499
21. Jensen TE, Schjerling P, Viollet B, Wojtaszewski JFP, Richter EA. AMPK alpha1 activation is required for stimulation of glucose uptake by twitch contraction, but not by H2O2, in mouse skeletal muscle. *PLoS One* 2008;3:e2102

22. Lefort N, St-Amand E, Morasse S, Côté CH, Marette A. The alpha-subunit of AMPK is essential for submaximal contraction-mediated glucose transport in skeletal muscle in vitro. *Am J Physiol Endocrinol Metab* 2008;295:E1447–E1454
23. Mu J, Brozinick JT Jr., Valladares O, Bucan M, Birnbaum MJ. A role for AMP-activated protein kinase in contraction- and hypoxia-regulated glucose transport in skeletal muscle. *Mol Cell* 2001;7:1085–1094
24. Karlsson HKR, Chibalin AV, Koistinen HA, et al. Kinetics of GLUT4 trafficking in rat and human skeletal muscle. *Diabetes* 2009;58:847–854
25. Yang J, Holman GD. Insulin and contraction stimulate exocytosis, but increased AMP-activated protein kinase activity resulting from oxidative metabolism stress slows endocytosis of GLUT4 in cardiomyocytes. *J Biol Chem* 2005;280:4070–4078
26. Yang J, Holman GD. Long-term metformin treatment stimulates cardiomyocyte glucose transport through an AMP-activated protein kinase-dependent reduction in GLUT4 endocytosis. *Endocrinology* 2006;147:2728–2736
27. Lantier L, Fentz J, Mounier R, et al. AMPK controls exercise endurance, mitochondrial oxidative capacity, and skeletal muscle integrity. *FASEB J* 2014;28:3211–3224
28. Cokorinos EC, Delmore J, Reyes AR, et al. Activation of skeletal muscle AMPK promotes glucose disposal and glucose lowering in non-human primates and mice. *Cell Metab* 2017;25:1147–1159.e10
29. Chadt A, Immisch A, de Wendt C, et al. Deletion of both Rab-GTPase-activating proteins TBC1D1 and TBC1D4 in mice eliminates insulin- and AICAR-stimulated glucose transport [published correction appears in *Diabetes* 2015;64:1492]. *Diabetes* 2015;64:746–759
30. Fentz J, Kjøbsted R, Birk JB, et al. AMPK α is critical for enhancing skeletal muscle fatty acid utilization during in vivo exercise in mice. *FASEB J* 2015;29:1725–1738
31. Kjøbsted R, Munk-Hansen N, Birk JB, et al. Enhanced muscle insulin sensitivity after contraction/exercise is mediated by AMPK. *Diabetes* 2017;66:598–612
32. Kjøbsted R, Treebak JT, Fentz J, et al. Prior AICAR stimulation increases insulin sensitivity in mouse skeletal muscle in an AMPK-dependent manner. *Diabetes* 2015;64:2042–2055
33. Lowry OH, Passonneau JV. Typical fluorometric procedures for metabolite assays. In *A Flexible System of Enzymatic Analysis*. New York, Academic Press, 1972, p. 68–92
34. Treebak JT, Taylor EB, Witzczak CA, et al. Identification of a novel phosphorylation site on TBC1D4 regulated by AMP-activated protein kinase in skeletal muscle. *Am J Physiol Cell Physiol* 2010;298:C377–C385
35. Vichaiwong K, Purohit S, An D, et al. Contraction regulates site-specific phosphorylation of TBC1D1 in skeletal muscle. *Biochem J* 2010;431:311–320
36. Steinberg GR, O'Neill HM, Dzamko NL, et al. Whole body deletion of AMP-activated protein kinase β 2 reduces muscle AMPK activity and exercise capacity. *J Biol Chem* 2010;285:37198–37209
37. Barnes BR, Marklund S, Steiler TL, et al. The 5'-AMP-activated protein kinase gamma3 isoform has a key role in carbohydrate and lipid metabolism in glycolytic skeletal muscle. *J Biol Chem* 2004;279:38441–38447
38. Hutber CA, Hardie DG, Winder WW. Electrical stimulation inactivates muscle acetyl-CoA carboxylase and increases AMP-activated protein kinase. *Am J Physiol* 1997;272:E262–E266
39. Vendelbo MH, Møller AB, Treebak JT, et al. Sustained AS160 and TBC1D1 phosphorylations in human skeletal muscle 30 min after a single bout of exercise. *J Appl Physiol* (1985) 2014;117:289–296
40. Kjøbsted R, Pedersen AJT, Hingst JR, et al. Intact regulation of the AMPK signaling network in response to exercise and insulin in skeletal muscle of male patients with type 2 diabetes: illumination of AMPK activation in recovery from exercise. *Diabetes* 2016;65:1219–1230
41. Funai K, Schweitzer GG, Sharma N, Kanzaki M, Cartee GD. Increased AS160 phosphorylation, but not TBC1D1 phosphorylation, with increased postexercise insulin sensitivity in rat skeletal muscle. *Am J Physiol Endocrinol Metab* 2009;297:E242–E251
42. Funai K, Schweitzer GG, Castorena CM, Kanzaki M, Cartee GD. In vivo exercise followed by in vitro contraction additively elevates subsequent insulin-stimulated glucose transport by rat skeletal muscle. *Am J Physiol Endocrinol Metab* 2010;298:E999–E1010
43. Pehmøller C, Brandt N, Birk JB, et al. Exercise alleviates lipid-induced insulin resistance in human skeletal muscle-signaling interaction at the level of TBC1 domain family member 4. *Diabetes* 2012;61:2743–2752
44. Liu Y, Lai Y-C, Hill EV, et al. Phosphatidylinositol 3-phosphate 5-kinase (PIKfyve) is an AMPK target participating in contraction-stimulated glucose uptake in skeletal muscle. *Biochem J* 2013;455:195–206
45. An D, Toyoda T, Taylor EB, et al. TBC1D1 regulates insulin- and contraction-induced glucose transport in mouse skeletal muscle. *Diabetes* 2010;59:1358–1365
46. Stöckli J, Meoli CC, Hoffman NJ, et al. The RabGAP TBC1D1 plays a central role in exercise-regulated glucose metabolism in skeletal muscle. *Diabetes* 2015;64:1914–1922
47. Fujii N, Hirshman MF, Kane EM, et al. AMP-activated protein kinase alpha2 activity is not essential for contraction- and hyperosmolarity-induced glucose transport in skeletal muscle. *J Biol Chem* 2005;280:39033–39041
48. Fujii N, Seifert MM, Kane EM, et al. Role of AMP-activated protein kinase in exercise capacity, whole body glucose homeostasis, and glucose transport in skeletal muscle -insight from analysis of a transgenic mouse model-. *Diabetes Res Clin Pract* 2007;77(Suppl. 1):S92–S98
49. Merry TL, Steinberg GR, Lynch GS, McConell GK. Skeletal muscle glucose uptake during contraction is regulated by nitric oxide and ROS independently of AMPK. *Am J Physiol Endocrinol Metab* 2010;298:E577–E585
50. Sylow L, Møller LLV, Kleinert M, et al. Rac1 and AMPK account for the majority of muscle glucose uptake stimulated by ex vivo contraction but not in vivo exercise. *Diabetes* 2017;66:1548–1559
51. O'Neill HM, Maarbjerg SJ, Crane JD, et al. AMP-activated protein kinase (AMPK) beta1beta2 muscle null mice reveal an essential role for AMPK in maintaining mitochondrial content and glucose uptake during exercise. *Proc Natl Acad Sci U S A* 2011;108:16092–16097
52. Abbott MJ, Bogachus LD, Turcotte LP. AMPK α 2 deficiency uncovers time dependency in the regulation of contraction-induced palmitate and glucose uptake in mouse muscle. *J Appl Physiol* (1985) 2011;111:125–134
53. Chen ZP, McConell GK, Michell BJ, Snow RJ, Canny BJ, Kemp BE. AMPK signaling in contracting human skeletal muscle: acetyl-CoA carboxylase and NO synthase phosphorylation. *Am J Physiol Endocrinol Metab* 2000;279:E1202–E1206
54. Fujii N, Hayashi T, Hirshman MF, et al. Exercise induces isoform-specific increase in 5'AMP-activated protein kinase activity in human skeletal muscle. *Biochem Biophys Res Commun* 2000;273:1150–1155
55. Wojtaszewski JF, Nielsen P, Hansen BF, Richter EA, Kiens B. Isoform-specific and exercise intensity-dependent activation of 5'-AMP-activated protein kinase in human skeletal muscle. *J Physiol* 2000;528:221–226
56. Musi N, Fujii N, Hirshman MF, et al. AMP-activated protein kinase (AMPK) is activated in muscle of subjects with type 2 diabetes during exercise. *Diabetes* 2001;50:921–927
57. Mortensen B, Hingst JR, Frederiksen N, et al. Effect of birth weight and 12 weeks of exercise training on exercise-induced AMPK signaling in human skeletal muscle. *Am J Physiol Endocrinol Metab* 2013;304:E1379–E1390
58. Frøsig C, Roepstorff C, Brandt N, et al. Reduced malonyl-CoA content in recovery from exercise correlates with improved insulin-stimulated glucose uptake in human skeletal muscle. *Am J Physiol Endocrinol Metab* 2009;296:E787–E795
59. Blomstrand E, Saltin B. Effect of muscle glycogen on glucose, lactate and amino acid metabolism during exercise and recovery in human subjects. *J Physiol* 1999;514(Pt 1):293–302.
60. Bangsbo J, Gollnick PD, Graham TE, Saltin B. Substrates for muscle glycogen synthesis in recovery from intense exercise in man. *J Physiol* 1991;434:423–440
61. Henriksson J, Knol M. A single bout of exercise is followed by a prolonged decrease in the interstitial glucose concentration in skeletal muscle. *Acta Physiol Scand* 2005;185:313–320

62. Jensen TE, Angin Y, Sylow L, Richter EA. Is contraction-stimulated glucose transport feedforward regulated by Ca²⁺? *Exp Physiol* 2014;99:1562–1568
63. Szekeres F, Chadt A, Tom RZ, et al. The Rab-GTPase-activating protein TBC1D1 regulates skeletal muscle glucose metabolism. *Am J Physiol Endocrinol Metab* 2012;303:E524–E533
64. Chen L, Chen Q, Xie B, et al. Disruption of the AMPK-TBC1D1 nexus increases lipogenic gene expression and causes obesity in mice via promoting IGF1 secretion. *Proc Natl Acad Sci U S A* 2016;113:7219–7224
65. Maarbjerg SJ, Jørgensen SB, Rose AJ, et al. Genetic impairment of AMPK α 2 signaling does not reduce muscle glucose uptake during treadmill exercise in mice. *Am J Physiol Endocrinol Metab* 2009;297:E924–E934
66. Chen Q, Xie B, Zhu S, et al. A Tbc1d1^{Ser231Ala}-knockin mutation partially impairs AICAR- but not exercise-induced muscle glucose uptake in mice. *Diabetologia* 2017;60:336–345
67. Lee-Young RS, Griffee SR, Lynes SE, et al. Skeletal muscle AMP-activated protein kinase is essential for the metabolic response to exercise in vivo. *J Biol Chem* 2009;284:23925–23934



TBC1D4 Is Necessary for Enhancing Muscle Insulin Sensitivity in Response to AICAR and Contraction

Rasmus Kjøbsted,¹ Alexandra Chadt,^{2,3} Nicolas O. Jørgensen,¹ Kohei Kido,¹ Jeppe K. Larsen,¹ Christian de Wendt,^{2,3} Hadi Al-Hasani,^{2,3} and Jørgen F.P. Wojtaszewski¹

Diabetes 2019;68:1756–1766 | <https://doi.org/10.2337/db18-0769>

Muscle insulin sensitivity for stimulating glucose uptake is enhanced in the period after a single bout of exercise. We recently demonstrated that AMPK is necessary for AICAR, contraction, and exercise to enhance muscle and whole-body insulin sensitivity in mice. Correlative observations from both human and rodent skeletal muscle suggest that regulation of the phosphorylation status of TBC1D4 may relay this insulin sensitization. However, the necessity of TBC1D4 for this phenomenon has not been proven. Thus, the purpose of this study was to determine whether TBC1D4 is necessary for enhancing muscle insulin sensitivity in response to AICAR and contraction. We found that immediately after contraction and AICAR stimulation, phosphorylation of AMPK α -Thr172 and downstream targets were increased similarly in glycolytic skeletal muscle from wild-type and TBC1D4-deficient mice. In contrast, 3 h after contraction or 6 h after AICAR stimulation, enhanced insulin-stimulated glucose uptake was evident in muscle from wild-type mice only. The enhanced insulin sensitivity in muscle from wild-type mice was associated with improved insulin-stimulated phosphorylation of TBC1D4 (Thr649 and Ser711) but not of TBC1D1. These results provide genetic evidence linking signaling through TBC1D4 to enhanced muscle insulin sensitivity after activation of the cellular energy sensor AMPK.

Impaired insulin-stimulated glucose uptake in skeletal muscle is a key defect in the pathogenesis of type 2 diabetes (1). Importantly, the ability of a single bout of exercise to improve insulin-stimulated glucose uptake in skeletal muscle has been demonstrated by several studies in both healthy and insulin-resistant rodents (2–4) and humans

(5–8), highlighting the therapeutic potential of exercise. In vivo enhanced insulin-stimulated glucose uptake is likely mediated by a coordinated increase in microvascular perfusion (9) and GLUT4 translocation to the plasma membrane (10) in response to insulin without enhanced proximal insulin signaling (4,8,11–13). We recently reported that prior activation of AMPK in skeletal muscle is necessary to improve muscle and whole-body insulin sensitivity in response to AICAR, contraction, and exercise (14,15). TBC1D4 is regulated by Akt-mediated phosphorylation during insulin stimulation that has been suggested to be important for insulin-stimulated GLUT4 translocation and glucose uptake in skeletal muscle (16,17). TBC1D4 is also regulated by AMPK-mediated phosphorylation, but this seems insufficient in itself to promote glucose uptake (18). A number of studies have reported that elevated insulin-stimulated phosphorylation of TBC1D4 occurs in parallel with improved muscle insulin sensitivity after a single bout of exercise, contraction, and AICAR stimulation (8,13–15,19,20). Importantly, this relationship is abolished in AMPK-deficient muscle (14,15), suggesting that an AMPK-TBC1D4 signaling axis is mediating the insulin-sensitizing effect of these stimuli. However, direct evidence linking AMPK and TBC1D4 to improved muscle insulin sensitivity has not been established.

To address the hypothesis that TBC1D4 is required for enhancing muscle insulin sensitivity after pharmacological- and contraction-induced activation of AMPK, we applied a genetic approach and took advantage of our previously established *ex vivo* and *in situ* experimental protocols (14,15).

¹Section of Molecular Physiology, Department of Nutrition, Exercise and Sports, Faculty of Science, University of Copenhagen, Copenhagen, Denmark

²German Diabetes Center, Leibniz Center for Diabetes Research at the Heinrich Heine University Düsseldorf, Düsseldorf, Germany

³German Center for Diabetes Research (DZD), München-Neuherberg, Germany

Corresponding author: Jørgen F.P. Wojtaszewski, jwojtaszewski@nexs.ku.dk

Received 14 July 2018 and accepted 3 June 2019

This article contains Supplementary Data online at <http://diabetes.diabetesjournals.org/lookup/suppl/doi:10.2337/db18-0769/-/DC1>.

© 2019 by the American Diabetes Association. Readers may use this article as long as the work is properly cited, the use is educational and not for profit, and the work is not altered. More information is available at <http://www.diabetesjournals.org/content/license>.

RESEARCH DESIGN AND METHODS

Animals

All animal experiments complied with the European Union Convention for the Protection of Vertebrates Used for Scientific Purposes and were approved by the State Agency for Nature, Environment and Consumer Protection (LANUV, North Rhine-Westphalia, Germany) Ethics Committee and the Danish Animal Experiments Inspectorate. Animals used in this study were whole-body *Tbc1d4* knock-out (D4KO) female mice (21) and CRISPR/Cas9-generated muscle-specific *Tbc1d4* KO (mD4KO) male and female mice (Supplementary Data) with corresponding wild-type (WT) littermates as controls. Mice (17 ± 6 weeks [mean \pm SD]) were maintained on a 12:12-h light-dark cycle with free access to standard rodent chow and water.

Ex Vivo Muscle Incubations After AICAR Stimulation

Fed whole-body *Tbc1d4* KO female mice (21) and WT littermates were anesthetized by an intraperitoneal injection of tribromoethanol (Avertin) (50 mg/100 g body wt) or pentobarbital (10 mg/100 g body wt) before extensor digitorum longus (EDL) muscles were isolated and suspended in incubation chambers (Multi Wire Myograph System; Danish Myo Technology, Aarhus, Denmark) containing Krebs-Ringer buffer (KRB) supplemented with 0.1% BSA, 8 mmol/L mannitol, and 2 mmol/L pyruvate, as previously described (14). In short, after 10 min of preincubation, EDL muscles were incubated for 50 min in 100% human serum in the absence or presence of 1 mmol/L AICAR (Toronto Research Chemicals, Toronto, Ontario, Canada). Serum was obtained from a young, healthy man after an overnight fast in accordance with a protocol approved by the Ethics Committee of Copenhagen (#H-18045268).

Muscles were allowed to recover for 6 h in KRB supplemented with 0.1% BSA, 5 mmol/L D-glucose, and 5 mmol/L mannitol, after which they were incubated in KRB supplemented with 0.1% BSA, 2 mmol/L pyruvate, and 8 mmol/L mannitol, with or without a submaximal or a maximal insulin concentration (100 and 10,000 μ U/mL), for 30 min. 2-Deoxyglucose uptake was measured during the last 10 of the 30-min stimulation period by adding 1 mmol/L [3 H]2-deoxyglucose (0.028 MBq/mL) and 7 mmol/L [14 C]mannitol (0.0083 MBq/mL) to the incubation medium. For glucose uptake measurements in response to acute AICAR stimulation, EDL muscles were incubated in 100% human serum for 50 min in the absence or presence of 1 mmol/L of AICAR. Subsequently, muscles were washed for 1 min in KRB supplemented with 0.1% BSA, 8 mmol/L mannitol, and 2 mmol/L pyruvate, after which 2-deoxyglucose uptake was measured during a 10 min incubation period as described above. Also present in the wash and transport buffers was 1 mmol/L AICAR. For all incubations, 2-deoxyglucose uptake was determined as previously described (15).

Ex Vivo Muscle Incubations After In Situ Contraction

Fed CRISPR/Cas9-generated muscle-specific *Tbc1d4* KO male and female mice as well as WT littermates were

anesthetized by an intraperitoneal injection of pentobarbital (10 mg/100 g body wt), after which electrodes were connected to the common peroneal nerve of both legs of the animals. Half of the animals served as sham-operated controls. Immediately after 10 min of in situ contraction (duration: 0.5 s, frequency: 100 Hz, width: 0.1 ms, voltage: 5 V, repeated every 1.5 s) tibialis anterior muscles were dissected and frozen in liquid nitrogen to study the acute response of contraction on intracellular signaling and glycogen levels. After dissection of the tibialis anterior muscles, EDL muscles were dissected and suspended in incubation chambers containing KRB supplemented with 0.1% BSA, 5 mmol/L D-glucose, and 5 mmol/L mannitol to study the submaximal insulin response after contraction, as previously described (15). In short, EDL muscles were incubated for 180 min during which the incubation buffer was replaced every 30 min to maintain a glucose concentration of \sim 5 mmol/L. Muscles were subsequently incubated in KRB supplemented with 0.1% BSA, 2 mmol/L pyruvate, and 8 mmol/L mannitol, with or without a submaximal insulin concentration (100 μ U/mL), for 30 min. Uptake of 2-deoxyglucose was measured during the last 10 min of the 30-min stimulation period as described above.

Muscle Processing, SDS-PAGE, and Western Blot Analyses

Muscles were homogenized, and lysates were collected and frozen (-80°C) for subsequent analyses as previously described (14). The bicinchoninic acid method was used to determine total protein abundance in muscle lysates. Lysates were boiled in Laemmli buffer and subjected to SDS-PAGE and immunoblotting as previously described (14).

Muscle Glycogen

Glycogen concentration in tibialis anterior muscle was measured on 500 μ g of muscle protein homogenate after acid hydrolysis. In short, muscle homogenates were heated (100°C) for 2 h in 2 mol/L HCl. Glucosyl units were determined in a fraction of the supernatant (22) and related to protein concentration.

Antibodies

Primary antibodies against Akt2, phosphorylated (p)Akt-Ser473, pAkt-Thr308, Erk1/2, pErk1/2 Thr202/Tyr204, pAMPK α -Thr172, pACC-Ser79/212, pTBC1D4-Thr642, pTBC1D1-Thr590, TBC1D1, and hexokinase II were from Cell Signaling Technology. Antibody against pTBC1D1-Ser231 was from Millipore, and antibody against TBC1D4 (AS160) was from Millipore and Abcam. Antibody against AMPK α 2 was from Santa Cruz Biotechnology as well as donated by Dr. D. Grahame Hardie (School of Life Sciences, University of Dundee). GLUT4 antibody was from Thermo-Fisher Scientific, and ACC protein was detected using horseradish peroxidase-conjugated streptavidin from Jackson ImmunoResearch. pTBC1D4-Ser711 was detected using antibody donated by Dr. Laurie J. Goodyear (Joslin Diabetes Center and Harvard Medical School) (18).

Statistics

Data are presented as the means \pm SEM unless stated otherwise. Two-way ANOVA with repeated measures and paired/unpaired Student *t* tests were used to assess statistical significance within and between genotypes, where appropriate. The Student-Newman-Keuls test was used for post hoc testing. Statistical significance was defined as $P < 0.05$.

RESULTS

Glucose Uptake and AMPK Signaling Increase Similarly in EDL Muscle From WT and Whole-Body *Tbc1d4* KO Mice During AICAR Stimulation

Glucose uptake increased similarly in EDL muscle from *Tbc1d4* WT and KO mice during AICAR stimulation (Fig. 1A), as also previously reported (21). Acute AICAR stimulation also increased phosphorylation of AMPK α -Thr172 (Fig. 1B) and downstream targets ACC-Ser212 (Fig. 1C) and TBC1D1-Ser231 (Fig. 1D) in EDL muscle from both genotypes. As expected, acute AICAR stimulation increased phosphorylation of TBC1D4-Ser711 in WT EDL muscle only (Fig. 1E). Immediately after AICAR stimulation, total protein abundance of AMPK α 2, ACC, and TBC1D4 was not altered; however, we detected a slight but significant increase in TBC1D1 protein in EDL muscle from both genotypes. Collectively, these results suggest that immediately after AICAR stimulation, AMPK activity increased to a similar extent in EDL muscle from WT and whole-body *Tbc1d4* KO mice.

AMPK Signaling and Glycogen Content Are Similar in Skeletal Muscle From WT and Muscle-Specific *Tbc1d4* KO Mice Immediately After Contraction

In response to in situ contraction, glycogen content decreased to a similar extent in skeletal muscle from WT and muscle-specific *Tbc1d4* KO mice (Fig. 2A). In addition, in situ contraction increased phosphorylation of Erk1/2-Thr202/Tyr204 (Fig. 2B), AMPK α -Thr172 (Fig. 2C), ACC-Ser212 (Fig. 2D), and TBC1D1-Ser231 (Fig. 2E) in skeletal muscle to an extent that did not differ between genotypes. This indicates that the in situ contraction protocol induced similar metabolic stress and relevant cellular signaling in both WT and *Tbc1d4*-deficient skeletal muscle. TBC1D4 protein was not detected in skeletal muscle from muscle-specific *Tbc1d4* KO mice, and thus, in situ contraction increased phosphorylation of TBC1D4-Ser711 in WT skeletal muscle only (Fig. 2F and G). Besides a small ($\sim 30\%$) significant decrease in AMPK α 2, total protein abundance of Erk1/2, ACC, TBC1D1, and TBC1D4 were not affected in skeletal muscle from either genotype immediately after in situ contraction (Fig. 2G).

Prior AICAR Stimulation Enhances Submaximal Insulin-Stimulated Glucose Uptake and Phosphorylation of TBC1D4 in WT Muscle Only

To clarify whether the AMPK-dependent increase in muscle insulin sensitivity after AICAR stimulation is dependent on TBC1D4, we measured submaximal and maximal

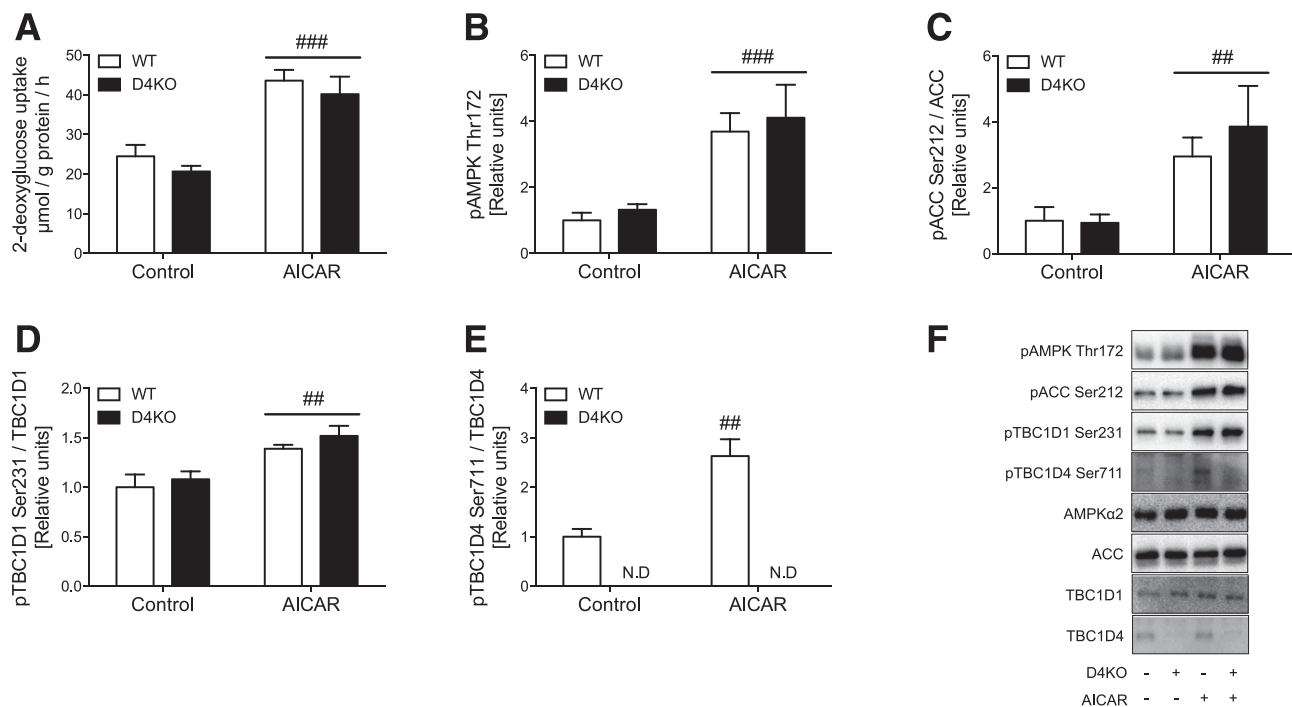


Figure 1—Acute AICAR stimulation increases muscle glucose uptake and AMPK signaling in WT and *Tbc1d4* KO mice. 2-Deoxyglucose uptake (A), pAMPK-Thr172 (B), pACC-Ser212 (C), pTBC1D1-Ser231 (D), and pTBC1D4-Ser711 (E) in isolated EDL muscle from WT and whole-body D4KO mice immediately after 50 min of AICAR stimulation. Data were analyzed by a two-way repeated measures ANOVA (A–D) and a paired Student *t* test (E). ### $P < 0.001$ and ## $P < 0.01$ effect of AICAR. Lines indicate main effect of AICAR. F: Representative Western blot images. Values are means \pm SEM ($n = 6$ in all groups). N.D., not detectable.

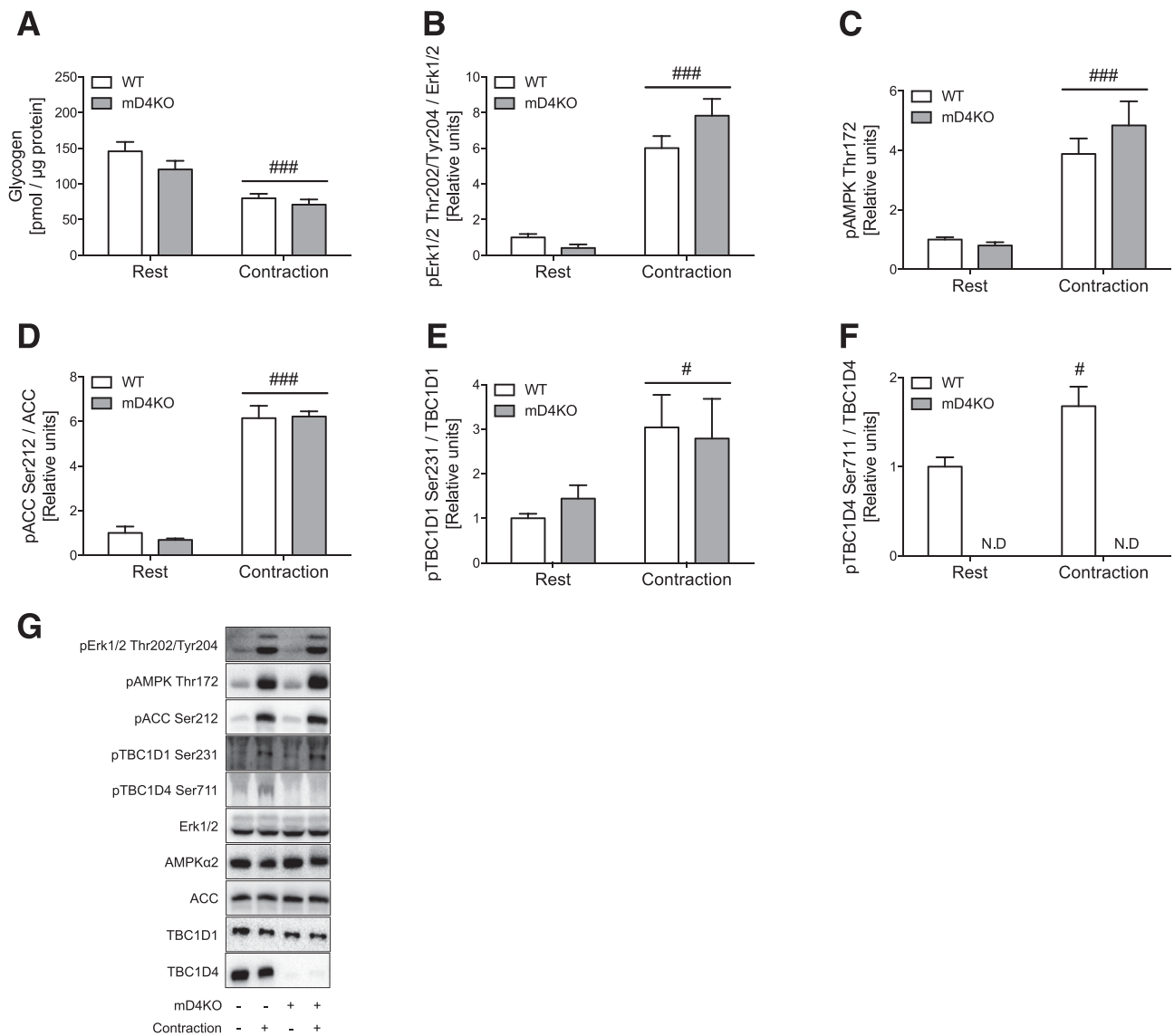


Figure 2—Acute in situ contraction affects glycogen levels and AMPK signaling similarly in skeletal muscle from WT and mD4KO mice. Glycogen (A), pErk1/2-Thr202/Tyr204 (B), pAMPK-Thr172 (C), pACC-Ser212 (D), pTBC1D1-Ser231 (E), and pTBC1D4-Ser711 (F) in tibialis anterior muscle from WT and mD4KO mice immediately after 10 min of in situ contraction. Data were analyzed by a two-way repeated measures ANOVA (A–E) and a paired Student *t* test (F). ### $P < 0.001$ and # $P < 0.05$ effect of in situ contraction. Lines indicate main effect of contraction. G: Representative Western blot images. Values are means \pm SEM ($n = 6$ –8 in WT groups, $n = 4$ –5 in *Tbc1d4* KO groups). N.D., not detectable.

insulin-stimulated glucose uptake in EDL muscle 6 h after AICAR stimulation. At this time point, the acute effect of AICAR on noninsulin-stimulated glucose uptake (Fig. 1A) had returned to near control levels in muscle from both WT and whole-body *Tbc1d4* KO mice (Fig. 3A). Interestingly, prior AICAR stimulation improved submaximal insulin-stimulated glucose uptake in isolated EDL muscle from WT mice only (Fig. 3A). Thus, the incremental increase in submaximal insulin-stimulated glucose uptake was significantly higher ($\sim 70\%$) in prior AICAR-stimulated EDL muscle from WT mice only (Fig. 3B).

We next investigated the phosphorylation pattern of TBC1D4. We found that activation of AMPK by prior AICAR stimulation increased submaximal insulin-stimulated

phosphorylation of TBC1D4-Ser711 and TBC1D4-Thr649 in WT EDL muscle (Fig. 3C and D). This occurred despite that proximal insulin signaling measured at the level of phosphorylated Akt-Thr308 and -Ser473 was not enhanced by prior AICAR stimulation (Fig. 3E and F). As expected, no changes in total muscle protein abundance of Akt2, TBC1D4, HKII, and GLUT4 were found 6 h after AICAR stimulation (Fig. 3G).

Prior In Situ Contraction Enhances Submaximal Insulin-Stimulated Glucose Uptake and Phosphorylation of TBC1D4 in WT Muscle Only

Noninsulin-stimulated glucose uptake was slightly elevated 3 h after in situ contraction in EDL muscle from

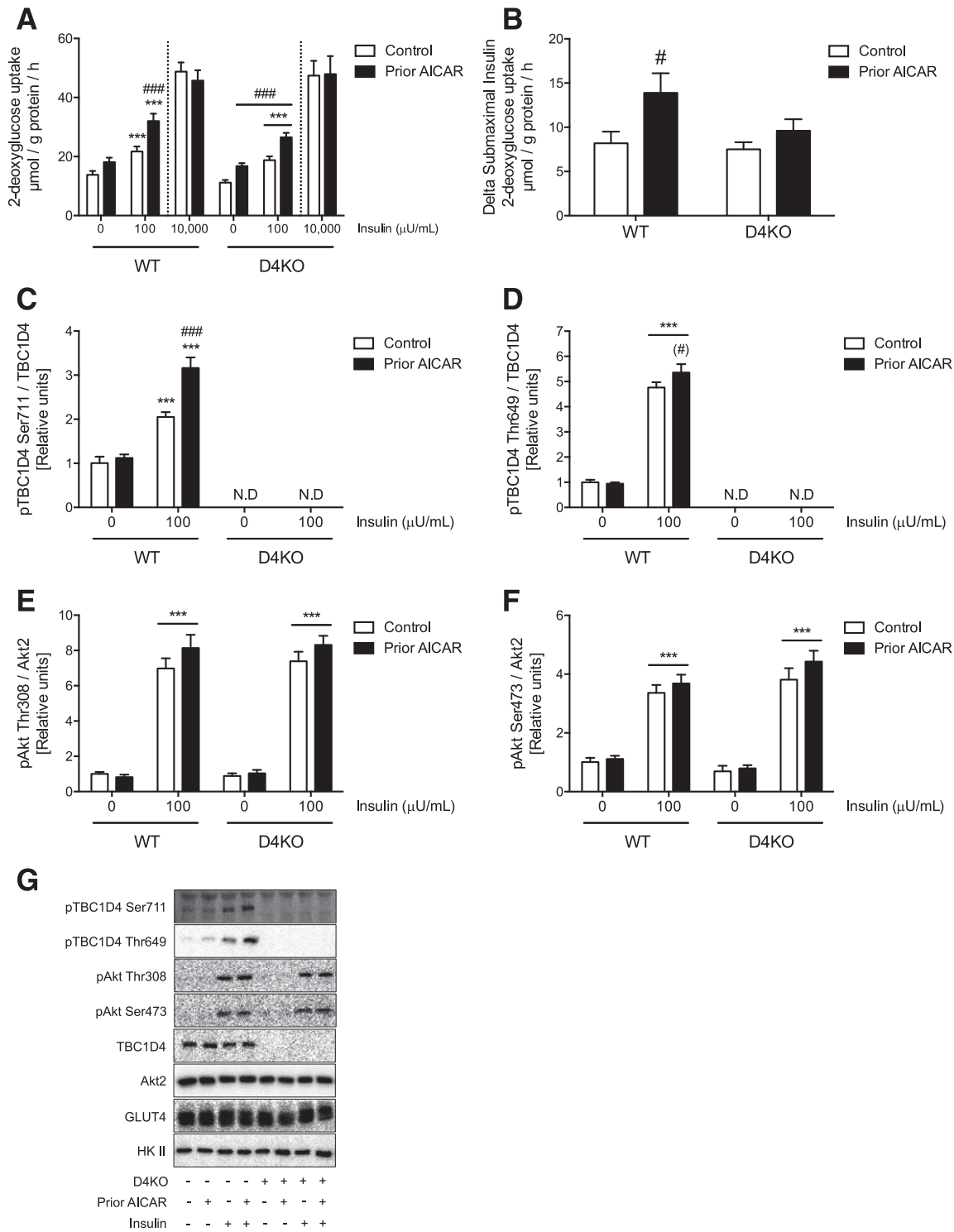


Figure 3—TBC1D4 is necessary for enhancing muscle insulin sensitivity 6 h after AICAR stimulation. 2-Deoxyglucose uptake (A) and Δ 2-deoxyglucose uptake (submaximal insulin minus basal) (B) in isolated EDL muscle from WT and whole-body D4KO mice incubated with or without a submaximal (100 $\mu\text{U}/\text{mL}$) or a maximal (10,000 $\mu\text{U}/\text{mL}$) insulin concentration 6 h after prior control or AICAR treatment. pTBC1D4-Ser711 (C), pTBC1D4-Thr649 (D), pAkt-Thr308 (E), and pAkt-Ser473 (F) in isolated EDL muscle from WT and whole-body D4KO mice incubated with or without a submaximal insulin concentration (100 $\mu\text{U}/\text{mL}$) 6 h after prior control or AICAR treatment. Data on basal and submaximal insulin-stimulated glucose uptake were analyzed by a two-way repeated measures ANOVA (A) and an unpaired Student *t* test (B) within each genotype, respectively. A: Data on maximal insulin-stimulated glucose uptake were analyzed by a paired Student *t* test within each genotype. C–F: Data on muscle signaling were analyzed by a two-way repeated measures ANOVA within each genotype. ###*P* < 0.001, #*P* < 0.05, and (#)*P* = 0.08 indicate effect of prior AICAR stimulation. ****P* < 0.001 indicates effect of insulin. A and C: WT: AICAR \times insulin interaction (*P* < 0.05). Lines indicate main effect of AICAR or insulin. G: Representative Western blot images. Values are means \pm SEM (*n* = 17–18 in basal and submaximal insulin groups, *n* = 6 in maximal insulin groups).

both WT and muscle-specific *Tbc1d4* KO mice (Fig. 4A). However, prior in situ contraction enhanced submaximal insulin-stimulated glucose uptake in isolated EDL muscle from WT mice only (Fig. 4A). Thus, a significant incremental increase in submaximal insulin-stimulated glucose uptake (~150%) was observed in prior contracted EDL muscle from WT mice (Fig. 4B). When examining the phosphorylation pattern of TBC1D4, we found that prior in situ contraction increased submaximal insulin-stimulated phosphorylation of TBC1D4-Ser711 and TBC1D4-Thr649 in WT EDL muscle (Fig. 4C and D). This also occurred without significant enhanced insulin-stimulated phosphorylation of Akt-Thr308 and -Ser473 (Fig. 4E and F). In addition, no changes in total muscle protein abundance of Akt2, TBC1D4, HKII, and GLUT4 were found 3 h after prior in situ contraction (Fig. 4G).

AMPK Signaling Is Elevated in Skeletal Muscle in the Recovery Period After AICAR Stimulation

We have previously reported that AMPK activity and downstream signaling are increased in skeletal muscle in the recovery period after AICAR stimulation (14). In accordance, we found that the phosphorylation of AMPK α -Thr172, ACC-Ser212, TBC1D1-Ser231, and TBC1D1-Thr590 was increased in EDL muscle from WT and *Tbc1d4* KO mice 6 h after AICAR stimulation (Fig. 5A–D). On average, the increase in phosphorylation of AMPK α -Thr172, ACC-Ser212, and TBC1D1-Ser231 represented ~38%, ~80%, and ~90%, respectively, of the increase observed immediately after AICAR stimulation (Fig. 1). In addition, insulin increased the phosphorylation of TBC1D1-Thr590 in both control and prior AICAR-stimulated muscles independent of genotype (Fig. 5D). We did not detect any changes in total protein abundance of AMPK α 2, ACC, and TBC1D1 6 h after AICAR stimulation (Fig. 5E).

AMPK Signaling Had Returned to Resting Levels in Skeletal Muscle 3 h After In Situ Contraction

In contrast to findings 6 h after AICAR stimulation, we observed that the phosphorylation of AMPK α -Thr172, ACC-Ser212, and TBC1D1-Ser231 had returned to resting levels in EDL muscle 3 h after in situ contraction (Fig. 6A–C) as also previously reported (15). The phosphorylation of TBC1D1-Thr590 was not different between rest and prior contracted muscle but increased in response to insulin in both genotypes (Fig. 6D). We did not detect any changes in total protein abundance of AMPK α 2, ACC, and TBC1D1 3 h after in situ contraction (Fig. 6E). Collectively, no differences between genotypes were observed for AMPK signaling in skeletal muscle after in situ contraction and AICAR stimulation.

DISCUSSION

Skeletal muscle insulin resistance is a key risk factor for developing type 2 diabetes. Importantly, a marked and persistent increase in insulin sensitivity is observed in the previously active muscle after a single bout of exercise

(2,3,5,7,11), highlighting the therapeutic potential of exercise. We and others have shown that pharmacological activation of AMPK in isolated muscle is sufficient to increase insulin sensitivity (12,14), and we recently reported that AMPK is also necessary for contraction and exercise to improve muscle insulin sensitivity (15). Moreover, we have provided proof-of-concept that direct pharmacological activation of AMPK in skeletal muscle improves glucose homeostasis in diet-induced obese mice and nonhuman primates (23). Here we provide the first genetic evidence to support that the AMPK downstream target TBC1D4 is necessary for enhancing insulin sensitivity in glycolytic EDL muscle after pharmacological and contraction-mediated activation of AMPK. Because AICAR and in situ contraction fail to increase insulin sensitivity in WT soleus muscle (14,15) and insulin-stimulated glucose uptake is abrogated in soleus muscle from *Tbc1d4* KO mice (21), we were unable to determine the role of TBC1D4 in regulating insulin sensitivity in isolated oxidative soleus muscle.

Since the seminal observations in rat skeletal muscle by Arias et al. (19), elevated phosphorylation of TBC1D4 has emerged as an attractive candidate for mediating improvements in muscle insulin sensitivity after a single bout of exercise. Indeed, we reported in several human studies that improved muscle insulin sensitivity after acute exercise coincides with elevated insulin-stimulated phosphorylation of TBC1D4 in the prior exercised muscle (8,9,20). Furthermore, we showed that improved insulin sensitivity after prior contraction and AICAR stimulation is positively associated with elevated phosphorylation of TBC1D4-Thr649 and -Ser711 in WT EDL mouse muscle (14,15). Interestingly, such interplay is lost in AMPK-deficient muscle, supporting the notion of an AMPK-TBC1D4 signaling axis regulating muscle insulin sensitivity.

Evidence suggests that insulin stimulates glucose uptake by Akt-mediated phosphorylation of TBC1D4 (16). Phosphorylation of TBC1D4-Thr649 seems to be the site primarily responsible for enhancing GLUT4 translocation and glucose uptake in skeletal muscle in response to insulin (17). TBC1D4 is also phosphorylated at Ser711 in response to insulin and activation of AMPK, but this seems insufficient in itself to promote glucose uptake (18). However, when a TBC1D4-Ser711Ala mutant is overexpressed in skeletal muscle by gene electrotransfer, the ability of insulin to enhance phosphorylation of TBC1D4-Thr649 is impaired (14), suggesting that Ser711 phosphorylation increases the potential of upstream kinase Akt to phosphorylate TBC1D4. This seemingly increased effect of Akt on TBC1D4 several hours after prior AMPK activation by AICAR and contraction may be mediated by altered cellular localization of TBC1D4 and/or a decreased ability of phosphatases to dephosphorylate TBC1D4 during submaximal insulin concentrations (24,25). Taken together, our observations may suggest that activation of AMPK in some way primes TBC1D4 for a subsequent insulin stimulus, which leads to enhanced insulin-stimulated glucose uptake.

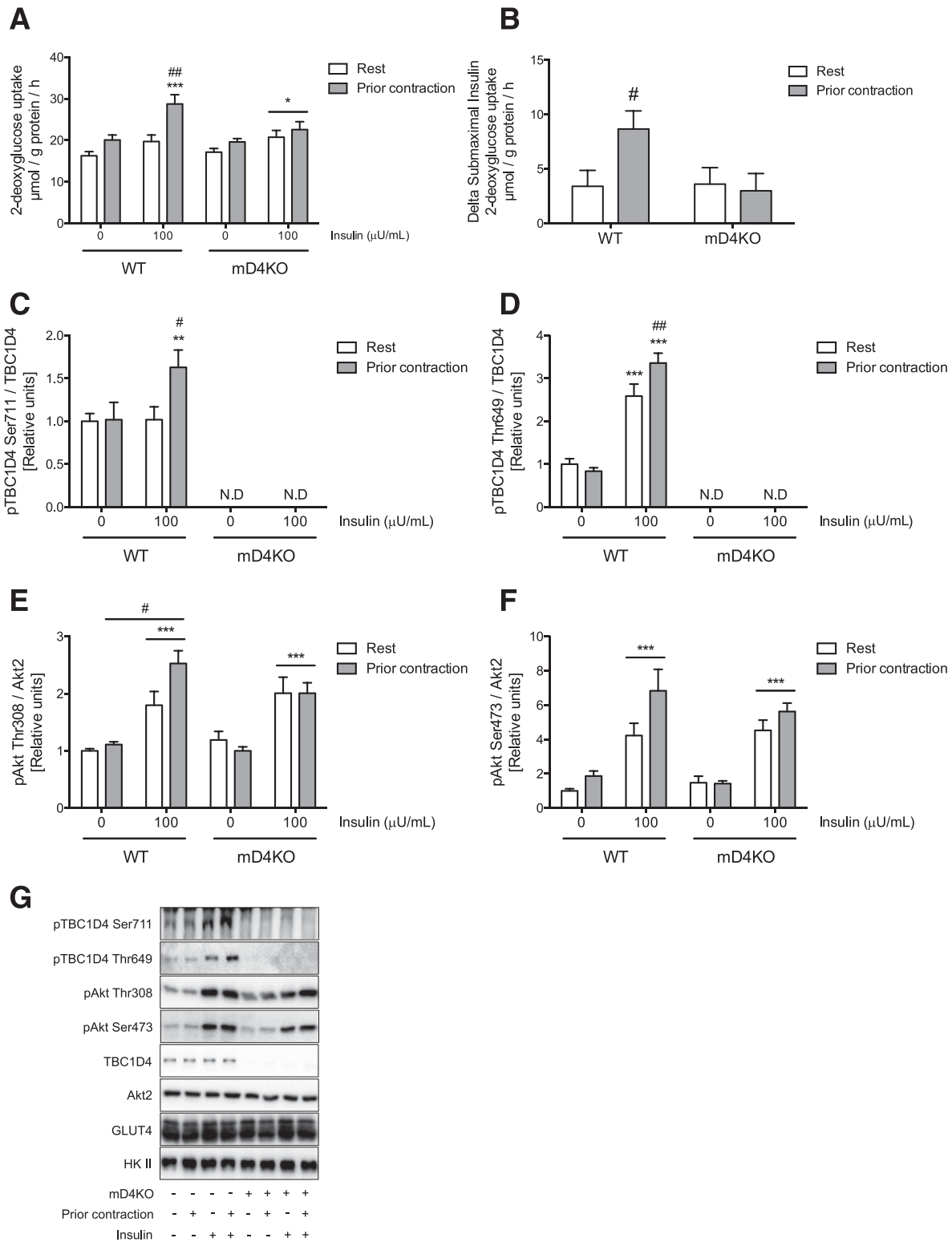


Figure 4—TBC1D4 is necessary for enhancing muscle insulin sensitivity 3 h after in situ contraction. 2-Deoxyglucose uptake (A), Δ 2-deoxyglucose uptake (submaximal insulin minus basal) (B), pTBC1D4-Ser711 (C), pTBC1D4-Thr649 (D), pAkt-Thr308 (E), and pAkt-Ser473 (F) in isolated EDL muscle from WT and mD4KO mice incubated with or without a submaximal (100 μU/mL) insulin concentration 3 h after rest or in situ contraction. Data on basal and submaximal insulin-stimulated glucose uptake were analyzed by a two-way repeated measures ANOVA (A) and an unpaired Student *t* test (B) within each genotype, respectively. C–F: Data on muscle signaling were analyzed by a two-way repeated measures ANOVA within each genotype. ^{##}*P* < 0.01 and [#]*P* < 0.05 indicate effect of in situ contraction. ^{***}*P* < 0.001, ^{**}*P* < 0.01, and ^{*}*P* < 0.05 indicate effect of insulin. A, C, and D: WT: contraction × insulin interaction (*P* < 0.05). Lines indicate main effect of contraction or insulin. G: Representative Western blot images. Values are means ± SEM (*n* = 5–9 per group). N.D., not detectable.

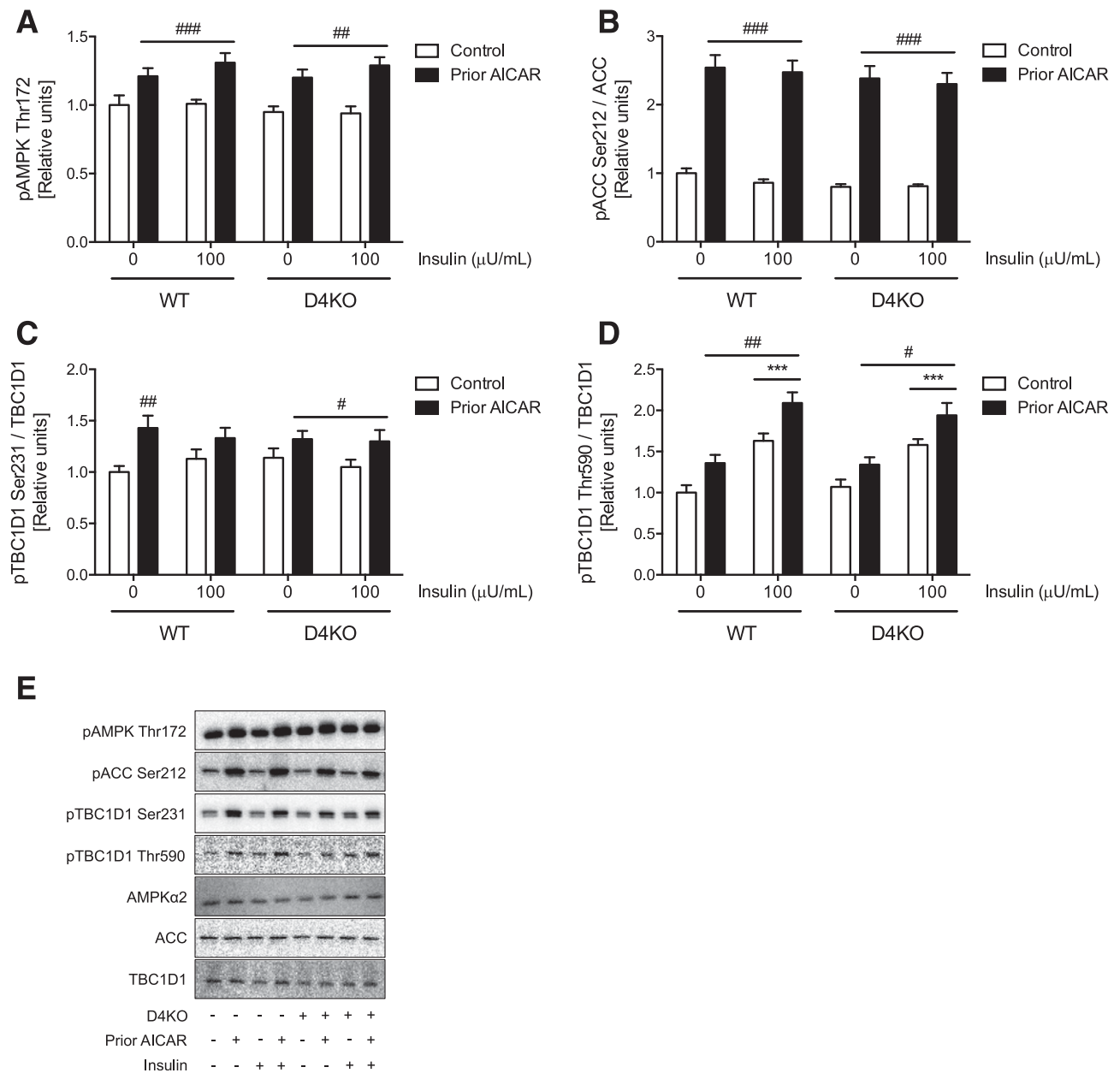


Figure 5—AMPK signaling is elevated in prior AICAR-stimulated muscle from WT and whole-body D4KO mice. pAMPK-Thr172 (A), pACC-Ser212 (B), pTBC1D1-Ser231 (C), and pTBC1D1-Thr590 (D) in isolated EDL muscle from WT and whole-body D4KO mice incubated with or without insulin (100 μU/mL) 6 h after control or AICAR treatment. Data were analyzed by a two-way repeated measures ANOVA within each genotype. ###*P* < 0.001, ##*P* < 0.01, and #*P* < 0.05 indicate the effect of AICAR. ****P* < 0.001 indicates the effect of insulin. Lines indicate the main effect of AICAR or insulin. E: Representative Western blot images. Values are means ± SEM (*n* = 16–18 per group).

Several heterotrimeric complexes of AMPK exist in skeletal muscle (26). We have shown that the insulin-sensitizing effect of prior AICAR stimulation occurs via the AMPKα2β2γ3 complex (14) and that this complex likely phosphorylates TBC1D4-Ser711 during contraction (15). Based on these findings, we propose that AICAR and contraction enhance muscle insulin sensitivity by activating the AMPKα2β2γ3 complex, which subsequently phosphorylates TBC1D4-Ser711. Thus, in the period after contraction and AICAR stimulation, internalized GLUT4

may relocate to specific intracellular compartments that are highly susceptible to recruitment by a subsequent insulin stimulus leading to enhanced insulin-stimulated glucose uptake as previously hypothesized (27). Alternatively, more TBC1D4 protein may associate with GLUT4 as it moves from the cell surface membrane into the cell. If the recently internalized GLUT4 associates with more protein that senses the insulin signal (i.e., TBC1D4), this could also explain the increase in insulin sensitivity as previously suggested (28).

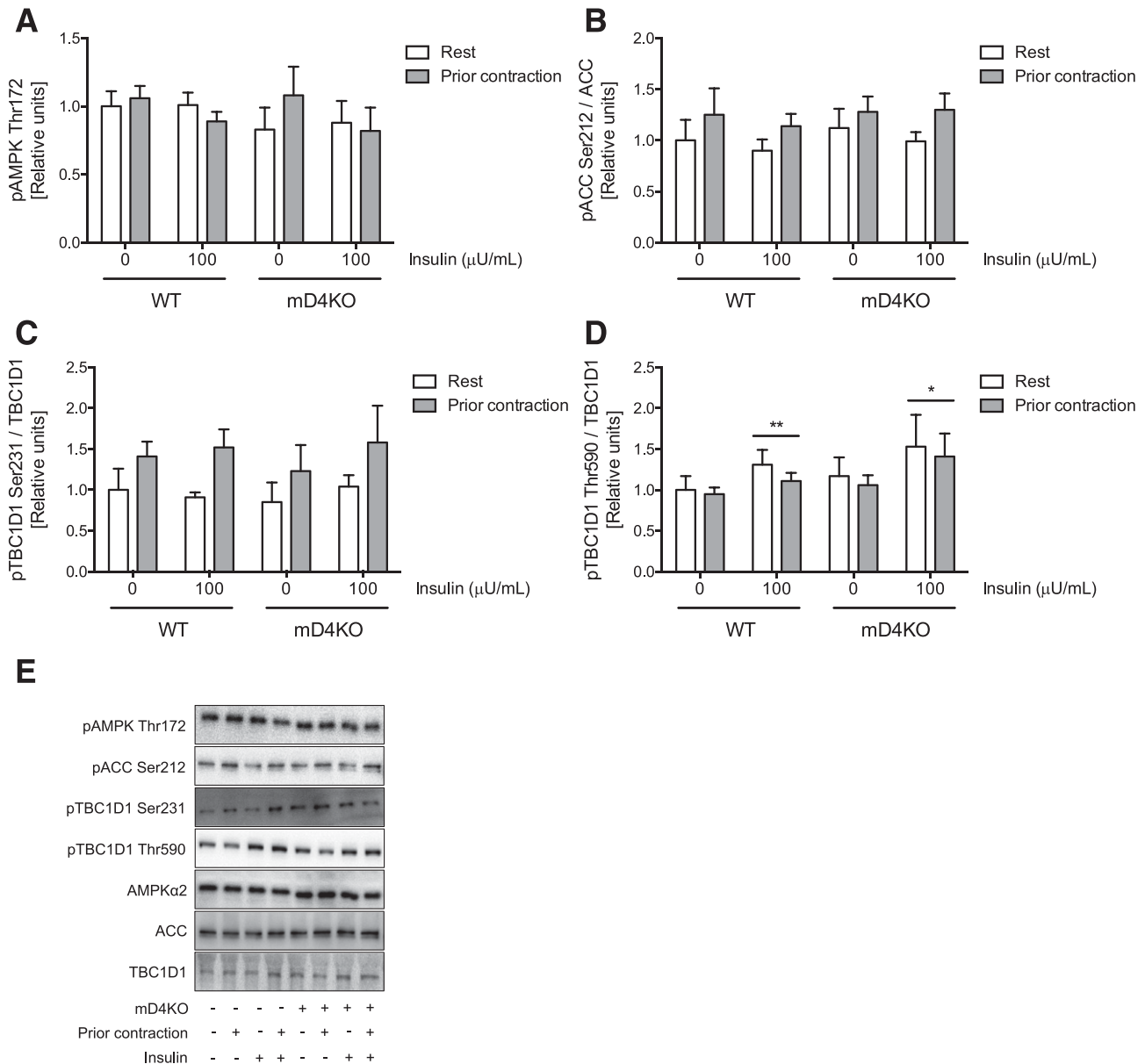


Figure 6—AMPK signaling has returned to resting levels in muscle from WT and mD4KO mice 3 h after in situ contraction. pAMPK-Thr172 (A), pACC-Ser212 (B), pTBC1D1-Ser231 (C), and pTBC1D1-Thr590 (D) in isolated EDL muscle from WT and mD4KO mice incubated with or without insulin (100 μU/mL) 3 h after rest or in situ contraction. Data were analyzed by a two-way repeated measures ANOVA within each genotype. ***P* < 0.01 and **P* < 0.05 indicate effect of insulin. E: Representative Western blot images. Values are means ± SEM (*n* = 5–9 per group).

Similar to our previous study (14), we observed elevated AMPK downstream signaling 6 h after prior AICAR stimulation, which likely derives from a persistent increase in AMPK activity (14). We presume that this is not due to changes in the adenosine nucleotide pools but rather to a lasting effect of 5-amino-4-imidazole carboxamide ribonucleoside 5'-phosphate (ZMP) in skeletal muscle, because accumulation of ZMP after AICAR stimulation does not seem to affect concentrations of AMP, ADP, or ATP in cells and isolated skeletal muscle (29,30). Although the action of AICAR/ZMP in skeletal muscle is likely not confined to AMPK alone, we previously showed in AMPK transgenic

animals that the insulin-sensitizing effect of prior AICAR stimulation is indeed mediated via AMPK in skeletal muscle (14).

Because GLUT4 and HKII protein abundance have been shown to be important for insulin-stimulated muscle glucose uptake (31), improved insulin sensitivity or the lack thereof several hours after contraction and AICAR stimulation could potentially be due to changes in muscle protein abundance of GLUT4 and HKII. However, we did not detect changes in total muscle protein abundance of GLUT4 and HKII, suggesting that these proteins are not essential for the insulin-sensitizing effect of contraction

and AICAR in EDL muscle from WT mice or the lack thereof in EDL muscle from TBC1D4-deficient mice.

Studies have reported that improved muscle insulin sensitivity after prior AICAR stimulation and contraction occurs without enhanced proximal insulin signaling (12,14). In line, we found that insulin-stimulated phosphorylation of Akt-Thr308 and -Ser473 was not enhanced by prior AICAR stimulation or contraction. These results are similar to findings showing normal proximal insulin signaling in prior exercised and insulin-sensitized muscle (4,8,11,13).

Similar to TBC1D4, it has been shown that TBC1D1 is targeted by both Akt and AMPK and that TBC1D1 may function to regulate glucose uptake in skeletal muscle (32–34). Because the phosphorylation pattern of TBC1D1 was similar in skeletal muscle from WT and *Tbc1d4*-deficient mice, this indicates that TBC1D1 is not involved in mediating the insulin-sensitizing effect of prior contraction and AICAR stimulation in WT EDL muscle. Nevertheless, we cannot rule out a potential role of TBC1D1 because it may function to regulate muscle insulin sensitivity only in the presence of TBC1D4.

In conclusion, we show for the first time that the ability of AMPK to regulate muscle insulin sensitivity is dependent on TBC1D4 because *in situ* contraction and AICAR fail to increase insulin sensitivity in mouse EDL muscle lacking TBC1D4. Future studies will have to determine the involved mechanism of interplay between AMPK and TBC1D4, but we hypothesize that phospho-regulation of TBC1D4-Ser711 is important. Furthermore, because insulin-stimulated glucose uptake and phosphorylation of TBC1D4-Ser711 are also potentiated in human skeletal muscle after exercise (8,9), we hypothesize that an AMPK-TBC1D4 signaling axis is also regulating muscle insulin sensitivity in humans.

Acknowledgments. The authors thank Irene Bech Nielsen (Department of Nutrition, Exercise and Sports, Faculty of Science, University of Copenhagen) for her skilled technical assistance and also thank Dr. Laurie J. Goodyear (Joslin Diabetes Center and Harvard Medical School, Boston, MA) and Dr. D. Grahame Hardie (School of Life Sciences, University of Dundee, Dundee, Scotland, U.K.) for the donation of phospho-specific TBC1D4-Ser711 and AMPK α 2 antibody, respectively.

Funding. This work was supported by grants from the Danish Council for Independent Research – Medical Sciences (FSS8020-00288B) and the Novo Nordisk Foundation (NNF160C0023046), as well as funded in part by a grant from the Deutsche Forschungsgemeinschaft to A.C. (CH1659). This work was also supported by a research grant from the Danish Diabetes Academy, which is funded by the Novo Nordisk Foundation, grant number NNF17SA0031406.

Duality of Interest. No potential conflicts of interest relevant to this article were reported.

Author Contributions. R.K. conceived and designed the research, performed the experiments, analyzed the data, and drafted the manuscript. A.C., N.O.J., K.K., J.K.L., and C.d.W. performed the experiments. H.A.-H. provided founder mice for the study cohort. J.F.P.W. conceived and designed the research and contributed to drafting the manuscript. All authors interpreted the results, contributed to the discussion, edited and revised the manuscript, and read and approved the final version of the manuscript. J.F.P.W. is the guarantor of this work and, as such, had full access to all the data in the study and takes responsibility for the integrity of the data and the accuracy of the data analysis.

Prior Presentation. Parts of this study were presented in abstract form at the Danish Diabetes Academy Summer School on Diabetes & Metabolism, Ebberup, Denmark, 3–6 September 2018.

References

- DeFronzo RA, Tripathy D. Skeletal muscle insulin resistance is the primary defect in type 2 diabetes. *Diabetes Care* 2009;32(Suppl. 2):S157–S163
- Richter EA, Garetto LP, Goodman MN, Ruderman NB. Muscle glucose metabolism following exercise in the rat: increased sensitivity to insulin. *J Clin Invest* 1982;69:785–793
- Cartee GD, Young DA, Sleeper MD, Zierath J, Wallberg-Henriksson H, Holloszy JO. Prolonged increase in insulin-stimulated glucose transport in muscle after exercise. *Am J Physiol* 1989;256:E494–E499
- Castorena CM, Arias EB, Sharma N, Cartee GD. Postexercise improvement in insulin-stimulated glucose uptake occurs concomitant with greater AS160 phosphorylation in muscle from normal and insulin-resistant rats. *Diabetes* 2014;63:2297–2308
- Wojtaszewski JFP, Hansen BF, Kiens B, Richter EA. Insulin signaling in human skeletal muscle: time course and effect of exercise. *Diabetes* 1997;46:1775–1781
- Mikines KJ, Sonne B, Farrell PA, Tronier B, Galbo H. Effect of physical exercise on sensitivity and responsiveness to insulin in humans. *Am J Physiol* 1988;254:E248–E259
- Richter EA, Mikines KJ, Galbo H, Kiens B. Effect of exercise on insulin action in human skeletal muscle. *J Appl Physiol* (1985) 1989;66:876–885
- Pehmøller C, Brandt N, Birk JB, et al. Exercise alleviates lipid-induced insulin resistance in human skeletal muscle—signaling interaction at the level of TBC1 domain family member 4. *Diabetes* 2012;61:2743–2752
- Sjøberg KA, Frøsig C, Kjøbsted R, et al. Exercise increases human skeletal muscle insulin sensitivity via coordinated increases in microvascular perfusion and molecular signaling. *Diabetes* 2017;66:1501–1510
- Hansen PA, Nolte LA, Chen MM, Holloszy JO. Increased GLUT-4 translocation mediates enhanced insulin sensitivity of muscle glucose transport after exercise. *J Appl Physiol* (1985) 1998;85:1218–1222
- Wojtaszewski JF, Hansen BF, Gade, et al. Insulin signaling and insulin sensitivity after exercise in human skeletal muscle. *Diabetes* 2000;49:325–331
- Fisher JS, Gao J, Han D-H, Holloszy JO, Nolte LA. Activation of AMP kinase enhances sensitivity of muscle glucose transport to insulin. *Am J Physiol Endocrinol Metab* 2002;282:E18–E23
- Funai K, Schweitzer GG, Sharma N, Kanzaki M, Cartee GD. Increased AS160 phosphorylation, but not TBC1D1 phosphorylation, with increased postexercise insulin sensitivity in rat skeletal muscle. *Am J Physiol Endocrinol Metab* 2009;297:E242–E251
- Kjøbsted R, Treebak JT, Fentz J, et al. Prior AICAR stimulation increases insulin sensitivity in mouse skeletal muscle in an AMPK-dependent manner. *Diabetes* 2015;64:2042–2055
- Kjøbsted R, Munk-Hansen N, Birk JB, et al. Enhanced muscle insulin sensitivity after contraction/exercise is mediated by AMPK. *Diabetes* 2017;66:598–612
- Kramer HF, Witczak CA, Taylor EB, Fujii N, Hirshman MF, Goodyear LJ. AS160 regulates insulin- and contraction-stimulated glucose uptake in mouse skeletal muscle. *J Biol Chem* 2006;281:31478–31485
- Chen S, Wasserman DH, MacKintosh C, Sakamoto K. Mice with AS160/TBC1D4-Thr649Ala knockin mutation are glucose intolerant with reduced insulin sensitivity and altered GLUT4 trafficking. *Cell Metab* 2011;13:68–79
- Trebak JT, Taylor EB, Witczak CA, et al. Identification of a novel phosphorylation site on TBC1D4 regulated by AMP-activated protein kinase in skeletal muscle. *Am J Physiol Cell Physiol* 2010;298:C377–C385
- Arias EB, Kim J, Funai K, Cartee GD. Prior exercise increases phosphorylation of Akt substrate of 160 kDa (AS160) in rat skeletal muscle. *Am J Physiol Endocrinol Metab* 2007;292:E1191–E1200
- Trebak JT, Frøsig C, Pehmøller C, et al. Potential role of TBC1D4 in enhanced post-exercise insulin action in human skeletal muscle. *Diabetologia* 2009;52:891–900

21. Chadt A, Immisch A, de Wendt C, et al. Deletion of both Rab-GTPase-activating proteins TBC1D1 and TBC1D4 in mice eliminates insulin- and AICAR-stimulated glucose transport [corrected] [published correction appears in *Diabetes* 2015;64:1492]. *Diabetes* 2015;64:746–759
22. Fentz J, Kjøbsted R, Birk JB, et al. AMPK α is critical for enhancing skeletal muscle fatty acid utilization during in vivo exercise in mice. *FASEB J* 2015;29:1725–1738
23. Cokorinos EC, Delmore J, Reyes AR, et al. Activation of skeletal muscle AMPK promotes glucose disposal and glucose lowering in non-human primates and mice. *Cell Metab* 2017;25:1147–1159.e10
24. Zheng X, Cartee GD. Insulin-induced effects on the subcellular localization of AKT1, AKT2 and AS160 in rat skeletal muscle. *Sci Rep* 2016;6:39230
25. Arias EB, Wang H, Cartee GD. Akt substrate of 160 kDa dephosphorylation rate is reduced in insulin-stimulated rat skeletal muscle after acute exercise. *Physiol Res* 2018;67:143–147
26. Treebak JT, Birk JB, Hansen BF, Olsen GS, Wojtaszewski JFP. A-769662 activates AMPK beta1-containing complexes but induces glucose uptake through a PI3-kinase-dependent pathway in mouse skeletal muscle. *Am J Physiol Cell Physiol* 2009;297:C1041–C1052
27. Holloszy JO. Exercise-induced increase in muscle insulin sensitivity. *J Appl Physiol* (1985) 2005;99:338–343
28. Geiger PC, Han DH, Wright DC, Holloszy JO. How muscle insulin sensitivity is regulated: testing of a hypothesis. *Am J Physiol Endocrinol Metab* 2006;291:E1258–E1263
29. Corton JM, Gillespie JG, Hawley SA, Hardie DG. 5-aminoimidazole-4-carboxamide ribonucleoside. A specific method for activating AMP-activated protein kinase in intact cells? *Eur J Biochem* 1995;229:558–565
30. Merrill GF, Kurth EJ, Hardie DG, Winder WW. AICA riboside increases AMP-activated protein kinase, fatty acid oxidation, and glucose uptake in rat muscle. *Am J Physiol* 1997;273:E1107–E1112
31. Wasserman DH, Kang L, Ayala JE, Fueger PT, Lee-Young RS. The physiological regulation of glucose flux into muscle in vivo. *J Exp Biol* 2011;214:254–262
32. Pehmøller C, Treebak JT, Birk JB, et al. Genetic disruption of AMPK signaling abolishes both contraction- and insulin-stimulated TBC1D1 phosphorylation and 14-3-3 binding in mouse skeletal muscle. *Am J Physiol Endocrinol Metab* 2009;297:E665–E675
33. Vichaiwong K, Purohit S, An D, et al. Contraction regulates site-specific phosphorylation of TBC1D1 in skeletal muscle. *Biochem J* 2010;431:311–320
34. An D, Toyoda T, Taylor EB, et al. TBC1D1 regulates insulin- and contraction-induced glucose transport in mouse skeletal muscle. *Diabetes* 2010;59:1358–1365



The RabGAPs TBC1D1 and TBC1D4 Control Uptake of Long-Chain Fatty Acids Into Skeletal Muscle via Fatty Acid Transporter SLC27A4/FATP4

Tim Benninghoff,^{1,2} Lena Espelage,^{1,2} Samaneh Eickelschulte,^{1,2} Isabel Zeinert,¹ Isabelle Sinowenka,¹ Frank Müller,¹ Christina Schöndeling,¹ Hannah Batchelor,¹ Sandra Cames,^{1,2} Zhou Zhou,¹ Jörg Kotzka,^{1,2} Alexandra Chadt,^{1,2} and Hadi Al-Hasani^{1,2}

Diabetes 2020;69:2281–2293 | <https://doi.org/10.2337/db20-0180>

The two closely related RabGTPase-activating proteins (RabGAPs) TBC1D1 and TBC1D4 play a crucial role in the regulation of GLUT4 translocation in response to insulin and contraction in skeletal muscle. In mice, deficiency in one or both RabGAPs leads to reduced insulin- and contraction-stimulated glucose uptake and to elevated fatty acid (FA) uptake and oxidation in both glycolytic and oxidative muscle fibers without altering mitochondrial copy number and the abundance of proteins for oxidative phosphorylation. Here we present evidence for a novel mechanism of skeletal muscle lipid utilization involving the two RabGAPs and the FA transporter SLC27A4/FATP4. Both RabGAPs control the uptake of saturated and unsaturated long-chain FAs (LCFAs) into skeletal muscle and knockdown (Kd) of a subset of RabGAP substrates, *Rab8*, *Rab10*, or *Rab14*, decreased LCFA uptake into these cells. In skeletal muscle from *Tbc1d1* and *Tbc1d4* knockout animals, SLC27A4/FATP4 abundance was increased and depletion of SLC27A4/FATP4 but not FAT/CD36 completely abrogated the enhanced FA oxidation in RabGAP-deficient skeletal muscle and cultivated C2C12 myotubes. Collectively, our data demonstrate that RabGAP-mediated control of skeletal muscle lipid metabolism converges with glucose metabolism at the level of downstream RabGTPases and involves regulated transport of LCFAs via SLC27A4/FATP4.

As direct downstream effectors of both, AKT (protein kinase B) and AMP-dependent kinase AMPK, the two

RabGTPase-activating proteins (RabGAPs) TBC1D1 and TBC1D4 have been shown in previous studies to act as critical regulators of skeletal muscle glucose metabolism (1–5). RabGAPs accelerate the intrinsic GTP hydrolysis activity of Rab proteins, a large family of small GTPases that control a multiplicity of cellular vesicle trafficking and organelle translocation processes (6–8). In the past, several Rab proteins were described to be direct targets of the two RabGAPs and, in addition, to be associated to GLUT4 vesicles, namely Rab8a, Rab10, Rab14, and Rab28 (3,4,9–11). Rab8b, in addition, has been described as a direct downstream effector of TBC1D1, but its role in skeletal muscle substrate metabolism is not yet clear (4,12). Interestingly, both TBC1D1 and TBC1D4 have been implicated to play an important role in lipid metabolism as well. Deficiency in either *Tbc1d1* or *Tbc1d4* as well as the combined knockout of both RabGAPs in mice leads to enhanced in vivo lipid utilization, indicated by a lowered respiratory quotient (5,13). In fact, TBC1D-family GAPs reciprocally regulate glucose uptake and fatty acid oxidation (FAO) in skeletal muscle through independent signaling pathways and, at least in mice, this control is dependent on the muscle fiber composition (5). We have previously demonstrated that insulin- and AICAR-stimulated glucose uptake is normal in glycolytic extensor digitorum longus (EDL) muscle from *Tbc1d4*-deficient (D4KO) mice, whereas EDL muscles from *Tbc1d1*-deficient (D1KO) mice show impaired response toward these stimuli (5). In accordance, EDL muscle from D1KO but not D4KO mice

¹Institute for Clinical Biochemistry and Pathobiochemistry, German Diabetes Center, Leibniz Center for Diabetes Research at Heinrich Heine University Düsseldorf, Medical Faculty, Düsseldorf, Germany

²German Center for Diabetes Research, München-Neuherberg, Germany

Corresponding author: Alexandra Chadt, alexandra.chadt@ddz.de

Received 20 February 2020 and accepted 24 August 2020

This article contains supplementary material online at <https://doi.org/10.2337/figshare.12857771>.

© 2020 by the American Diabetes Association. Readers may use this article as long as the work is properly cited, the use is educational and not for profit, and the work is not altered. More information is available at <https://www.diabetesjournals.org/content/license>.

shows lower abundance of GLUT4, presumably resulting from missorting of the protein, and may, in part, explain the reduced glucose transport. At that point, it seems to be clear that insulin- and AMPK-signaling pathways converge at the level of the two RabGAPs and that TBC1D1 and TBC1D4 are required for sorting of GLUT4 in skeletal muscle with TBC1D1 representing the major signal transducer for glucose transport in glycolytic skeletal muscle and TBC1D4 in oxidative skeletal muscle and adipose tissue (1,5,14,15). Most importantly, basal FAO is equally elevated in EDL muscle from D1KO and D4KO mice, but only the former shows this increase also in the oxidative soleus (SOL) muscle (5). These data indicate that despite the fact that both RabGAPs contribute to the effect on FAO, this influence is not directly related to skeletal muscle glucose uptake, as D4KO mice demonstrate normal glucose uptake but increased FAO in EDL muscle. Importantly, these effects are strictly dependent on the functional GAP domain since no changes in lipid utilization were monitored in cultivated muscle cells overexpressing a non-functional R941K mutant of *Tbc1d1* (16).

Skeletal muscle FA uptake has been shown to be dependent on several distinct mechanisms including diffusion through the plasma membrane, as postulated for short-chain FAs (SCFAs), and complex transport systems specific for long-chain FAs (LCFAs) involving a variety of different membrane transporter and binding proteins (17,18). At least three different FA transporters have been described to control skeletal muscle LCFA uptake (19). The most extensively studied FA transporter is FAT/CD36, which exclusively binds LCFAs and has been implicated in lipid storage of different tissues and also pathophysiological impairments such as obesity and type 2 diabetes (20). Besides FAT/CD36, at least two more FA transporters, both members of the *SLC27* family of FA transport proteins (FATP), have been reported to be relevant in skeletal muscle lipid metabolism, FATP1 (*SLC27A1*) and FATP4 (*SLC27A4*) (21). In L6 rat muscle cells, *Tbc1d4* deficiency led to enhanced influx of FAs associated with an increase in FA translocase FAT/CD36 and FABPpm expression (22), and in mouse cardiomyocytes, knockdown (Kd) of *Tbc1d4* led to redistribution of FAT/CD36 to the cell surface (23). Of note, previous studies have provided evidence for the involvement of a regulated translocation mechanism for FA uptake facilitators (e.g., FAT/CD36, FATP1, and FATP4) (19,24–26) in analogy to the mechanism described for the uptake of glucose through GLUT4 in insulin-sensitive cells (27,28). However, there are no data available so far on the specificity of RabGAP-regulated lipid metabolism with regard to the FA species (17–19).

The aim of the current study was to characterize the molecular mechanisms that are responsible for the increased FA use upon inactivation of *Tbc1d1* or *Tbc1d4* in skeletal muscle cells and to determine the responsible downstream targets of the two RabGAPs.

RESEARCH DESIGN AND METHODS

Chemicals and Buffer

Chemicals and buffer ingredients are listed in Supplementary Table 1. Buffers and cell culture media are listed in Supplementary Table 2.

Experimental Animals

Mice were kept in accordance with the National Institutes of Health guidelines for the care and use of laboratory animals, and all experiments were approved by the ethics committee of the State Ministry of Agriculture, Nutrition and Forestry (Reference numbers 84–02.04.2013.A352 and 84–02.04.2017.A345, State of North Rhine-Westphalia, Germany). Unless indicated otherwise, three to six mice per cage were housed at 22°C and a 12-h light–dark cycle with ad libitum access to food and water. After weaning, animals received a standard chow diet (Ssniff, Soest, Germany). Male mice were used at the age of 12–25 weeks. Generation of D1KO and D4KO mice was described previously (5,16,29). Heterozygous *Cd36*-knockout (CD36KO) mice (30) were bred with either D1KO or D4KO mice and the F1 generation was intercrossed to generate homozygous double-deficient D1/CD36KO and D4/CD36KO mice. Isolation of genomic DNA from mouse tail tips was performed with the InViSorb Genomic DNA Kit II (Invitex, Berlin, Germany). Genotyping of mice was performed by PCR with primers for the *Tbc1d1* and *Tbc1d4* knockout as described (5). Genotyping of the *Cd36* knockout was conducted as described (30). Sequences of all genotyping primers are listed in Supplementary Table 3.

In Vivo Muscle Electroporation

The in vivo electroporation (IVE) protocol was adapted from previous reports (31–33). Briefly, mice were anesthetized using isoflurane, and their hind limbs were shaved. Then 30 μ L saline containing 15 units hyaluronidase (Sigma-Aldrich, Steinheim, Germany) were injected in the proximal and distal part of the front and the back of the shank to target EDL and SOL muscle. Following a 1-h recovery in their cages, the mice were anesthetized again with isoflurane and 4 μ g siRNA oligonucleotides specific for *Rab8a*, *Rab10*, or *Slc27a4/Fatp4*, respectively, in 30 mL sterile saline were injected into the same leg regions as before. *Slc27a4/Fatp4* siRNA oligonucleotides were mixed with InvivoFectamine 2.0 (Invitrogen, Carlsbad, CA) according to the manufacturer's instructions to a final concentration of 0.7 mg/mL. In each animal, one muscle was used as a control and therefore injected with non-target (NT) siRNA oligonucleotides. The siRNA injection was followed by the application of a pair of tweezer electrodes across the distal limb connected to an ECM-830 electroporator device (Square Wave Electroporation System ECM 830; BTX). Eight pulses (80 V, 20 ms, 1 Hz) were applied to each leg following recovery of the animals. Three (*Slc27a4/Fatp4*) or seven (Rab-GTPases) days after IVE

intervention, mice were subjected to *ex vivo* experiments. Only muscle samples with a minimum Rab protein reduction of 20% were considered for further statistical analysis.

Cell Culture

C2C12 myoblasts were grown to 80% confluence in DMEM (PAA Laboratories) supplemented with 10% FBS and 1% penicillin/streptomycin at 37°C and 5% CO₂. Myotube differentiation was induced by switching to DMEM containing 3% horse serum. Cells were used for assays when fully differentiated (usually 7 days). For Kd of *Tbc1d1*, *Tbc1d4*, the different RabGTPases or FA transporters, C2C12 cells were transfected with 50 nmol/L siRNA duplexes using DharmaFECT1 on day 3 of differentiation. Experiments were conducted at day 6 of differentiation. Sequences from siRNA oligonucleotides used are listed in Supplementary Table 4.

FA Uptake and Oxidation in C2C12 Myotubes

C2C12 myotubes (6 days after differentiation) were serum-starved for 2 h (DMEM [high glucose, 4.5 g/L] supplemented with 1% FA-free BSA) before adding Krebs-Ringer-HEPES buffer (see Supplementary Table 2), supplemented with 40 μmol/L FA-free BSA. To start the uptake assay, a Krebs-Ringer-HEPES-based buffer (radioactive "HOT" buffer) containing either 8.5 nmol/L ³H-palmitate, ³H-oleate, or ³H-butyrate (Supplementary Table 5), 2.5 μmol/L FA-free BSA and 5 μmol/L unlabeled palmitate, bound in a molar ratio of 2:1 to BSA, was added to each well for 5 min at 37°C/5% CO₂. Afterward, cells were placed on ice, HOT buffer was immediately aspirated, and each well was intensively washed three times with ice-cold washing buffer. Residual washing buffer was completely aspirated, and cells were lysed in protein lysis buffer (with protease and phosphatase inhibitor cocktail) and cleared protein lysates were prepared. A total of 50 μL of the lysates were used for liquid scintillation counting, the rest was used for protein measurement. Radioactivity was measured by scintillation counting and normalized to protein concentrations. [¹⁻¹⁴C]-palmitic acid oxidation assays were performed essentially as described (29,34). Briefly, C2C12 myotubes in 48-well plates were incubated with HOT oxidation buffer (11.8 μmol/L ¹⁴C-palmitate, 6.24 μmol/L FA-free BSA and 1 μmol/L L-carnitine in C2C12 differentiation medium) for 4 h at 37°C/5% CO₂. Then, supernatants were transferred to fresh 48-well plates, acidified with 1 mol/L HCl and incubated overnight with NaOH-soaked filter papers. The remaining cells were washed with PBS and analyzed for protein content. Trapped radioactivity was determined by scintillation counting and normalized to the amount of cellular protein.

Palmitate Oxidation in Intact Isolated Skeletal Muscles

Assays were done essentially as described (16). Briefly, EDL and SOL muscles were incubated in Krebs-Henseleit buffer containing 15 mmol/L mannitol, 5 mmol/L glucose, 3.5% FA-free BSA, 4 mCi/mL ³H-palmitate, and 300 mmol/L unlabeled palmitate at 30°C for 2 h. After absorption of

FAs to activated charcoal, FAO was determined by measuring tritiated water using a scintillation counter.

Sample Processing, SDS-PAGE, and Western Blotting

Protein lysates (10–30 μg) were separated by 8–12% SDS-PAGE and transferred onto nitrocellulose membranes by tank blotting (Amersham Protran 0.45 μm). Membranes were blocked for 1 h with 5% fat-free powdered milk in Tris-buffered saline with Tween (Supplementary Table 2), incubated with primary antibodies and secondary horseradish peroxidase-conjugated antibodies as described in Supplementary Table 6 and developed with enhanced chemiluminescence reagent (Perkin Elmer). For analysis of SLC27A4/FATP4 membrane localization, Kd of *Tbc1d1* was conducted in C2C12 myotubes as described above and subjected to a fractionation protocol modified from (35). Briefly, cells were dissolved in homogenization buffer A and centrifuged at 500g for 5 min at 4°C to remove cell debris. A fraction of the supernatant was stored for later determination of total SLC27A4/FATP4, the rest was subjected to an ultracentrifugation step (100,000g, 4°C, 30 min) to spin down membranes. Supernatants were discarded and crude membrane pellets were resuspended in homogenization buffer B. Buffer compositions are listed in Supplementary Table 2. Fractions A and B were analyzed via Western blot analysis as described above.

RNA Extraction, cDNA Synthesis, and Quantitative Real-time PCR

RNA was isolated using RNeasy Mini Kit and cDNA was synthesized using GoScript Reverse Transcriptase Kit (Promega) with 1 μg RNA and random hexanucleotide primers (Roche). For quantitative real-time PCR (qPCR), specific primers were used with the GoTaq quantitative PCR Master Mix on a StepOne Plus device (Applied Biosystems). Primer sequences are shown in Supplementary Table 7. Analysis was performed using the 2^{-ΔΔCt}-method (36) with *Tbp* (TATA-box binding protein) as reference gene. Quantification of *Tbc1d1* and *Tbc1d4* copy number was performed as described previously (29).

Lipid Profiling

Skeletal muscle total FA (TFA) content and specific fractional compositions of FAs were determined by gas chromatography (37). FA data were further used to calculate the Δ9-desaturase index (C16:1/C16:0 or C18:1/C18:0) and the Δ5-desaturase index (C18:2/C20:4) as well as the sums of TFA, nonsaturated FAs, monounsaturated FAs (MUFAs), saturated FAs (SFAs), essential FAs (C18:2 + C18:3) or nonessential FAs (C16:0 + C16:1 + C18:0 + C18:1) (38,39). Nomenclature used indicates C_x:y (x, number of carbons in the FA; y, number of double bonds in the FAs).

Statistical Analysis

All experiments were performed with at least *n* = 3 independent samples and are shown as mean values ± SEM.

Statistical significance ($P < 0.05$) was calculated with appropriate tests (unpaired or paired two-tailed Student t test and one- or two-way ANOVA) using GraphPad Prism 8 software as detailed in the respective figure legends.

Data and Resource Availability

The data and critical resources supporting their reported findings, methods, and conclusions are available from the corresponding author upon reasonable request.

RESULTS

TBC1D1 and TBC1D4 Regulate FA Influx Into Skeletal Muscle Cells and Specifically Control LCFA Metabolism

To investigate the mechanism of RabGAP-regulated FA utilization, we performed siRNA-mediated Kd of *Tbc1d1* and *Tbc1d4* in differentiated C2C12 myotubes and, subsequently, determined the uptake of the LCFAs ^3H -palmitate and ^3H -oleate or the SCFA ^3H -butyrate, respectively. The rationale behind this experiment was to determine the specificity for the uptake of distinct lipid species such as saturated versus unsaturated (palmitate, oleate) and LCFA versus SCFA in RabGAP-deficient muscle cells. To validate successful Kd of the two target genes, expression of *Tbc1d1* and *Tbc1d4* mRNA was determined via qPCR. Treatment of the cells with target-specific siRNA oligonucleotides reduced the mRNA expression of *Tbc1d1* or *Tbc1d4* by 70–85% (Fig. 1A and B). ^3H -palmitate uptake was increased in C2C12 myotubes after Kd of *Tbc1d1* and *Tbc1d4* compared with cells transfected with unspecific NT siRNA duplexes (Fig. 1A and B). Moreover, both *Tbc1d1* and *Tbc1d4* deficiency led to a significantly increased oxidation of ^{14}C -palmitate (Fig. 1C). Interestingly, Kd of *Tbc1d1* and *Tbc1d4* resulted in increased uptake of ^3H -oleate into the muscle cells as well (Fig. 1D). In contrast, uptake of ^3H -butyrate was unchanged in C2C12 myotubes following either *Tbc1d1* or *Tbc1d4* depletion (Fig. 1E). To assess the relative contribution of each of the two RabGAPs in skeletal muscle FA uptake and oxidation, we determined expression levels of *Tbc1d1* and *Tbc1d4* transcripts by measuring mRNA copy numbers via qPCR using a standard calibration curve as described (29). *Tbc1d1* gene expression increased during the course of differentiation, whereas *Tbc1d4* transcript levels were unchanged in differentiated C2C12 myotubes compared with the undifferentiated myoblasts (Fig. 1F).

Uptake and Oxidation of LCFAs in Skeletal Muscle Cells Is Dependent on Distinct RabGTPases Downstream of TBC1D1 and TBC1D4

We conducted Kd experiments of the previously reported RabGAP-target RabGTPases *Rab8a*, *Rab8b*, *Rab10*, *Rab14*, and *Rab28* in C2C12 myotubes and analyzed ^3H -palmitate uptake in these cells. Gene expression levels of the different *Rab* genes were reduced between 40 and 60% 4 days after transfection of target-specific siRNA oligonucleotides (Fig. 2A–E). Although ^3H -palmitate uptake was significantly reduced in C2C12 myotubes after Kd of *Rab8a*, *Rab8b*,

Rab10, *Rab14*, depletion of *Rab28* did not result in alterations of FA influx (Fig. 2A–E). Next, we conducted Kd of *Rab8a* and *Rab10* in skeletal muscle from C57BL/6J mice via IVE as described in the RESEARCH DESIGN AND METHODS section. The Kd efficiency was $\sim 35\%$ in the EDL and $\sim 41\%$ in the SOL muscle (Supplementary Fig. 1A). Seven days after transfection of siRNA, ^3H -palmitate oxidation was measured ex vivo in intact skeletal muscles. Interestingly, FAO was decreased by $\sim 24\%$ in the oxidative SOL muscle but not in the glycolytic EDL muscle following *Rab8a* silencing (Fig. 2F). *Rab10* Kd, however, did not lead to changes in ^3H -palmitate oxidation (Supplementary Fig. 1B). Gene expression levels of *Rab8a*, *Rab10*, and *Rab14* were not affected by either *Tbc1d1* or *Tbc1d4* Kd in C2C12 myotubes (Supplementary Fig. 1C and D).

FA Transporter SLC27A4/FATP4 but Not FAT/CD36 Is Elevated in *Tbc1d1*- and *Tbc1d4*-Deficient Skeletal Muscle

To further elucidate the function of the RabGAPs as a signaling hub between lipid and glucose metabolism in skeletal muscle, we determined gene expression as well as protein abundance of key enzymes of energy substrate flux in RabGAP-deficient skeletal muscle and cultured muscle cells (Supplementary Fig. 2). *Pdk4* mRNA and protein were increased in *Tbc1d1* Kd myotubes and tibialis anterior (TA) skeletal muscle from D1KO mice (Supplementary Fig. 2A) but not in EDL and SOL muscle from D1KO and D4KO animals (Fig. 3A–D). Also, proteins for oxidative phosphorylation (OXPHOS) in EDL and SOL muscle were not altered compared with wildtype (WT) controls (Supplementary Fig. 2D–G). The FA transporter FAT/CD36 has been shown to contribute to FA uptake in skeletal muscle (20). However, protein abundance of FAT/CD36 was not altered in either EDL or SOL muscle from D1KO and D4KO mice, respectively (Fig. 3A–D), or in *Tbc1d1* Kd myotubes and TA muscle from D1KO animals (Supplementary Figs. 2B and 3A). In contrast, protein abundance of the FA transporter SLC27A4/FATP4 was significantly increased in both EDL and SOL muscles from D1KO and D4KO mice compared with the WT littermate controls (Fig. 3A, B, G, and H). However, this difference did not reach significance level in TA muscle from D1KO animals or C2C12 myotubes following *Tbc1d1* Kd (Supplementary Figs. 2C and 3A).

FA Transporter 4 (SLC27A4/FATP4) but Not FAT/CD36 Contributes to Increased FA Uptake in RabGAP-Deficient Muscle Cells

To study the relation of *Cd36*, *Tbc1d1*, and *Tbc1d4*, we generated global *Cd36*-RabGAP double-deficient mice by crossbreeding CD36KO animals with either D1KO or D4KO animals, respectively, as described in the RESEARCH DESIGN AND METHODS section. Intact isolated skeletal muscles from 12- to 16-week-old male knockout mice and respective WT littermate controls were used to analyze FA uptake ex vivo. As illustrated in Fig. 4A, uptake of ^3H -palmitate

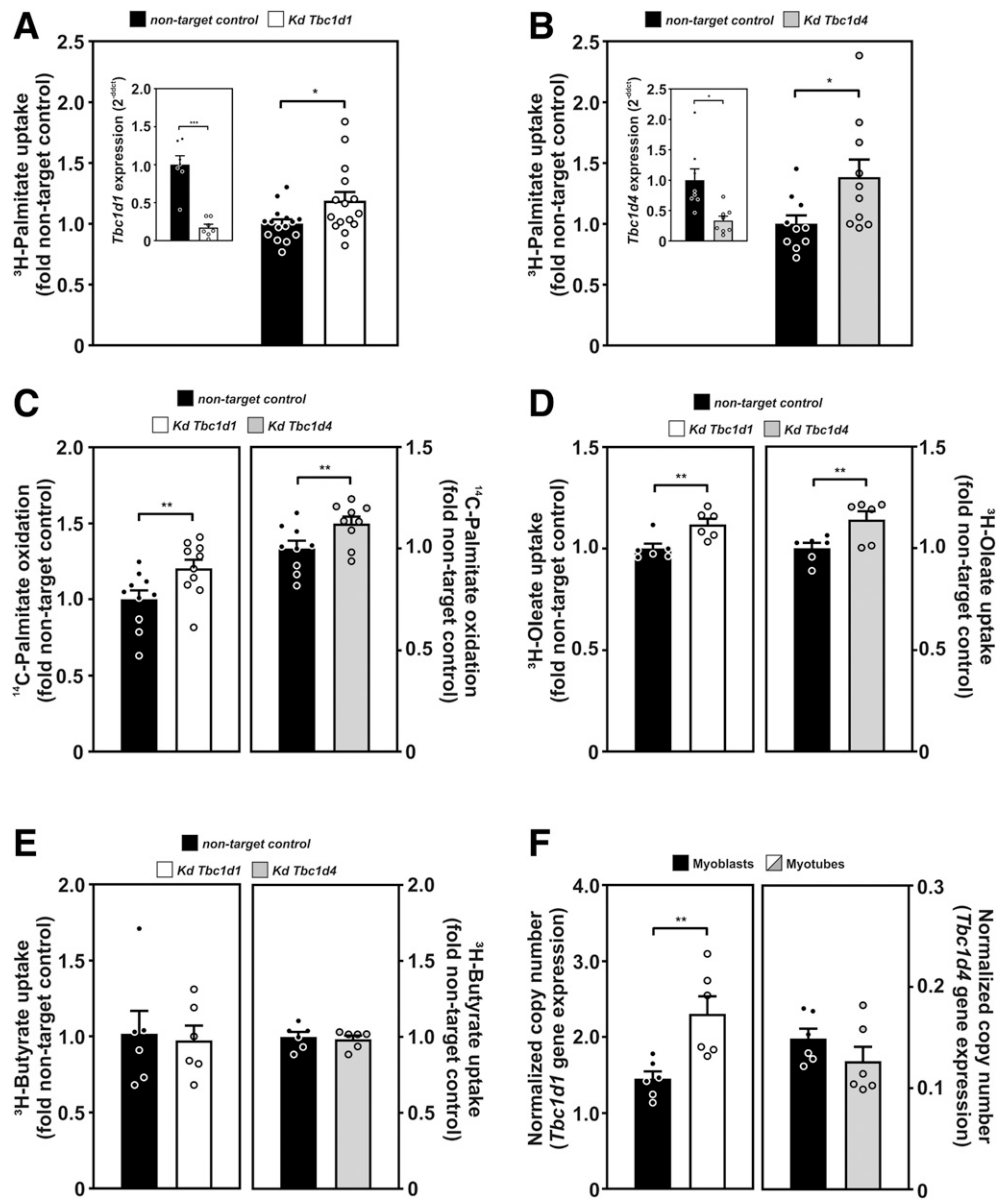


Figure 1—*Tbc1d1* and *Tbc1d4* deficiency increases LCFA uptake in vitro. Uptake of ³H-palmitate into C2C12 myotubes after siRNA-mediated *Tbc1d1* (A) and *Tbc1d4* (B) Kd, respectively. Kd efficiency for both RabGAPs can be seen in the interlaced graph of either A or B. Oxidation of ³H-palmitate after silencing of *Tbc1d1* and *Tbc1d4*, respectively (C). Uptake of ³H-Oleate (D) and ³H-Butyrate (E) after silencing of either *Tbc1d1* or *Tbc1d4*. Data are presented as mean ± SEM (n = 6–10). *P < 0.05, **P < 0.01, NT control vs. *Tbc1d1* siRNA or *Tbc1d4* siRNA kd (paired two-tailed Student *t* test). Normalized mRNA expression of *Tbc1d1* and *Tbc1d4* in C2C12 myoblasts and myotubes, respectively (F). ΔCt-values (with the geometric mean of *Tbp* and *Rplp0* as housekeeping genes) were measured by qPCR, corrected, and normalized using standard concentration curves (29). Data are presented as mean ± SEM (n = 6). **P < 0.01, myoblasts vs. myotubes (unpaired two-tailed Student *t* test).

was moderately reduced in EDL muscles from CD36KO animals, but substantially increased in D1KO or D4KO muscles, respectively. Importantly, the elevated FA uptake in muscles from D1KO mice was maintained or even further increased in muscles double-deficient in *Cd36* and *Tbc1d1* (D1/CD36KO). Similarly, *Tbc1d4* knockout increased FA uptake in *Cd36*-deficient muscles (D4/CD36KO). Interestingly, D1/CD36KO muscles showed higher FA uptake than D4/CD36KO muscles (Fig. 4A).

To investigate the contribution of SLC27A4/FATP4 in the elevated FA uptake in RabGAP-deficient muscle cells, we conducted Kd experiments in C2C12 myotubes and measured ³H-palmitate uptake following depletion of *Slc27a4/Fatp4* and *Cd36*, respectively, as well as combined Kd of *Slc27a4/Fatp4* plus *Tbc1d1* or *Tbc1d4* (Kd efficiency shown in Supplementary Fig. 3B). In C2C12 myotubes, Kd of *Slc27a4/Fatp4* resulted in a moderate reduction in ³H-palmitate uptake that did not reach statistical significance

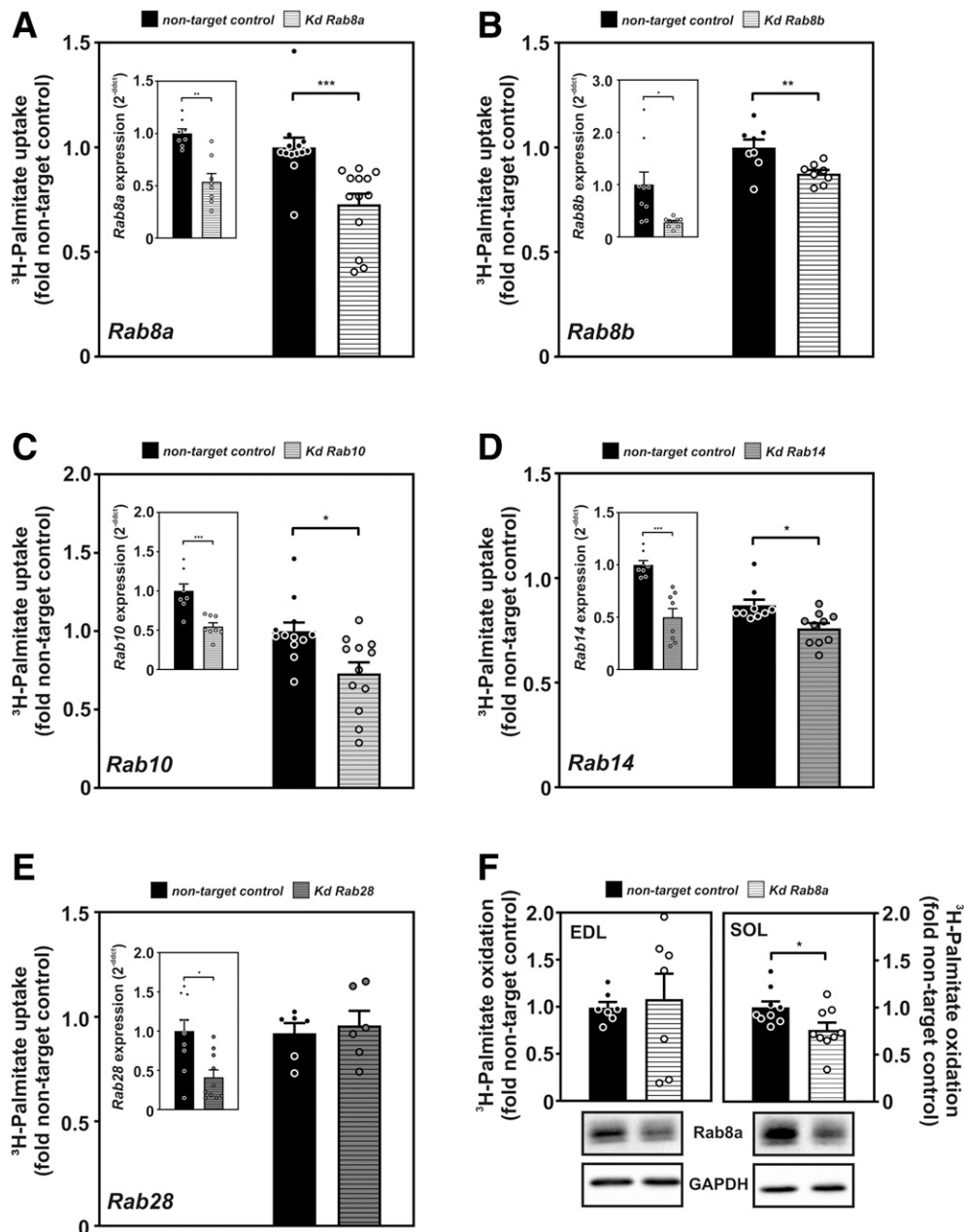


Figure 2—Downstream targets of TBC1D1 and TBC1D4 critically regulate FA uptake and oxidation in vitro and ex vivo. Uptake of ^3H -palmitate into C2C12 myotubes after siRNA-mediated Kd of *Rab8a* (A), *Rab8b* (B), *Rab10* (C), *Rab14* (D), and *Rab28* (E). Kd efficiency for all five *Rab* genes can be seen in the interlaced graph of either A–E. Ex vivo ^3H -palmitate oxidation of EDL and SOL skeletal muscles (F) after in vivo electrotransfection-mediated Kd of *Rab8a*. Data are presented as mean \pm SEM ($n = 7$ –13). * $P < 0.05$, ** $P < 0.01$, *** $P < 0.001$, NT control vs. respective *Rab* siRNA Kd (paired two-tailed Student t test).

(Fig. 4B), whereas *Cd36* depletion had no effect on FA uptake (Supplementary Fig. 3C). Conversely, Kd of *Tbc1d1* or *Tbc1d4* resulted in a substantial increase in FA uptake compared with control cells. Combined Kd of *Slc27a4/Fatp4* and each of the RabGAPs completely abrogated the increase in FA transport observed in either *Tbc1d1* or *Tbc1d4* Kd cells (Fig. 4B). Kd of *Slc27a4/Fatp4* did not lead to changes in *Cd36* gene expression and vice versa (Supplementary Fig. 3D).

To further investigate the potential mechanism of RabGAP-regulated FA transport, we conducted siRNA-mediated Kd experiments of *Tbc1d1* in C2C12 myotubes and measured plasma membrane and total SLC27A4/FATP4 abundance via Western blot analysis. Interestingly, membrane SLC27A4/FATP4 localization was increased upon *Tbc1d1*-deficiency compared with NT control cells (Fig. 4C). In accordance to our previous results (5), ex vivo FAO was enhanced in EDL muscle from D1KO and D4KO and SOL muscle from D1KO

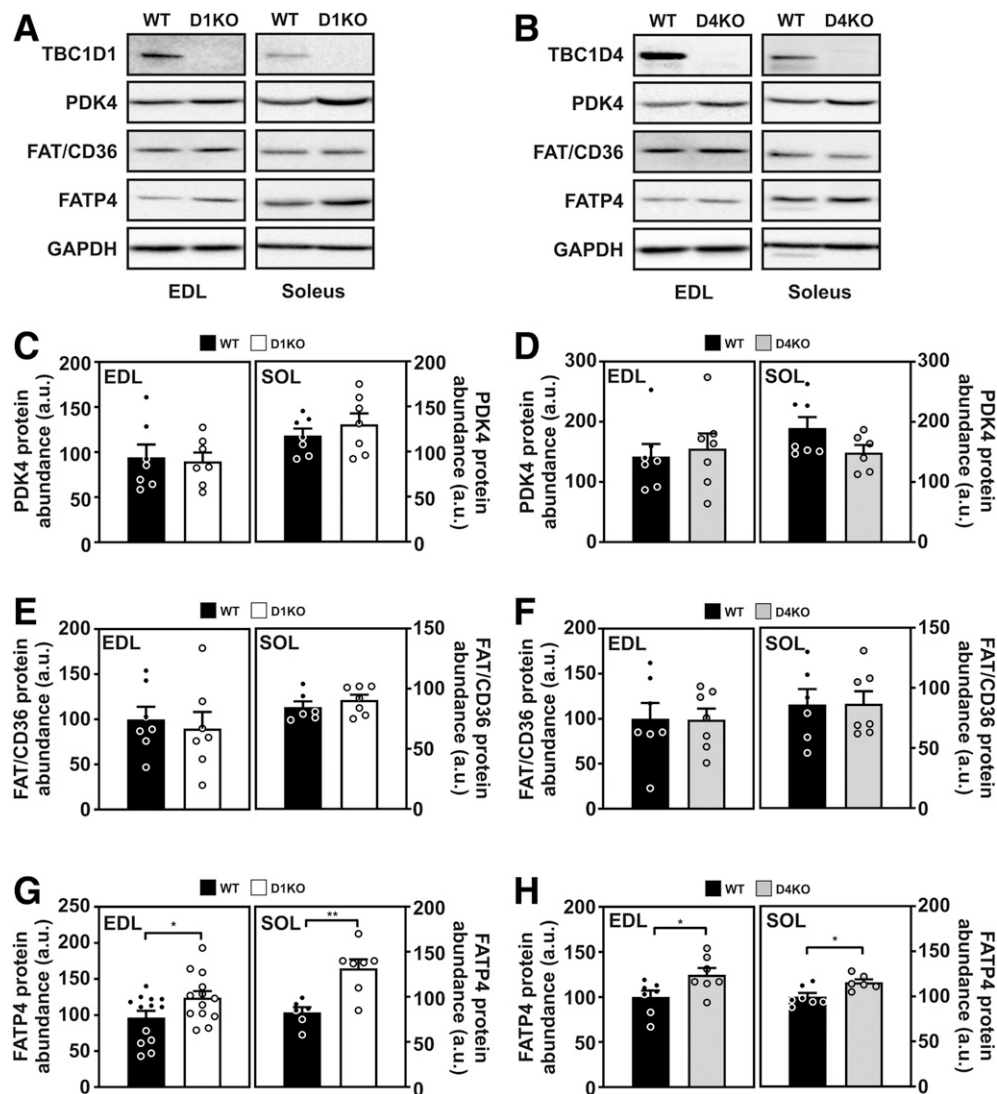


Figure 3—*Tbc1d1* and *Tbc1d4* deficiency leads to increased SLC27A4/FATP4 but not to PDK4 or FAT/CD36 protein abundance in EDL and SOL skeletal muscles. Representative Western blot membranes from D1KO (A) and D4KO (B) skeletal muscles after analysis of TBC1D1, TBC1D4, PDK4, FAT/CD36, and FATP4. Quantification of protein abundance for PDK4 (C and D), FAT/CD36 (E and F), and FATP4 (G and H) in EDL and SOL muscles from D1KO and D4KO animals, respectively. Data are presented as mean \pm SEM ($n = 6$ –13). * $P < 0.05$, ** $P < 0.01$, WT vs. RabGAP-KO (unpaired two-tailed Student t test).

mice, respectively, following IVE of NT siRNA oligonucleotides. Most notable, Kd of *Slc27a4/Fatp4* via IVE technology abolished the elevated rate of FAO in EDL and SOL muscle of D1KO and D4KO, respectively (Fig. 4D–F).

***Tbc1d1*-Deficiency Leads to a Redistribution of FA Species in Skeletal Muscle**

Next, we investigated distribution of different lipid species in skeletal muscle from D1KO mice. Despite the fact that the overall gene expression profile of cultured muscle cells or skeletal muscle after TBC1D1 depletion did not show marked changes (Supplementary Fig. 4A and C), we speculated that the proportions of cellular lipid species might be altered due to the enhanced FA uptake and oxidation in

D1KO skeletal muscle. Total amount of FAs showed a trend to increase in gastrocnemius muscle of D1KO (Fig. 5A) with changes in the composition of different FA species. In skeletal muscle from D1KO mice, the amount of SFA was reduced (Fig. 5B and E), MUFA content was increased (Fig. 5C and E), and no change in polyunsaturated FA levels were observed (Fig. 5D and E). A more detailed analysis of the individual percent of distinct FA species within the muscle revealed that the amount of four distinct FA species was different between the two genotypes. Skeletal muscle from D1KO mice showed lower amounts of saturated palmitic acid (C16:0) and polyunsaturated arachidonic acid (C20:4). In contrast, levels of monounsaturated palmitoleic acid (C16:1) and oleic acid (C18:1) were significantly increased in gastrocnemius muscle samples from D1KO

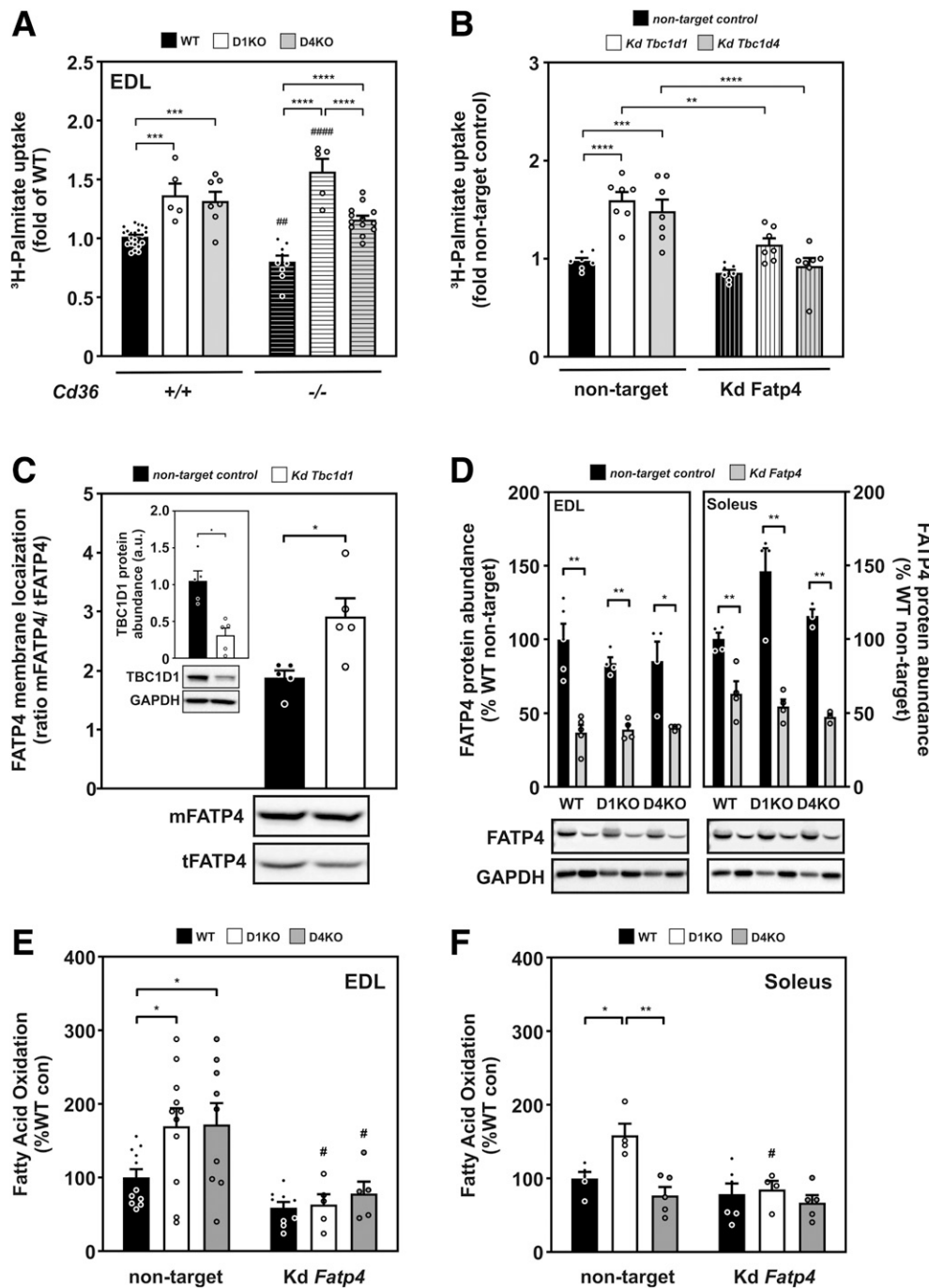


Figure 4—FA transporter FATP4 but not FAT/CD36 is specifically regulating RabGAP-dependent FA uptake into skeletal muscle. Ex vivo ^3H -palmitate uptake in mouse EDL muscles from WT, D1KO, D4KO, CD36KO, *Tbc1d1/Cd36* (D1CD36KO), and *Tbc1d4/Cd36* double-deficient (D4CD36KO) animals (A). Data are presented as mean \pm SEM ($n = 5$ –22). *** $P < 0.001$, **** $P < 0.0001$ between RabGAP genotypes; ## $P < 0.01$, #### $P < 0.0001$ compared with the WT control (two-way ANOVA with Tukey post hoc test). In vitro ^3H -palmitate uptake into C2C12 myotubes after silencing of *Slc27a4* (FATP4), *Tbc1d1*, *Tbc1d4*, or combined siRNA-mediated Kd of *Tbc1d1* and *Slc27a4/Fatp4*, or *Tbc1d4* and *Slc27a4/Fatp4*, respectively (B). Data presented as mean \pm SEM ($n = 7$). ** $P < 0.01$, *** $P < 0.001$, **** $P < 0.0001$ between indicated groups (two-way ANOVA with Tukey post hoc test). FATP4 membrane localization following Kd of *Tbc1d1* in C2C12 myotubes using siRNA-technology (C). *Tbc1d1* Kd efficiency can be seen in the interlaced graph of the panel figure, depicted as protein abundance measured by Western blot analysis. FATP4 membrane localization was calculated as ratio between membrane FATP4 (mFATP4) and total FATP4 (tFATP4), both determined by Western blot analysis. Data are presented as mean \pm SEM ($n = 5$). * $P < 0.05$, NT control vs. *Tbc1d1* kd (paired two-tailed Student *t* test). FATP4 protein abundance following Kd of *Slc27a4/Fatp4* in EDL and SOL muscles from D1KO and D4KO animals and respective WT controls using siRNA and IVE (D). *Slc27a4/Fatp4* Kd efficiency was determined by Western blot analysis. Data are presented as mean \pm SEM ($n = 3$ –5). * $P < 0.05$, ** $P < 0.01$ NT control vs. *Tbc1d1* kd (paired two-tailed Student *t* test). Ex vivo oxidation of ^3H -palmitate after silencing of *Slc27a4/Fatp4* in EDL (E) and SOL (F) muscles from D1KO and D4KO animals, respectively, via IVE technology. Data are presented as mean \pm SEM ($n = 5$ –11). * $P < 0.05$, ** $P < 0.01$ between indicated genotypes; # $P < 0.05$ NT control vs. *Slc27a4/Fatp4* Kd (mixed model two-way ANOVA with repeated measures analysis for the Kd condition and Tukey post hoc test). Kd conditions were treated as pairs in the analysis due to the experimental design (one leg transfected with NT, the second leg transfected with Kd siRNA oligonucleotides), whereas comparisons between genotypes were treated as independent parameters.

animals (Fig. 5F). Deduced from the measured values for each FA, enzyme activity of stearoyl-CoA desaturase-1, an enzyme that catalyzes the conversion of C16:0 and C18:0 SFAs into the MUFAs palmitoleic acid (C16:1) (Fig. 5G) and oleic acid (C18:1) (Fig. 5H) was increased in D1KO skeletal muscle. In contrast, activity of Δ^5 -desaturase, calculated as the ratio of arachidonic acid (C20:4) and α -Linoleic acid

(C18:3) was significantly decreased in gastrocnemius muscle from D1KO mice (Fig. 5I).

DISCUSSION

In the current study, we investigated the contribution of the RabGAPs TBC1D1 and TBC1D4 to FA uptake and oxidation in skeletal muscle. Our results demonstrate

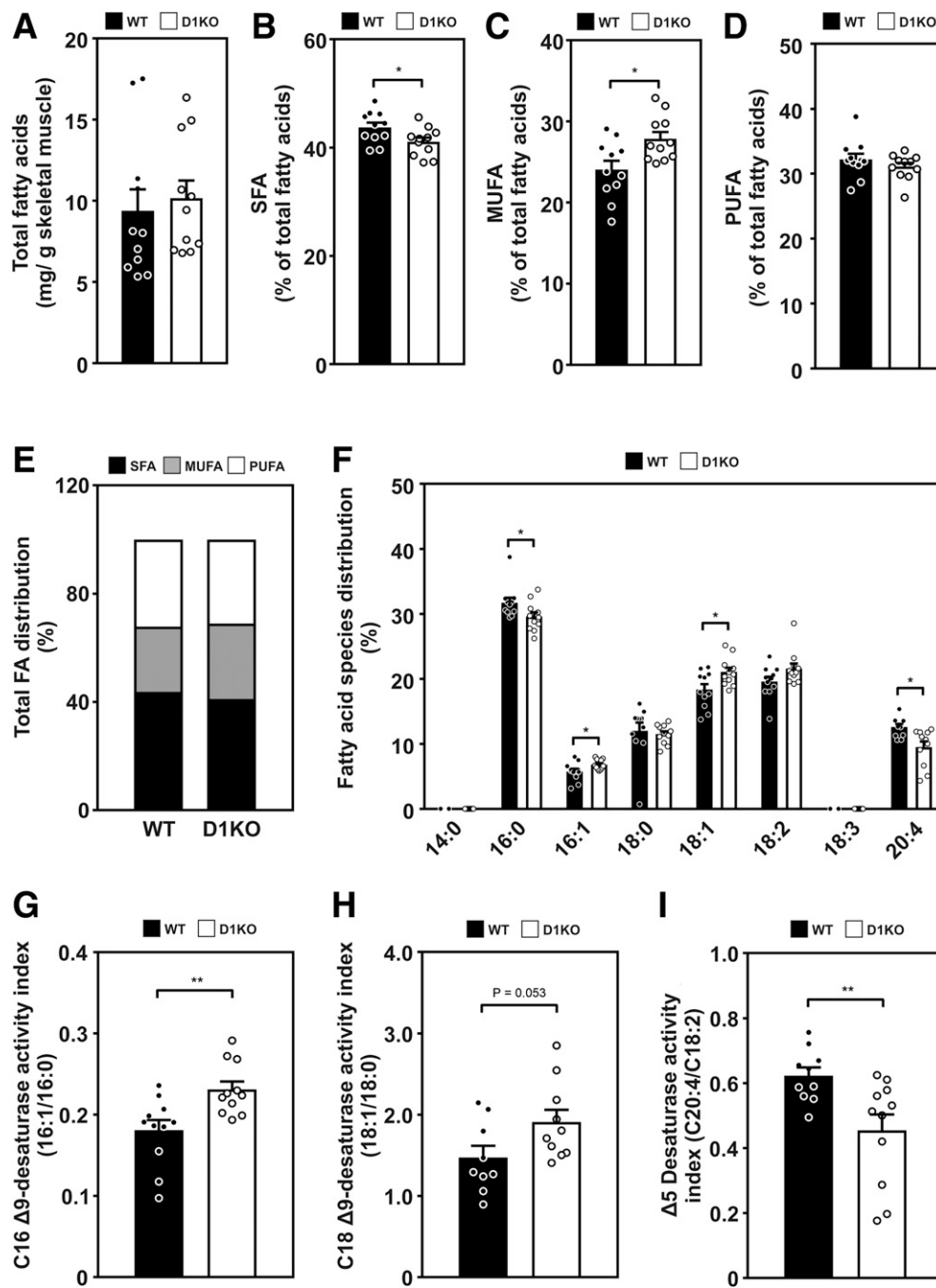


Figure 5—FA profile in gastrocnemius skeletal muscle from WT vs. D1KO mice differs with regard to the FA saturation grade. Amount of TFAs (A). Percentage of SFAs (B), MUFAs (C), and polyunsaturated FAs (PUFAs) (D) of TFA content. The results are summarized as contribution of each class to TFA content (E). Total evaluated FA profile as percentage of TFAs measured (F). Calculated C16 Δ^9 -desaturase activity index (16:1/16:0) (G), C18 Δ^9 -desaturase activity index (18:1/18:0) (H), and Δ^5 -desaturase activity index (C20:4/C18:2) (I). Data presented as mean \pm SEM ($n = 9$ –11). * $P < 0.05$, ** $P < 0.01$, WT vs. D1KO gastrocnemius skeletal muscle samples (unpaired two-tailed Student t test).

that both RabGAPs regulate entry of LCFAs through a RabGTPase-dependent pathway that involves the LCFA transport protein 4 (SLC27A4/FATP4).

Previous studies showed that ablation of either *Tbc1d1*, *Tbc1d4*, or both RabGAPs in skeletal muscle results in greatly reduced insulin-stimulated glucose uptake due to compromised trafficking of the GLUT4 transporter (1,5,13–16,40,41). Moreover, we and others reported that RabGAP-deficiency also results in increased uptake and oxidation of palmitic acid in skeletal muscle and cultured muscle cells (16,42). Because overexpression of intact *Tbc1d1*, but not a GAP-inactive R941K mutant, decreased palmitate uptake and oxidation in both isolated skeletal muscle and cultured muscle cells (16,43), we speculated that the two RabGAPs may regulate uptake of glucose and FAs through distinct Rab-dependent pathways.

Neither the abundance of proteins involved in mitochondrial OXPHOS, nor mitochondrial copy number or citrate synthase activity was altered in *Tbc1d1*-deficient skeletal muscle (40). Electroporation-mediated overexpression of *Tbc1d1* was reported to reduce FAO and β -hydroxyacyl-CoA dehydrogenase activity, a key enzyme of mitochondrial β -oxidation (43) whereas β -hydroxyacyl-CoA dehydrogenase activity was unaltered in skeletal muscle from *Tbc1d1* knockout rats that displayed increased in vivo and ex vivo skeletal muscle fat oxidation (42). In this study, mitochondrial OXPHOS proteins were not altered in EDL and SOL muscle of D1KO and D4KO mice, and consistent differences in key enzymes for energy metabolism, such as PDK4 were not observed in the muscles, presumably reflecting the complexity of energy metabolism in different muscle types and fibers (44,45). An increased influx of LCFAs may therefore not be driven by increased mitochondrial activity but rather result from elevated activity or abundance of FA transporters or other nonmitochondrial metabolizing enzymes (46). In accordance with previous studies in skeletal muscle (16,42), we show here that Kd of both *Tbc1d1* or *Tbc1d4* specifically increases uptake of both saturated and unsaturated LCFAs, whereas uptake of SCFAs into skeletal muscle cells remains unaltered. This indicates that RabGAP-deficiency increases FA transport via specialized LCFA transporter enzymes rather than activating passive diffusion through the plasma membrane, which has been proposed to be the predominant mechanism for SCFA uptake (19,20,47).

Several RabGTPases have been implicated to play roles in the translocation of GLUT4 including Rab4, Rab8a, Rab8b, Rab10, Rab11, Rab13, and Rab14 (48,49). Here, we show that Kd of *Rab8a*, *Rab8b*, *Rab10*, and *Rab14* decreases palmitate uptake in both basal and insulin-stimulated muscle cells (Supplementary Fig. 4B), whereas depletion of *Rab28*, which is also a substrate for TBC1D1 and TBC1D4 (3), has no effect (Fig. 2E). These data suggest that FA uptake utilizes a specific subset of RabGTPases downstream of TBC1D1 and TBC1D4, which partially overlaps with the substrate specificity of the RabGAPs in vitro (3). More specifically, Rab8a may represent the major RabGAP substrate mediating FAO as Kd of *Rab8a* but not *Rab10* in intact isolated skeletal muscle via IVE

technology led to a decrease of ^3H -palmitate oxidation (Fig. 2F and Supplementary Fig. 1B). A reduction in FAO was detected following *Rab8a* Kd in intact SOL but not EDL muscle, indicating a more complex relationship between RabGAP-RabGTPase interaction and different types of skeletal muscle fibers. Divergent mechanisms of lipid accumulation and mitochondrial function have already been described for oxidative/slow-twitch and glycolytic/fast-twitch muscle fibers (50,51). Further studies are required to investigate the specific contribution of individual RabGTPases to FA uptake and metabolism in muscle cells.

Our findings indicate a possible involvement of LCFA-specific metabolizing enzymes and/or transporters expressed in skeletal muscle including FA translocase FAT/CD36 and FA transporters of the FATP protein family (25,52). FAT/CD36 has been implicated in FA uptake in skeletal muscle and the heart (30,53). In analogy to the insulin-regulated GLUT4, FAT/CD36 was found to undergo recruitment from intracellular pools to the plasma membrane in response to insulin and contraction (24,54,55). Consistent with a possible role of RabGAPs in the regulation of FAT/CD36 traffic and subcellular localization, Kd of *Tbc1d4* as well as overexpression of constitutively active *Rab8a*, *Rab10*, and *Rab14* led to a redistribution of FAT/CD36-associated immunofluorescence to the plasma membrane in cardiomyocytes (23). In previous studies, RabGAPs were also related to the expression levels of *Cd36*. Mikłosz et al. (22,56) found in rat L6 myotubes that *Tbc1d4* silencing increased the expression levels of *Cd36*, whereas transient overexpression of *Tbc1d1* in mouse skeletal muscle led to reduced palmitate oxidation without altering FAT/CD36 protein abundance (43). *Tbc1d1*-deficient TA muscles from our knockout mice did not display increased mRNA and protein levels of FAT/CD36, although there was a trend toward increased levels of expression. For further in-depth analysis of a possible function of FAT/CD36 in RabGAP deficiency, we followed a genetic approach by generating *Cd36*/RabGAP double-deficient mice (D1/CD36KO; D4/CD36KO) and analyzing FA uptake into intact isolated skeletal muscle. As expected, skeletal muscle from CD36KO mice displayed reduced uptake of palmitate compared with WT littermates as reported previously (30). However, muscles from D1/CD36KO and D4/CD36KO double knockout animals showed similarly elevated FA uptake as compared with the single RabGAP knockout muscles with an intact *Cd36* gene. These findings rule out a major contribution of FAT/CD36 in the observed elevated FA uptake in response to RabGAP-deficiency in mouse skeletal muscle. In addition to FAT/CD36, the FA transport protein SLC27A4/FATP4 has been reported to catalyze uptake of LCFAs into skeletal muscle where its intrinsic acyl-CoA activity may contribute to its transport activity (57). Similar to FAT/CD36, plasma membrane SLC27A4/FATP4 was found to be increased in response to stimuli such as insulin and contraction in skeletal muscle (54). EDL and SOL skeletal muscle from both D1KO and D4KO mice displayed an increase in SLC27A4/FATP4 protein, indicating that this transporter might contribute at least in part to the elevated FAO in RabGAP-deficient skeletal muscle.

However, a contribution of this FA transporter in the elevated fat utilization of the animals may not be strictly dependent on protein amount alone but involve intracellular trafficking and translocation processes. As FATP4-null mice display neonatal lethality (58,59), crossbreeding and generation of FATP4/RabGAP double-deficient mice was not possible. Therefore, we first analyzed palmitate uptake in cultured muscle cells after Kd of the FATP4 gene *Slc27a4* and each of the two RabGAPs, revealing that the increase in palmitate uptake in RabGAP-deficiency is strictly dependent on the presence of SLC27A4/FATP4 in these cells. Likewise, Kd of *Slc27a4/FATP4* completely abrogated the elevated FAO in intact isolated EDL and SOL muscle from D1KO and D4KO mice. Interestingly, Kd of *Tbc1d1* or *Tbc1d4* was associated with an enrichment of *Slc27a4/FATP4* protein in the plasma membrane, indicating that RabGAPs may regulate both abundance and subcellular localization of the protein. However, further studies are required to elucidate the precise molecular mechanism of RabGAP-dependent regulation of FA transport.

Global *Tbc1d1* deficiency in mice is associated with a moderate increase in MUFA and a concomitant decrease of SFAs in skeletal muscle. As MUFA content of muscle lipids is increased with insulin resistance and obesity and has been shown to correlate with $\Delta 9$ -desaturase activity in human muscle cells, it appears that RabGAPs may contribute to systemic insulin sensitivity through alterations in lipid composition (60). A recent study in L6 myotubes showed that Kd of *Tbc1d4* also led to alterations in the ratio of SFA and MUFA (56). Interestingly, indigenous people of Greenland frequently carry a loss-of-function mutation in the related *TBC1D4* gene, which may reflect a genetic adaptation to the traditional hypoglycemic, fat-rich diet of the Inuits (61,62). However, the alterations in the FA profile of gastrocnemius muscle from D1KO mice were rather minor, which might be due to the diet and age of the mice, as well as the skeletal muscle type analyzed. Further studies are required to investigate alteration in metabolic fluxes of RabGAP-deficient muscle tissue.

Collectively, our data demonstrate that both TBC1D1 and TBC1D4 specifically control entry of LCFAs into skeletal muscle through a mechanism that requires a subset of RabGTPases involved also in GLUT4 translocation. FA transporter SLC27A4/FATP4 is a likely candidate mediating RabGAP-dependent lipid uptake, resulting in an altered lipid composition. A possible regulatory pathway of RabGAP-dependent SLC27A4/FATP4 trafficking within the muscle cell can be hypothesized, the exact mechanisms, however, remain to be determined. Unraveling the mechanisms underlying RabGAP-dependent lipid flux in skeletal muscle is an important step toward the understanding of skeletal muscle adaptations during the pathophysiology of insulin resistance and type 2 diabetes.

Acknowledgments. The authors thank Angelika Horrigs, Anette Kurowski, Heidrun Podini, Carina Heitmann, Dagmar Gröttner, Antonia Osmer, Annette Schöber, Lothar Bohne, Martina Schiller, Jennifer Schwettmann, and Denise Schauer (all from

German Diabetes Center, Leibniz Center for Diabetes Research at Heinrich Heine University Düsseldorf) for expert technical assistance. The authors also thank Dr. Maria Febbraio (Cleveland Clinic, Cleveland, OH) for generously providing the Cd36 knockout mice.

Funding. This work was supported by the German Center for Diabetes Research (DZD) (82DZD00202 to H.A.-H.) of the Federal Ministry for Education and Research and the Ministry of Science and Research of the State North Rhine-Westphalia and was funded, in part, by grants from the Deutsche Forschungsgemeinschaft (CH1659/1-1 to A.C.), and the European Foundation for the Study of Diabetes (EFS)/Novo Nordisk program (to H.A.-H.).

Duality of Interest. No potential conflicts of interest relevant to this article were reported.

Author Contributions. T.B., A.C., and H.A.-H. wrote the manuscript and analyzed and interpreted the data. T.B., L.E., S.E., I.Z., I.S., F.M., C.S., H.B., S.C., Z.Z., and J.K. performed the experiments and analyzed data. A.C. and H.A.-H. were involved in the study design and contributed to data interpretation. A.C. is the guarantor of this work and, as such, had full access to all of the data in the study and takes responsibility for the integrity of the data and the accuracy of the data analysis.

References

- Hargrett SR, Walker NN, Keller SR. Rab GAPs AS160 and Tbc1d1 play nonredundant roles in the regulation of glucose and energy homeostasis in mice. *Am J Physiol Endocrinol Metab* 2016;310:E276–E288
- Mafakheri S, Chadt A, Al-Hasani H. Regulation of RabGAPs involved in insulin action. *Biochem Soc Trans* 2018;46:683–690
- Zhou Z, Menzel F, Benninghoff T, et al. Rab28 is a TBC1D1/TBC1D4 substrate involved in GLUT4 trafficking. *FEBS Lett* 2017;591:88–96
- Roach WG, Chavez JA, Miinea CP, Lienhard GE. Substrate specificity and effect on GLUT4 translocation of the Rab GTPase-activating protein Tbc1d1. *Biochem J* 2007;403:353–358
- Chadt A, Immisch A, de Wendt C, et al. Deletion of both Rab-GTPase-activating proteins TBC1D1 and TBC1D4 in mice eliminates insulin- and AICAR-stimulated glucose transport [published correction appears in *Diabetes* 2014;64:746–759]. *Diabetes* 2015;64:746–759
- Eathiraj S, Pan X, Ritacco C, Lambright DG. Structural basis of family-wide Rab GTPase recognition by rabenosyn-5. *Nature* 2005;436:415–419
- Novick P. Regulation of membrane traffic by Rab GEF and GAP cascades. *Small GTPases* 2016;7:252–256
- Stenmark H. Rab GTPases as coordinators of vesicle traffic. *Nat Rev Mol Cell Biol* 2009;10:513–525
- Miinea CP, Sano H, Kane S, et al. AS160, the Akt substrate regulating GLUT4 translocation, has a functional Rab GTPase-activating protein domain. *Biochem J* 2005;391:87–93
- Görgens SW, Benninghoff T, Eckardt K, et al. Hypoxia in combination with muscle contraction improves insulin action and glucose metabolism in human skeletal muscle via the HIF-1 α pathway. *Diabetes* 2017;66:2800–2807
- Mafakheri S, Flörke RR, Kanngießer S, et al. AKT and AMP-activated protein kinase regulate TBC1D1 through phosphorylation and its interaction with the cytosolic tail of insulin-regulated aminopeptidase IRAP. *J Biol Chem* 2018;293:17853–17862
- Ishikura S, Klip A. Muscle cells engage Rab8A and myosin Vb in insulin-dependent GLUT4 translocation. *Am J Physiol Cell Physiol* 2008;295:C1016–C1025
- Hargrett SR, Walker NN, Hussain SS, Hoehn KL, Keller SR. Deletion of the Rab GAP Tbc1d1 modifies glucose, lipid, and energy homeostasis in mice. *Am J Physiol Endocrinol Metab* 2015;309:E233–E245
- Lansley MN, Walker NN, Hargrett SR, Stevens JR, Keller SR. Deletion of Rab GAP AS160 modifies glucose uptake and GLUT4 translocation in primary skeletal muscles and adipocytes and impairs glucose homeostasis. *Am J Physiol Endocrinol Metab* 2012;303:E1273–E1286
- Wang HY, Ducommun S, Quan C, et al. AS160 deficiency causes whole-body insulin resistance via composite effects in multiple tissues. *Biochem J* 2013;449:479–489

16. Chadt A, Leicht K, Deshmukh A, et al. Tbc1d1 mutation in lean mouse strain confers leanness and protects from diet-induced obesity. *Nat Genet* 2008;40:1354–1359
17. Charney AN, Micic L, Egnor RW. Nonionic diffusion of short-chain fatty acids across rat colon. *Am J Physiol* 1998;274:G518–G524
18. Kamp F, Hamilton JA. How fatty acids of different chain length enter and leave cells by free diffusion. *Prostaglandins Leukot Essent Fatty Acids* 2006;75:149–159
19. Schwenk RW, Holloway GP, Luiken JJ, Bonen A, Glatz JF. Fatty acid transport across the cell membrane: regulation by fatty acid transporters. *Prostaglandins Leukot Essent Fatty Acids* 2010;82:149–154
20. Glatz JFC, Luiken JJFP. Dynamic role of the transmembrane glycoprotein CD36 (SR-B2) in cellular fatty acid uptake and utilization. *J Lipid Res* 2018;59:1084–1093
21. Anderson CM, Stahl A. SLC27 fatty acid transport proteins. *Mol Aspects Med* 2013;34:516–528
22. Miklosz A, Łukaszuk B, Żendzian-Piotrowska M, Kurek K, Chabowski A. The effects of AS160 modulation on fatty acid transporters expression and lipid profile in L6 myotubes. *Cell Physiol Biochem* 2016;38:267–282
23. Samovski D, Su X, Xu Y, Abumrad NA, Stahl PD. Insulin and AMPK regulate FA translocase/CD36 plasma membrane recruitment in cardiomyocytes via Rab GAP AS160 and Rab8a Rab GTPase. *J Lipid Res* 2012;53:709–717
24. Luiken JJ, Dyck DJ, Han XX, et al. Insulin induces the translocation of the fatty acid transporter FAT/CD36 to the plasma membrane. *Am J Physiol Endocrinol Metab* 2002;282:E491–E495
25. Nickerson JG, Alkhateeb H, Benton CR, et al. Greater transport efficiencies of the membrane fatty acid transporters FAT/CD36 and FATP4 compared with FABPpm and FATP1 and differential effects on fatty acid esterification and oxidation in rat skeletal muscle. *J Biol Chem* 2009;284:16522–16530
26. Glatz JF, Nabben M, Heather LC, Bonen A, Luiken JJ. Regulation of the subcellular trafficking of CD36, a major determinant of cardiac fatty acid utilization. *Biochim Biophys Acta* 2016;1861:1461–1471
27. Sun Y, Bilan PJ, Liu Z, Klip A. Rab8A and Rab13 are activated by insulin and regulate GLUT4 translocation in muscle cells. *Proc Natl Acad Sci U S A* 2010;107:19909–19914
28. Stöckli J, Fazakerley DJ, James DE. GLUT4 exocytosis. *J Cell Sci* 2011;124:4147–4159
29. Stermann T, Menzel F, Weidlich C, et al. Deletion of the RabGAP TBC1D1 leads to enhanced insulin secretion and fatty acid oxidation in islets from male mice. *Endocrinology* 2018;159:1748–1761
30. Febbraio M, Abumrad NA, Hajjar DP, et al. A null mutation in murine CD36 reveals an important role in fatty acid and lipoprotein metabolism. *J Biol Chem* 1999;274:19055–19062
31. Cleasby ME, Davey JR, Reinten TA, et al. Acute bidirectional manipulation of muscle glucose uptake by in vivo electrotransfer of constructs targeting glucose transporter genes. *Diabetes* 2005;54:2702–2711
32. Satkuskas S, Bureau MF, Puc M, et al. Mechanisms of in vivo DNA electrotransfer: respective contributions of cell electroporation and DNA electrophoresis. *Mol Ther* 2002;5:133–140
33. Wiza C, Chadt A, Blumensatt M, et al. Over-expression of PRAS40 enhances insulin sensitivity in skeletal muscle. *Arch Physiol Biochem* 2014;120:64–72
34. Lambernd S, Taube A, Schober A, et al. Contractile activity of human skeletal muscle cells prevents insulin resistance by inhibiting pro-inflammatory signalling pathways. *Diabetologia* 2012;55:1128–1139
35. Czech MP, Buxton JM. Insulin action on the internalization of the GLUT4 glucose transporter in isolated rat adipocytes. *J Biol Chem* 1993;268:9187–9190
36. Livak KJ, Schmittgen TD. Analysis of relative gene expression data using real-time quantitative PCR and the 2^{-ΔΔC_T} Method. *Methods* 2001;25:402–408
37. Knebel B, Fahlbusch P, Poschmann G, et al. Adipokine signatures in obese mouse models reflect adipose tissue health and are associated with serum lipid composition. *Int J Mol Sci* 2019;20:2559
38. Cinci G, Guerranti R, Pagani R, et al. Fatty acid composition of phospholipids, triglycerides and cholesterol in serum of castrated and estradiol treated rats. *Life Sci* 2000;66:1647–1654
39. Knebel B, Fahlbusch P, Dille M, et al. Fatty liver due to increased *de novo* lipogenesis: alterations in the hepatic peroxisomal proteome. *Front Cell Dev Biol* 2019;7:248
40. Dokas J, Chadt A, Nolden T, et al. Conventional knockout of Tbc1d1 in mice impairs insulin- and AICAR-stimulated glucose uptake in skeletal muscle. *Endocrinology* 2013;154:3502–3514
41. Xie B, Chen Q, Chen L, Sheng Y, Wang HY, Chen S. The inactivation of RabGAP function of AS160 promotes lysosomal degradation of GLUT4 and causes postprandial hyperglycemia and hyperinsulinemia. *Diabetes* 2016;65:3327–3340
42. Whitfield J, Pagliarunga S, Smith BK, et al. Ablating the protein TBC1D1 impairs contraction-induced sarcolemmal glucose transporter 4 redistribution but not insulin-mediated responses in rats. *J Biol Chem* 2017;292:16653–16664
43. Maher AC, McFarlan J, Lally J, Snook LA, Bonen A. TBC1D1 reduces palmitate oxidation by inhibiting β-HAD activity in skeletal muscle. *Am J Physiol Regul Integr Comp Physiol* 2014;307:R1115–R1123
44. Pette D. The adaptive potential of skeletal muscle fibers. *Can J Appl Physiol* 2002;27:423–448
45. Lacour JR. Muscle activity and energy expenditure. *Rev Mal Respir* 2011;28:1278–1292 [in French]
46. Ikeda S, Miyazaki H, Nakatani T, et al. Up-regulation of SREBP-1c and lipogenic genes in skeletal muscles after exercise training. *Biochem Biophys Res Commun* 2002;296:395–400
47. Luiken JJ, Miskovic D, Arumugam Y, Glatz JF, Bonen A. Skeletal muscle fatty acid transport and transporters. *Int J Sport Nutr Exerc Metab* 2001;11(Suppl.):S92–S96
48. Jaldin-Fincati JR, Pavarotti M, Frenedo-Cumbo S, Bilan PJ, Klip A. Update on GLUT4 vesicle traffic: a cornerstone of insulin action. *Trends Endocrinol Metab* 2017;28:597–611
49. Foster LJ, Klip A. Mechanism and regulation of GLUT-4 vesicle fusion in muscle and fat cells. *Am J Physiol Cell Physiol* 2000;279:C877–C890
50. Komiya Y, Sawano S, Mashima D, et al. Mouse soleus (slow) muscle shows greater intramyocellular lipid droplet accumulation than EDL (fast) muscle: fiber type-specific analysis. *J Muscle Res Cell Motil* 2017;38:163–173
51. Warren BE, Lou PH, Lucchinetti E, et al. Early mitochondrial dysfunction in glycolytic muscle, but not oxidative muscle, of the fructose-fed insulin-resistant rat. *Am J Physiol Endocrinol Metab* 2014;306:E658–E667
52. Glatz JF, Luiken JJ, Bonen A. Membrane fatty acid transporters as regulators of lipid metabolism: implications for metabolic disease. *Physiol Rev* 2010;90:367–417
53. Coburn CT, Knapp FF Jr., Febbraio M, Beets AL, Silverstein RL, Abumrad NA. Defective uptake and utilization of long chain fatty acids in muscle and adipose tissues of CD36 knockout mice. *J Biol Chem* 2000;275:32523–32529
54. Jain SS, Chabowski A, Snook LA, et al. Additive effects of insulin and muscle contraction on fatty acid transport and fatty acid transporters, FAT/CD36, FABPpm, FATP1, 4 and 6. *FEBS Lett* 2009;583:2294–2300
55. Steinbusch LK, Schwenk RW, Ouwens DM, Diamant M, Glatz JF, Luiken JJ. Subcellular trafficking of the substrate transporters GLUT4 and CD36 in cardiomyocytes. *Cell Mol Life Sci* 2011;68:2525–2538
56. Miklosz A, Łukaszuk B, Żendzian-Piotrowska M, Brańska-Januszewska J, Ostrowska H, Chabowski A. Challenging of AS160/TBC1D4 alters intracellular lipid milieu in L6 myotubes incubated with palmitate. *J Cell Physiol* 2017;232:2373–2386
57. Coe NR, Smith AJ, Frohner BI, Watkins PA, Bernlohr DA. The fatty acid transport protein (FATP1) is a very long chain acyl-CoA synthetase. *J Biol Chem* 1999;274:36300–36304
58. Herrmann T, van der Hoeven F, Grone HJ, et al. Mice with targeted disruption of the fatty acid transport protein 4 (*Fatp4*, *Slc27a4*) gene show features of lethal restrictive dermopathy. *J Cell Biol* 2003;161:1105–1115

59. Gimeno RE, Hirsch DJ, Punreddy S, et al. Targeted deletion of fatty acid transport protein-4 results in early embryonic lethality. *J Biol Chem* 2003;278:49512–49516
60. Hulver MW, Berggren JR, Carper MJ, et al. Elevated stearoyl-CoA desaturase-1 expression in skeletal muscle contributes to abnormal fatty acid partitioning in obese humans. *Cell Metab* 2005;2:251–261
61. Fumagalli M, Moltke I, Grarup N, et al. Greenlandic Inuit show genetic signatures of diet and climate adaptation. *Science* 2015;349:1343–1347
62. Moltke I, Grarup N, Jørgensen ME, et al. A common Greenlandic TBC1D4 variant confers muscle insulin resistance and type 2 diabetes. *Nature* 2014;512:190–193



Contraction-Mediated Glucose Transport in Skeletal Muscle Is Regulated by a Framework of AMPK, TBC1D1/4, and Rac1

Christian de Wendt,^{1,2} Lena Espelage,^{1,2} Samaneh Eickelschulte,^{1,2} Christian Springer,^{1,2} Laura Toska,¹ Anna Scheel,^{1,2} Awovi Didi Bedou,^{1,2} Tim Benninghoff,¹ Sandra Comes,¹ Torben Stermann,¹ Alexandra Chadt,^{1,2} and Hadi Al-Hasani^{1,2}

Diabetes 2021;70:2796–2809 | <https://doi.org/10.2337/db21-0587>

The two closely related RabGTPase-activating proteins (RabGAPs) TBC1D1 and TBC1D4, both substrates for AMPK, play important roles in exercise metabolism and contraction-dependent translocation of GLUT4 in skeletal muscle. However, the specific contribution of each RabGAP in contraction signaling is mostly unknown. In this study, we investigated the cooperative AMPK-RabGAP signaling axis in the metabolic response to exercise/contraction using a novel mouse model deficient in active skeletal muscle AMPK combined with knockout of either *Tbc1d1*, *Tbc1d4*, or both RabGAPs. AMPK deficiency in muscle reduced treadmill exercise performance. Additional deletion of *Tbc1d1* but not *Tbc1d4* resulted in a further decrease in exercise capacity. In oxidative soleus muscle, AMPK deficiency reduced contraction-mediated glucose uptake, and deletion of each or both RabGAPs had no further effect. In contrast, in glycolytic extensor digitorum longus muscle, AMPK deficiency reduced contraction-stimulated glucose uptake, and deletion of *Tbc1d1*, but not *Tbc1d4*, led to a further decrease. Importantly, skeletal muscle deficient in AMPK and both RabGAPs still exhibited residual contraction-mediated glucose uptake, which was completely abolished by inhibition of the GTPase Rac1. Our results demonstrate a novel mechanistic link between glucose transport and the GTPase signaling framework in skeletal muscle in response to contraction.

In the presence of insulin, skeletal muscle accounts for up to ~85% of peripheral glucose disposal from the blood

(1). In addition to insulin stimulation, glucose uptake into skeletal muscle is increased by contraction during exercise. Both stimuli lead to the redistribution of the facilitative GLUT4 from intracellular storage vesicles to the cell surface, resulting in increased glucose clearance from the blood stream (2,3). The process of contraction-mediated GLUT4 translocation is tightly regulated and, up to now, not fully understood (4). A major mechanism linking muscle contraction to GLUT4 translocation involves the activation of the serine/threonine protein kinase AMPK by AMP (5,6). In a contracting muscle, cellular AMP levels increase as a result of the amplified energy demand. AICAR is a known chemical activator of AMPK and is thus frequently used as an *in vitro* contraction mimetic (7). However, contraction signaling is clearly more complex and involves more players in addition to AMPK. For instance, AMPK-related kinases (ARKs) have been discussed to facilitate AMPK-independent contraction- or exercise-induced glucose uptake. Kinases belonging to this group share the commonality of being activated by their upstream kinase liver kinase B1 (LKB1) (8,9).

As another very relevant component of contraction-mediated glucose transport into skeletal muscle, the Rho GTPase Ras-related C3 botulinum toxin substrate 1 (Rac1) has emerged recently. Rac1 is activated by mechanical stress or stretching of the muscle during contraction, a process that is independent from the mainly metabolic signaling pathways involving AMPK (10–12). Both AMPK and Rac1 display an extraordinary degree of evolutionary

¹Institute for Clinical Biochemistry and Pathobiochemistry, German Diabetes Center (DDZ), Leibniz Center for Diabetes Research at Heinrich Heine University Düsseldorf, Düsseldorf, Germany

²German Center for Diabetes Research (DZD), Partner Düsseldorf, München-Neuherberg, Germany

Corresponding author: Alexandra Chadt, alexandra.chadt@ddz.de

Received 30 June 2021 and accepted 17 September 2021

This article contains supplementary material online at <https://doi.org/10.2337/figshare.16645567>.

C.d.W. and L.E. contributed equally to this work.

© 2021 by the American Diabetes Association. Readers may use this article as long as the work is properly cited, the use is educational and not for profit, and the work is not altered. More information is available at <https://www.diabetesjournals.org/content/license>.

conservation, emphasizing the physiological relevance of at least two redundant mechanisms to secure glucose clearance from the blood stream upon physical activity (13,14). When combined, Rac1 and AMPK inhibition constitute nearly the complete contraction-dependent glucose disposal into skeletal muscle (15). Activation, and thus phosphorylation, of AMPK eventually triggers a complex signaling cascade, resulting in an insulin-independent elevation of glucose transport. Two main downstream effectors of AMPK are the RabGTPase-activating proteins (RabGAPs) TBC1D1 and TBC1D4. Previously, we demonstrated fiber type-dependent regulation of the two RabGAPs through AICAR stimulation of muscles (16). Whereas *Tbc1d1*-deficient (D1KO) animals display substantially impaired insulin- and AICAR-stimulated glucose transport into glycolytic extensor digitorum longus (EDL) but not oxidative soleus muscle, adverse observations have been described for *Tbc1d4* knockout (D4KO) mice. These results are in line with the RabGAPs' expression pattern, where TBC1D1 is the predominant isoform in glycolytic skeletal muscle and TBC1D4 shows the highest abundance in oxidative skeletal muscle and adipocytes (16–18). Likewise, GLUT4 protein abundance is reduced in oxidative skeletal muscle and white adipose tissue from D4KO and in glycolytic skeletal muscle from D1KO mice (19–22). Of note, fiber type specificity of *Tbc1d1* and *Tbc1d4* expression patterns appear to differ between mouse and human skeletal muscle (23,24). Double-deficient *Tbc1d1/4* (D1/4KO) mice present a combined muscular phenotype with impaired insulin- as well as AICAR-mediated glucose transport and reduced GLUT4 content in all muscle types. In addition, these mice display deteriorated whole-body glycemia, unlike the single-knockout mice, and presumably because of a compensatory action of the remaining RabGAP (16,25).

Interestingly, several seemingly redundant cellular pathways have been identified in addition to the activation of AMPK mediating contraction-stimulated glucose uptake, including, but not limited to, Rac1/actin and CAMK signaling (26–28). For instance, a transgenic mouse strain overexpressing a dominant inhibitory mutant of the AMPK α 2 subunit (AMPK-DN) in muscular tissues shows completely ablated AICAR-stimulated glucose uptake into skeletal muscle, whereas a contraction stimulus still results in a reduced, but significantly elevated transport of glucose into the muscle (29,30). The complexity of this regulation supposedly represents the evolutionarily conserved need to maintain muscle energy supply in situations of high energy demand, such as physical activity. The aim of the current study was to segregate the individual contribution of TBC1D1, TBC1D4, and AMPK to skeletal muscle glucose metabolism in vivo as well as in different skeletal muscle types.

RESEARCH DESIGN AND METHODS

Chemicals and Buffer

Chemicals and buffer ingredients are listed in Supplementary Table 1.

Experimental Animals

All animal experiments were approved by the ethics committee of the State Ministry of Agriculture, Nutrition and Forestry (State of North Rhine-Westphalia, Germany). Three to six male (12–30 weeks old) mice per cage were housed at 22°C on a 12-h light-dark cycle (lights on at 6:00 A.M.) with ad libitum access to food and water. After weaning, animals received a standard chow diet containing 22.1% (wt/wt) protein (30% of calories), 4.5% fat (11% of calories), and 53.35% carbohydrates (53% of calories) containing 3.3 kcal/g energy (ssniff-Spezialdiäten, Soest, Germany). Unless otherwise indicated, all interventions were conducted during the morning and in random-fed animals. Generation of C57BL/6J D1KO, D4KO, and D1/4KO mice has previously been described (16). Transgenic mice overexpressing AMPK-DN, a kinase-dead α ₂-subunit of the AMPK enzyme, under the control of the muscle creatine kinase promoter (29) were a gift from Morris J. Birnbaum (University of Pennsylvania, Philadelphia, PA) and crossbred with RabGAP-deficient animals to obtain the five experimental genotypes: wild type (WT), transgenic AMPK α 2-DN (DN), AMPK α 2-DN-D1KO (D1KO-DN), AMPK α 2-DN-D4KO (D4KO-DN), and AMPK α 2-DN-*Tbc1d1/Tbc1d4* double-deficient (D1/4KO-DN) mice. Sequences of all genotyping primers are listed in Supplementary Table 2.

Tolerance Tests

For glucose tolerance tests, sterile glucose (2 g/kg body weight, 20% solution) was injected intraperitoneally into 16-h fasted animals. Compared with humans, a 16-h period is a comparatively long time for mice to fast. However, to reduce variability in basal blood glucose levels, it is beneficial to expose mice to an overnight fast (31). For AICAR tolerance tests, nonfasted mice were injected intraperitoneally with AICAR (250 mg/kg body weight; Toronto Research Chemicals, Toronto, Ontario, Canada), and blood samples were taken from the tail tip at 0, 15, 30, 60, and 120 min. Blood glucose was determined with a glucometer (Contour; Bayer, Leverkusen, Germany). On the basis of fasting plasma, an insulin- and glucose-level HOMA of insulin resistance (HOMA-IR) index was calculated according to the following equation (32): HOMA-IR = fasting insulin (ng/mL) \times fasting blood glucose (mg/dL)/405.

Determination of Insulin and Nonesterified Fatty Acids in Mouse Plasma

Plasma insulin was measured with ELISA (Insulin Mouse Ultrasensitive ELISA; DRG Instruments, Marburg, Germany). Nonesterified fatty acids (NEFAs) in plasma were determined by an NEFA-HR(2) enzymatic colorimetric assay (Wako Chemicals, Richmond, VA) according to the manufacturer's instructions.

In Vivo Running Performance

Mice were familiarized with a calorimetric treadmill system (TSE Systems, Bad Homburg, Germany) at low speed

(15 cm * s⁻¹, 5° incline) for 5 min the day before performing the exercise test. Acute exercise testing consisted of a run to exhaustion starting at 15 cm * s⁻¹ (5° incline) for the first 2 min and then continuously increasing speed by 5 cm * s⁻¹ every 2 min. Time to exhaustion was defined as the time point when the mouse was no longer able to maintain its normal running position and showed frequent contact with the grid at the rear of the treadmill. VO_{2max} (mL * min⁻¹ * kg^{-0.75}) and respiratory exchange ratios (RERs) (VCO₂ * VO₂⁻¹; average RER during the exercise test or RER at VO_{2max}) were determined with PhenoMaster software (TSE Systems).

In Vitro Kinase Assay

Recombinant full-length His₆-*Tbc1d1* and His₆-*Nuak1* (AMP-activated protein kinase-related kinase 5 [ARK5]) were cloned, expressed in *Sf9* cells using the baculovirus system, and purified by IMAC using Ni-NTA resins (QIAGEN, Hilden, Germany) as previously described (33). Activation of purified His₆-ARK5 was confirmed by Western blotting of pThr211 (data not shown). Phosphorylation reactions were carried out at room temperature for 20 min in the presence of 3 pmol ARK5, 40 mmol/L Tris-HCl (pH 7.4), 8 mmol/L MgCl₂, 200 μmol/L AMP, 2 mmol/L ATP, and 0.4 mmol/L dithiothreitol in a volume of 100 μL as previously described (33,34).

Analysis of Glucose Uptake Into Isolated Skeletal Muscles

Glucose uptake was assessed by the accumulation of [³H]2-deoxyglucose (Hartmann Analytic, Braunschweig, Germany) in muscle with the use of [¹⁴C]mannitol (Perkin-Elmer, Waltham, MA) as an extracellular marker. Mice were anesthetized (500 mg/kg Avertin [2,2,2-tribromoethanol] via intraperitoneal injection), and intact EDL and soleus muscles were removed. Isolated muscles were mounted in a Muscle Strip Myograph chamber (Danish Myo Technology, Aarhus, Denmark) and incubated for 15 min in preoxygenated (95% oxygen/5% carbon dioxide) Krebs-Henseleit buffer (Supplementary Table 3) containing 5 mmol/L HEPES and supplemented with 8 mmol/L pyruvate and 15 mmol/L mannitol. Rac1 inhibition was achieved after 50-min preincubation with NSC23766 (200 μmol/L; Sigma-Aldrich) or DMSO as vehicle control, both diluted in Krebs-Henseleit buffer containing 1% BSA, 15 mmol/L mannitol, and 8 mmol/L pyruvate. All incubation steps were conducted under continuous gassing (95% oxygen/5% carbon dioxide) at 30°C. After recovery, a basal mechanical tension was applied (2–3 mN to EDL and 4–5 mN to soleus muscle), and muscles were again incubated for 30 min. Then, muscles were electrically stimulated to contract with 300-ms trains of 0.1-ms pulses at 160 Hz every second in the presence of 1 mmol/L [³H]2-deoxyglucose and 19 mmol/L [¹⁴C]mannitol. After 10 min of stimulation and an additional 10 min of radioactive incubation, muscles were immediately frozen in liquid nitrogen and

stored at –20°C. Cleared protein lysates were used to determine incorporated radioactivity by scintillation counting. [¹⁴C]Mannitol counts were used to correct for the extracellular space.

Sample Processing, SDS-PAGE, and Western Blotting

Protein lysates (10–30 μg) were separated by 8–12% SDS-PAGE and transferred by tank blotting onto nitrocellulose membranes (Amersham Protran 0.45 μm). Membranes were blocked for 1 h with 5% fat-free powdered milk in Tris-buffered saline with Tween (Supplementary Table 3), incubated with primary antibodies and secondary horseradish peroxidase-conjugated antibodies as described in Supplementary Table 4, and developed with ECL reagent (PerkinElmer). Protein abundances were normalized to the housekeeping protein GAPDH.

RNA Extraction, cDNA Synthesis, and Quantitative Real-Time PCR

RNA was extracted using QIAzol Lysis Reagent (QIAGEN, Hilden, Germany) according to the manufacturer's instructions, and cDNA was synthesized with a GoScript Reverse Transcriptase system (Promega, Madison, WI). Real-time quantitative PCR was performed using self-designed SYBR Green PCR primers (Supplementary Table 5), and data were normalized to *Gapdh* (gastrocnemius muscle) or *Rps29* (liver) according to the 2^{-ΔΔCt} method (35).

Determination of Triglycerides and Glycogen

Male mice were sacrificed in the morning after 4 h of fasting, and plasma samples and homogenized tissue (40 mg liver and gastrocnemius muscle) were analyzed using a triglycerides assay kit (Trigs; Randox, Crumlin, U.K.) according to the manufacturer's guidelines. Glycogen content was determined using the amyloglucosidase method (36) using a glucose oxidase-based colorimetric detection kit (Glucose liquicolor; HUMAN Diagnostics, Taunusstein, Germany) according to the manufacturer's instructions.

Statistics

Unless otherwise stated, data are reported as mean ± SEM. Significant differences were determined by one-way or two-way ANOVA (post hoc test, Tukey correction, Šidák correction, or Fisher least significant difference) or paired two-tailed Student *t* test, as indicated in the figure legends. *P* < 0.05 was considered statistically significant.

RESULTS

TBC1D1 and TBC1D4 Exert Nonredundant Functions on Postprandial and Postexercise Glycemia and Contraction-Stimulated Glucose Uptake in Different Skeletal Muscle Fiber Types

Both TBC1D1 and TBC1D4 have been shown to play crucial roles in skeletal muscle glucose transport. To investigate the contribution of each of the two RabGAPs to glycemic control, we subjected D1KO, D4KO, or D1/4KO

mice to an overnight fast followed by 1 h of ad libitum refeeding. While there were no alterations in blood glucose or plasma insulin levels among the genotypes in the fasted state, D4KO and D1/4KO mice showed markedly increased blood glucose and plasma insulin levels compared with WT littermates after 1 h of refeeding. In contrast, D1KO mice displayed neither increased blood glucose levels nor elevated plasma insulin levels in the refed state (Fig. 1A and B). We and others previously demonstrated disturbed insulin- and AICAR-stimulated glucose transport into oxidative soleus muscle from D4KO and D1/4KO mice and glycolytic EDL muscle from D1KO and D1/4KO mice, respectively (16,25). However, glucose transport in response to contraction has not been investigated in D4KO and D1/4KO animals. Thus, we sought to investigate the specific roles of TBC1D1 and TBC1D4 in the regulation of contraction-mediated glucose transport into different skeletal muscle fiber types, subjecting isolated EDL and soleus muscles from D1KO, D4KO, and D1/4KO mice to ex vivo analyses of contraction-stimulated glucose uptake in a myograph chamber. D1KO and

D1/4KO mice showed ~50% reduced contraction-stimulated glucose uptake compared with WT controls in glycolytic EDL muscle. Basal glucose transport was also impaired in EDL muscle from D1KO and D1/4KO but not D4KO mice (Fig. 1C). In contrast, basal glucose uptake was unaltered among the genotypes in oxidative soleus muscle, and contraction-stimulated glucose transport was reduced exclusively in muscles from D1/4KO mice (Fig. 1D). Strikingly, skeletal muscle lacking either TBC1D1, TBC1D4, or both RabGAPs displayed significant residual stimulation of glucose transport in response to contraction, indicating spare signaling capacity. Contraction force determined as time for half-capacity was unaltered among the genotypes (Supplementary Fig. 1).

Lack of TBC1D1, but not TBC1D4, Combined With Muscle-Specific AMPK Inactivation Leads to Impairments in Whole-Body Glycemia in the Fasted State

We generated a new mouse line by crossbreeding muscle-specific AMPK-DN mice with RabGAP-deficient animals

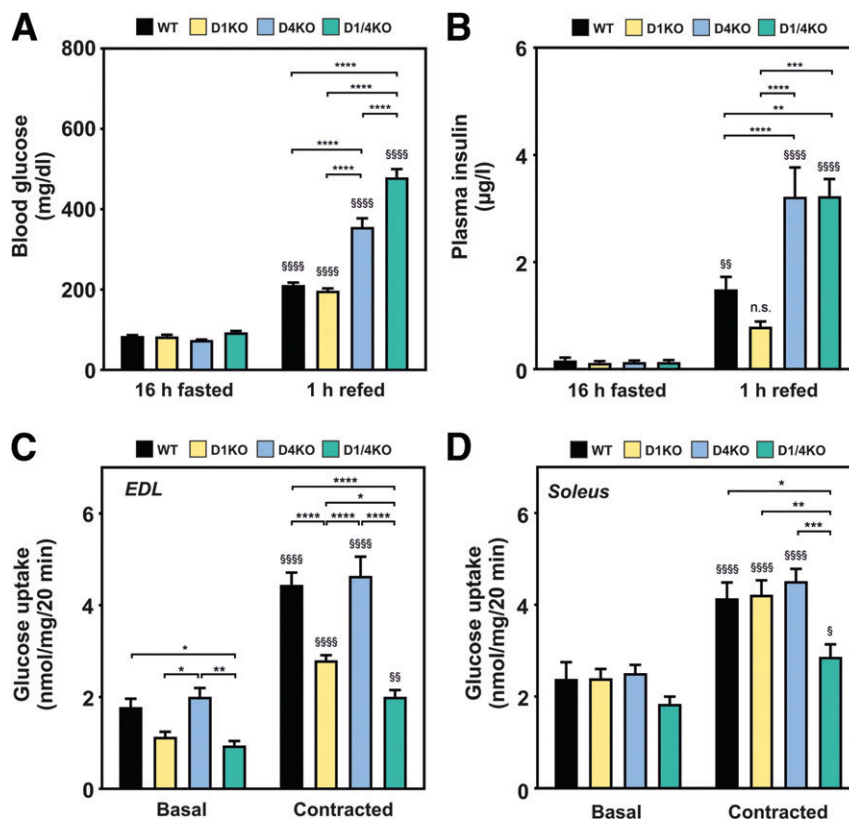


Figure 1—TBC1D1 and TBC1D4 exert nonredundant functions on postprandial and postexercise glycemia and contraction-stimulated glucose uptake in different skeletal muscle fiber types. Mice were subjected to an overnight fast with 1 h of ad libitum refeeding. A and B: Blood glucose and plasma insulin levels were measured after the fasting period and refeeding. *n* = 5–22. C and D: To investigate the specific role of TBC1D1 and TBC1D4 in skeletal muscle contraction, ex vivo 2-deoxy-D-glucose uptake was measured at basal or contraction-stimulated conditions in isolated EDL and soleus muscles from D1KO, D4KO, and D1/4KO mice. *n* = 8–10. Data are presented as mean ± SEM. **P* < 0.05, ***P* < 0.01, ****P* < 0.001, *****P* < 0.0001, WT vs. D1KO vs. D4KO vs. D1/4KO by two-way ANOVA with Tukey correction; §*P* < 0.05, §§*P* < 0.01, §§§§*P* < 0.0001, basal vs. contracted by two-way ANOVA with Šidák correction. n.s., not significant.

on a C57BL/6J background (16,29). Overexpression of an inactive AMPK α 2 subunit did not alter the abundance of TBC1D1 in D1KO or D4KO mouse skeletal muscles, and all genotypes overexpressing the AMPK-DN allele displayed a strong signal for AMPK (Fig. 2A and B). Despite some tendencies, both 6-h fasted blood glucose and plasma insulin levels were not significantly altered between the genotypes (Fig. 2C and D). The estimated HOMA-IR index revealed an impaired insulin sensitivity as a result of a combined inactivation of AMPK and *Tbc1d1*-deficiency

(D1KO-DN). Interestingly, D4KO-DN completely ablated the increased HOMA-IR in D1KO-DN mice (Fig. 2E). No major differences were determined in body weight and body composition between the genotypes. Moreover, glucose tolerance was not altered because of AMPK or RabGAP deficiency (Supplementary Fig. 2A–D). During an intraperitoneal AICAR tolerance test, DN mice presented slightly elevated blood glucose levels after AICAR injection (Fig. 2F). In accordance with our previous findings, GLUT4 abundance was reduced in gastrocnemius skeletal muscle

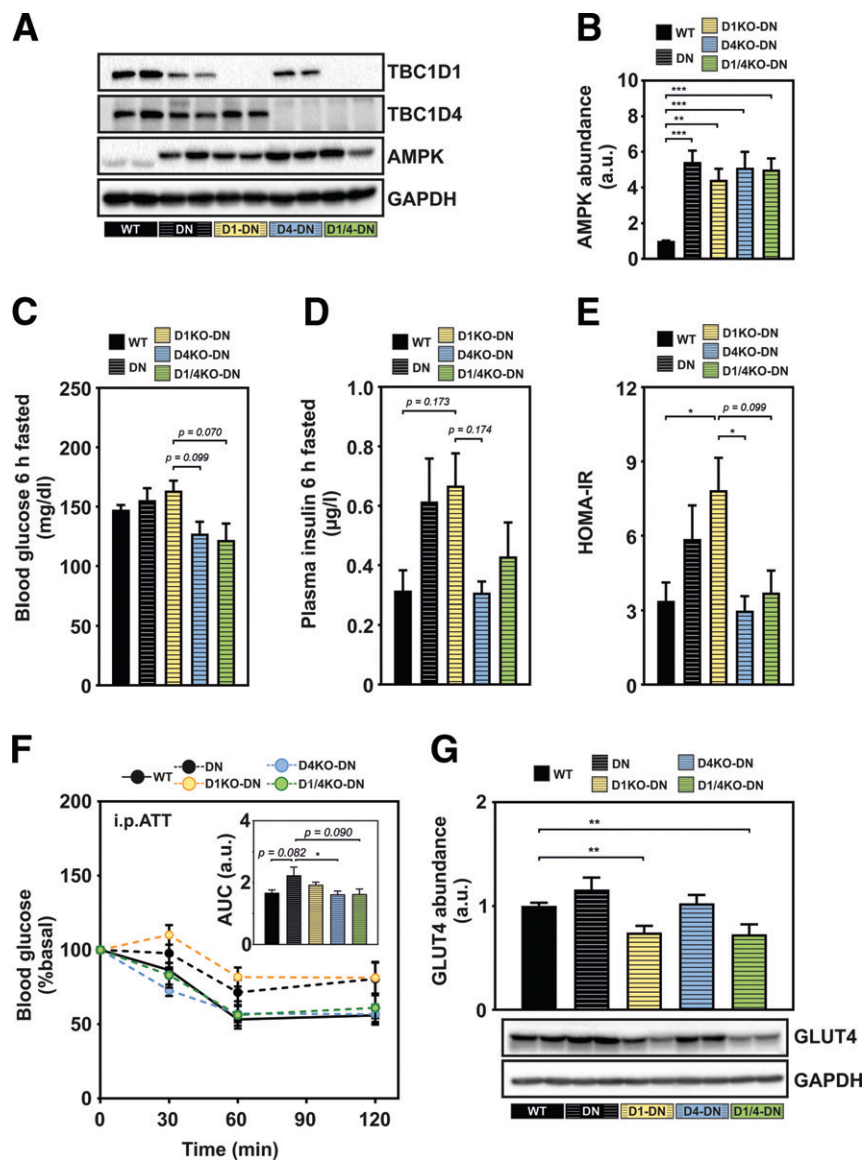


Figure 2—Lack of TBC1D1, but not TBC1D4, combined with muscle-specific AMPK inactivation leads to impairments in whole-body glycemia in the fasted state. **A**: Representative Western blots of TBC1D1, TBC1D4, and AMPK in gastrocnemius muscle from WT, DN, D1KO-DN, D4KO-DN, and D1/4KO-DN mice. **B**: Quantification of AMPK in gastrocnemius muscle of WT, DN, D1KO-DN, D4KO-DN, and D1/4KO-DN mice. Protein abundance was normalized to GAPDH. $n = 7$ –9. **C–E**: To investigate the specific role of the RabGAPs in AMPK-independent glycemia, blood glucose and plasma insulin levels were measured after a 6-h fasting period, and the HOMA-IR index was determined. **F**: AICAR tolerance was measured after intraperitoneal injection of AICAR (250 mg/kg body weight), and the area under the curve (AUC) was determined for quantification. $n = 7$ –10. **G**: GLUT4 protein abundance as determined in gastrocnemius muscle and normalized to GAPDH. Data are mean \pm SEM. * $P < 0.05$, ** $P < 0.01$, *** $P < 0.001$, WT vs. DN vs. D1KO-DN vs. D4KO-DN vs. D1/4KO-DN by one-way ANOVA with Tukey correction. a.u., arbitrary units; i.p.ATT, intraperitoneal AICAR tolerance test.

from D1KO-DN and D1/4KO-DN but not DN and D4KO-DN animals, and GLUT1 abundance was unchanged among the groups (Fig. 2G and Supplementary Fig. 2E).

Lack of TBC1D4, but not TBC1D1, Combined With Muscle-Specific AMPK Inactivation Leads to Impairments in Whole-Body Glycemia in the Postprandial State

Next, we subjected all five genotypes of the AMPK-DN RabGAP mouse line to a fasting-refeeding experiment with 16-h overnight fasting and 1 h of ad libitum refeeding. Fasted plasma blood glucose as well as fasted and refeed plasma insulin levels were equal in all genotypes. In contrast, following 1 h of ad libitum refeeding, postprandial blood glucose levels were increased in D4KO-DN and D1/4KO-DN animals compared with WT controls (Fig. 3A and B). Following 16 h of fasting, plasma triglycerides were significantly increased in DN mice compared with WT littermates, an effect that was almost completely abolished by additive deficiency of both RabGAPs (D1/4KO-DN), whereas there were no differences among the

genotypes in the refeed state (Fig. 3C). Interestingly, the increased plasma free fatty acids in DN and D4KO-DN animals following 16 h of fasting were restored to WT levels in D1KO-DN mice (Fig. 3D).

Reciprocal Energy Storage in the Liver of DN-RabGAP Animals Is Independent From the Inactivation of AMPK in Muscle

We analyzed liver triglyceride and glycogen content as well as the abundance and phosphorylation status of regulatory enzymes in all genotypes. Liver triglycerides were not different in DN mice compared with WT littermates but increased in D1KO-DN, D4KO-DN, D1/4KO-DN mice (Fig. 4A). In contrast, protein abundance of PEPCK1 (PCK1) was only slightly elevated in D1/4KO-DN mice but not in the other genotypes, and no changes were observed for PEPCK2 (PCK2) (Fig. 4B). Liver glycogen content was slightly reduced in D4KO-DN and D1/4KO-DN animals compared with the DN genotype but unaltered in DN and D1KO-DN mice compared with WT

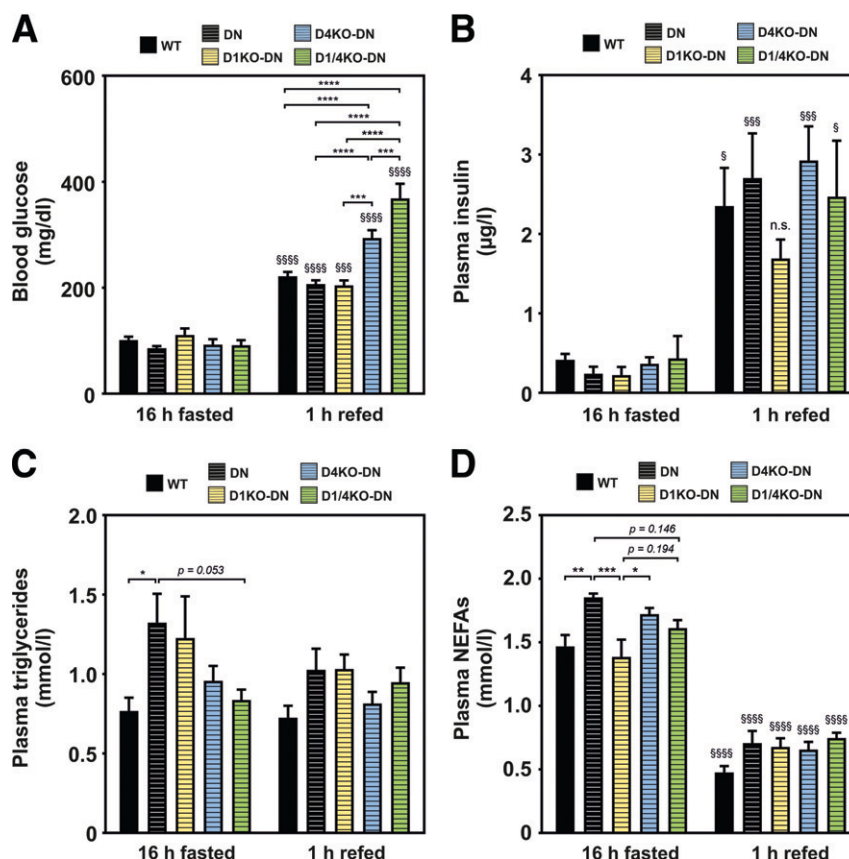


Figure 3—Lack of TBC1D4, but not TBC1D1, combined with muscle-specific AMPK inactivation leads to impairments in whole-body glycemia in the postprandial state. *A–D*: A fasting and refeeding experiment was performed, and blood glucose, plasma insulin, plasma triglyceride, and plasma NEFA levels were measured after 16 h of fasting and 1 h of refeeding. $n = 4–12$. Data are mean \pm SEM. * $P < 0.05$, ** $P < 0.01$, *** $P < 0.001$, **** $P < 0.0001$, WT vs. DN vs. D1KO-DN vs. D4KO-DN vs. D1/4KO-DN by two-way ANOVA with Tukey correction; $\$P < 0.05$, $\$\$P < 0.001$, $\$\$\$P < 0.0001$, 16-h fasted vs. 1-h refeed mice by two-way ANOVA with Sidák correction. n.s., not significant.

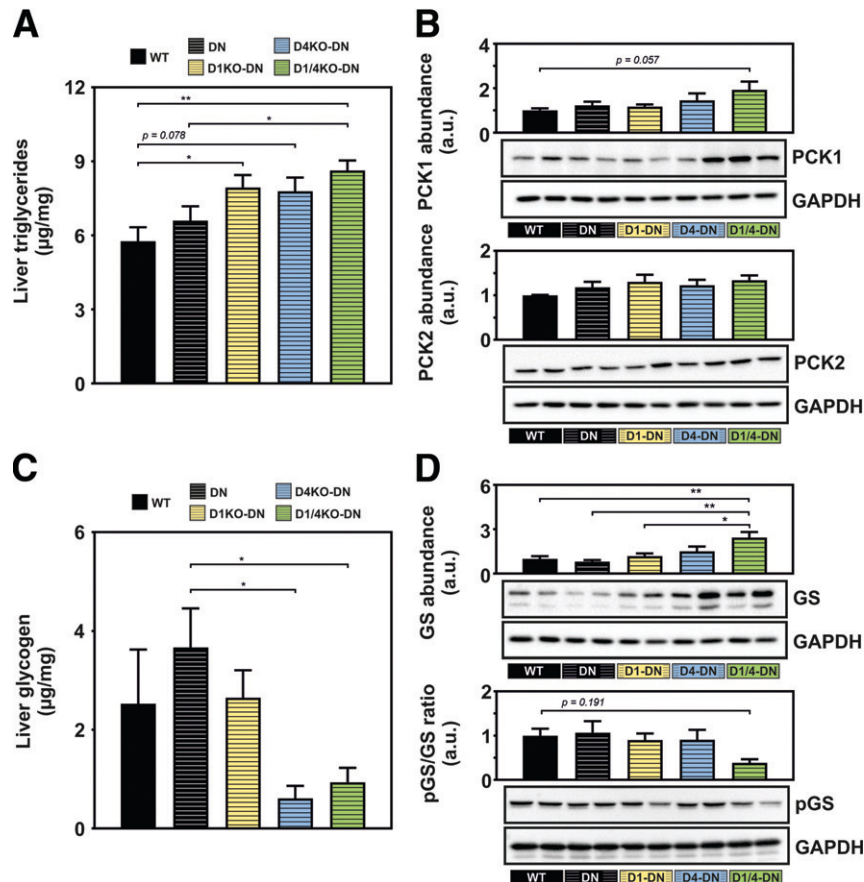


Figure 4—Reciprocal energy storage in the liver from DN-RabGAP animals is independent from the inactivation of AMPK in muscle. **A** and **B**: To gain a more global overview on energy metabolism in RabGAP-deficient animals with muscle-specific AMPK inactivation, liver triglyceride content was measured, and Western blot analysis of PCK1 and PCK2 from WT, DN, D1KO-DN, D4KO-DN, and D1/4KO-DN normalized to GAPDH was performed. **C** and **D**: Liver glycogen content was measured, and liver GS protein abundance and pGS/GS ratio was determined from WT, DN, D1KO-DN, D4KO-DN, and D1/4KO-DN mice normalized to GAPDH. $n = 6$ – 17 . Data are mean \pm SEM. * $P < 0.05$, ** $P < 0.01$ by one-way ANOVA with Tukey correction. a.u., arbitrary units.

controls (Fig. 4C). D1/4KO-DN animals displayed increased glycogen synthase (GS) protein abundance, but the ratio of phosphorylated (Ser641) to total GS (pGS/GS) was slightly decreased (Fig. 4D).

Lack of TBC1D1, but not TBC1D4, Combined With Muscle-Specific AMPK Inactivation Leads to Impairments in Exercise Performance

We determined the exercise capacity of DN, D1KO-DN, D4KO-DN, and D1/4KO-DN mice on treadmills. Muscle-specific inactivation of AMPK α 2 (DN mice) led to a significantly reduced time to exhaustion compared with WT animals. Interestingly, both D1KO-DN and D1/4KO-DN mice showed an additional impairment in running capacity compared with the DN animals. In contrast, additional ablation of *Tbc1d4* in D4KO-DN mice did not affect exercise performance to a larger extent than AMPK inactivation alone (Fig. 5A). These results were also reflected by significantly lower VO_{2max} values of DN and D1KO-DN mice compared with WT animals (Fig. 5B). The RER and the RER at VO_{2max} , however, were not changed among

the five different genotypes (Fig. 5C and D). No genotype-dependent differences were observed for skeletal muscle triglyceride or glycogen content (Fig. 5E and F).

Deletion of Both RabGAPs and Inactivation of AMPK Are Sufficient to Abolish Contraction Response in Oxidative Soleus Muscle, but Additional Inhibition of the Small Rho GTPase Rac1 Is Required in EDL Muscle to Completely Block Contraction-Mediated Glucose Uptake

Intact isolated EDL and soleus muscles from WT, DN, D1KO-DN, D4KO-DN, and D1/4KO-DN mice were *in vivo* contracted in a myograph chamber, and [3 H]2-deoxyglucose uptake was measured. Compared with WT animals, EDL muscles from AMPK-inactive DN mice displayed only a very minor reduction in the basal state but substantially decreased glucose transport in the contracted state. In accordance with the impaired exercise performance *in vivo*, D1KO-DN and D1/4KO-DN, but not D4KO-DN, animals demonstrated substantially impaired contraction-mediated glucose uptake into EDL muscle in

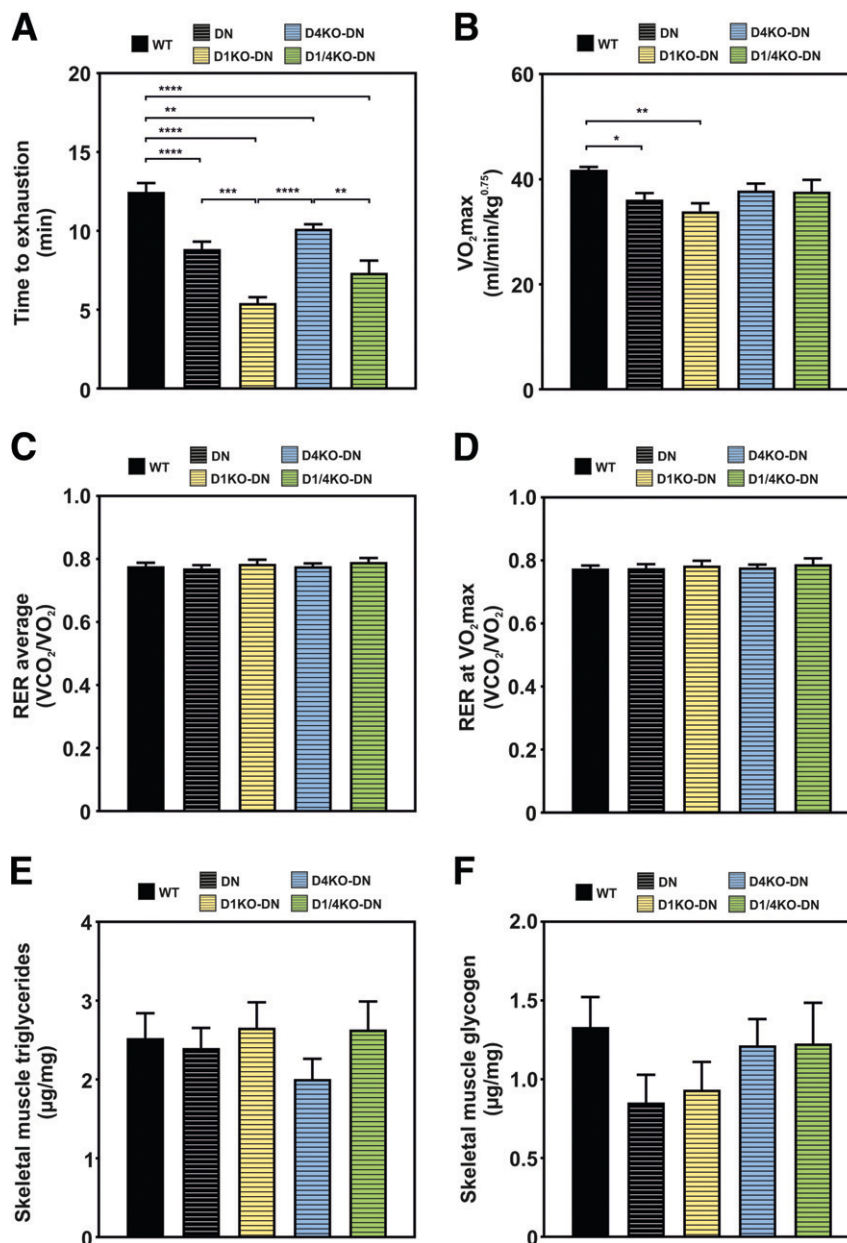


Figure 5—Lack of TBC1D1, but not TBC1D4, combined with muscle-specific AMPK inactivation leads to impairments in exercise performance and depletion of skeletal muscle glycogen. To address the question about the role of TBC1D1 and TBC1D4 downstream of AMPK α 2 in skeletal muscle exercise metabolism, *in vivo* exercise capacity on a calorimetric treadmill was elucidated. *A–D*: Running performance, VO₂max values, average RER, and RER at VO₂max from WT, DN, D1KO-DN, D4KO-DN, and D1/4KO-DN mice were determined. *n* = 4–11. *E* and *F*: Triglyceride and glycogen content from gastrocnemius muscle was measured. *n* = 4–17. Data are mean \pm SEM. **P* < 0.05, ***P* < 0.01, ****P* < 0.001, *****P* < 0.0001 by one-way ANOVA with Tukey correction.

addition to the reduction caused by AMPK inactivation (Fig. 6A). In isolated soleus muscle, AMPK inactivation led to a clearly impaired contraction-stimulated glucose transport rate. However, RabGAP deficiency did not result in any further decline in contraction-stimulated glucose uptake (Fig. 6B). Ablation of both RabGAPs in combination with muscle-specific AMPK inactivation (D1/4KO-DN) resulted in a blunted contraction response in the

oxidative soleus muscle. In contrast, contraction-mediated glucose transport was still moderately increased in the glycolytic EDL muscle from D1/4KO-DN mice compared with the basal state (Fig. 6A and B). We found reduced GLUT4 abundance in EDL muscle from D1KO-DN and D1/4KO-DN mice, whereas GLUT4 abundance in DN and D4KO-DN mice was unaltered (Fig. 6C). In contrast, GLUT4 content was diminished in soleus muscle from

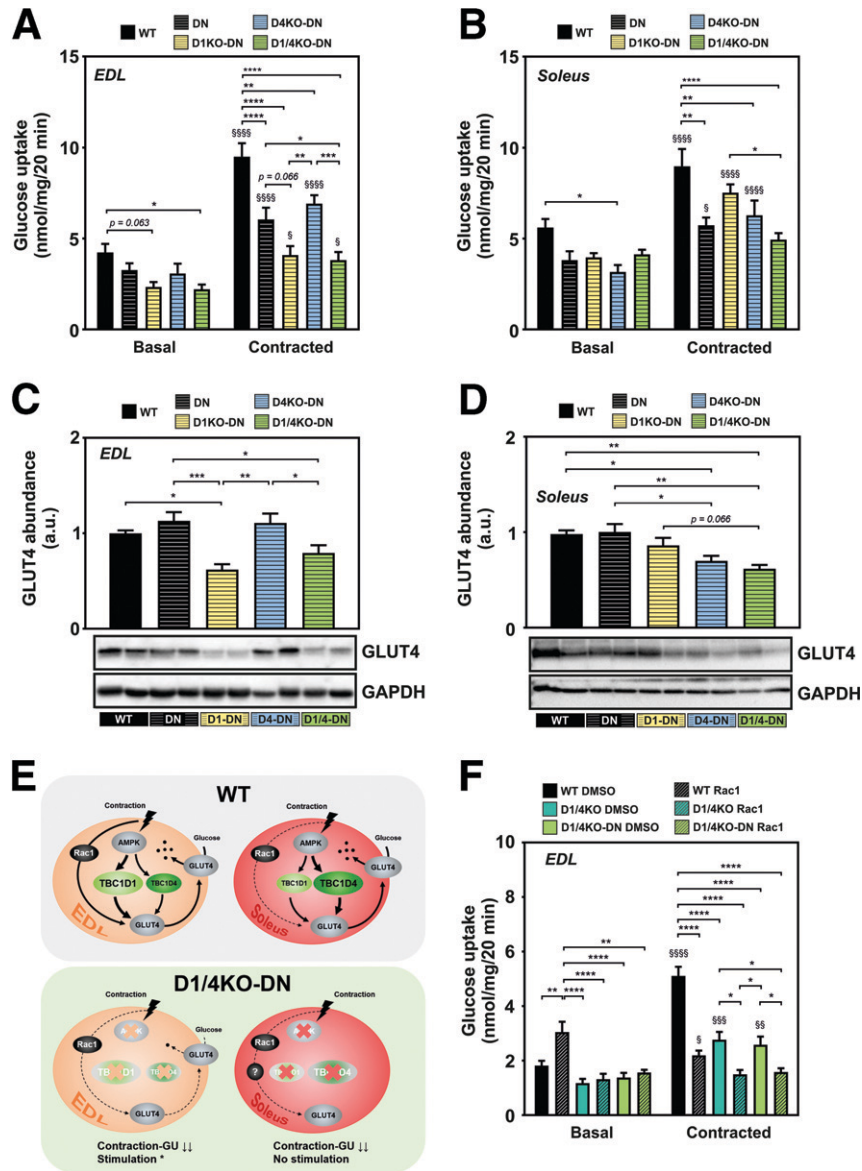


Figure 6—Deletion of both RabGAPs and inactivation of AMPK are sufficient to abolish contraction response in oxidative soleus muscle, but additional inhibition of the small Rho GTPase Rac1 is required in EDL muscle to completely abolish contraction-mediated glucose uptake. *A* and *B*: Basal and contraction-stimulated 2-deoxy-D-glucose (2-DOG) uptake in intact isolated EDL and soleus muscles were determined using a myograph chamber. *n* = 7–11. *C* and *D*: Western blot analysis of GLUT4 in EDL and soleus normalized to GAPDH from WT, DN, D1KO-DN, D4KO-DN, and D1/4KO-DN mice. *n* = 7–8. *E*: Schematic overview on differences in contraction-stimulated glucose uptake into EDL and soleus muscle from WT and D1/4KO-DN animals. **P* < 0.05 basal vs. contracted. *F*: Basal and contraction-stimulated 2-DOG uptake in intact isolated EDL muscle was determined using a myograph chamber after preincubation with either a Rac1 inhibitor or DMSO as vehicle control. *n* = 5–10. Data are mean ± SEM. **P* < 0.05, ***P* < 0.01, ****P* < 0.001, *****P* < 0.0001, WT vs. DN vs. D1KO-DN vs. D4KO-DN vs. D1/4KO-DN by two-way ANOVA with Tukey correction; §*P* < 0.05, §§*P* < 0.01, §§§*P* < 0.001, §§§§*P* < 0.0001, §*P* < 0.05, basal vs. contracted by two-way ANOVA with Sidák correction. a.u., arbitrary units; GU, glucose uptake.

D4KO-DN and D1/4KO-DN but not from D1KO-DN mice (Fig. 6D). Inactivation of AMPK alone, however, did not affect GLUT4 content in either EDL or soleus muscles. An overview on the different responses in contraction-mediated glucose uptake between the two muscle types can be found in Fig. 6E.

We investigated the residual contraction response in EDL muscle from D1/4KO-DN animals and determined ex vivo contraction-mediated glucose uptake after preincubation

with either DMSO or the Rac1 inhibitor NSC23766. The small Rho GTPase Rac1 has been described as an important factor in AMPK-independent contraction signaling (13,15), and Rac1 inhibition led to a pronounced increase of basal glucose transport into EDL muscles from WT mice. Contraction-stimulated glucose transport, in contrast, was substantially impaired in WT muscles as a result of Rac1 inhibition. Similarly, both D1/4KO and D1/4KO-DN muscles had markedly reduced contraction-stimulated glucose uptake. Of

note, WT muscles after Rac1 inhibition as well as D1/4KO and D1/4KO-DN muscles treated with DMSO still showed a significant response to the ex vivo contraction stimulus. Additional Rac1 inhibition in D1/4KO and D1/4KO-DN muscles, in contrast, completely ablated the residual contraction-stimulated glucose transport (Fig. 6F). Rac1 inhibition as well as the applied contraction tension did not affect Rac1 protein abundance in EDL muscle (Supplementary Fig. 3A). In addition, the GTPase activity of Rac1 was not directly altered by TBC1D1 or TBC1D4 in vitro (Supplementary Fig.

3B and C). Supplementary Fig. 4 summarizes the observed mouse phenotypes that depend on either the AMPK inactivity or the RabGAP deficiency.

AMP-Activated Protein Kinase-Related Kinase 5 (ARK5)/Novel Kinase Family 1 (NUAK1) Phosphorylates TBC1D1 at Ser660 and Ser700 but not Ser231

We analyzed mRNA and protein expression of AMPK-related kinases (ARKs) downstream of LKB1, *Nuak1*, *Nuak2*, and *Sik1*, 2, and 3, respectively, but found no genotype-dependent

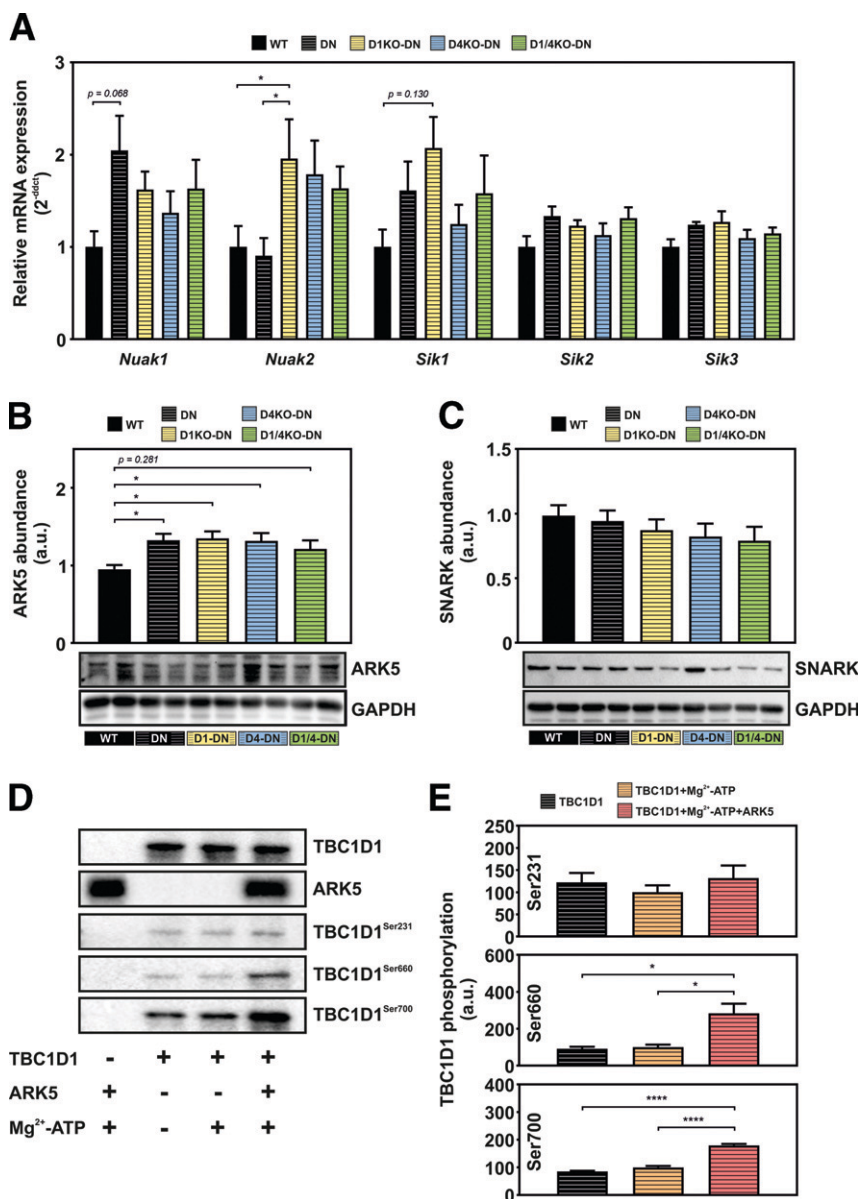


Figure 7—ARK5/NUAK1 phosphorylates TBC1D1 at sites Ser660 and Ser700 but not Ser231. **A**: Gene expression analysis of ARKs *Nuak1*, *Nuak2*, *Sik1*, *Sik2*, and *Sik3* in gastrocnemius muscle of WT, DN, D1KO-DN, D4KO-DN, and D1/4KO-DN mice. **B** and **C**: Representative Western blot of ARK5 and sucrose nonfermenting AMPK-related kinase (SNARK) from WT, DN, D1KO-DN, D4KO-DN, and D1/4KO-DN mice normalized to GAPDH. *n* = 6–15. **P* < 0.05 by one-way ANOVA with Tukey correction. **D**: Purified full-length TBC1D1 was phosphorylated in vitro for 20 min at room temperature in the presence of purified ARK5. **E**: Phosphorylation was confirmed by Western blot analysis using phosphosite-specific antibodies against pSer231, pSer660, and pSer700; quantification of TBC1D1 phosphorylation by ARK5. *n* = 3. Data are mean ± SEM. **P* < 0.05, *****P* < 0.0001, TBC1D1 and TBC1D1 + Mg²⁺-ATP vs. TBC1D1 + Mg²⁺-ATP + ARK5 by one-way ANOVA with Tukey correction. a.u., arbitrary units.

alterations in D1/4KO-DN muscles (Fig. 7A–C). However, to study possible kinase/substrate interactions, we expressed and purified both ARK5 kinase and full-length TBC1D1 using the baculovirus system and conducted phosphorylation assays *in vitro* as described in RESEARCH DESIGN AND METHODS. As illustrated in Fig. 7D and E, incubation of TBC1D1 with recombinant ARK5 led to phosphorylation of AMPK target sites Ser660 and Ser700 but not Ser231.

DISCUSSION

In the current study, we investigated the contribution of AMPK, TBC1D1, and TBC1D4 to contraction-stimulated glucose transport by using novel mouse models that combine deficiency in both AMPK and RabGAP functions. Our results identify a nonredundant fiber type-specific framework of GTPase signaling that controls contraction-dependent glucose transport into skeletal muscle.

We recently analyzed insulin- and AICAR-stimulated glucose transport into intact isolated skeletal muscle from mice lacking either one or both RabGAPs (16,25). Because AICAR may only partially act as a contraction mimetic in skeletal muscle, we conducted in the current study *ex vivo* electrical stimulation and contraction of muscles from KO mice and measured glucose transport. In concordance with AICAR stimulation, contraction-induced glucose uptake in EDL muscle was strongly reduced in D1KO and D1/4KO but not in D4KO muscles, indicating that TBC1D1 has a critical function in glycolytic muscle and that AICAR indeed mimics contraction. However, contraction-induced glucose uptake was normal in the oxidative soleus muscle, whereas AICAR-stimulated glucose uptake was markedly reduced (16), hence dissociating the stimulatory effect of AICAR from muscle contraction. Only combined lack of TBC1D1 and TBC1D4 led to strong reduction in contraction-stimulated glucose transport in soleus muscle.

These findings indicate, at least in oxidative fibers, that 1) TBC1D4 is not essential for contraction-mediated glucose disposal *ex vivo* and 2) the single ablation of each RabGAP isoform leads to compensatory action of the remaining TBC1D protein and that only the complete lack of RabGAPs is sufficient to block the contraction response. Of note, contraction-stimulated glucose uptake was not completely ablated in either muscle type from D1/4KO animals, indicating the involvement of additional factors in this process, one of them most likely being AMPK. To delineate the AMPK-RabGAP signaling axis, we generated animals with muscle-specific AMPK α 2 inactivity (DN) in combination with the deficiency in either one or both RabGAPs. Expectedly, inactivation of the AMPK α 2 subunit led to a substantial decrease in contraction-mediated glucose transport into both soleus and EDL muscle (29). However, in EDL muscle, combined inactivation of AMPK and both RabGAPs was not sufficient to fully abolish contraction-stimulated glucose transport, in contrast to soleus muscle. This indicates that the relevance of the RabGAP-AMPK signaling axis may

depend on divergent metabolic properties of muscle fibers, expression of AMPK subunit isoforms, and intensity/duration of the applied contraction stimulus (38–40). The residual contraction response in D1/4KO-DN EDL muscle, however, suggests the presence of an additional pathway circumventing canonical AMPK-RabGAP signaling, presumably to ensure the integrity of contraction-mediated glucose transport.

The small Rho GTPase Rac1 becomes activated independently of AMPK by mechanical stress or stretching of skeletal muscle during contraction (10–12). Inhibition of Rac1 or KO partially decreased contraction-stimulated glucose uptake in EDL muscle (14). Moreover, Sylov et al. (15) demonstrated that combined inhibition of Rac1 and AMPK only partially prevents glucose uptake in response to contraction, indicating the involvement of multiple signaling routes in this pathway. Here, we show that pharmacological Rac1 inhibition completely abolished contraction-stimulated glucose transport into D1/4KO and D1/4KO-DN EDL muscles, demonstrating that TBC1D RabGAPs and Rac1 operate in concert with AMPK to regulate the GLUT4 translocation machinery. While RabGAPs are believed to regulate critical Rabs localized to GLUT4-containing vesicles, Rac1 is involved in remodeling of the actin cytoskeleton in skeletal muscle (14). Another potentially relevant compound of contraction-mediated glucose transport we identified is the AMPK-related kinase ARK5 as a novel upstream regulator of TBC1D1. ARK5 phosphorylated TBC1D1 at two of the three known AMPK phosphorylation sites, Ser660 and Ser700, while phosphorylation of Ser231, another major AMPK site (41), was not significantly increased by ARK5, possibly because of prephosphorylation of this site.

Previous studies have shown that either muscle contraction, AICAR, or insulin leads to enhanced ARK5 phosphorylation (42). It has been implicated that a muscle-specific loss of ARK5 can prevent high-fat diet-induced glucose intolerance, presumably by suppressing glucose uptake through negative regulation of insulin signaling in skeletal muscle (43). Thus, the ARK5-TBC1D1 interaction may present a key pathway linking muscle contraction to insulin sensitivity. Further studies need to focus on the interface between the two pathways.

Of note, there are clear discrepancies in muscle physiology between *ex vivo* and *in vitro* contraction and *in vivo* exercise. Because of the lack of neuronal interconnectedness and substrate provisioning by the capillary system, both *in vitro* and *ex vivo* systems do not fully reflect the complexity of skeletal muscle metabolism. However, they present useful tools to study specific cellular pathways in a reliable way that may not be possible during *in vivo* studies where circulating and environmental factors add an extensive degree of complexity to the system, potentially hampering the clarity of data interpretation (44,45). Consistent with the impaired contraction-stimulated glucose uptake into isolated skeletal muscles, we found that DN mice exhibit reduced exercise capacity

on treadmills (46). Notably, time to exhaustion was further reduced in D1KO-DN and D1/4KO-DN but not D4KO-DN animals, implying a higher relevance for TBC1D1 in the AMPK-mediated control of physical fitness. In addition, VO_{2max} and skeletal muscle glycogen content (by trend) were exclusively decreased in DN and D1KO-DN animals, again highlighting the tight relationship between this particular RabGAP isoform in controlling exercise performance. Our data concur with that of Stöckli et al. (47), who demonstrated impaired exercise endurance in *Tbc1d1* KO mice, and AMPK-DN mice were shown to be unable to perform high-intensity, but not low-intensity, treadmill exercise (48). Moreover, it has been observed that the activation of the AMPK-TBC1D1 signaling nexus is increased in cyclophilin-D KO mice, thus enabling higher exercise endurance in these mice (49). Nevertheless, reduced mitochondrial oxidative capacity, associated with decreased mitochondrial gene expression of peroxisome proliferator-activated receptor γ coactivator 1 α , cytochrome C, and citrate synthase, may also contribute to impaired exercise tolerance in muscle-specific AMPK α 1, α 2 double KO mice (50).

We found marked differences in the impact of *Tbc1d1* or *Tbc1d4* deficiency on postprandial glycemia and exercise physiology. Lack of TBC1D4, but not TBC1D1, leads to increased postprandial blood glucose and insulin levels, indicating a more prominent role of TBC1D4 in the regulation of postprandial blood glucose levels and insulin action. Accordingly, postprandial hyperglycemia is also strongly associated with a loss-of-function variant of *TBC1D4* that is common in Arctic populations (51). Interestingly, this effect is more pronounced in mice deficient in both RabGAPs (D1/4KO mice), pointing toward potential RabGAP interactions.

After 6 h of fasting, the combined *Tbc1d1* deficiency and AMPK inactivation (D1KO-DN) led to impaired insulin sensitivity, whereas the HOMA-IR index was normal in D4KO-DN and D1/4KO-DN mice. Thus, AMPK, but not TBC1D1, is required for maintaining skeletal muscle insulin sensitivity in the fasted state. In contrast, depletion of *Tbc1d4* leads to a restoration of insulin sensitivity despite the muscular AMPK inactivation, emphasizing the importance of the AMPK-TBC1D4 axis in the regulation of glycemia during fasting. The disparate impact of *Tbc1d1* and *Tbc1d4* deficiency on fasting glycemia and AICAR tolerance, however, cannot be explained by opposite changes in GLUT4 abundance. Instead, GLUT4 abundance in the different muscle types follows the previously observed expression pattern dependent on the RabGAP isoform (16), without further impact because of AMPK inactivation. In accordance with previous results (16), an adverse distribution of energy substrates is associated with RabGAP deficiency but independent from AMPK inactivation. Presumably secondary to the skeletal muscle insulin resistance, liver glycogen stores were depleted, whereas triglyceride levels were increased in RabGAP-deficient animals. In addition, muscle-specific

overexpression of the AMPK-DN variant alone affects hepatic lipid metabolism, as reflected by increased fasting plasma free fatty acid and triglyceride levels in our study. These findings are in accordance with data from other metabolic studies in muscle-specific transgenic mice, demonstrating a complex regulatory pattern of whole-body glycemia involving a diversity of target tissues and organ crosstalk (52–54).

Collectively, our data demonstrate a nonredundant function for TBC1D1 and TBC1D4 in exercise- and insulin-mediated regulation of whole-body glycemia and, more specifically, contraction-induced glucose transport into skeletal muscle. We identify a new signaling axis consisting of two independent GTPase regulators, Rac1 and TBC1D1/4, both direct/indirect targets of AMPK and presumably other kinases, that act in concert to achieve the full contraction-mediated glucose uptake response in skeletal muscle. Shedding light onto these regulatory circuits represents one more step toward the understanding of mechanisms involved in glucose homeostasis.

Acknowledgments. The authors thank Angelika Horrigths, Anette Kurovski, Antonia Osmer, Carina Heitmann, Jennifer Schwettmann, Peter Herdt, and Cornelia Köllmer, German Diabetes Center (DDZ), Leibniz Center for Diabetes Research, Heinrich Heine University Düsseldorf, Germany, for expert technical assistance, support, and consultation. They also thank Dr. Annette Schürmann, Department of Experimental Diabetology, German Institute of Human Nutrition Potsdam-Rehbruecke, Nuthetal, Germany, and German Center for Diabetes Research (DZD), Partner Potsdam-Rehbruecke, München-Neuherberg, Germany, for providing GLUT1 antibodies and Dr. Morris Birnbaum, Pfizer Inc., Cambridge, MA, for providing the transgenic AMPK-DN mouse model. The authors thank Dr. James Hastie, Division of Signal Transduction Therapy, University of Dundee, Dundee, Scotland, U.K., for providing phosphorylated TBC1D1 antibodies.

Funding. This work was supported in part by grants from the Deutsche Forschungsgemeinschaft (DFG-RTG 2576 vivid to H.A.-H. and A.C.; CH1659 to A.C.), Deutsche Diabetes Gesellschaft (DDG), EFSD/Novo Nordisk Programme for Diabetes Research, the Ministry of Science and Research of the State North Rhine-Westphalia, and the German Federal Ministry of Health.

Duality of Interest. No potential conflicts of interest relevant to this article were reported.

Author Contributions. C.d.W., L.E., S.E., C.S., and L.T. performed the experiments and analyzed data. C.d.W., L.E., A.C., and H.A.-H. were involved in the study design, contributed to the data analysis and interpretation, and wrote the manuscript. A.S., A.D.B., T.B., S.C., and T.S. contributed to the data interpretation. A.C. is the guarantor of this work and, as such, had full access to all the data in the study and takes responsibility for the integrity of the data and the accuracy of the data analysis.

References

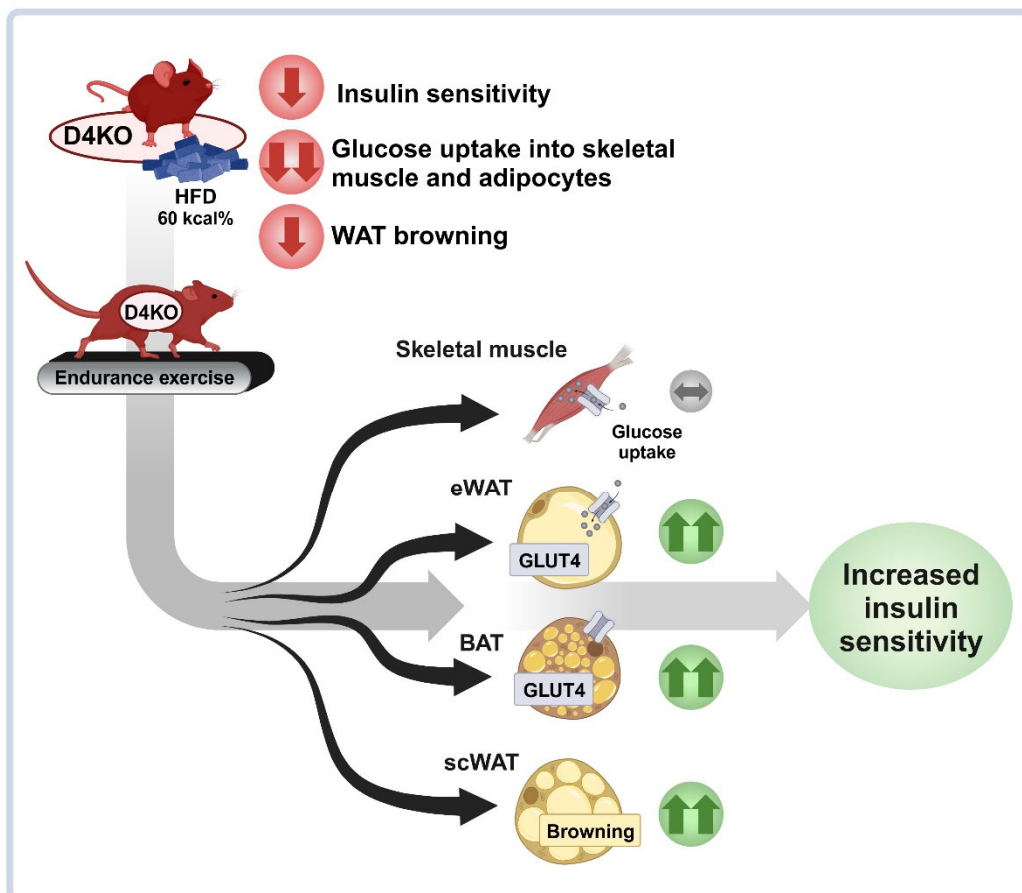
1. DeFronzo RA, Jacot E, Jequier E, Maeder E, Wahren J, Felber JP. The effect of insulin on the disposal of intravenous glucose. Results from indirect calorimetry and hepatic and femoral venous catheterization. *Diabetes* 1981;30:1000–1007
2. Watson RT, Pessin JE. GLUT4 translocation: the last 200 nanometers. *Cell Signal* 2007;19:2209–2217

3. Rose AJ, Jeppesen J, Kiens B, Richter EA. Effects of contraction on localization of GLUT4 and v-SNARE isoforms in rat skeletal muscle. *Am J Physiol Regul Integr Comp Physiol* 2009;297:R1228–R1237
4. Richter EA, Hargreaves M. Exercise, GLUT4, and skeletal muscle glucose uptake. *Physiol Rev* 2013;93:993–1017
5. Coven DL, Hu X, Cong L, et al. Physiological role of AMP-activated protein kinase in the heart: graded activation during exercise. *Am J Physiol Endocrinol Metab* 2003;285:E629–E636
6. Hayashi T, Hirshman MF, Kurth EJ, Winder WW, Goodyear LJ. Evidence for 5' AMP-activated protein kinase mediation of the effect of muscle contraction on glucose transport. *Diabetes* 1998;47:1369–1373
7. Merrill GF, Kurth EJ, Hardie DG, Winder WW. AICA riboside increases AMP-activated protein kinase, fatty acid oxidation, and glucose uptake in rat muscle. *Am J Physiol* 1997;273:E1107–E1112
8. Jeppesen J, Maarbjerg SJ, Jordy AB, et al. LKB1 regulates lipid oxidation during exercise independently of AMPK. *Diabetes* 2013;62:1490–1499
9. Hardie DG, Alessi DR. LKB1 and AMPK and the cancer-metabolism link – ten years after. *BMC Biol* 2013;11:36
10. Ito Y, Obara K, Ikeda R, et al. Passive stretching produces Akt- and MAPK-dependent augmentations of GLUT4 translocation and glucose uptake in skeletal muscles of mice. *Pflugers Arch* 2006;451:803–813
11. Chambers MA, Moylan JS, Smith JD, Goodyear LJ, Reid MB. Stretch-stimulated glucose uptake in skeletal muscle is mediated by reactive oxygen species and p38 MAP-kinase. *J Physiol* 2009;587:3363–3373
12. Sylow L, Møller LL, Kleinert M, Richter EA, Jensen TE. Stretch-stimulated glucose transport in skeletal muscle is regulated by Rac1. *J Physiol* 2015;593:645–656
13. Sylow L, Nielsen IL, Kleinert M, et al. Rac1 governs exercise-stimulated glucose uptake in skeletal muscle through regulation of GLUT4 translocation in mice. *J Physiol* 2016;594:4997–5008
14. Sylow L, Møller LL, Kleinert M, Richter EA, Jensen TE. Rac1—a novel regulator of contraction-stimulated glucose uptake in skeletal muscle. *Exp Physiol* 2014;99:1574–1580
15. Sylow L, Møller LL, Kleinert M, et al. Rac1 and AMPK account for the majority of muscle glucose uptake stimulated by ex vivo contraction but not in vivo exercise. *Diabetes* 2017;66:1548–1559
16. Chadt A, Immisch A, de Wendt C, et al. “Deletion of both Rab-GTPase-activating proteins TBC1D1 and TBC1D4 in mice eliminates insulin- and AICAR-stimulated glucose transport [corrected]. *Diabetes* 2015;64:746–759
17. Espelage L, Al-Hasani H, Chadt A. RabGAPs in skeletal muscle function and exercise. *J Mol Endocrinol* 2020;64:R1–R19
18. Szekeres F, Chadt A, Tom RZ, et al. The Rab-GTPase-activating protein TBC1D1 regulates skeletal muscle glucose metabolism. *Am J Physiol Endocrinol Metab* 2012;303:E524–E533
19. Chadt A, Leicht K, Deshmukh A, et al. Tbc1d1 mutation in lean mouse strain confers leanness and protects from diet-induced obesity. *Nat Genet* 2008;40:1354–1359
20. Dokas J, Chadt A, Nolden T, et al. Conventional knockout of Tbc1d1 in mice impairs insulin- and AICAR-stimulated glucose uptake in skeletal muscle. *Endocrinology* 2013;154:3502–3514
21. Wang HY, Ducommun S, Quan C, et al. AS160 deficiency causes whole-body insulin resistance via composite effects in multiple tissues. *Biochem J* 2013;449:479–489
22. Lansley MN, Walker NN, Hargrett SR, Stevens JR, Keller SR. Deletion of Rab GAP AS160 modifies glucose uptake and GLUT4 translocation in primary skeletal muscles and adipocytes and impairs glucose homeostasis. *Am J Physiol Endocrinol Metab* 2012;303:E1273–E1286
23. Taylor EB, An D, Kramer HF, et al. Discovery of TBC1D1 as an insulin-, AICAR-, and contraction-stimulated signaling nexus in mouse skeletal muscle. *J Biol Chem* 2008;283:9787–9796
24. Albers PH, Pedersen AJ, Birk JB, et al. Human muscle fiber type-specific insulin signaling: impact of obesity and type 2 diabetes. *Diabetes* 2015;64:485–497
25. Hargrett SR, Walker NN, Keller SR. Rab GAPs AS160 and Tbc1d1 play nonredundant roles in the regulation of glucose and energy homeostasis in mice. *Am J Physiol Endocrinol Metab* 2016;310:E276–E288
26. JeBailey L, Wanono O, Niu W, Roesler J, Rudich A, Klip A. Ceramide- and oxidant-induced insulin resistance involve loss of insulin-dependent Rac-activation and actin remodeling in muscle cells. *Diabetes* 2007;56:394–403
27. Tsakiridis T, Vranic M, Klip A. Disassembly of the actin network inhibits insulin-dependent stimulation of glucose transport and prevents recruitment of glucose transporters to the plasma membrane. *J Biol Chem* 1994;269:29934–29942
28. Wright DC, Hucker KA, Holloszy JO, Han DH. Ca²⁺ and AMPK both mediate stimulation of glucose transport by muscle contractions. *Diabetes* 2004;53:330–335
29. Mu J, Brozinick JT Jr, Valladares O, Bucan M, Birnbaum MJ. A role for AMP-activated protein kinase in contraction- and hypoxia-regulated glucose transport in skeletal muscle. *Mol Cell* 2001;7:1085–1094
30. Jørgensen SB, Viollet B, Andreelli F, et al. Knockout of the alpha2 but not alpha1 5'-AMP-activated protein kinase isoform abolishes 5-aminoimidazole-4-carboxamide-1-beta-4-ribofuranoside but not contraction-induced glucose uptake in skeletal muscle. *J Biol Chem* 2004;279:1070–1079
31. Jensen TL, Kiersgaard MK, Sørensen DB, Mikkelsen LF. Fasting of mice: a review. *Lab Anim* 2013;47:225–240
32. Roza NA, Possignolo LF, Palanch AC, Gontijo JA. Effect of long-term high-fat diet intake on peripheral insulin sensibility, blood pressure, and renal function in female rats. *Food Nutr Res* 2016;60:28536
33. Mafakheri S, Förke RR, Kannigießer S, et al. AKT and AMP-activated protein kinase regulate TBC1D1 through phosphorylation and its interaction with the cytosolic tail of insulin-regulated aminopeptidase IRAP. *J Biol Chem* 2018;293:17853–17862
34. Eickelschulte S, Hartwig S, Leiser B, et al. AKT/AMPK-mediated phosphorylation of TBC1D4 disrupts the interaction with insulin-regulated aminopeptidase. *J Biol Chem* 2021;296:100637
35. Livak KJ, Schmittgen TD. Analysis of relative gene expression data using real-time quantitative PCR and the 2(-delta)Ct method. *Methods* 2001;25:402–408
36. Passonneau JV, Lauderdale VR. A comparison of three methods of glycogen measurement in tissues. *Anal Biochem* 1974;60:405–412
37. Sun X, Gao L, Chien HY, Li WC, Zhao J. The regulation and function of the NUA family. *J Mol Endocrinol* 2013;51:R15–R22
38. Medler S. Mixing it up: the biological significance of hybrid skeletal muscle fibers. *J Exp Biol* 2019;222:jeb200832
39. Chen Z, Heierhorst J, Mann RJ, et al. Expression of the AMP-activated protein kinase beta1 and beta2 subunits in skeletal muscle. *FEBS Lett* 1999;460:343–348
40. MacInnis MJ, Gibala MJ. Physiological adaptations to interval training and the role of exercise intensity. *J Physiol* 2017;595:2915–2930
41. Vichaiwong K, Purohit S, An D, et al. Contraction regulates site-specific phosphorylation of TBC1D1 in skeletal muscle. *Biochem J* 2010;431:311–320
42. Fisher JS, Ju JS, Oppelt PJ, Smith JL, Suzuki A, Esumi H. Muscle contractions, AICAR, and insulin cause phosphorylation of an AMPK-related kinase. *Am J Physiol Endocrinol Metab* 2005;289:E986–E992
43. Inazuka F, Sugiyama N, Tomita M, Abe T, Shioi G, Esumi H. Muscle-specific knock-out of NUA family SNF1-like kinase 1 (NUAK1) prevents high fat diet-induced glucose intolerance. *J Biol Chem* 2012;287:16379–16389
44. Carter S, Solomon TPJ. In vitro experimental models for examining the skeletal muscle cell biology of exercise: the possibilities, challenges and future developments. *Pflugers Arch* 2019;471:413–429
45. Kjøbsted R, Kido K, Larsen JK, et al. Measurement of insulin- and contraction-stimulated glucose uptake in isolated and incubated mature skeletal muscle from mice. *J Vis Exp* 2021;(171):e61398

46. Mu J, Barton ER, Birnbaum MJ. Selective suppression of AMP-activated protein kinase in skeletal muscle: update on 'lazy mice'. *Biochem Soc Trans* 2003;31:236–241
47. Stöckli J, Meoli CC, Hoffman NJ, et al. The RabGAP TBC1D1 plays a central role in exercise-regulated glucose metabolism in skeletal muscle. *Diabetes* 2015;64:1914–1922
48. Miura S, Kai Y, Kamei Y, et al. Alpha2-AMPK activity is not essential for an increase in fatty acid oxidation during low-intensity exercise. *Am J Physiol Endocrinol Metab* 2009;296:E47–E55
49. Radhakrishnan J, Baetiong A, Kaufman H, et al. Improved exercise capacity in cyclophilin-D knockout mice associated with enhanced oxygen utilization efficiency and augmented glucose uptake via AMPK-TBC1D1 signaling nexus. *FASEB J* 2019;33:11443–11457
50. Lantier L, Fentz J, Mounier R, et al. AMPK controls exercise endurance, mitochondrial oxidative capacity, and skeletal muscle integrity. *FASEB J* 2014;28:3211–3224
51. Moltke I, Grarup N, Jørgensen ME, et al. A common Greenlandic TBC1D4 variant confers muscle insulin resistance and type 2 diabetes. *Nature* 2014;512:190–193
52. Bertholdt L, Gudiksen A, Jessen H, Pilegaard H. Impact of skeletal muscle IL-6 on regulation of liver and adipose tissue metabolism during fasting. *Pflugers Arch* 2018;470:1597–1613
53. Knudsen JG, Gudiksen A, Bertholdt L, et al. Skeletal muscle IL-6 regulates muscle substrate utilization and adipose tissue metabolism during recovery from an acute bout of exercise. *PLoS One* 2017;12:e0189301
54. Zhang W, Yang D, Yuan Y, et al. Muscular G9a regulates muscle-liver-fat axis by musclin under overnutrition in female mice. *Diabetes* 2020;69:2642–2654

Depletion of TBC1D4 Improves the Metabolic Exercise Response by Overcoming Genetically Induced Peripheral Insulin Resistance

Christian Springer, Christian Binsch, Deborah Weide, Laura Toska, Anna L. Cremer, Heiko Backes, Anna K. Scheel, Lena Espelage, Jörg Kotzka, Sebastian Sill, Anette Kurowski, Daebin Kim, Sandra Karpinski, Theresia M. Schnurr, Torben Hansen, Sonja Hartwig, Stefan Lehr, Sandra Cames, Jens C. Brüning, Matthias Lienhard, Ralf Herwig, Stefan Böro, Bernd Timmermann, Hadi Al-Hasani, and Alexandra Chadt



BAT, brown adipose tissue; D4KO, *Tbc1d4*-deficient; eWAT, epididymal white adipose tissue; HFD, high-fat diet; scWAT, subcutaneous white adipose tissue; WAT, white adipose tissue. Figure created with BioRender.com



Depletion of TBC1D4 Improves the Metabolic Exercise Response by Overcoming Genetically Induced Peripheral Insulin Resistance

Christian Springer,^{1,2} Christian Binsch,^{1,2} Deborah Weide,^{1,2} Laura Toska,^{1,2} Anna L. Cremer,³ Heiko Backes,³ Anna K. Scheel,^{1,2} Lena Espelage,^{1,2} Jörg Kotzka,^{1,2} Sebastian Sill,^{1,2} Anette Kurowski,¹ Daebin Kim,¹ Sandra Karpinski,¹ Theresia M. Schnurr,⁴ Torben Hansen,⁴ Sonja Hartwig,^{1,2} Stefan Lehr,^{1,2} Sandra Cames,^{1,2} Jens C. Brüning,³ Matthias Lienhard,⁵ Ralf Herwig,⁵ Stefan Börho,⁵ Bernd Timmermann,⁵ Hadi Al-Hasani,^{1,2} and Alexandra Chadt^{1,2}

Diabetes 2024;73:1058–1071 | <https://doi.org/10.2337/db23-0463>

The Rab-GTPase-activating protein (RabGAP) TBC1D4 (AS160) represents a key component in the regulation of glucose transport into skeletal muscle and white adipose tissue (WAT) and is therefore crucial during the development of insulin resistance and type 2 diabetes. Increased daily activity has been shown to be associated with improved postprandial hyperglycemia in allele carriers of a loss-of-function variant in the human TBC1D4 gene. Using conventional Tbc1d4-deficient mice (D4KO) fed a high-fat diet, we show that moderate endurance exercise training leads to substantially improved glucose and insulin tolerance and enhanced expression levels of markers for mitochondrial activity and browning in WAT from D4KO animals. Importantly, in vivo and ex vivo analyses of glucose uptake revealed increased glucose clearance in interscapular brown adipose tissue and WAT from trained D4KO mice. Thus, chronic exercise is able to overcome the genetically induced insulin resistance caused by Tbc1d4 depletion. Gene variants in TBC1D4 may be relevant in future precision medicine as determinants of exercise response.

Insulin resistance represents an important hallmark in the pathophysiology of type 2 diabetes (1). As major target tissues for insulin action, the skeletal muscle and the white adipose

ARTICLE HIGHLIGHTS

- The study was conducted to unravel the mechanistic basis of exercise-mediated improvements of insulin resistance.
- We wanted to answer whether genetically induced insulin resistance as present upon deletion of the insulin signaling factor TBC1D4 can be rescued by endurance exercise training in *Tbc1d4*-deficient mice.
- We show that deletion of *Tbc1d4* leads to an enhanced exercise response as presented by improved insulin sensitivity, especially in the adipose tissue.
- *TBC1D4* gene variants may serve as potential predictive markers for precision medicine approaches.

tissue (WAT) are of vital importance in glucose disposal. In response to insulin stimulation, GLUT4 translocates from intracellular storage vesicles to the plasma membrane, thereby facilitating enhanced glucose clearance from the blood stream (2). In both skeletal muscle and WAT, GLUT4 translocation is induced by multiple phosphorylation events downstream of the insulin receptor, eventually resulting in activation of the serine/threonine kinase AKT. Interestingly, muscle contraction

¹Institute for Clinical Biochemistry and Pathobiochemistry, Medical Faculty, German Diabetes Center (DDZ), Leibniz-Center for Diabetes Research at the Heinrich Heine University, Düsseldorf, Germany

²German Center for Diabetes Research, Partner Düsseldorf, München-Neuherberg, Germany

³Max Planck Institute for Metabolism Research, Department of Neuronal Control of Metabolism, Cologne, Germany

⁴Novo Nordisk Foundation Center for Basic Metabolic Research, Faculty of Health and Medical Sciences, University of Copenhagen, Copenhagen, Denmark

⁵Max Planck Institute for Molecular Genetics, Berlin, Germany

Corresponding authors: Alexandra Chadt, alexandra.chadt@ddz.de, and Hadi Al-Hasani, hadi.al-hasani@ddz.de

Received 12 June 2023 and accepted 2 April 2024

This article contains supplementary material online at <https://doi.org/10.2337/figshare.25578054>.

© 2024 by the American Diabetes Association. Readers may use this article as long as the work is properly cited, the use is educational and not for profit, and the work is not altered. More information is available at <https://www.diabetesjournals.org/journals/pages/license>.

leads to an AKT (and thus insulin)-independent increase in GLUT4 translocation mainly, but not exclusively, via the activation of another serine/threonine kinase, AMPK (3,4). As a direct downstream target of both AKT and AMPK, the Rab-GTPase-activating protein (RabGAP) TBC1D4 holds a key role in conveying GLUT4 translocation by catalyzing the GTP hydrolysis activity of small Rab-GTPases located in GLUT4 storage vesicles (5). We and others previously demonstrated that depletion of TBC1D4 in mice leads to substantially impaired insulin- and contraction-stimulated glucose transport into oxidative skeletal muscle. In addition, D4KO animals display severely reduced insulin-stimulated uptake of glucose into adipose tissue (6–12). These findings are in line with a strong reduction of GLUT4 protein abundance in the respective tissue type due to the *Tbc1d4* deficiency. TBC1D4 has also been implicated to play an important role in human metabolic disorders. A premature stop mutation (R363X) in the human *TBC1D4* gene was shown to lead to extreme postprandial hyperinsulinemia, presumably by interfering with its wild-type (WT) counterpart in a dominant-negative fashion and reducing GLUT4 membrane localization (13,14). More recently, a muscle-specific nonsense *TBC1D4* p.Arg684Ter stop mutation was described in Arctic populations, defining a specific subtype of nonautoimmune diabetes characterized by elevated postprandial glucose levels and increased type 2 diabetes risk (15,16). Strikingly, an increase of daily physical activity, as assessed using retrospective survey data, was shown to be associated with improved whole-body glycemia, especially in homozygous *TBC1D4* risk allele carriers, providing a rationale for the implementation of exercise as lifestyle intervention therapy in Arctic populations (17). How exactly exercise can overcome peripheral insulin resistance and which contribution to exercise-related improvements of insulin sensitivity is being made by TBC1D4 are not yet understood.

To clarify the mechanisms underlying the impact of TBC1D4 on exercise-mediated improvements in insulin sensitivity, we conducted a chronic exercise intervention study using conventional *Tbc1d4*-deficient (D4KO) mice. The overarching goal of this research was to unravel the complex relationship between specific cellular compounds of the insulin signaling pathway and exercise physiology with the hope to eventually enable new approaches in precision medicine and provide recommendations for patients experiencing disturbed insulin sensitivity.

RESEARCH DESIGN AND METHODS

Chemicals and Buffers

Chemicals, buffer ingredients, and buffers are listed in Supplementary Tables 1 and 2.

Experimental Animals

Male WT and D4KO mice were generated as previously described (7). Animals were kept in accordance with the National Institutes of Health guidelines for the care and use of laboratory animals. All experiments were approved by the ethics committee of the State Ministry of Agriculture, Nutrition

and Forestry (State of North Rhine-Westphalia, Germany). Three to six males per cage (Makrolon type III) were housed with ad libitum access to food and water at 22°C and a 12-h light-dark cycle. After weaning, animals received a standard diet (9% kcal from fat). At the age of 10 weeks, animals received a high-fat diet (HFD) (60% kcal from fat) or remained on the standard diet until the end of the intervention. Detailed compositions of the animal diets are listed in Supplementary Table 3. Tissues and plasma of mice were harvested 24 h after the last exercise bout in week 18. Genotyping of mice was performed by PCR as previously described (7). Sequences of genotyping primers are listed in Supplementary Table 4.

Treadmill Training and Exhaustion Running Test

Mice were subjected to 4 weeks of moderate endurance training on treadmills (TSE Systems, Bad Homburg, Germany), with training sessions 5 days per week, one training session per day starting in week of life 14, or they remained sedentary (18). A detailed description of the treadmill training can be found in the Supplementary Methods.

Tolerance Tests

For tolerance tests, sterile glucose (2 g/kg body weight, 20% solution for the glucose tolerance test [GTT]), human recombinant insulin (1 unit/kg body weight for the insulin tolerance test [ITT]), or sterile pyruvate (1 g/kg body weight, 10% solution for the pyruvate tolerance test [PTT]) was injected intraperitoneally (i.p.) into 6-h-fasted (i.p.GTT), random-fed (i.p.ITT), or 16-h-fasted (i.p.PTT) animals ($n = 6–11$) in the final week of training. Blood samples were taken at 0, 15, 30, 60, and 120 min (i.p.GTT, i.p.PTT) or 0, 15, 30, and 60 min (i.p.ITT) from the tail tip.

Plasma Analysis

Blood glucose concentrations were determined with a glucometer (Contour; Bayer, Leverkusen, Germany). Plasma insulin levels were measured using ELISA (DRG Instruments, Marburg, Germany) in $n = 6–9$ mice per group. The HOMA of insulin resistance (HOMA-IR) index was calculated from blood glucose and plasma insulin data as described previously (12).

Body Composition

Body weight was measured with an electronic scale (Sartorius, Göttingen, Germany), and body composition was analyzed with an MRI (EchoMRI, Houston, TX) in $n = 6–9$ mice.

Glucose Uptake Into Isolated Skeletal Muscles and White Adipocytes

Glucose uptake in intact isolated skeletal muscles ($n = 11–12$) was assessed ex vivo by measuring the incorporation of radioactively labeled [^3H]2-deoxyglucose (Hartmann Analytic, Braunschweig, Germany) as described previously (19). Glucose uptake in isolated white adipocytes (WACs) ($n = 12$) was assessed ex vivo by measuring the incorporation of

radioactively labeled [^{14}C]D-glucose (Hartmann Analytic) as described previously (7). Detailed protocols of glucose uptake assays can be found in the Supplementary Methods.

Sample Processing, SDS-PAGE, and Western blotting

Protein lysates (20 μg) were separated by SDS-PAGE using 8–12% custom-made or precast stain-free (UCP-1, Any kD Mini-PROTEAN TGX; Bio-Rad Laboratories, Hercules, CA) gels. Immunoblotting and detection was performed as described previously (9). Antibodies are depicted in Supplementary Table 5.

Positron Emission Tomography Imaging of Whole-Body Glucose Uptake

Whole-body glucose uptake of sedentary and trained D4KO mice ($n = 4\text{--}6$) was measured via positron emission tomography (PET)/CT scanner (Inveon; Siemens Healthineers, Erlangen, Germany) using (^{18}F)-2-fluoro-deoxy-D-glucose as a tracer after intravenous injection of glucose. A detailed protocol is listed in the Supplementary Methods.

Skeletal Muscle Fiber Type Composition

Fiber type-specific antibodies (Supplementary Table 6) were produced as described previously (20) using myosin heavy chain-specific mouse hybridoma cell lines and purified via Protein G Sepharose affinity chromatography or concentrated using Amicon filters. Mouse muscles ($n = 7\text{--}10$ per group) were embedded in gum tragacanth and snap frozen in liquid nitrogen-cooled isopentane, and cross sections were prepared using a precooled cryostat. A detailed purification and staining protocol is shown in the Supplementary Methods.

Lipid Profiling

Skeletal muscle total fatty acid (FA) content and specific fractional composition of FAs from all groups ($n = 6$) were determined by gas chromatography in gastrocnemius muscle as described previously (21). The FA nomenclature adheres to that of the International Union of Pure and Applied Chemistry (22).

RNA Extraction, cDNA Synthesis, and Real-Time PCR

RNA from $n = 8\text{--}15$ mice was extracted using the miRNeasy Mini Kit (QIAGEN, Hilden, Germany), and cDNA was synthesized using the GoScript Reverse Transcriptase system (Promega, Madison, WI) with 1 μg RNA using random hexanucleotide primers (Roche, Mannheim, Germany). Quantitative real-time PCR was performed using SYBR Green PCR primers (Supplementary Table 7). Expression was normalized to *Hprt* according to the $2^{-\Delta\Delta\text{Ct}}$ method (23).

RNA Sequencing and Transcriptome Analysis

RNA from sedentary and trained D4KO mice ($n = 4\text{--}6$) was isolated using the miRNeasy Mini Kit, and Illumina sequencing of stranded mRNA and subsequent Ingenuity

Pathway Analysis (IPA) was performed as described in the Supplementary Methods. The cutoff for differentially expressed genes in the IPA was set at an adjusted $P < 0.05$ for all analyses.

Statistical Analysis

Data are reported as mean \pm SEM. Significant differences were determined by two-way ANOVA (post hoc test, Bonferroni correction) or unpaired, two-tailed Student t test, as indicated in the figure legends. $P < 0.05$ was considered statistically significant.

Data and Resource Availability

Data supporting the findings of this study are available upon reasonable request from the corresponding authors. RNA sequencing data have been deposited in the BioProject/Sequence Read Archive database (accession no. PRJNA957970).

RESULTS

D4KO Mice Fed a Standard Diet Show Unaltered Insulin Sensitivity Independent of Chronic Exercise Training

We first sought to explore the effect of a moderate-intensity endurance exercise training on whole-body glycemia in D4KO and respective WT littermates kept on a standard chow diet. Consistent with our previous findings (7), glucose tolerance was not impaired in sedentary D4KO mice fed a standard diet, and 4 weeks of chronic exercise training did not alter glucose tolerance in WT or D4KO mice (Fig. 1A). Comparing the physical capacity before and after the exercise intervention, WT mice displayed significantly increased time to exhaustion post the intervention (Fig. 1B). Although not showing a significant increase, running capacity in trained D4KO mice was comparable to WT littermates. A similar pattern of physical capacity was observed when comparing age-matched sedentary and trained mice at the end of the intervention (Supplementary Fig. 1A). Body weight before and after the exercise training was not different between the groups (Supplementary Fig. 1B).

Chronic Exercise Improves Insulin Sensitivity and Running Capacity in D4KO Mice Fed an HFD

To induce a moderate degree of insulin resistance to the relative diabetes-resistant C57BL/6J (B6) genetic background, D4KO and WT mice were subjected to an HFD with 60% kcal from fat and trained for 4 weeks with the same moderate-intensity treadmill protocol as the standard diet cohort. Eight weeks of HFD feeding led to moderately increased 6-h-fasted blood glucose and plasma insulin levels in WT and D4KO mice (Supplementary Fig. 1C–F), resulting in an increased HOMA-IR for the HFD-fed animals (Fig. 1C). D4KO mice showed the highest degree of insulin resistance, which was prevented after chronic exercise training. Moreover, D4KO mice demonstrated markedly improved glucose and insulin tolerance in response to exercise, as indicated by decreased blood glucose levels during the tolerance tests

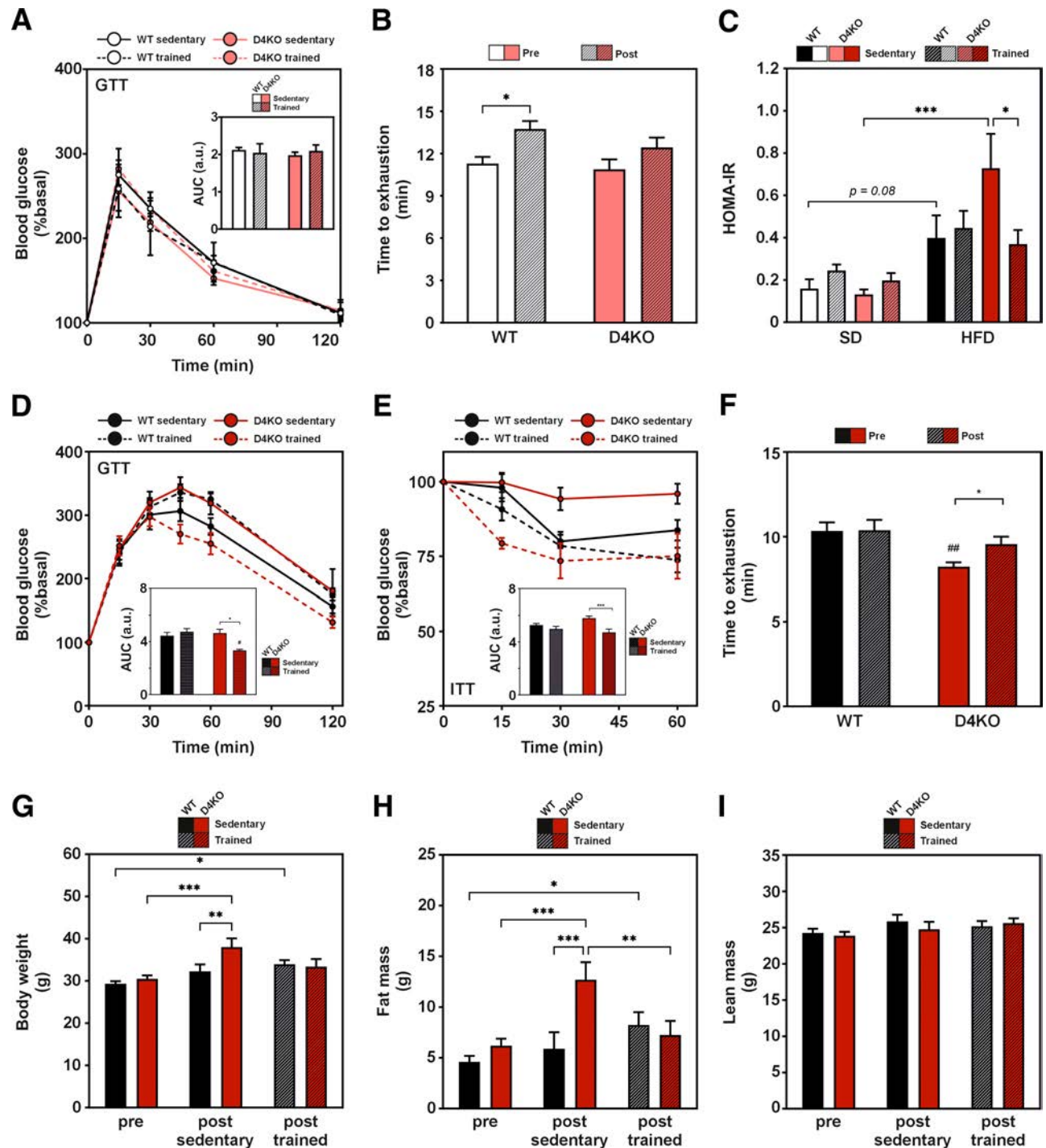


Figure 1—Chronic exercise improves insulin sensitivity and enhances physical capacity in D4KO mice fed an HFD. **A:** Blood glucose concentrations and area under the curve (AUC) (inset) of blood glucose clearance during i.p.GTT of sedentary and trained WT and D4KO male mice fed a standard chow diet ($n = 6$). **B:** Time to exhaustion during exhaustion running tests performed in trained WT and D4KO male mice fed a standard diet before (pre) and after (post) the 4-week exercise intervention ($n = 6$). **C:** HOMA-IR index calculated from 6-h-fasted blood glucose and plasma insulin concentrations from sedentary and trained WT and D4KO male mice fed a standard diet or an HFD ($n = 6-9$). **D:** Blood glucose concentrations and AUC (inset) of blood glucose clearance during i.p.GTT of sedentary and trained WT and D4KO male mice fed an HFD ($n = 8-9$). **E:** Blood glucose concentrations and AUC (inset) of blood glucose clearance during i.p.ITT of sedentary and trained WT and D4KO male mice ($n = 8-9$). **F:** Time to exhaustion during exhaustion running tests performed in trained WT and D4KO male mice pre and post the 4-week exercise intervention ($n = 8$). **G-I:** Body weight (G), body fat content (H), and lean mass (I) of sedentary and trained WT and D4KO male mice pre and post the 4-week exercise intervention ($n = 8-9$). Data are mean \pm SEM. * $P < 0.05$, ** $P < 0.01$, *** $P < 0.001$ between indicated groups; # $P < 0.05$, ## $P < 0.01$ in D4KO vs. corresponding WT control (two-way ANOVA with Bonferroni correction). a.u., arbitrary unit.

(Fig. 1D and E). In exhaustion running tests, untrained D4KO mice demonstrated reduced time to exhaustion compared with WT mice. Chronic exercise training ablated this impairment, with D4KO mice showing a comparable running duration to WT controls (Fig. 1F). Of note, trained WT mice did not show improved running capacity before and after the intervention but exhibited enhanced time to exhaustion after 4 weeks of training compared with age-matched sedentary controls (Supplementary Fig. 2A). Neither $\dot{V}O_{2\max}$ nor the respiratory exchange ratio during the exhaustion running test or blood lactate levels before and after one exercise bout were different between the groups (Supplementary Fig. 2B–D). Sedentary D4KO mice showed a significant increase of body weight and fat mass after 4 weeks of HFD feeding, which was prevented in trained D4KO mice (Fig. 1G and H). Lean mass of all groups remained unchanged (Fig. 1I).

Enhanced Insulin Sensitivity in Trained D4KO Mice Is Not Associated With Improved Skeletal Muscle Glucose Uptake

We next investigated whether the improved insulin sensitivity in trained D4KO mice was associated with improved skeletal muscle glycemia. In accordance with previous results (7,8,10,11), *ex vivo* insulin-stimulated glucose uptake into isolated soleus muscle was abrogated in sedentary D4KO mice. Exercise training led to significantly improved insulin-stimulated glucose uptake in both WT and D4KO mice; however, in D4KO muscle, it was not restored to WT levels after the training period (Fig. 2A). Moreover, expressing the data as fold over basal showed that the insulin-stimulated glucose uptake was almost abolished in D4KO mice independent of the training status (Supplementary Fig. 2E). Subsequent Western blot analyses did not reveal significant differences in abundance or phosphorylation of skeletal muscle AKT at Ser473 or AMPK at Thr172 (Fig. 2B–D). In oxidative soleus muscle, GLUT4 protein abundance was markedly reduced in sedentary D4KO mice compared with WT mice, without further changes after exercise training (Fig. 2E). In contrast, there were no alterations in insulin-stimulated glucose uptake or GLUT4 abundance in glycolytic extensor digitorum longus (EDL) muscle between the groups (Supplementary Fig. 2F and G). Abundances of muscular GLUT1 and hexokinase 2 (HKII) proteins were not altered upon exercise training in D4KO mice (Fig. 2F and G). In addition, abundance of TBC1D1, the closest homolog of TBC1D4, was not changed between the groups in soleus muscle (Supplementary Fig. 2H). Skeletal muscle glycogen content was slightly elevated in trained WT mice compared with sedentary controls but unchanged in D4KO animals (Supplementary Fig. 2I). We determined skeletal muscle fiber type composition by immunohistochemistry. Composition of glycolytic type II B, type II X, and glycolytic-oxidative type II A fibers were not changed in EDL muscle from either WT or D4KO mice after training (Fig. 2H). In the oxidative soleus muscle, only a few glycolytic fibers could be detected in some of the groups, and composition of type II A and purely oxidative type I fibers were not changed in WT or D4KO mice (Fig. 2I). We further

investigated a possible impact of *Tbc1d4* deficiency on hepatic glucose output. Pyruvate tolerance as a marker for hepatic gluconeogenesis was moderately, but not significantly improved in WT mice after training but was unchanged in trained versus sedentary D4KO mice (Supplementary Fig. 3).

Skeletal Muscle FA Metabolism Is Elevated in Trained D4KO Mice

Since TBC1D4 is important in the regulation of not only glucose but also skeletal muscle lipid metabolism (7,21), we further examined whether chronic exercise training led to altered lipid use in this tissue. Determination of total FA content in gastrocnemius muscle by gas chromatography showed that compared with WT controls, total FAs were elevated in sedentary D4KO mice but significantly reduced after exercise training (Fig. 3A). Determination of total triglyceride content in skeletal muscle demonstrated a similar trend between the groups (Supplementary Fig. 4A). Lipid species analysis revealed a reduced content of saturated FAs in sedentary D4KO versus WT mice, which was increased to WT levels after chronic exercise (Fig. 3B), whereas the amount of monounsaturated FAs was increased in the sedentary state but reduced after training in D4KO mice (Fig. 3C). Levels of total polyunsaturated FAs were not different between the groups (Fig. 3D). Amounts of C18:0 (octadecanoic acid) and C20:4 (arachidonic acid) were increased, but C16:1 (palmitoleic acid) content was decreased in trained versus sedentary D4KO mice (Fig. 3E and F). D9-desaturase indices were also reduced in trained D4KO mice, whereas the D6-desaturase index was not significantly altered (Fig. 3G and Supplementary Fig. 4B and C). The amount of essential FAs was increased in sedentary D4KO mice but reduced after chronic exercise, whereas levels of nonesterified FAs were unaltered between the groups (Supplementary Fig. 4D and E). RNA sequencing was performed in gastrocnemius muscle from sedentary and trained D4KO mice. IPA of differentially expressed genes (Fig. 3H) showed upregulation of the oxidative phosphorylation (OXPHOS) pathway and increased expression of related genes in trained versus sedentary D4KO mice (Fig. 3I and J). Moreover, genes regulating oxidative metabolism, such as *Ppargc1a* and *Pparg*, were identified as the top activated upstream regulators in trained D4KO mice (Fig. 3I and K).

Transcriptome Analysis Reveals Increased Expression Levels of Browning Genes in WAT From Trained D4KO Mice

Since trained D4KO mice showed enhanced OXPHOS in skeletal muscle, we also investigated gene expression levels of markers for mitochondrial activity in WAT and BAT, tissues with high TBC1D4 expression (8). RNA sequencing and subsequent IPA of differentially expressed genes from WAT of sedentary versus trained D4KO mice (Fig. 4A) revealed downregulation of pathways and upstream regulators (*Tnf*, *Il-6*, and *Il-4*) mainly related to immune response and inflammation (Fig. 4B). Moreover, transforming growth factor β -1 (*Tgfb1*) signaling was identified as one of the top

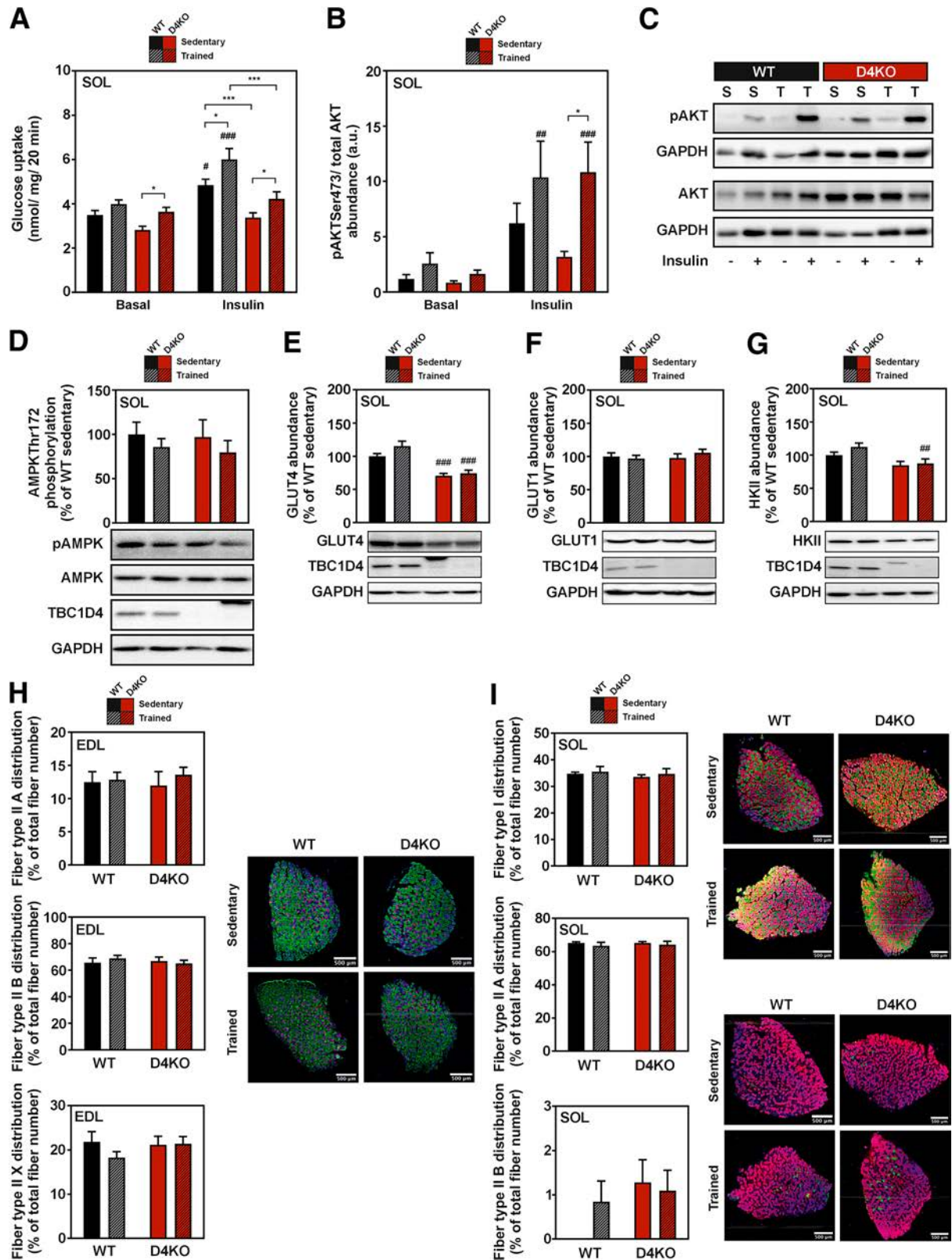


Figure 2—Skeletal muscle glucose uptake and fiber type composition is unaltered in trained D4KO mice. *A*: Ex vivo glucose uptake in isolated soleus (SOL) muscles of sedentary and trained WT and D4KO male mice at basal or insulin-stimulated conditions ($n = 11$ – 12). *B* and *C*: Abundance of phosphorylated AKT (pAKT) at Ser473 in relation to total AKT content from ex vivo glucose uptake muscle samples ($n = 6$ – 8) and representative Western blot images. *D*–*G*: Abundances of pAMPK at Thr172 (*D*), GLUT4 (*E*), GLUT1 (*F*), and HKII (*G*) in SOL muscle of sedentary and trained WT and D4KO male mice ($n = 5$ – 9). Detection of TBC1D4 served as an additional genotyping control for WT and D4KO mice. *H*: Fiber type composition in EDL muscle of sedentary and trained WT and D4KO male mice. EDL cross sections were

reduced upstream regulators (Fig. 4C). Since reduced *Tgfb1* signaling was shown to be related to increased mitochondrial activity and browning in adipocytes (24), we screened our RNA sequencing data specifically for the expression levels of known browning genes. Expression levels of *Adrb3*, *Ces1d*, *Cidea*, *Cyp2e1*, and *Pparg1a* were increased in trained D4KO mice compared with sedentary controls (Fig. 4D). Additional real-time PCR analysis of browning genes in WAT demonstrated an overall tendency toward reduced expression levels of the browning genes *Cidea* and *Cox8b* in sedentary D4KO mice, which were rescued after chronic exercise (Fig. 4E). Moreover, expression of *Pparg1a* and *P2rx5* were significantly elevated in trained D4KO mice, while expression of *Cd137* and *Prdm16* as well as expression of other selected browning genes were not elevated (Fig. 4E and Supplementary Fig. 5A). Importantly, mRNA expression as well as protein abundance of the main regulator of thermogenesis and browning UCP-1 was markedly increased in WAT from trained D4KO mice (Fig. 4F and G). In BAT, expression of a number of thermogenic markers was moderately upregulated in trained D4KO mice (Supplementary Fig. 5B and C). In addition, IPA in BAT revealed a mildly upregulated OXPHOS pathway and increased expression levels of related genes (Supplementary Fig. 5D and E).

Chronic Exercise Increases Glucose Uptake and GLUT4 Abundance in WAT and BAT From D4KO Mice

We next investigated whether the improved insulin sensitivity in trained D4KO mice was associated with improved adipocyte function. We analyzed in vivo glucose uptake into interscapular BAT (iBAT), an organ compartment describing the BAT and surrounding WAT, via PET/CT. Whereas glucose uptake into iBAT of WT mice remained unchanged after chronic exercise, trained D4KO mice showed a marked increase into this tissue (Fig. 5A–C). Western blot analysis of GLUT4 protein in BAT and WAT from D4KO mice showed a GLUT4 reduction of ~50% compared with sedentary WT animals (Fig. 5D and E). However, in both fat depots from D4KO mice, GLUT4 content was significantly increased after the training intervention compared with sedentary controls, and even elevated to WT levels in the WAT, whereas GLUT1 levels were unchanged (Fig. 5F and G). Abundance of TBC1D1 was not altered in WAT from sedentary or trained WT and D4KO mice (Supplementary Fig. 6). In addition, we determined ex vivo glucose transport into isolated primary epididymal WACs (eWACs). Sedentary D4KO mice demonstrated significantly impaired insulin-stimulated glucose uptake into eWACs compared with WT littermates. Following the

training intervention, WT mice displayed substantially enhanced insulin-stimulated glucose uptake into the eWACs. Notably, trained D4KO animals also revealed a clearly improved insulin-stimulated glucose transport into fat cells, almost completely abolishing the initially observed impairment in this genotype (Fig. 5H).

DISCUSSION

With the current study, we are the first to determine the impact of TBC1D4 on exercise-induced improvements in systemic and organ-specific insulin sensitivity. We and other researchers have shown that deletion of TBC1D4 leads to impaired insulin sensitivity (7,25). We now demonstrate that *Tbc1d4* deficiency on HFD feeding also leads to improved sensitivity to moderate endurance training, as evidenced by improved whole-body insulin sensitivity, increased expression of markers of mitochondrial activity and browning in WAT, and increased glucose uptake in iBAT and WAT.

Analogous to our previous results (7), D4KO mice fed a standard diet did not show impaired glucose tolerance compared with WT littermates. In contrast, 8 weeks of HFD feeding impaired insulin sensitivity in D4KO mice, as reflected by increased HOMA-IR. However, glucose and insulin tolerance was only slightly, but not significantly, impaired in the D4KO animals. This mild expression of insulin resistance was also observed in other studies where glucose and insulin tolerance of animals with TBC1D4 depletion or functional limitation was either only slightly impaired or not impaired at all after HFD feeding (26–28). In contrast, the combined deletion of TBC1D4 and its closest homolog TBC1D1 resulted in impaired glucose and insulin tolerance in standard diet-fed mice, suggesting at least partially compensatory mechanisms at the physiological level (7,25). However, potential compensation is not achieved by increased expression levels of the remaining RabGAP after depletion of TBC1D1 or TBC1D4, as shown in the current and previous studies (6–8).

We found an initially impaired physical fitness of D4KO mice fed an HFD that was rescued after the exercise intervention. In contrast, running capacity of D4KO mice kept on a standard diet was comparable to WT littermates, suggesting that the impaired fitness was not primarily due to the lack of TBC1D4 but also due to the additional impact of the HFD on the TBC1D4 deficiency. Interestingly, HFD-fed D4KO mice exhibited a slightly increased body fat content before the training intervention, which may relate to the observed reduction in running capacity.

stained with SC-71 (myosin heavy chain [MyHC] type IIA, red), BF-F3 (MyHC type IIB, green), and laminin (cell membranes, blue) and respective fluorophore-labeled secondary antibodies. Unstained fibers represent type II X fibers. *l*: Fiber type composition in SOL muscle of sedentary and trained WT and D4KO male mice. SOL cross sections were stained with either BA-D5 (MyHC type I, green), SC-71 (MyHC type IIA, red), or laminin (cell membranes, blue) (top) or with SC-71 (red), BF-F3 (MyHC type IIB, green), and laminin (bottom) and respective fluorophore-labeled secondary antibodies. Scale bar in all images is 500 μm ($n = 7-10$). Data are mean \pm SEM. * $P < 0.05$, *** $P < 0.001$ between indicated groups; # $P < 0.05$, ## $P < 0.01$, ### $P < 0.001$ in insulin-stimulated vs. basal of indicated group (A and B) or D4KO vs. corresponding WT control (E and G) (two-way ANOVA with Bonferroni correction). a.u., arbitrary unit; S, sedentary; T, trained.

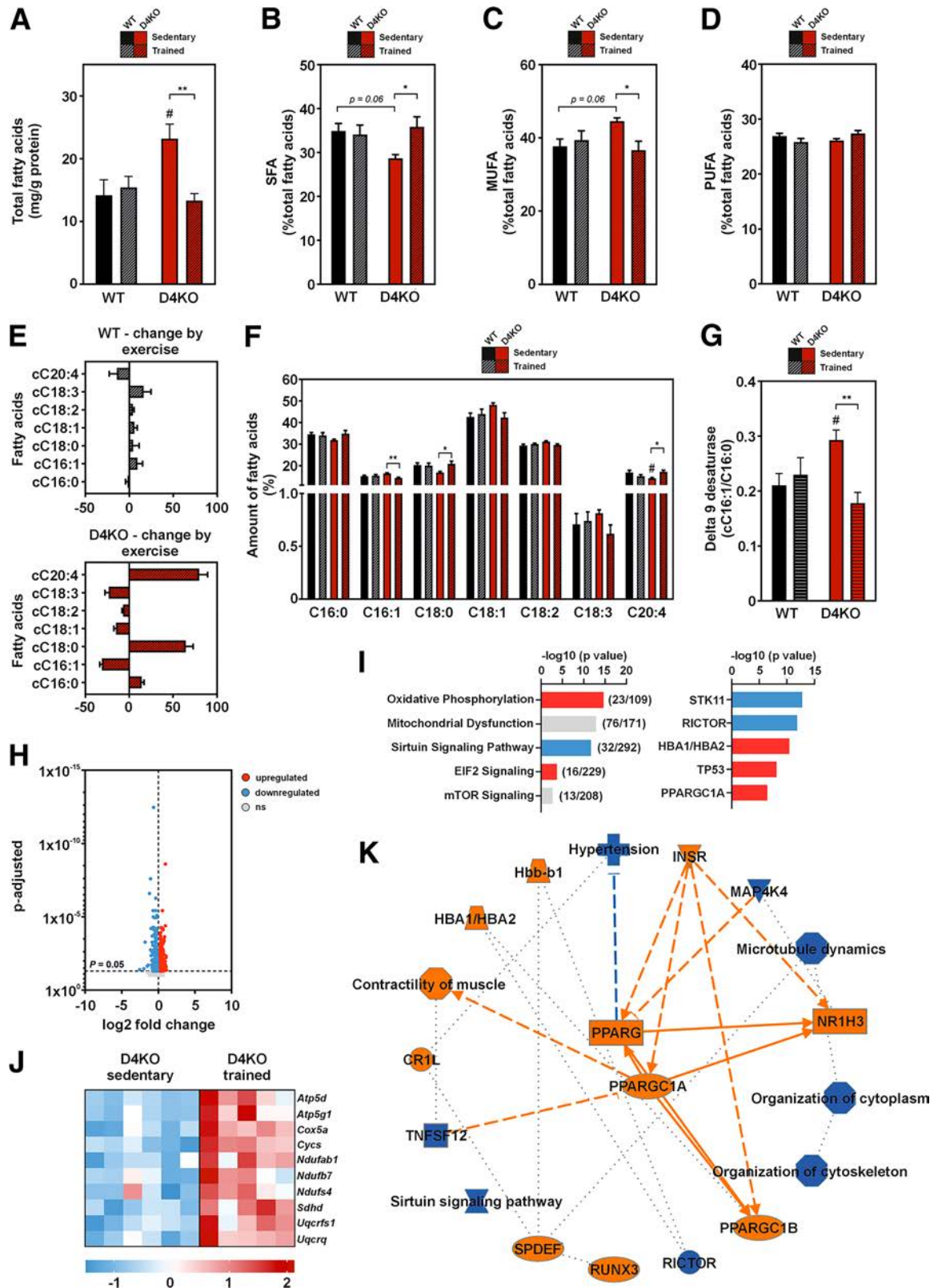


Figure 3—Skeletal muscle of trained D4KO mice exhibits altered FA composition and increased mitochondrial OXPHOS gene expression. **A**: Total FA content in gastrocnemius muscle from sedentary and trained WT and D4KO male mice determined by lipid profiling. **B–D**: Percentage of saturated FA (SFA) (**B**), monounsaturated FA (MUFA) (**C**), and polyunsaturated FA (PUFA) (**D**) of total FA content. **E** and **F**: Detailed analysis of skeletal muscle FA species distribution as percentage of total FA content. (**E** highlights percent changes of FA species in trained vs. sedentary male animals of each genotype.) **G**: Calculated D9-desaturase index (C16:1/C16:0) from lipid profiling data ($n = 6$). **H**: Volcano plot of differentially expressed genes at a threshold of adjusted $P < 0.05$ in gastrocnemius muscle of sedentary vs. trained D4KO

In our study, the improved insulin sensitivity in trained D4KO mice was associated with modestly enhanced skeletal muscle glucose uptake but not with a full rescue of the initial impairment. Severe impairments of insulin-stimulated glucose uptake into skeletal muscle and adipocytes have been related to reduced protein abundance and/or translocation defects of the insulin-responsive GLUT4 in *Tbc1d4*-deficient oxidative skeletal muscle and adipocytes (7,10,11,29). In contrast, a number of studies have demonstrated that regular exercise training leads to both increased GLUT4 amount and enhanced GLUT4 translocation to the plasma membrane, resulting in improved skeletal muscle insulin sensitivity (30). Of note, not all training interventions lead to increased GLUT4 mRNA or protein expression in human or rodent studies, dependent on training intensity, frequency, and metabolic state of the individuals (31–35). In skeletal muscle from D4KO mice, neither was GLUT4 protein content increased after chronic exercise nor was the abundance of HKII, which regulates the rate-limiting phosphorylation of glucose for skeletal muscle glucose uptake during exercise (31,36), or the distribution of glycolytic fiber types. These findings are similar to a recent study using a D4KO rat model that exhibited reduced postexercise skeletal muscle glucose uptake and abrogated GLUT4 content. These parameters, however, were only determined after a single bout of exercise (32). Compared with D4KO mice, trained WT mice showed enhanced glucose uptake into oxidative soleus muscle after exercise training. The magnitude of this increase could have been affected by the increased skeletal muscle glycogen content of WT mice, which was not evident in the trained D4KO muscle. In contrast, exercise training did not result in any improvement in insulin-stimulated glucose uptake in the glycolytic EDL muscle of either WT or D4KO mice. The response to the training program may differ depending on the muscle fiber type (33,34). Both genotypes showed improvement in insulin-stimulated glucose uptake as a result of treadmill training exclusively in the soleus muscle. Improving insulin sensitivity exclusively in oxidative muscle types is unlikely to significantly impact whole-body glycemia because of the small proportion of type I fibers in larger muscles, such as the quadriceps or the gastrocnemius (35,37). Therefore, the observed improvement in adipocyte insulin sensitivity after training may be either a primary effect specific to D4KO fat tissue or a secondary effect mediated from the trained D4KO skeletal muscle to the D4KO adipocytes, e.g., via alterations in the myokine secretion profile.

A major feature of insulin resistance in skeletal muscle is a high degree of metabolic inflexibility characterized by a disturbed on-demand switching ability from lipid to carbohydrate substrates (38). In general, excess accumulation of certain lipid species in skeletal muscle is negatively correlated with insulin sensitivity (21,39). A role as metabolic switch between glucose and lipid metabolism has been attributed to both TBC1D1 and TBC1D4 in the past. Previously, we demonstrated increased whole-body lipid use and skeletal muscle FA oxidation in D4KO mice already in the sedentary state when fed a standard diet (6,7,21). In our current study, the improved insulin sensitivity in trained D4KO mice was associated with reduced body fat content, reduced skeletal muscle total FA and monounsaturated FA content, as well as reduced stearoyl-CoA desaturase activity. Increased stearoyl-CoA desaturase 1 activity together with reduced FA oxidation in skeletal muscle has been associated with obesity in humans (40). These findings indicate an elevated lipid use in response to the exercise intervention in skeletal muscle from HFD-fed D4KO animals, potentially contributing to the observed improved insulin sensitivity.

Endurance exercise training in D4KO mice led to enhanced expression of thermogenic markers in WAT. Originally discovered as a cold-induced phenomenon in rodents, the increase in thermogenic and mitochondrial genes in WACs, the so-called browning, has gained attention as a relevant mechanism in response to exercise interventions as well. Since mitochondrial dysfunction in adipocytes has been widely accepted to strongly correlate with the development of insulin resistance, physical activity presents an attractive treatment or preventive measure for these disorders (41,42). Current research now focuses on the translational potential of exercise-induced browning and its therapeutic potential, the majority of studies so far having been conducted in rodents (43–45). In our study, we saw a general reduction in gene expression levels of browning markers in sedentary D4KO mice that were increased to WT levels after endurance exercise. In addition, protein abundance of UCP-1 was increased in WAT from trained D4KO mice, and TGFB1 was revealed as a major upstream regulator of the training-induced alterations. Previous studies identified *TGFB1* as a central regulator of exercise response in humans (46). More importantly, inhibition of TGF β signaling has been shown to be involved in the activation of adipocyte browning processes in murine and human adipocyte cells (24). In line with these findings, our data suggest that reduced TGFB1 signaling may

male mice ($n = 6$ per group) from RNA sequencing analysis. Blue dots, genes downregulated in trained D4KO; red dots, genes upregulated in trained D4KO mice; gray dots, genes not significantly regulated. *I*: Canonical pathways (left) and upstream regulators (right) of differentially regulated transcripts identified by IPA in gastrocnemius muscle of sedentary vs. trained D4KO male mice. Red bars, positive z score (activated in trained D4KO); blue bars, negative z score (inhibited in trained D4KO); gray bars, undetermined directionality. *J*: Heat map of differentially regulated genes (z scores) related to the OXPHOS pathway. *K*: Graphical summary of IPA in gastrocnemius muscle from sedentary and trained D4KO male mice. Orange nodes, predicted activation (z score ≥ 2); blue nodes, predicted inhibition (z score ≤ -2) in trained D4KO mice. * $P < 0.05$, ** $P < 0.01$ between indicated groups; # $P < 0.05$ in D4KO vs. corresponding WT control (two-way ANOVA with Bonferroni correction).

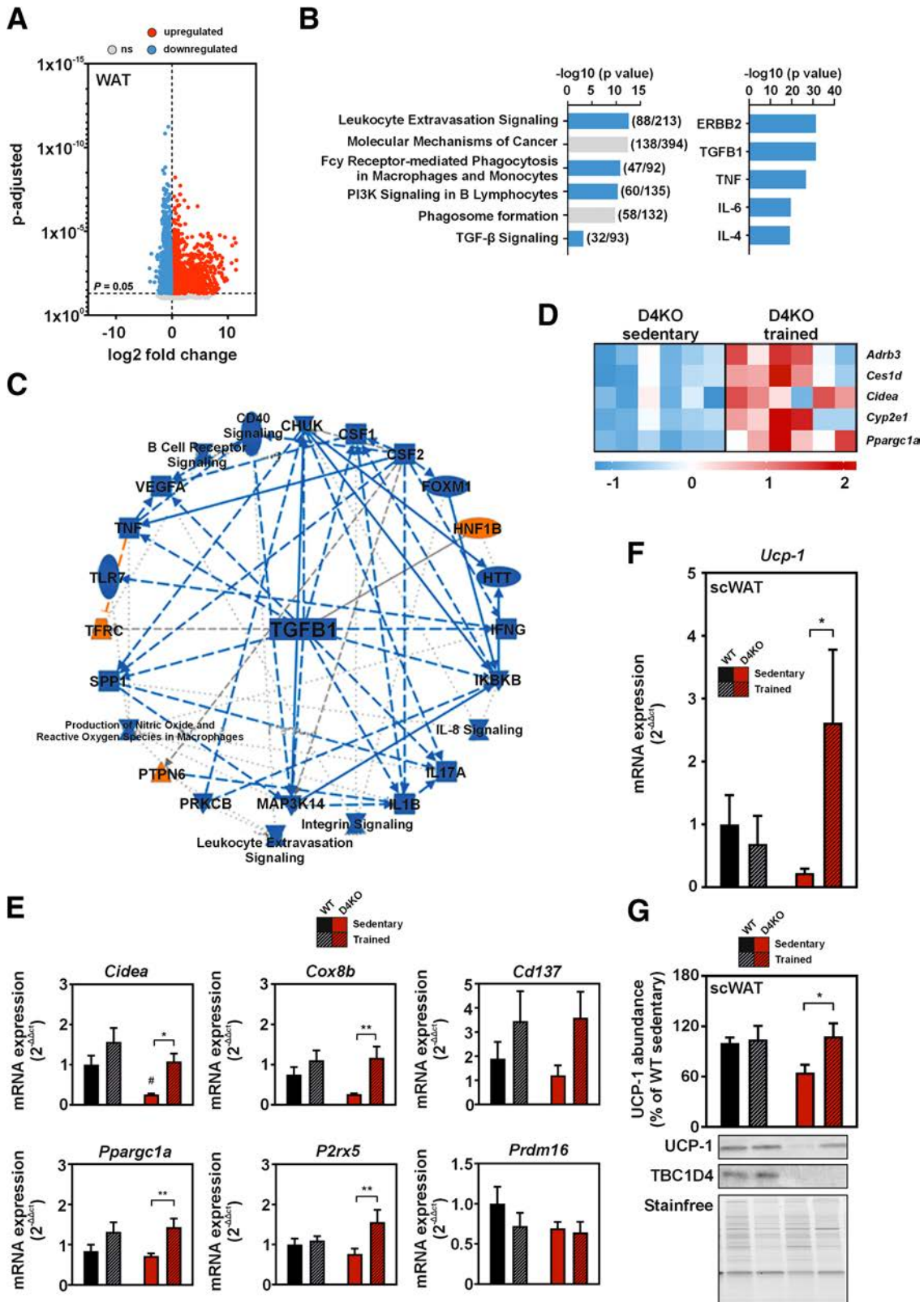


Figure 4—Transcriptome analysis in trained D4KO mice shows enhanced markers for mitochondrial activity and browning in WAT. **A**: Volcano plot of differentially expressed genes at a threshold of adjusted $P < 0.05$ in WAT of sedentary vs. trained D4KO male mice ($n = 6$ per group). Blue dots, genes downregulated in trained D4KO; red dots, genes upregulated in trained D4KO mice; gray dots, genes not significantly regulated. **B**: Canonical pathways (left) and upstream regulators (right) of differentially regulated transcripts identified by IPA in WAT of sedentary vs. trained D4KO male mice. Blue bars, negative z score (inhibited in D4KO trained); gray bars, undetermined directionality. **C**: IPA graphical summary of top upstream regulator *Tgfb1* and its relation to other target genes and canonical pathways in WAT of sedentary vs. trained D4KO male

be associated with enhanced browning processes in D4KO adipose tissue.

In contrast to skeletal muscle, GLUT4 abundance was substantially increased in WAT from trained D4KO mice. Despite the fact that the adipose tissue accounts for <10% of whole-body glucose uptake, studies in adipocyte-specific GLUT4 knockout mice demonstrated the major importance of this tissue for the maintenance of healthy glucose homeostasis, as these mice developed marked muscular and hepatic insulin resistance and became heavily diabetic (47,48). In accordance with the increased GLUT4 levels in WAT and BAT, glucose transport into isolated adipocytes as well as into iBAT from D4KO mice was rescued to WT levels, identifying an important role for the adipose tissue in increasing glucose clearance in trained D4KO mice. Increased glucose uptake into BAT was shown to be associated with increased thermogenesis (49). In our study, a number of thermogenic markers were moderately upregulated in the BAT from trained D4KO mice. Further functional studies are needed to elucidate the exact link between increased glucose uptake and thermogenesis in *Tbc1d4*-deficient adipose tissue.

Decreased fat mass and, consequently, improved adipocyte function may explain at least in part the pronounced effects on insulin sensitivity and glucose homeostasis in D4KO mice. Studies in mice have indicated that regular physical activity targets the adipose tissue, which partly contributes to improved whole-body glycemia (45,50). Therefore, we speculate that exercising muscles deficient in *Tbc1d4* may release previously unknown secreted factors, such as myokines and/or metabolites, that increase insulin sensitivity in other cell types such as adipocytes. In addition, TBC1D4 has been shown to be associated with vesicle transport (5,51), and deficiency in this RabGAP may also alter secretory processes. Future studies are necessary to elucidate a possible muscle-adipose tissue crosstalk caused by a modified secretory profile of D4KO skeletal muscles.

Interestingly, these findings are similar to the observations made in our earlier collaborative study in which increased daily physical activity, as assessed using retrospective survey data, was associated with greater improvements of postprandial hyperglycemia in homozygous allele carriers of a *TBC1D4* *p.Arg684Ter* loss-of-function variant compared with nonallele carriers (15,17,52). Lack of TBC1D4 apparently enables individuals to significantly benefit even from moderate endurance training (in the present mouse study) or an increase in daily activity (in the human study), with substantial

improvements seen in overall insulin sensitivity. In this study, we chose a moderate-intensity exercise protocol that mimics a more active lifestyle rather than a rigorous and frequent high-intensity exercise program that may not be feasible for many people. This protocol did not result in very pronounced improvements in body fat content or insulin sensitivity in the WT controls. This is in line with previous studies training WT mice on a B6 background that used similar moderate-intensity training protocols (53,54). Even increasing the training intensity did not always lead to reductions in body adiposity or improved glucose tolerance in WT mice on a B6 background (55), highlighting the interindividual heterogeneity of this mouse strain in response to exercise, particularly regarding glycemic end points. Presumably, a more intense or prolonged exercise training protocol would result in greater improvements in glycemic control, body adiposity, and skeletal muscle glucose uptake. In the case of *Tbc1d4* deficiency, on the other hand, even moderate endurance training is sufficient to bring about a significant improvement in insulin sensitivity. Based on the finding that sedentary D4KO mice had greater adiposity at the end of the training intervention than their WT littermates, the training may have been more intensive for certain individuals.

Collectively, our data demonstrate that impairments in whole-body glycemia caused by *Tbc1d4* deficiency can be rescued by moderate endurance exercise training, mainly by improving adipose tissue insulin sensitivity. According to our study, *Tbc1d4* deficiency improves exercise response in individuals with insulin resistance. Although the effect of *TBC1D4* variants on insulin sensitivity has so far only been described in genetically isolated populations or individual cases, there may be other as-yet unknown gene variants in the general population that determine the magnitude of exercise-mediated glycemic improvements in individuals. Thus, *TBC1D4* gene variants may be relevant targets for the prediction of exercise response in individuals with insulin resistance in the future.

Acknowledgments. The authors thank Angelika Horrigs, Birgit Knobloch, Heidrun Podini, Antonia Osmer, Carina Heitmann, Martina Schiller, Jennifer Schwettmann, Denise Schauer, Lisa Ditges, Jürgen Weiß, Kay Jeruschke, and Carmen Weidlich, German Diabetes Center (DDZ), Leibniz Center for Diabetes Research, Heinrich Heine University Düsseldorf, for expert technical assistance and support and consultation. The authors also thank Prof. Annette Schürmann, Department of Experimental Diabetology, German Institute of Human Nutrition Potsdam-Rehbruecke, and German Center for Diabetes Research (DZD), Partner Potsdam-Rehbruecke, for providing GLUT1 antibodies.

Funding. This work was supported in part by Deutsche Forschungsgemeinschaft grants DFG-RTG 2576 vivid (to H.A.-H. and A.C.) and CH1659 (to A.C.),

mice. Orange nodes, predicted activation (z score ≥ 2) in trained D4KO mice; blue nodes, predicted inhibition (z score ≤ -2) in trained D4KO mice. *D*: Heat map of differentially regulated browning genes (z scores) in WAT of sedentary vs. trained D4KO male mice. *E* and *F*: mRNA expression of selected genes (*E*) related to enhanced mitochondrial activity and browning and expression of master regulator of browning *Ucp-1* (*F*) in subcutaneous WAT (scWAT) of sedentary and trained WT and D4KO male mice ($n = 8-15$). *G*: Protein abundance of UCP-1 in scWAT of sedentary and trained WT and D4KO male mice normalized to total protein content ($n = 10-12$). Detection of TBC1D4 served as an additional genotyping control for WT and D4KO mice. Data in *E-G* are mean \pm SEM. * $P < 0.05$, ** $P < 0.01$ between indicated groups; # $P < 0.05$ in D4KO vs. corresponding WT control (two-way ANOVA with Bonferroni correction).

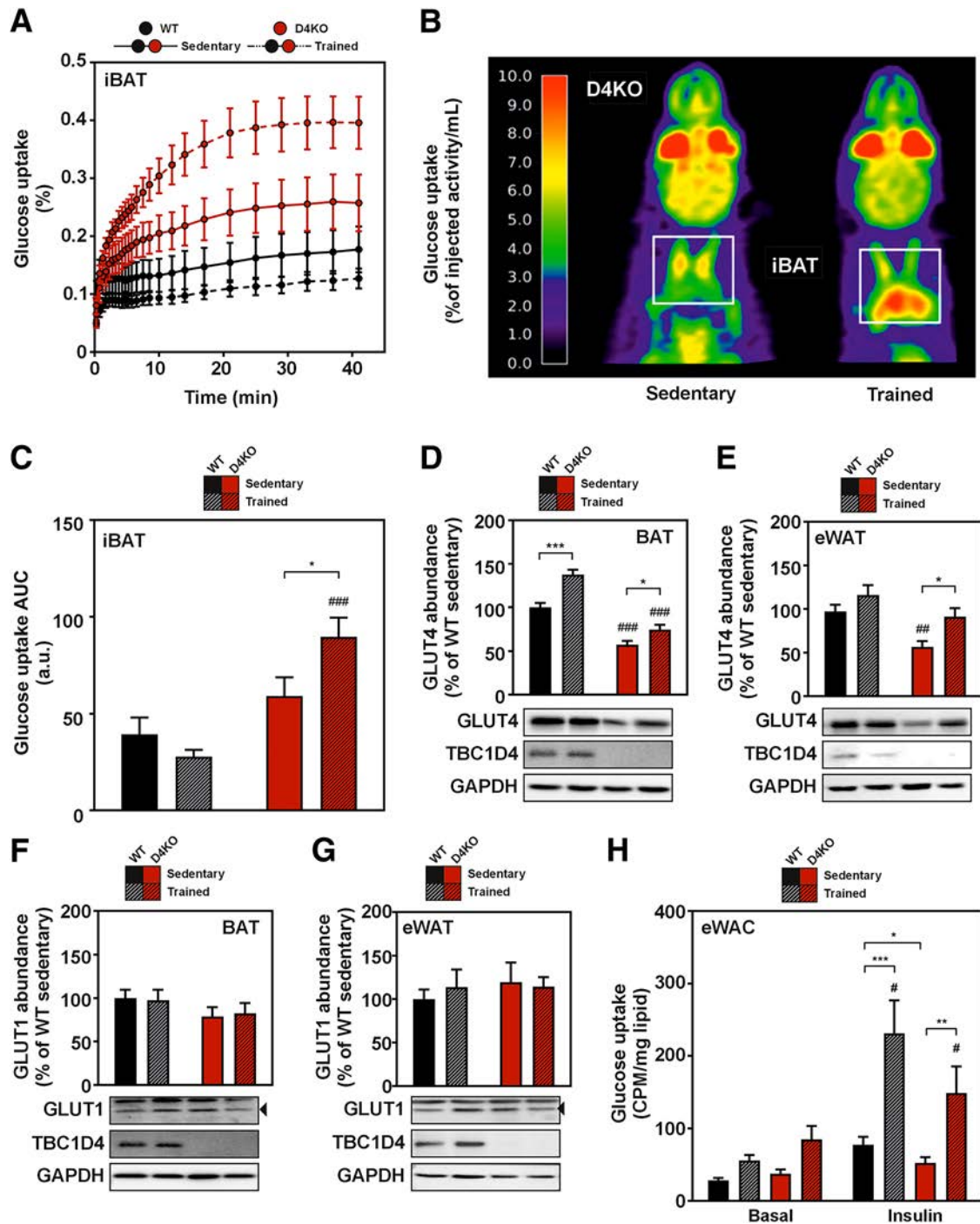


Figure 5—Increased insulin sensitivity in trained D4KO mice is associated with improved glucose uptake in BAT and WAT. **A**: Glucose uptake into iBAT of sedentary and trained WT and D4KO male mice after intravenous injection with (^{18}F)-2-fluoro-deoxy-D-glucose (^{18}FDG) followed by PET. **B**: Representative PET scan of iBAT tissue (square) in sedentary (left) and trained (right) D4KO male mice. Red color indicates higher glucose uptake within the respective area. **C**: Area under the curve (AUC) quantification of ^{18}FDG uptake ($n = 4-6$). **D-G**: Abundances of GLUT4 in BAT (**D**) and epididymal WAT (eWAT) (**E**) and abundance of GLUT1 in BAT (**F**) and eWAT (**G**) of sedentary and trained WT and D4KO male mice ($n = 8-18$). Detection of TBC1D4 served as an additional genotyping control for WT and D4KO mice. **H**: Ex vivo glucose uptake in isolated adipocytes from eWACs of sedentary and trained WT and D4KO male mice at basal or insulin-stimulated conditions ($n = 12$). Data are mean \pm SEM. * $P < 0.05$, ** $P < 0.01$, *** $P < 0.001$ between indicated groups; # $P < 0.05$, ## $P < 0.01$, ### $P < 0.001$ in D4KO vs. corresponding WT control (**C-E**) or insulin-stimulated vs. basal of indicated group (**H**) (two-way ANOVA with Bonferroni correction). a.u., arbitrary unit; CPM, counts per minute.

Deutsche Diabetes Gesellschaft (DDG) (to C.S.), EFSD/Novo Nordisk Program for Diabetes Research (to H. A.-H.), the Ministry of Science and Research of the State North Rhine-Westphalia, the German Center for Diabetes Research, and the German Federal Ministry of Health (BMG).

Duality of Interest. No potential conflicts of interests relevant to this article were reported.

Author Contributions. C.S., C.B., D.W., L.T., A.L.C., H.B., A.K.S., L.E., J.K., S.S., A.K., D.K., S.K., S.H., S.L., S.C., M.L., R.H., S.B., and B.T. performed the experiments and analyzed data. C.S., T.M.S., T.H., J.B., H.A.-H., and A.C. were involved in the study design and contributed to the data interpretation. C.S., H.A.-H., and A.C. wrote the manuscript and analyzed and interpreted the data. A.C. is the guarantor of this work and, as such, had full access to all the data in the study and takes responsibility for the integrity of the data and the accuracy of the data analysis.

Prior Presentation. Parts of this study were presented in an oral presentation at the Jahrestagung der Deutschen Diabetes-Gesellschaft (DDG), Berlin, Germany, 17–20 May 2023.

References

- Samuel VT, Shulman GI. Mechanisms for insulin resistance: common threads and missing links. *Cell* 2012;148:852–871
- Watson RT, Pessin JE. Intracellular organization of insulin signaling and GLUT4 translocation. *Recent Prog Horm Res* 2001;56:175–193
- Hilder TL, Baer LA, Fuller PM, et al. Insulin-independent pathways mediating glucose uptake in hindlimb-suspended skeletal muscle. *J Appl Physiol* (1985) 2005;99:2181–2188
- Musi N, Goodyear LJ. AMP-activated protein kinase and muscle glucose uptake. *Acta Physiol Scand* 2003;178:337–345
- Jaladin-Fincati JR, Pavarotti M, Frendo-Cumbo S, Bilan PJ, Klip A. Update on GLUT4 Vesicle Traffic: A Cornerstone of Insulin Action. *Trends Endocrinol Metab* 2017;28:597–611
- Chadt A, Leicht K, Deshmukh A, et al. Tbc1d1 mutation in lean mouse strain confers leanness and protects from diet-induced obesity. *Nat Genet* 2008;40:1354–1359
- Chadt A, Immisch A, de Wendt C, et al. Deletion of both Rab-GTPase-activating proteins TBC1D1 and TBC1D4 in mice eliminates insulin- and AICAR-stimulated glucose transport [corrected]. *Diabetes* 2015;64:746–759
- Szekeress F, Chadt A, Tom RZ, et al. The Rab-GTPase-activating protein TBC1D1 regulates skeletal muscle glucose metabolism. *Am J Physiol Endocrinol Metab* 2012;303:E524–E533
- Dokas J, Chadt A, Joost HG, Al-Hasani H. Tbc1d1 deletion suppresses obesity in leptin-deficient mice. *Int J Obes* 2016;40:1242–1249
- Lansley MN, Walker NN, Hargrett SR, Stevens JR, Keller SR. Deletion of Rab GAP AS160 modifies glucose uptake and GLUT4 translocation in primary skeletal muscles and adipocytes and impairs glucose homeostasis. *Am J Physiol Endocrinol Metab* 2012;303:E1273–E1286
- Wang HY, Ducommun S, Quan C, et al. AS160 deficiency causes whole-body insulin resistance via composite effects in multiple tissues. *Biochem J* 2013;449:479–489
- de Wendt C, Espelage L, Eickelschulte S, et al. Contraction-mediated glucose transport in skeletal muscle is regulated by a framework of AMPK, TBC1D1/4, and Rac1. *Diabetes* 2021;70:2796–2809
- Dash S, Langenberg C, Fawcett KA, et al. Analysis of TBC1D4 in patients with severe insulin resistance. *Diabetologia* 2010;53:1239–1242
- Dash S, Sano H, Rochford JJ, et al. A truncation mutation in TBC1D4 in a family with acanthosis nigricans and postprandial hyperinsulinemia. *Proc Natl Acad Sci U S A* 2009;106:9350–9355
- Moltke I, Grarup N, Jørgensen ME, et al. A common Greenlandic TBC1D4 variant confers muscle insulin resistance and type 2 diabetes. *Nature* 2014;512:190–193
- Andersen MK, Hansen T. Genetics of metabolic traits in Greenlanders: lessons from an isolated population. *J Intern Med* 2018;284:464–477
- Schnurr TM, Jørsboe E, Chadt A, et al. Physical activity attenuates postprandial hyperglycaemia in homozygous TBC1D4 loss-of-function mutation carriers. *Diabetologia* 2021;64:1795–1804
- Binsch C, Jelenik T, Pfitzer A, et al. Absence of the kinase S6k1 mimics the effect of chronic endurance exercise on glucose tolerance and muscle oxidative stress. *Mol Metab* 2017;6:1443–1453
- Klymenko O, Brecklinghaus T, Dille M, et al. Histone deacetylase 5 regulates interleukin 6 secretion and insulin action in skeletal muscle. *Mol Metab* 2020;42:101062
- Schiaffino S, Gorza L, Sartore S, et al. Three myosin heavy chain isoforms in type 2 skeletal muscle fibres. *J Muscle Res Cell Motil* 1989;10:197–205
- Benninghoff T, Espelage L, Eickelschulte S, et al. The RabGAPs TBC1D1 and TBC1D4 Control uptake of long-chain fatty acids into skeletal muscle via fatty acid transporter SLC27A4/FATP4. *Diabetes* 2020;69:2281–2293
- Knebel B, Fahlbusch P, Poschmann G, et al. Adipokine signatures in obese mouse models reflect adipose tissue health and are associated with serum lipid composition. *Int J Mol Sci* 2019;20:2559
- Livak KJ, Schmittgen TD. Analysis of relative gene expression data using real-time quantitative PCR and the 2^{-ΔΔC_T} method. *Methods* 2001;25:402–408
- Wankhade UD, Lee JH, Dagur PK, et al. TGF-β receptor 1 regulates progenitors that promote browning of white fat. *Mol Metab* 2018;16:160–171
- Hargrett SR, Walker NN, Keller SR. Rab GAPs AS160 and Tbc1d1 play nonredundant roles in the regulation of glucose and energy homeostasis in mice. *Am J Physiol Endocrinol Metab* 2016;310:E276–E288
- Binsch C, Barbosa DM, Hansen-Dille G, et al. Deletion of Tbc1d4/As160 abrogates cardiac glucose uptake and increases myocardial damage after ischemia/reperfusion. *Cardiovasc Diabetol* 2023;22:17
- Paglialunga S, Simnett G, Robson H, et al. The Rab-GTPase activating protein, TBC1D1, is critical for maintaining normal glucose homeostasis and β-cell mass. *Appl Physiol Nutr Metab* 2017;42:647–655
- Kjøbsted R, Kristensen JM, Eskesen NO, et al. TBC1D4-S711 controls skeletal muscle insulin sensitization after exercise and contraction. *Diabetes* 2023;72:857–871
- Xie B, Chen Q, Chen L, Sheng Y, Wang HY, Chen S. The inactivation of RabGAP function of AS160 promotes lysosomal degradation of GLUT4 and causes postprandial hyperglycemia and hyperinsulinemia. *Diabetes* 2016;65:3327–3340
- Richter EA, Hargreaves M. Exercise, GLUT4, and skeletal muscle glucose uptake. *Physiol Rev* 2013;93:993–1017
- Fueger PT, Heikkinen S, Bracy DP, et al. Hexokinase II partial knockout impairs exercise-stimulated glucose uptake in oxidative muscles of mice. *Am J Physiol Endocrinol Metab* 2003;285:E958–E963
- Zheng A, et al. The exercise-induced improvement in insulin-stimulated glucose uptake by rat skeletal muscle is absent in male AS160-knockout rats, partially restored by muscle expression of phosphomutated AS160, and fully restored by muscle expression of wildtype AS160. *Diabetes* 2022;71:219–232
- Takekura H, Yoshioka T. Different metabolic responses to exercise training programmes in single rat muscle fibres. *J Muscle Res Cell Motil* 1990;11:105–113
- Lee SM, Lee MC, Bae WR, Yoon KJ, Moon HY. Muscle fiber type-dependence effect of exercise on genomic networks in aged mice models. *Aging (Albany NY)* 2022;14:3337–3364
- Sher J, Cardasis C. Skeletal muscle fiber types in the adult mouse. *Acta Neurol Scand* 1976;54:45–56
- Fueger PT, Shearer J, Krueger TM, et al. Hexokinase II protein content is a determinant of exercise endurance capacity in the mouse. *J Physiol* 2005;566:533–541
- Mänttari S, Järvillehto M. Comparative analysis of mouse skeletal muscle fibre type composition and contractile responses to calcium channel blocker. *BMC Physiol* 2005;5:4

38. Galgani JE, Moro C, Ravussin E. Metabolic flexibility and insulin resistance. *Am J Physiol Endocrinol Metab* 2008;295:E1009–E1017
39. Gilbert M. Role of skeletal muscle lipids in the pathogenesis of insulin resistance of obesity and type 2 diabetes. *J Diabetes Investig* 2021;12:1934–1941
40. Hulver MW, Berggren JR, Carper MJ, et al. Elevated stearoyl-CoA desaturase-1 expression in skeletal muscle contributes to abnormal fatty acid partitioning in obese humans. *Cell Metab* 2005;2:251–261
41. Lee JH, Park A, Oh KJ, Lee SC, Kim WK, Bae KH. The role of adipose tissue mitochondria: regulation of mitochondrial function for the treatment of metabolic diseases. *Int J Mol Sci* 2019;20:4924
42. Martin AR, Chung S, Koehler K. Is exercise a match for cold exposure? Common molecular framework for adipose tissue browning. *Int J Sports Med* 2020;41:427–442
43. Lizcano F. The beige adipocyte as a therapy for metabolic diseases. *Int J Mol Sci* 2019;20:5058
44. McKie GL, Wright DC. Biochemical adaptations in white adipose tissue following aerobic exercise: from mitochondrial biogenesis to browning. *Biochem J* 2020;477:1061–1081
45. Scheel AK, Espelage L, Chadt A. Many ways to Rome: exercise, cold exposure and diet-do they all affect BAT activation and WAT browning in the same manner? *Int J Mol Sci* 2022;23:4759
46. Böhm A, Hoffmann C, Irmiler M, et al. TGF- β contributes to impaired exercise response by suppression of mitochondrial key regulators in skeletal muscle. *Diabetes* 2016;65:2849–2861
47. Abel ED, Peroni O, Kim JK, et al. Adipose-selective targeting of the GLUT4 gene impairs insulin action in muscle and liver. *Nature* 2001;409:729–733
48. Reitman ML, Gavrilova O. A-ZIP/F-1 mice lacking white fat: a model for understanding lipotrophic diabetes. *Int J Obes Relat Metab Disord* 2000;24(Suppl. 4):S11–S14
49. McNeill BT, Morton NM, Stimson RH. Substrate utilization by brown adipose tissue: what's hot and what's not? *Front Endocrinol (Lausanne)* 2020;11:571659
50. Stanford KI, Middelbeek RJ, Goodyear LJ. Exercise effects on white adipose tissue: beiging and metabolic adaptations. *Diabetes* 2015;64:2361–2368
51. Eickelschulte S, Hartwig S, Leiser B, et al. AKT/AMPK-mediated phosphorylation of TBC1D4 disrupts the interaction with insulin-regulated aminopeptidase. *J Biol Chem* 2021;296:100637
52. Manousaki D, Kent JW Jr, Haack K, et al. Toward precision medicine: TBC1D4 disruption is common among the Inuit and leads to underdiagnosis of type 2 diabetes. *Diabetes Care* 2016;39:1889–1895
53. Lezi E, Lu J, Burns JM, Swerdlow RH. Effect of exercise on mouse liver and brain bioenergetic infrastructures. *Exp Physiol* 2013;98:207–219
54. Chen W, Wang HJ, Shang NN, et al. Moderate intensity treadmill exercise alters food preference via dopaminergic plasticity of ventral tegmental area-nucleus accumbens in obese mice. *Neurosci Lett* 2017;641:56–61
55. Marcinko K, Sikkema SR, Samaan MC, Kemp BE, Fullerton MD, Steinberg GR. High intensity interval training improves liver and adipose tissue insulin sensitivity. *Mol Metab* 2015;4:903–915